DIRECTED METALLISATION USING MOLECULAR RECOGNITION TOOLS

Thesis submitted for the degree of

Doctor of Philosophy

at the University of Leicester

by

Ruggero Dondi

February 2012

Table of contents

ACKNOWLEDGMENTS

I would like to thank my supervisor Glenn for the fantastic opportunity that he gave me to work in his group. I want to thank all my friends in Leicester for the help they shared during the years spent in the laboratory. Most of all I would like to thank my family for allowing me to spend 4 years abroad and Joanna for all the psychological and material support she gave me. Lastly, I would like to thank everybody I consulted and helped me in any way throughout these years.

ABSTRACT

During this thesis a new infrastructure of methods to template functional materials at specific sites in a DNA architecture using molecular recognition of specific DNA duplexes has been developed. The project focused on the use of naturally occurring duplex DNA and the Tollens' reaction as a mild source of metal amenable to reduction in the presence of aldehyde functional groups. The advantages of this choice are:

1) The use of naturally-occurring DNA increases modularity;

2) The Tollens' reagent acts as a mild selective metallising reagent that enables the reduction of metal ions at specific sites along DNA. Molecules such as Pyrrole-Imidazole polyamides were prepared and were tested to determine whether selective metallisation of DNA nano-architectures can be achieved by confining the nucleation and growth of silver nanostructures to defined regions along a DNA duplex.

ABBREVIATIONS

AgNP@**(1)**: Silver nanoparticles prepared with compound **(1)**
AgNP: Silver nanoparticle
AuNP: Gold nanoparticle
ACN: Acetonitrile
ACTG: adenine, cytosine, thymine, guanine
Boc: Tert-butyloxycarbonyl
BSPP: Bis-(p-sulfonatophenyl)phenylphosphine dihydrate dipotassium salt
BTC: Bis(trichloromethyl) carbonate (Triphosgene)
Cbz: Benzyloxycarbonyl
Cy3: Cyanine dye containing 3 methines. 1-{6-[(2,5-Dioxo-1-pyrrolidinyl)oxy]-6-oxohexyl}-2-[(1E,3E)-3-(1-ethyl-3,3-dimethyl-5-sulfonato-1,3-dihydro-2H-indol-2-ylidene)-1-propen-1-yl]-3,3-dimethyl-3H-indolium-5-sulfonate
DABA: Diaminobutirric acid
DCC: Dicyclohexylcarbodiimide
DCM: Dichloromethane
DEAD: Diethylazodicarboxylate
DIEA: Diisopropylethylamine
DLS: Dynamic light scattering
DMEDA: N-N'-dimethylethylenediamine
DMF: Dimethylformamide
DMSO: Dimethylsulphoxide
DNA: Deoxyribonucleic acid
dsDNA: Double-stranded DNA
Dp: Di-methylaminopropylamine
EDTA: Ethylenediaminotetracetic acid
EI: Electronic impact
ESI: Electrospray ionisation
HPLC: High Performance Liquid Chromatography
Fmoc: Fluorenylmethyloxycarbonyl
Fcc: Face centered cubic
FWHM: Full witdth at half maximum
GABA: Gammaaminobutirric acid
HATU: 2-(1H-7-Azabenzotriazol-1-yl)- 1,1,3,3-tetramethyl uronium hexafluorophosphate
HOAt/HOBt: Hydroxyazabenzotriazole/Hydroxybenzotriazole
LAH: Lithium Aluminium Hydride
IR: Infrared
mL: Milliliter
Mp: Melting point
MS: Mass spectroscopy
NHS: N-hydroxy succinimide

NMP:	N-methylpyrrolidone
NMR:	Nuclear magnetic resonance
Nm:	Nanometer
PA:	Polyamide
PAM:	Oxymethylphenylacetamidomethyl resin
PCR:	Polymerase chain reaction
Py-Im PA:	Pyrrole imidazole polyamide
PB:	Phosphate buffer
PVA:	Polyvinyl alcohol
PVP:	Polyvinyl pyrrolidone
RNA:	Ribonucleic acid
r.t.:	Room temperature
TLC:	Thin layer chromatography
T:	Time
TBE:	Tris/Borate/EDTA buffer
TPW:	TFA/Phenol/Water
tRNA:	Transfer RNA
SAB:	Sulphonamidobutirryl
SAED:	Selected area electron diffraction
SPS:	Solid phase synthesis
ssDNA:	Single-stranded DNA
TEA:	Triethylamine
TEM:	Transmission electron microscopy
TEMED:	Tetramethylethylenediamine
HR-TEM:	High resolution TEM
TFA:	Trifluoroacetic acid
TOF:	Time of flight
UV-Vis:	Ultraviolet-visible

CHAPTER 1: INTRODUCTION

1.1 Nanotechnology

Nanotechnology today intersects many scientific fields such as chemistry, engineering, biology, physics and computing. It deals with structures and molecules in the range between 1 nm and 100 nm and is seeking to control the size, spatial location and properties of functional materials in this size regime. Achieving such control on the nanoscale would enable the creation of molecules, assemblies and devices that could exhibit unique chemical, physical and biological properties compared to materials made by existing methods.

1.1.1 What is nanotechnology and why it is important

Nanotechnology deals with structures at the nanometre scale. A requirement for the definition of being "nanotechnological" is that the structure should be man-made. Otherwise most of molecular biology should be included in the category. Moreover, size limitations (1-100 nm), while being useful to quickly tag novel structures and compounds, can build artificial boundaries that could limit the research. In this vision, a definition of nanotechnology should be unconstrained by size limitations. Raj Bawa offers an unconstrained and general definition:

"The design, characterization, production, and application of structures, devices, and systems by controlled manipulation of size and shape at the nanometer scale (atomic, molecular and macromolecular scale) that produces structures, devices and systems with at least one novel/superior characteristic or property"[1]

This definition of nanotechnology shows its importance in the future by focusing on the manufacturing process. Creating smaller electronics components and better

performance materials is a trend started 60 years ago, and nanotechnology is going to be a vital part of most companies and industries in the future.

1.1.2 Approaches to nanotechnology

There are two basic nanotechnological methodologies: the "bottom-up" approach and the "top-down" approach (Figure 1). The latter technique is based on using a large scale pattern or mechanism to produce the smaller scale features.

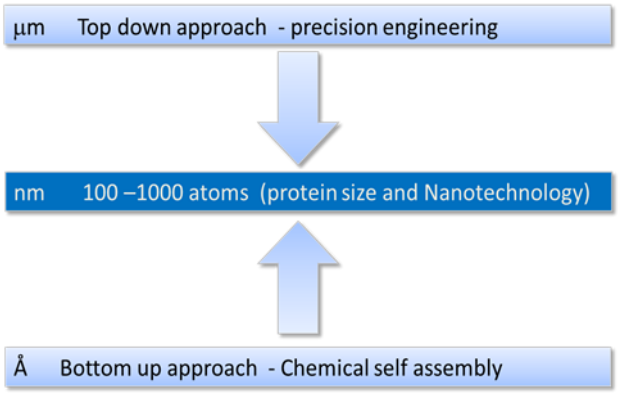

Figure 1: The two possible approaches to nanometre sized structures: "top-down" systems are the current approach for modern mass production techniques of micro and submicro sized devices; in "bottom-up" constructions many molecules self-assemble in parallel steps, as a function of their molecular recognition properties.

1.1.2.1 Top-down approaches to nanotechnology

An example of "top-down" is dip-pen lithography, where the tip of an atomic force microscope is used to "draw" the desired pattern by releasing and depositing in position molecules that can range from small thiols to complex proteins.[2,3] Another "top-down" technique is photolithography, currently used to mass produce most of the silicon-copper chips for computers around the world. A beam of light passes through a several meters wide mask then is focused onto a silicon

wafer covered with a photo-removable polymer. To reduce the size of the components on the wafer the industry is moving versus high energy photons, like UV (current technology) or x-rays.[4] X-rays have the disadvantage of being extremely hard to bend and focus and that the energy of the beam is already in the order of core shell electrons, causing the beam to degrade the surface before the etching can be completed. Electron beams have also been reported.[5]

1.1.2.2 Bottom-up approaches to Nanotechnology

"Bottom-up" nanotechnology uses the principles of molecular recognition. It permits the assembly of smaller structures that cannot be reached by the other methods with much higher feature densities. The modular nature of this approach permits the construction of nanocomponents followed by assembly into arrays or circuits. The bottom-up approach will enable material scientist to build 3D structures that cannot be accessed by lithographic methods. DNA nanotechnology is a subfield of the bottom-up approach, where the key player is DNA and its properties (see paragraph 1.3).

1.2 Nanomaterials

Nanoscaled materials are ubiquitous in nature. Bone in skeletons, seashells, clusters in micrometeorites and space dust are all formed by nanomaterials. Human-made nanomaterials can be classified by their dimensionality: zero dimensional (nanoparticles, quantum dots and fullerenes), one dimensional (nanofibers and carbon nanotubes), 2D (graphene) and 3D nanomaterials (zeolites).

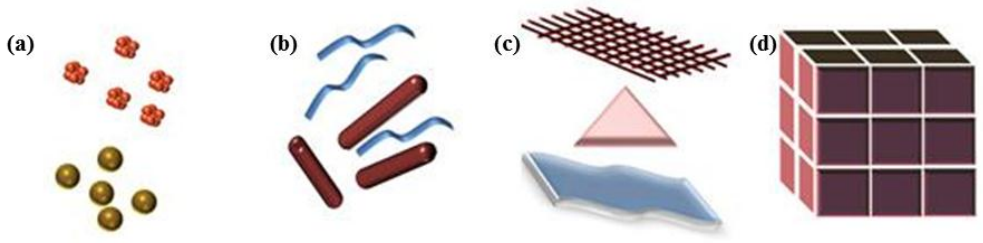

Figure 2: Examples of nanomaterials: A. 0D spheres and clusters. B. 1D nanofibers, wires, and rods. C. 2D films, plates, and networks. D. 3D nanomaterials (image reproduced from Ref.[6])

1.2.1 Nanoparticles

Nanoparticles are of great scientific interest as they are effectively a bridge between bulk materials and atomic or molecular structures.

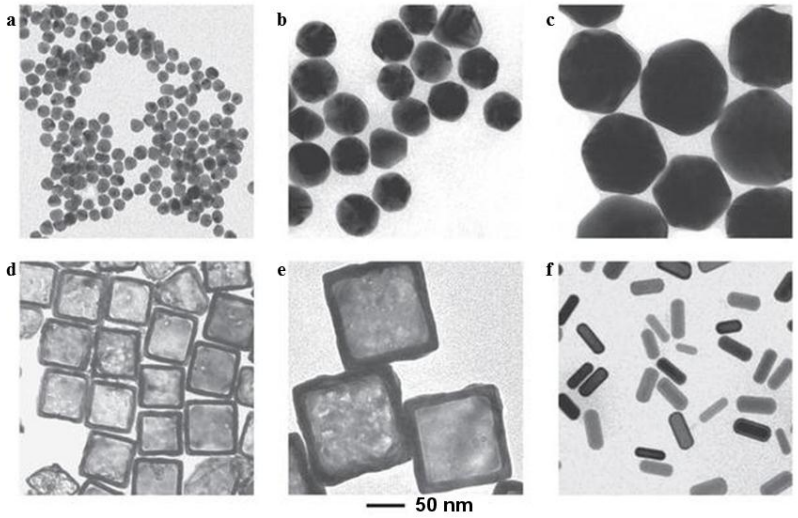

Figure 3: TEM images showing the six types of gold nanoparticles: 15 nm (diameter) nanospheres A, 54 nm nanospheres B, 100 nm nanospheres C, 62 nm (outer edge length) nanocages D, 118 nm nanocages E, nanorods F (16 nm × 40 nm, diameter by length). The 50 nm scale bar applies to all images. (image referenced from Ref.[7])

A bulk material has constant physical properties regardless of its size, but at the nano-scale this is often not the case.

1.2.1.1 Semiconducting nanoparticles

Size-dependent properties are observed such as quantum confinement in semiconductor particles. Quantum confinement is an effect that results when electrons or electron holes are confined into a dimension that approaches a critical quantum measurement, called the exciton Bohr radius. In current applications, a quantum dot confines in all three dimensions such as a small sphere, a quantum wire confines in two dimensions, and a quantum well confines in one dimension. Because quantization of the electronic energy levels occurs, this enabled material scientist to change the energy bandgap of the material by changing the size of the nanoparticles.

1.2.1.2 Metallic nanoparticles and their properties

Surface plasmons, also known as surface plasmon-polaritons, are surface electromagnetic waves that propagate in a direction parallel to the metal/dielectric (or metal/vacuum) interface[8] (Figure 4). Since the wave is on the boundary of the metal and the external medium (air or water for example), these oscillations are very sensitive to any change of this boundary, such as the adsorption of molecules to the metal surface. Only a tangential plane polarized light can generate a plasmon resonance, usually this is done by illumination of evanescent waves of a totally reflected beam of visible or infrared light (Figure 4). Typical distances of the metal surface where the plasmon is generated should be less than one third of the wavelength used.[9] Plasmonic circuits offer the potential to carry optical signals and electric currents through the same metal circuitry, thereby creating the

ability to combine the superior technical advantages of photonics and electronics on the same chip.

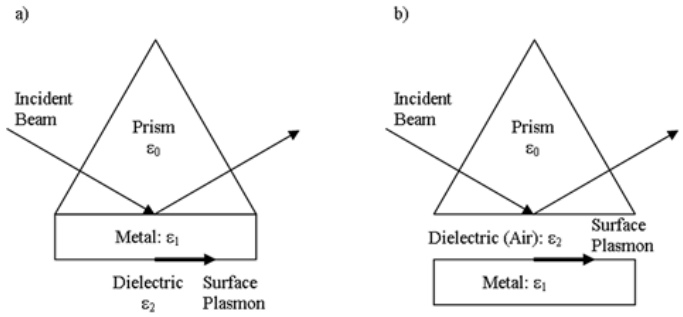

Figure 4: A. Kretschmann and B. Otto configuration of an Attenuated Total Reflection setup for coupling surface plasmons. In both cases, the surface plasmon propagates along the metal/dielectric interface

Metallic nanoparticles are subjected to intense research in the field of catalysis.[10] At the decrease of the size of the nanoparticles, an increase in the catalytic activity of the material is observed due to the enormous increase of the surface area. Gold nanoparticles of 2 nm or less have also shown the appearance of novel properties such as increased catalytic activity and selectivity[11] and magnetic properties such as superparamagnetism.[12] Recently, the shape of the nanoparticles has been recognized as an important factor to predict catalytic, optic and magnetic properties. Nanoparticles with approximately equal hydrodynamic diameter can have greatly different surface areas as shown in Table 1. As an example, cubic nanoparticles have approximately double the surface area of a spherical nanoparticle of the same hydrodynamic diameter. Shape-dependent catalytic activity has been observed for platinum nanoparticles.[13]

Polyhedron	Surface Area Formula by radius r of a unitary sphere	Surface Area r=1 (nm^2)	3D representation
sphere	$4\pi r^2$	12.57	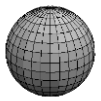
cube	$24r^2$	24	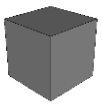
cylinder	$6\pi r^2$	18.85	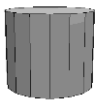
cone	$(1+\sqrt{5})\pi r^2$	10.17	
conical bi-pyramid	$(2+2\sqrt{2})\pi r^2$	15.17	
icosahedron (inscribed in the sphere vertexes touching the sphere)	$\frac{80\sqrt{3}}{10+2\sqrt{5}}r^2$	9.57	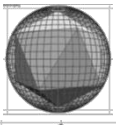
icosahedron (mid-radius, sphere touches the middle of each edge)	$\frac{40\sqrt{3}}{3+\sqrt{5}}r^2$	13.23	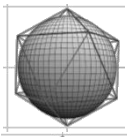
icosahedron (sphere inscribed tangent to icosahedral faces)	$\frac{20\sqrt{3}}{7+3\sqrt{5}}r^2$	15.16	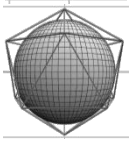
hexagonal prism (by circumcircle radius)	$6\left(\sqrt{\frac{21}{4}}+\sqrt{3}\right)r^2$	24.14	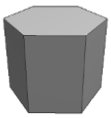

Table 1: Calculation of surface areas of polyhedral particles circumscribed or inscribed in a unitary sphere or with unitary edge length. The formulas calculate the surface area of the polyhedron from the radius (22) of the unitary sphere.

1.2.2 Bridging top-down with bottom-up approaches

Current top-down techniques allow the bulk production of nanodevices but lack in precision.[14] Moreover, they are restricted by size limitations; X-ray lithography for example, one of the most widely used top-down techniques, has a limitation of

~100nm as the minimum size.[15] Bottom-up approaches on the other hand, can handle very small sizes of 1-50 nm, are extremely precise and are cost efficient, and by spontaneous self-assembly large but defined structures can be created.[16] Their limitations however arise from their constrained dependence on molecular weight,[16] as large supramolecular molecules are highly time consuming to prepare. It is evident that a hybrid method utilising both approaches would be greatly beneficial in efficiency and precision, combining both the precision of bottom-up approaches to the large scale patterning of top-down techniques. In the middle between these two techniques lays DNA nanotechnology, a field that has the potential to combine the two previously discussed approaches.[17]

1.3 DNA

In the last 50-60 years, DNA research has been almost exclusively the province of biologists and biologically-oriented physical scientists, who have studied its biological impact and molecular properties. Recently, material scientists, nanotechnologists and computer engineers have begun to realize the potential of DNA as a nanomaterial and are now beginning to exploit DNA's chemical properties in a non-biological context.[18] From a material science perspective, DNA is an excellent construct for its use in nanotechnology.

DNA consists of two long polymers of simple units called nucleotides, with backbones made of sugars and phosphate groups joined by ester bonds. These two strands run in opposite (anti-parallel) directions to each other. Attached to each sugar is one of four types of molecules called bases. It is the sequence of these

four bases along the backbone that encodes the genetic information within a cell of a living organism.

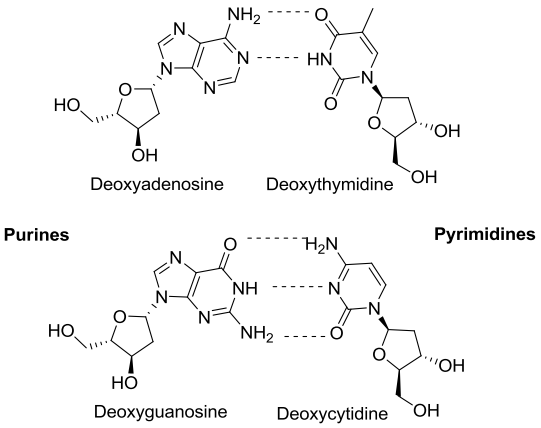

Figure 5: Structure of the four bases of DNA: deoxyadenosine, deoxythymidine, deoxyguanosine and deoxycytidine. Dashed lines represent Watson-Crick hydrogen bonding interactions.

This information is read by a myriad of transcriptional proteins using the hydrogen bond landscape as a read of the nucleotide sequence. DNA can assume in solution three main conformations named A, B and Z. Inside living organisms only conformations B and Z have been observed for pure DNA, while A form has been observed for DNA-RNA hybrids.

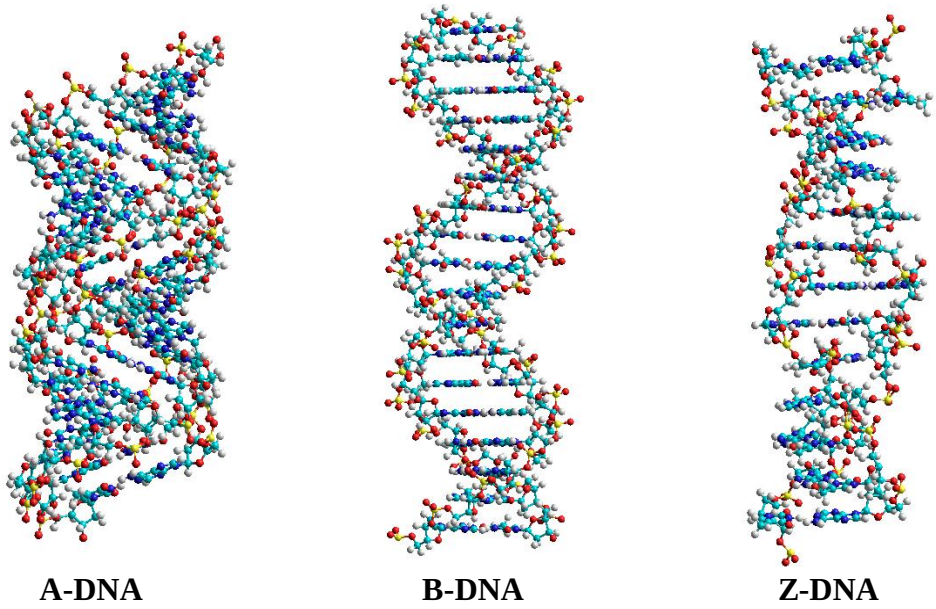

Figure 6: Ball and stick representation of A-DNA, B-DNA and Z-DNA.

Depending on chemical modifications such as methylation and other physical properties such as hydration level, one conformation can be more stable than others.[19] The underlying basis of DNA being such a good construct for nanotechnology is due to its structure. The most common B-DNA has a consistent width of 2.0 nm when in the double helical form with a distance between the bases of 0.34 nm along axis. Each turn consist of 10.5 bases (3.32 nm).[20] A-DNA has a more compact structure but with a larger width of 2.3 nm. The distance between the bases is of 0.24 nm along axis and each turn consist of 11 bases (2.46 nm).[21] In contrast with A- and B-DNA, Z-DNA is a left-handed helix. Z-DNA is a shallower and longer along the axis with a diameter of 1.8 nm. The distance between the bases is of 0.37 nm along axis and each turn consist of 12 bases (4.56 nm).[19] The spaces between the strands of the double helix are called grooves. B-DNA shows the presence of 2 distinct groove regions called major groove, which

is 2.2 nm wide, and minor groove, which is 1.2 nm wide.[22] These regions are important as they allow direct access to the hydrogen bonding landscape of the base pairs. Virtually all DNA sequence specific binders have interactions in these regions. The total length of DNA can be easily varied using either chemical (solid phase synthesis) or enzymatic (PCR) techniques, resulting in a highly modular construction material. Another attribute of the use of DNA as a nanomaterial is the predictability of its secondary structure. Computer programs have the ability to predict the type of secondary structures that DNA will adopt purely by knowing the primary nucleotide sequence; a feat that is very difficult to do for proteins.[23] In addition, computational methods can predict and generate DNA sequences that form non-natural secondary structures, leading to a greater variety of supramolecular architectures, both in 2D and in 3D. Moreover, biologists have already developed a large number of enzymes for processing DNA strands, thereby allowing the material scientist to manipulate the length of the DNA, cut out and troubleshoot errors in the synthetic process, resulting in an invaluable set of tools to modify the DNA architecture for nanotechnological applications.[24] Finally, DNA is readily available, thereby making it a useful and versatile material to use in nanotechnology.

1.3.1 DNA self-assembly properties

The assembly of small molecules in more sophisticated architectures reproducibly is considered one of the major goals in material science. It is also a feat that nature conducts regularly and with exquisite specificity. Duplex DNA is the pre-eminent example of a naturally-occurring intermolecular self-assembly process, where two

strands of polynucleotides self-assemble into stable helical structures based on the genetic code. This code depends uniquely on base pairing. Each type of base on one strand forms a hydrogen bond with one type of base on the other strand. This is called complementary base pairing. Here, purines form hydrogen bonds to pyrimidines, with A bonding more selectively with T, and C bonding only to G. This arrangement of two nucleotides binding together across the double helix is called a base pair. The two types of base pairs form different numbers of hydrogen bonds, A•T forming two hydrogen bonds, and G•C forming three hydrogen bonds.[a] Hydrogen bonds are considerably weaker than covalent bonds (typical hydrogen bonds have energies of 5-30 kJ/mol while weak covalent bonds have 155+ kJ/mol[25]), they can be broken and re-joined relatively easily. Therefore, the two strands of DNA in a double helix can be pulled apart like a zipper, either by a mechanical force or high temperature.[b]

Duplex DNA is a classic example of intermolecular self-assembly, yet naturally-occurring nucleic acids can also form a variety of alternative structures which rely on intramolecular recognition events, resulting in elaborate secondary and tertiary structures in DNA [e.g. quadruplex[26]], RNA [riboswitches[27], t-RNA structures[28]] and RNA-protein complexes [e.g. ribosome and the spliceosome[29]]. DNA can also self-assemble intermolecularly via sticky-ends.[30] A sticky end is a short single-stranded overhang protruding from the end of a double-stranded helical DNA

[a] Other pairing modes exist such as the Hoogsteen pairing.

[b] BIRD (blackbody infrared radiative dissociation) gas phase measurements give 115-160 KJ/mol for the Arrhenius activation energy of the dissociation of a 7-mer dsDNA at 300 K, solution phase dissociation enthalpies give similar results.[306] As a comparison, the E_a of the decomposition of N_2O_4 -> $2NO_2$ (an exothermic reaction with low potential barrier) is 161 KJ/mol, on the contrary a reaction with a high potential barrier is H_2O -> $H_2 + ½O_2$ with E_a=565 KJ/mol

molecule (Figure 7). Two molecules with complementary sticky ends have complementary arrangements of the nucleotide bases adenine, cytosine, guanine and thymine and will cohere to form a molecular complex. Sticky-ended cohesion is arguably the best example of programmable molecular recognition: there is significant diversity to possible sticky ends (4^N for N-base sticky ends), and the product formed at the site of this cohesion is the classic DNA double helix. Therefore, sticky ends offer both predictable control of intermolecular associations and predictable geometry at the point of cohesion.[31]

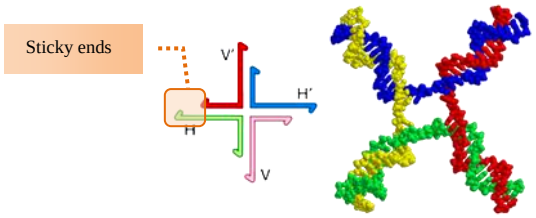

Figure 7: A special Holliday junction with sticky ends: each DNA strand ends with a single stranded part. V is complementary with V' and H is complementary with H', this enables the Holliday junction to form large self-assembling networks.[c]

1.3.1.1 Predictable self-assembling of DNA and DNA origami

The predictability of the self-assembling of DNA can be computer-computed. This has led many research groups to develop stable DNA nanostructures. Seeman constructed DNA cubes using specially prepared Holliday junctions, and folded the cube building each face separately to prevent polymerization of the material.[32] However the synthesis of a single cube is a complicated and low yielding process and the length of the sides of the cube make the nanostructure weak and deformable. Turberfield worked on another platonic solid: the tetrahedron.[33] The

[c] Image modified and reproduced from Ref.[30,31]

Turberfield tetrahedron self assembles from only 4 DNA strands, making the synthesis extremely quick and easy. A number of DNA tetrahedrons were constructed by simply adding together the four strands (the sequence of which were calculated computationally). The resultant tetrahedra can be visualized using AFM for structural rigidity and stability. The Turberfield group exploited the strength of the tetrahedral structure by preparing a variety of pyramidal structures of varying shapes and sizes. DNA tetrahedra are particularly attractive candidates for the encapsulation of other molecules: containers on all scales down to the molecular level have been used to protect and target the delivery of drugs.[34] Turberfield demonstrated the possibility of using his tetrahedron as containers by encapsulating a cytochrome C.[35] Aldaye showed how many other polyhedra can be prepared with the same technique, such as dodecahedrons and icosahedrons.[36,37] A further step in complexity is DNA origami. Developed by Rothemund, the process involves a long viral DNA strand "folded" using short matching staple-strands of complementary DNA. The resulting 2D-sheets of folded DNA have boundaries resulting in various shapes, such as a smiley face.[38] In an additional complexity step, if the staples are made longer or shorter than needed to fold the viral DNA, a curvature of the sheet can be induced. Computational analysis of this curvature lead to the creation of 3D DNA origami by stacking and stapling together multiple curved 2D DNA origami.[39]

1.3.2 Molecular recognition processes involved in DNA

Sequence specific recognition of DNA architectures is an extensively studied area with a variety of naturally-occurring and synthetic molecules known. The typical

binding modalities for DNA recognition are electrostatic binding, intercalation, major groove recognition and minor groove recognition.

1.3.2.1 Electrostatic interactions

Small molecules or ions that bind externally are usually non-specific both with respect to nucleotide sequence and location, their distribution being mainly directed by electrostatic interactions with the negatively charged phosphates of the DNA backbone. Ions like Na^+, K^+ and Li^+ all bind in this non-specific way, but with soft transition metal ions like Ag^+ and Hg^{2+} there are some examples that they can bind specifically to the actual nucleobase.[40,41] Polyamines are small molecules that are known to bind externally to DNA.[42] External binding, being electrostatic in nature and generally requiring insignificant changes of DNA structure, is characterized by fast binding kinetics approaching the diffusion limit ($k_a = 10^8 – 10^9\ M^{-1}s^{-1}$).

1.3.2.2 Intercalators

Intercalators associate with DNA by inserting themselves between adjacent base pairs, by doing so they cause elongation of DNA by about the height of one DNA base (3.4Å) and the corresponding local unwinding of the double helix.

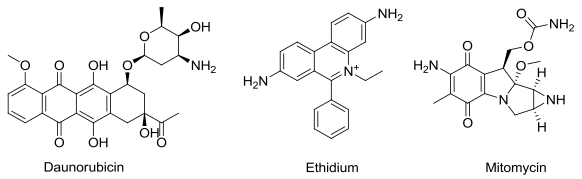

Figure 8: Structures of 3 known intercalators: Daunorubicin, Ethidium and Mitomycin.

These local distortions are much more pronounced than the ones occurring with groove binders and can extend over several base pairs surrounding the actual site of intercalation. In addition to an attractive electrostatic contribution to the free energy binding which is normally cationic, classical intercalators like ethidium bromide[43] (Figure 8), a substantial part of their binding energy derives from hydrophobic interactions with the surrounding base pairs (π-stacking). As a consequence, intercalative binding modes have a lower probability of being sequence specific.

1.3.2.3 Recognition of DNA duplexes: major and minor groove interactions

Groove binding agents associate with DNA in either the major or the minor groove. The majority of DNA-binding proteins penetrate into the major groove (2.2 nm): for example helix-turn-helix, Zn-fingers and leucine zippers are widespread protein motifs that bind the DNA in a sequence specific way (Figure 9).[44]

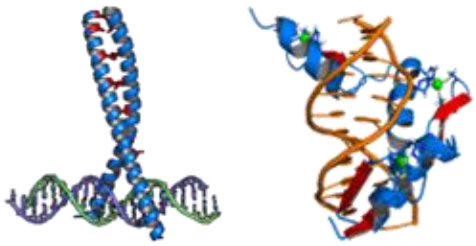

Figure 9: A leucine zipper on the left and a Zn-finger on the right are two examples of DNA major groove binders.

Most of the smaller molecules bind into the relatively narrow and deep minor groove (1.2 nm), which affords only a limited number of potential hydrogen bond interactions compared to its major counterpart. Binding in the minor groove may

in some cases be sequence selective mainly as a result of hydrogen bonding, but also Wan der Waals, hydrophobic contacts and electrostatic interaction can have a substantial contribute. Examples of small minor groove binders include DAPI,[45] Hoechst 33258,[46] distamycin and netropsin[47] (Figure 10), all of them preferentially bind to AT-rich regions of DNA. All the groove binders normally display binding kinetics that, like external binding, approaches the diffusion limit (k_a= ~10^8 $M^{-1}s^{-1}$) while their rate of dissociation can vary considerably (k_d= 10^{-1} – 10^3 s^{-1}).

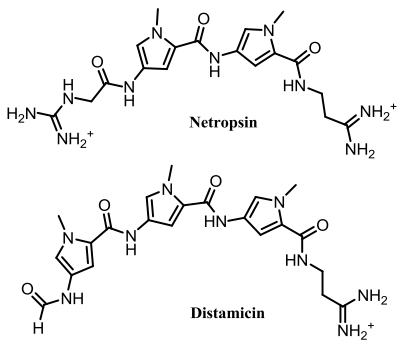

Figure 10: Structure of netropsin and distamycin, two minor groove binders of DNA

1.4 Challenges for molecular nanotechnology

The development of structural DNA nanotechnology (SDN) can provide a framework for the development of advanced nanosystems. Besides the required need of computational tools for SDN, the major challenges that nanotechnologists have to face are:

1) Stability of surfaces: the construction of "machine nanoparts" such as gears and cogs has been achieved with microfabrication techniques.[48] At this point of research it is not clear how stable these structures are. Due to the high surface they

present, they are consequently highly reactive. The same reasoning can be done for nanoclusters. For example, gold and silver nanoparticles have been shown to change shape and "shed", forming smaller nanoparticles.[49,50]

2) Brownian motion tolerance: at the nanoscale, structures are constantly in motion due to thermal noise. The engineering of complex nanomechanisms has to work against the constant wobbling of the Brownian motion.[51]

3) Friction and energy dissipation: for nanoconstructions with moving parts the relative amount of interfacial area increases at the decrease of the size of the nanoparts. Moreover, relatively weak surface forces (van der Waals) become important at the nanoscale. As smaller devices operate at higher power densities, even low levels of friction can generate high levels of local heating and damage the nanodevices.[52]

1.5 Global aim and objectives

The objective of this studentship is to develop a molecular toolkit which will enable the placement and growth of metallic nanoparticles along DNA architectures using DNA binding molecules. I will prepare DNA binding molecules with molecular functionalities that will bridge the hard-soft interface.

Aim: To develop a toolbox of synthetic methods that enables the use of minor groove polyamides to template functional materials along DNA architectures.

The aim of my project is to develop methods to template functional materials (eg. Nanoparticles, fluorophores) using molecular recognition processes over any DNA programmed nanostructure with 1D, 2D or 3D spatial distribution. This is important because the system that we are trying to develop is modular and it can

potentially template materials with greater precision than current methods. By exploiting the DNA recognition properties of polyamides I will link DNA to functional materials using a combination of solid phase synthesis and bio-conjugation strategies. Wide gaps still exist in DNA functionalization (such as reliable sequence specific functionalisations), and my project will provide a toolbox of methods for the material chemist to attach any arbitrary functional material on DNA taking advantage of the genetic code of the DNA itself to place these materials on the strands.

CHAPTER 2: DEVELOPING A NEW TEMPLATED APPROACH TO THE PREPARATION OF SILVER NANOPARTICLES

2.1 Introduction

Noble metal nanoparticles have unique catalytic, electric, magnetic, optical and mechanical properties[53–55] that are different from bulk materials such as quantum confinement and surface plasmon resonances as discussed in Chapter 1.2.

By virtue of their high fluorescence quantum yield and enhanced surface plasmon properties silver nanoparticles (AgNP) are excellent materials for applications in diagnostic systems,[56] biomedical delivery[57] and in catalysis.[58] It is well known that the catalytic reactivity of metal nanoparticles critically depends on both the size and shape of metal nanostructures. A key unmet challenge in the field is the development of facile and cost-effective methods which control both the size as well as the shape of AgNPs.[59] This is crucial to the field of nanoscience as both of these parameters have a direct bearing on their properties.

2.1.1 Current methods of preparation of AgNPs

AgNPs have traditionally been prepared using two types of methods: solution phase methods and physical methods. The latter includes sonochemical methods,[60–62] laser ablation,[63] electron beam irradiation,[64] exploding wire technique,[65] high temperature mixed alloy,[66] photochemical[67] or more traditional electrochemical methods.[68] These methods produce AgNPs of varying degrees of monodispersity and shape control. Currently there is no general method which produces AgNPs with a high degree of control over both of these parameters. For example, high energy methods like laser or electron beam ablation can produce consistently small nanoparticles of 1 nm or less, however with very high polydispersity. Photochemical and sonochemical methods with extended

irradiation times can produce highly monodisperse particles of large diameter (50-100 nm), which have limited use as biosensors due to their low fluorescence. An additional problem is that current physical methods are not easily amenable to scale-up, thus preventing wider utility in industry.

2.1.1.1 Preparation of AgNP using wet chemistry methods

Current protocols for the synthesis of AgNPs using wet chemistry methods focus on the production of small particles of 10 nm or less.[69] AgNPs prepared by these methods such as citrate reduction[70] are difficult to produce with the required monodispersity and biological stability for bionanotechnological applications and often, these silver particles are gold coated to provide additional stability.[71] Therefore, methods which can produce size and shape-controlled AgNPs that are both cost-effective and facile would be of high value for bionanotechnology.

Wet chemistry methods can be divided in various overlapping categories according to the choice of reducing agent, surfactants and stabilization/gelling agents (where present).[72]

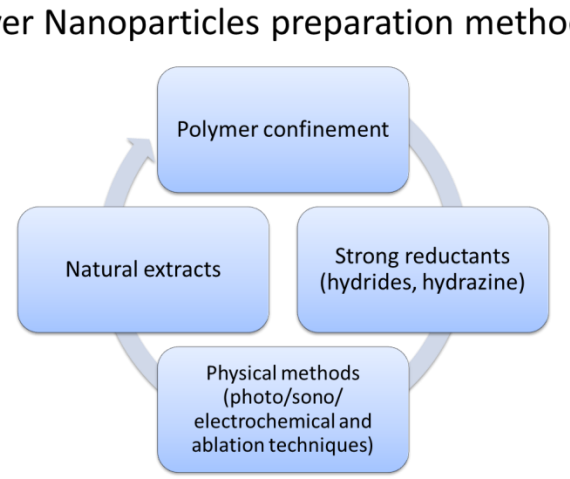

Figure 11: Silver nanoparticles preparation methods.

Most of these known preparations unfortunately require multi-step synthetic procedures in order to stabilise the particles, which render the reproducibility of the synthesis challenging.[73] For example, polymers such as polydispersed PVA,[74] PVP,[75] polyvinylacetone and polyacrylates[76] have been used to prepare AgNPs as small as 2 nm. These types of methods however have major disadvantages such as the inability of the particles to be diluted due to being stable only at particular gelling points of the matrices. Additionally, the use of polymers entraps the AgNPs thereby precluding key molecular interactions with their surfaces and preventing the use of these methods for biosensing applications.

The most widespread method of AgNP synthesis is to use strong inorganic reducing agents. These methods are cheap and facile and don't require expensive instruments. Examples are hydrogen reduction,[77] $NaBH_4$,[78,79] citrate,[70] paracetamol,[80] aniline[81] or hydrazine.[82] The main disadvantages of these methods are several. Firstly, size and shape control can be variable. Secondly, further derivatisation of AgNPs is required to render them biocompatible. Thirdly, the methods available for passivating the surface of AgNPs to produce biocompatible versions are not as robust as those developed for gold nanoparticles.[83]

Natural plant extracts such as lemon,[84] basil,[85] *Camellia Sinensis*,[86] geraniol,[87] silk sericin,[88] ginger,[89] *Euphorbia Hirta*[90] and garlic[91] have been used as reducing agents in "green" methods. Natural extracts of these plants contain reducing agents. Exact mechanisms of the reduction are still a matter of debate. Supporters of such methods claim that the AgNPs prepared don't need any

additional surfactant as the components of the natural extracts can passivate the surface of the particles and prevent aggregation. Unfortunately, the dispersity of the nanoparticles produced using these methods is inferior to classical $NaBH_4$ reduction.

2.1.1.2 Mechanisms of AgNP formation

AgNPs formation mechanism starts with the reduction of individual silver ions by action of a reductant (Figure 12).

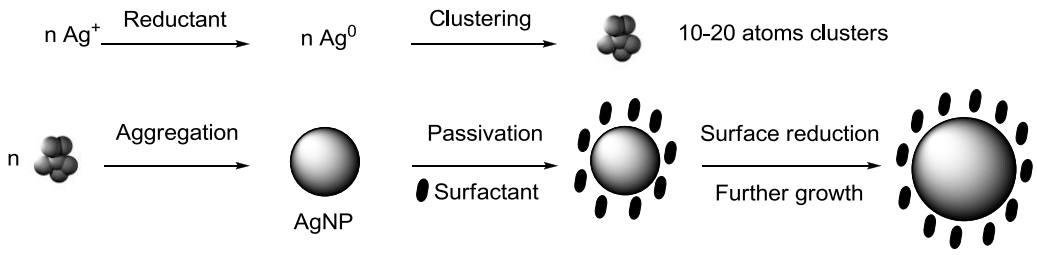

Figure 12: Reactions involved in the formation of small silver atom clusters.

Subsequently the reduced atoms cluster together to form small silver nanoclusters of two or more atoms.[92] The metal clusters can be long lived depending on the surfactants or their inherent stability. AgNPs have the ability to nucleate silver ions on their surface, consequently forming charged nanoparticles. The most known charged silver nanocluster is Ag_4^{2+},[93] which is at the base of silver photography methods[94,95] and it's formed from the simplest possible dimeric silver nanocluster Ag_2^0 over the surface of AgBr crystals (Scheme 1).

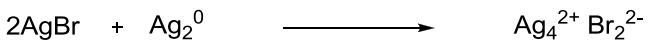

Scheme 1: Reaction scheme showing the formation of Ag_4 clusters

Condensation of these nanoclusters result in the formation of larger particles of 10-20 atoms, with a diameter under 1nm.[70] This clustering seems to be kinetically driven through dimerization processes instead of a thermodynamical pathway over a free energy barrier, as described by classical nucleation theory.[96] The mechanism has also been described as auto-catalytic as shown by Yadong Yin *et al*.[97] At a critical size, the growth of silver nanoparticles stops due to the formation of a strong repelling layer of surfactants and a second mechanism involving the reduction of Ag^{+} ions on the surface of the particles becomes prominent (Figure 13).[98]

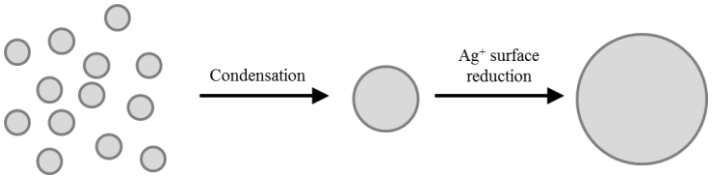

Figure 13: Schematic representation of the reactions involved in the AgNPs growth. Condensation refers to small silver nanoclusters assembling together to form larger AgNPs

2.1.1.3 Desirable properties of AgNPs for biosensing applications

A key property that underpins the potential utility of AgNPs for biosensing applications is their inherent stability to aqueous solutions containing high concentrations of salts. Salts are a known cause of colloid destabilisation, but they are highly necessary to manipulate DNA and other biological macromolecules.

2.1.1.4 Preparation of AgNP using the Tollen's reagent

Ammoniated silver salts (Tollens' reagent) are reducing agents in their own right and have been used to prepare silver nanoparticles, albeit currently with poor monospersity or low stability.[97,99–101] Of the various methods available for AgNP synthesis, the application of the Tollens'-reagent $[Ag(NH_3)_2]^+$ and reducing sugars has been under-utilized in literature despite exhibiting distinct advantages over traditional methods.

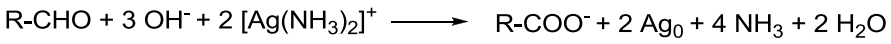

Scheme 2: reaction scheme between a generic aldehyde and the Tollens' reagent

These include:

Mild preparative conditions – AgNP synthesis proceeds at room temperature and involves mild oxidation of an aldehyde functionality present in reducing sugars as a hemiacetal. Derivatisation of the non-anomeric sites on the sugar could provide opportunities to incorporate of pendent functionality that would not withstand the typically harsh reducing environments required for other conventional preparative methods in a single step (Figure 14).

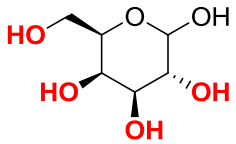

d-galactopyranose

Figure 14: Example of available positions for functionalization of D-galactose sugar (shown in red).

Facile one-pot synthesis – Reducing sugars act both as a Ag^+ reductant as well as a passivating ligand on the AgNP surface.

2.2 Aims of the study

The aim of this study is to develop a one-pot method to form highly size and shape selected AgNPs. The method of production must be mild and able to work in the presence of biological molecules with minimal degradation. DNA, *in primis*, is the bio-molecule that we have chosen as the initial example, as its programmability enables a sequence-selective readout of a molecular event.[17,102]

2.3 Results

2.3.1 Synthesis of reducing sugars

Azide sugars provide an excellent starting point to investigate the potential to tune both the size and shape of AgNPs. Azidosugars are metabolically inert sugars that can be introduced into living organisms to tag specific glycans on cells surfaces by using *click-chemistry* or Staudinger ligation.[103] Click-chemistry is a colloquial name devised by Sharpless for a copper(I)-catalysed Huisgen (3+2) cycloaddition (CuAAC) reaction between an azide and an alkyne.[104] As an example of click-chemistry involving azide sugars, in 2006 Carell and Burley prepared triazole sugars clicked to modified nucleic acids for DNA metallisation.[105] These sugars comprise multiple sugar-reducing moieties, a triazole spacer and an azide linker amenable to further derivatisation using click-chemistry protocols (Figure 15 and Figure 16).[105]

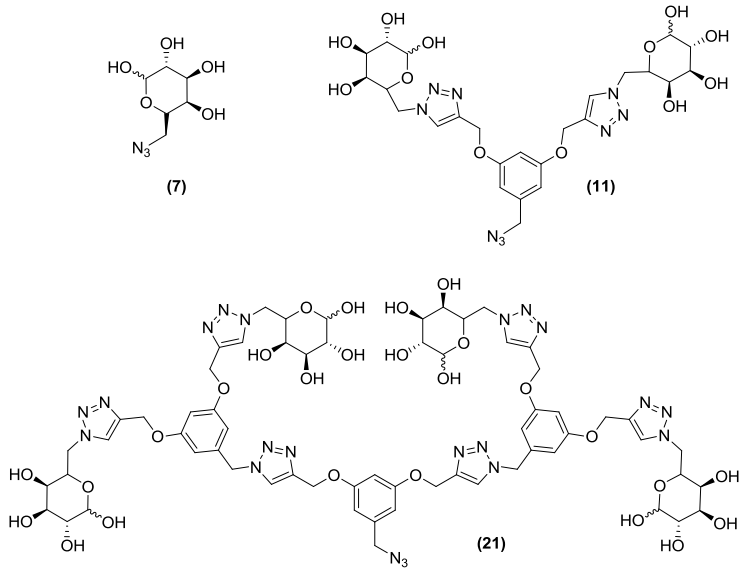

Figure 15: Dendrimeric sugar azides possessing 1,2 or 4 sugar moieties, a dendrimeric core assembled by click-chemistry via a modular design.

The azide linker can be used to form a triazole via a click-chemistry with a terminal alkyne-modified DNA strand to produce sugar-modified DNA. The sugars in this respect provide sites of metallisation using the Tollens' reagent (Figure 16).

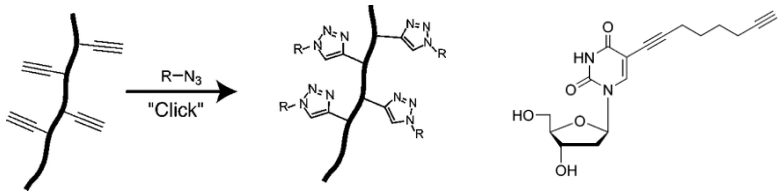

Figure 16: Schematic representation of functionalisation of alkyne-modified oligodeoxyribonucleotides with sugar azides and on the right structure of the alkyne-modified oligodeoxyribonucleotides (Images reproduced from Ref.[106]).

The sugar triazoles which were used in this study were designed with versatility in mind: the modular design allows each moiety of the molecule (linker, dendrimeric

core, sugars) to be changed independently and provide the ability to tune the properties of the silver nanoparticles produced by Tollens' metallisation.

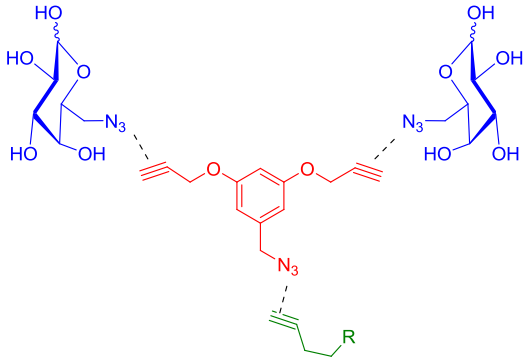

Figure 17: Versatility of dendrimeric sugars. The separate components sugars (blue), dendrimeric core (red) and linker (green) can be assembled efficiently by click-chemistry to create libraries of compounds to tune the properties.

2.3.2 Synthesis of AgNPs using sugar triazoles

In order to investigate the potential of sugar triazoles as a new scaffold to control the formation of AgNPs, we set out to prepare the following exemplars (**29, 30, 38**). Our first scaffold structure comprised a single sugar triazole prepared by copper catalysed (3+2) cycloaddition of azide **(7)** with 3-butyn-ol **(9)** (Scheme 4). The latter was chosen because of its commercial availability and on the basis of the following assumptions:

- 3-butyn-1-ol is a simple water soluble alcohol, and thus it would improve the solubility of the prototype system in water and would not interfere with the AgNP formation and stability.
- 3-butyn-1-ol is cheap, widely available, can be used in high-molar ratio during the click-chemistry reaction to provide complete conversion of the sugars and its excess can be easily removed by vacuum-distillation, HPLC or water-solvent partitioning.

2.3.3 Synthesis of the sugar (1) sugar (2) and sugar (3)

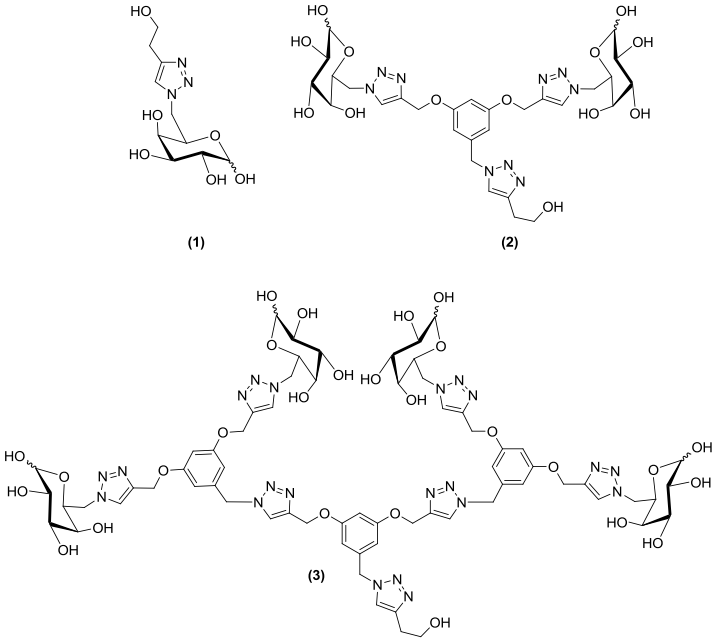

Figure 18: Structure of the sugars (1), (2) and (3).

A number of improvements were made on the previously reported synthesis[105] to deal with gram scale quantities and quicker purifications. Additional steps were executed to prepare the novel 3-butyn-1-ol **(9)** clicked sugars.

2.3.3.1 Synthesis of galactose-triazole: sugar1 (1)

Galactose azide **(7)** was prepared by the modification of a known method as outlined by Kong *et al* (Scheme 3).[107,108]

The synthesis involved an initial Mitsunobu reaction (not shown) between sugar **(4)** and sodium azide **(20)**, triphenylphosphine and imidazole, followed by DEAD; however the installation of the azide moiety proceeded in modest yield. Reverse addition to prepare the betaine[109] **(5a)** didn't improve the yield of the reaction, so a more robust and quicker two-step approach was devised as shown in Scheme 3.

Galactose **(4)** was first reacted with mesyl chloride **(38)** in DCM for 2 hours at 0°C and the resultant solution purified by precipitation in hexane and filtration to afford **(5)** in 99% yield. Subsequently, reaction of **(5)** with sodium azide at 120ºC in DMF resulted in complete conversion to azide **(6)** in 2 hours. Purification by column chromatography (hexane:ethyl acetate 90:10) gave pure galactose azide **(6)** as a clear oil in 99% yield. Acid deprotection of the isopropylidene groups with TFA at room temperature, followed by concentration *in vacuo*, afforded pure deprotected galactose azide **(7)** as a white powder in 94% yield.

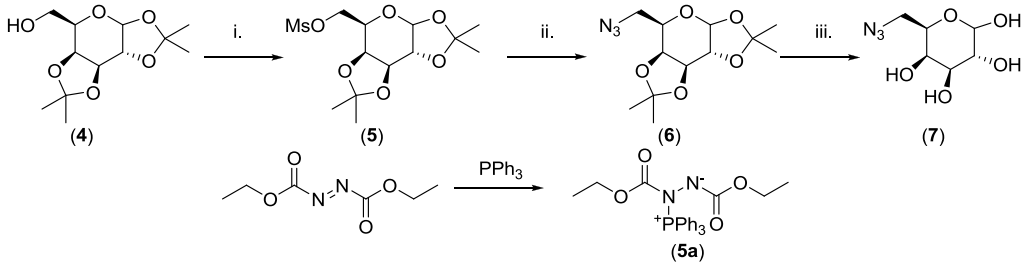

Scheme 3: Synthesis of compound (7) and structure of DEAD-PPh3 betaine (5a). i. MsCl, DCM, DIEA, 0°C ii. NaN_3, DMF, 120°C iii TFA, H_2O, 50°C

Sugar **(8)** was obtained by reaction of galactose azide **(6)** with 3-butyn-1-ol **(9)** in the presence of the solid click-chemistry catalyst PS-NHC-Cu(I) in DMSO;[110] the reaction was monitored by TLC until the reaction was complete (18 hours), then quenched by dilution with ethyl acetate followed by filtration to afford the triazole galactose **(8)** in 67% yield.[d] Deprotection of the triazole galactose **(8)** using TFA:H_2O at 80°C (8 hours), afforded pure deprotected galactose triazole **(1)** in quantitative yield.

[d] Synthesis of the click-chemistry catalyst[110] exploited Merrifield resin instead of activated SiO_2-Cl. Final resin loading was assumed to be the same as the loading of the resin; details of the synthesis are described in the Appendix.

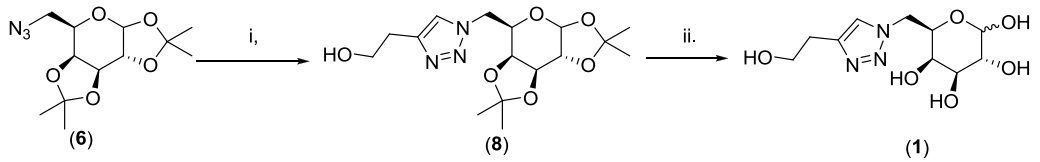

Scheme 4: Synthesis of sugar probe (1). i. (9), PS-NHC-Cu(I), 18h, 67% (42), DMSO ii. TFA, H_2O, 80°C, 8h, 99%

2.3.3.2 Synthesis of sugar2 (2)

The central resorcinol core **(11)** was chosen as the key scaffold for connecting the sugar residues **(7)**. This scaffold provides an excellent centre core to investigate factors which control size and shape in AgNP synthesis.[105] The synthetic scheme for the preparation of the core is highlighted in Scheme 5.

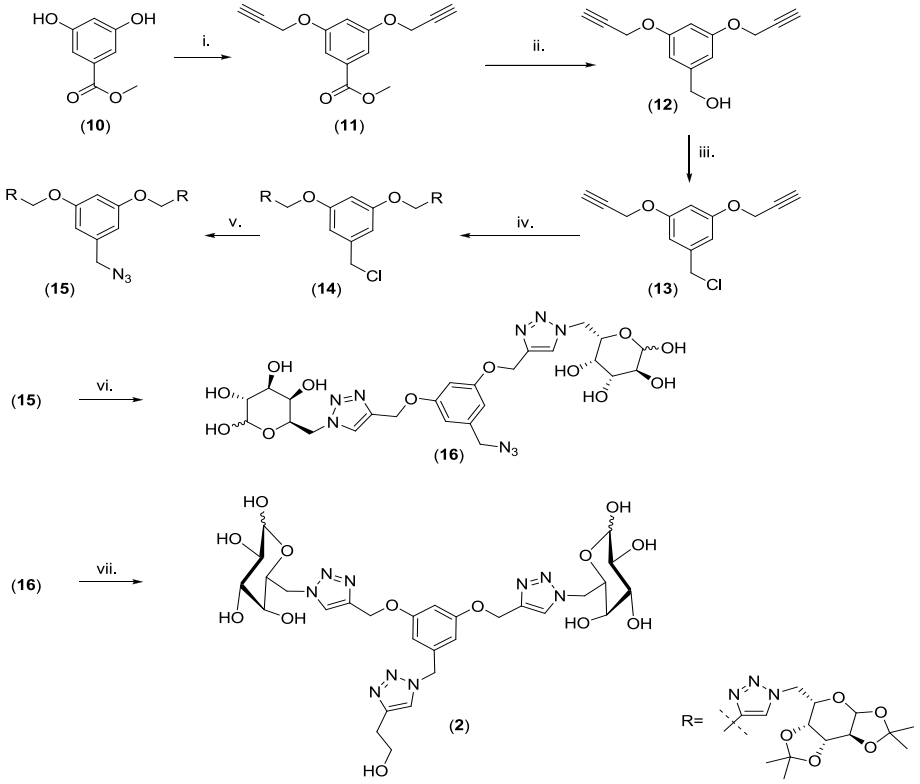

Scheme 5: Synthesis of sugar (2). i. Propargyl bromide (17), K_2CO_3, reflux, 24h, 70% ii. LAH, 74% iii. $SOCl_2$, 39% iv. Di-acetonide-6-azidogalactopyranose (6), $CuSO_4$-ascorbate, 21% v. NaN_3, 60% vi. TFA, 59% vii. (9), PS-NHC-Cu(I)[110], 92%.

The synthesis commenced with methyl-3,5-dihydroxybenzoate **(10)** heated to reflux in the presence of propargyl bromide **(17)** for 24h to obtain methyl 3,5-bis(prop-2-ynyloxy)benzoate **(11)** in 70% yield (reported 84% yield with dry acetone)[111]. Methyl 3,5-bis(prop-2-ynyloxy)benzoate **(11)** was then reduced using lithium aluminium hydride in THF to afford **(12)** as a white powder in 74% yield after recrystallisation (86% yield was obtained from a chromatographic column). Compound **(12)** was then reacted with thionyl chloride in DCM:pyridine in an attempt to form benzyl chloride **(13)**. This reaction proved to be highly sensitive to both moisture and to the thionyl chloride used. Reported conditions (room temperature for 24h)[111] resulted in modest yield, however heating the reaction mixture to reflux for 2 hours afforded crude **(13)** with a better conversion ratio. After work-up **(13)** was purified by simple filtration over a short Si-60 column using hexanes:ethyl acetate to afford a pale cream-coloured solid in 39% yield. Compound **(13)** was unstable to both moisture and light, and was found to darken in the fridge in less than a week. Recrystallization from MeOH afforded highly pure **(13)** as a white solid. An unknown impurity was identified by TLC. This formed a molecular ion corresponding to *m/z* 238 by EI-MS, however this impurity, when reacted in the following steps gave the desired product **(15)**. Compound **(13)** was reacted with galactose-azide **(6)** using copper sulphate in the presence of sodium ascorbate to obtain a di-galactoside-benzyl chloride **(14)** in 21% yield after purification by column chromatography. Compound **(14)** was heated to reflux in the presence of sodium azide for 3h in water:acetone to obtain

the di-galactoside-azide **(15)** in 60% yield as a white solid. The isopropylidene groups in compound **(15)** were deprotected with H_2O:TFA at r.t. for 18 hours and lyophilised to afford **(16)** in 59% yield. Click-chemistry between **(16)** and **(9)** was conducted in DMSO using a solid phase catalyst PS-NHC-Cu(I)[110] and purified by semi-preparative HPLC to obtain **(2)** as white powder in 92% yield.

2.3.3.3 Synthesis of (3)

The synthesis of compound **(3)** is outlined in Scheme 8. Compound **(15)** was reacted with **(13)** using copper sulphate in the presence of sodium ascorbate in THF:water. Product **(18)** was then heated to reflux in the presence of NaN_3 for 2 hours to afford the azide **(19)**. TLC was not a good technique to monitor the reaction as the starting material and products co-elute in all eluent mixtures that were tested.

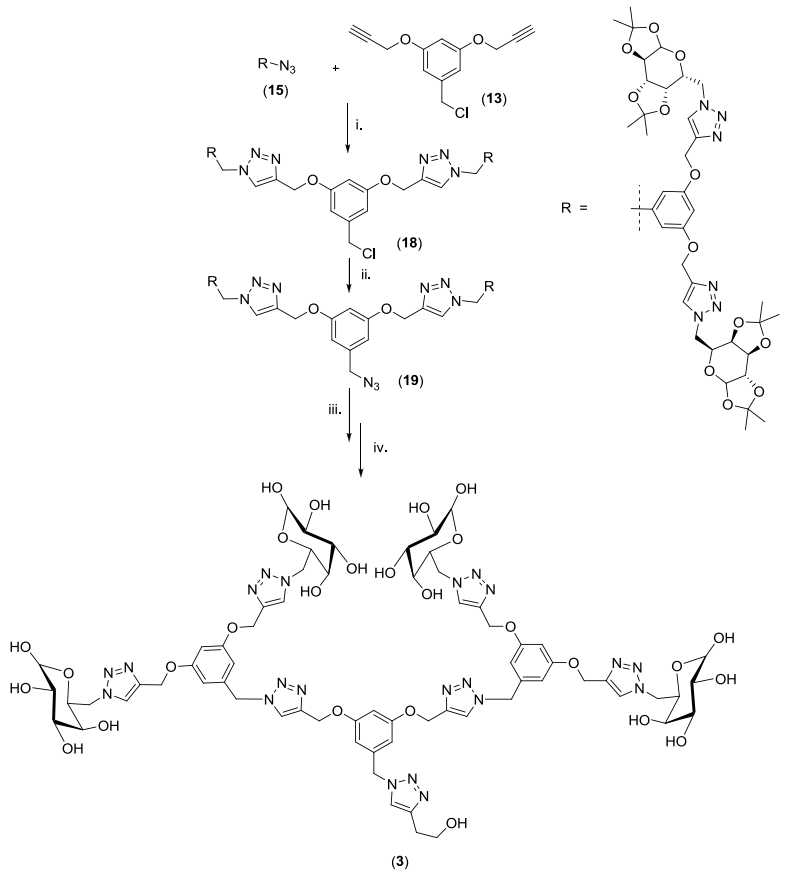

Scheme 6: Synthesis of compound (3). i. R-N_3 (15), (13), CuOTf benzene complex, Ascorbate, 24h, 20%; ii. NaN_3, 4h, 100ºC, 91%; iii. TFA-water, 6h, 65ºC, 48%; iv. PS-NHC-Cu(I) (42), DMSO, 18h, 92%

The crude reaction was therefore simply dissolved in TFA:water and heated to 80°C for 8 hours to deprotect all the isopropylidene groups. Product **(21)** was freeze-dried to afford a white solid with *m/z* 1545 $[M+H]^+$ by ESI-MS. Lastly, compound **(21)** was reacted in DMSO with PS-NHC-Cu(I) catalyst and 3-butyn-1-ol **(9)** overnight to afford crude **(3)**. This compound was purified by reverse-phase HPLC to obtain **(3)** in 88% yield.

2.3.4 Formation of AgNPs using sugars (1), (2) and (3) - Preliminary experiments

In order to determine the optimal conditions for the preparation of AgNPs using sugars **(1)**, **(2)** and **(3)**, parameters involving [Tollens' reagent] and [sugar] were screened. The "sweet spot" was defined as a concentration region of a multi-dimensional reaction matrix at which the AgNPs were formed in the highest yield as confirmed by UV/Vis. In collaboration with Ulrich Rant's group[e] the "sweet spot" of the formation of silver nanoparticles using a glucose-Tollens' bi-dimensional array was measured approximately at 100 μM [glucose] and 1 mM [Tollens'].[112]

2.3.4.1 The search of a "sweet spot" for the formation of AgNPs

Markus Schuster prepared silver nanoparticles using glucose and Tollens'.[112] He mapped the formation and the properties of the AgNP by screening the concentration of the sugar and Tollens' solution (Figure 19). The array was prepared over a large range of concentrations from 100 mM to 1 nM for glucose and between 1 μM to 125 mM for the Tollens' reagent. This ensured a deep analysis of the chemical space.

[e] Walter Schottky Institut, Technische Universität München, Am Coulombwall 3, D-85748, Garching, Germany. Phone: +49(0)89-289-11578 E-mail: Ulrich.Rant@wsi.tum.de

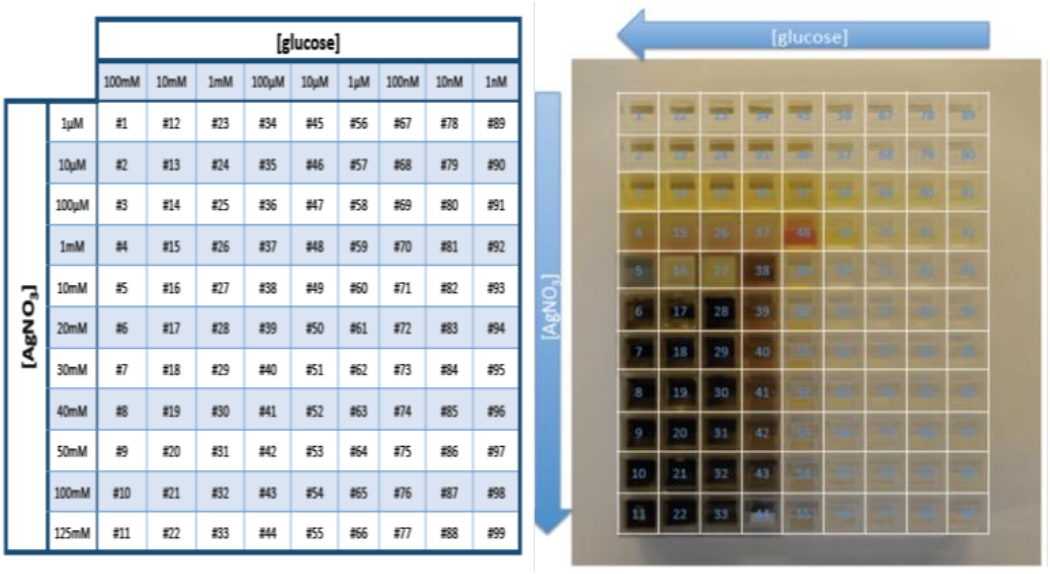

Figure 19: AgNP screening array prepared using glucose and Tollens' at different concentrations. AgNPs are clearly visible by the naked eye in wells 3, 14, 25, 36 and 47.

This powerful result allowed the selection of a desired physical property like absorption wavelength or diameter just by adjusting the initial concentrations of the reaction without the need of additional surfactants, as shown in Figure 20. The particles also show a certain degree of stability as the reaction is left running in open vials for 24h at room temperature without any apparent degradation of the quality of the particles.

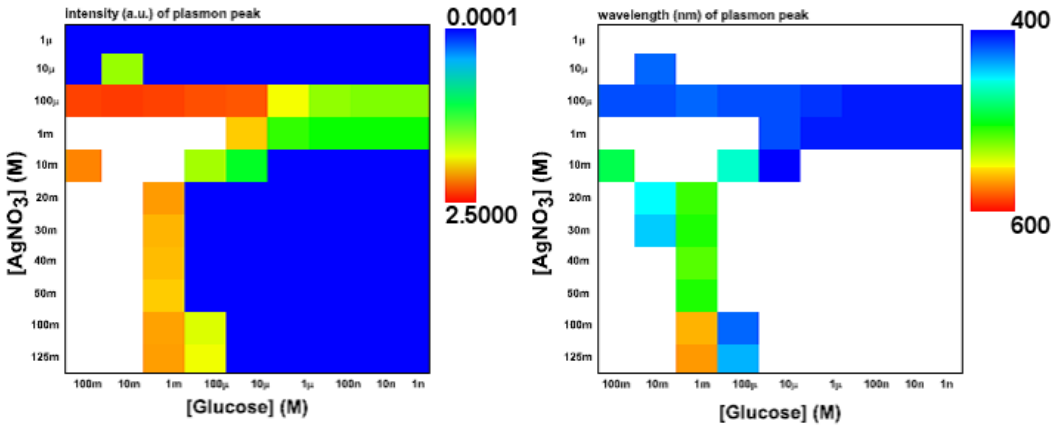

Figure 20: Intensity (in AU) and wavelength (in nm) distribution of the resonance plasmon peak of AgNPs prepared with glucose-Tollens'

A narrow region of formation of silver nanoparticles was observed in wells #3, #14, #25, #36 and #47. This was distinct compared to the region necessary to form a "silver mirror" (rectangular area formed between well #5 and well #44). All the remaining wells were clear with no formation of reduced silver.

There is a scarcity of references in literature on this topic as most scientists have used the Tollens' reaction for routine colorimetric sugar analysis or protein staining[113] and have most likely disregarded other behaviours of the reaction. Moreover, a ratio of 10:1 for the Ag^{+}:glucose concentrations led us to surmise that the process of formation of silver nanoparticles was due to a limiting reagent mechanism and not a general method. For example, gold nanoparticles form efficiently at relatively high dilution of ~50 mg/L in the classical Turkevich reaction,[114] however there is no direct evidence of a mechanism involving conditions in which a limiting reducing agent is used. In fact, most methods for the preparation of silver and gold nanoparticles have taken advantage of early

particle coating by keeping at all times the surfactant concentration greater than the metal concentration (Eg. citrate >> gold)[115].

Compound **(1)** was then tested for the formation of AgNPs with the Tollens' reagent. Tests were then conducted in open glass vials as show in Figure 21. A 200 μM stock solution of **(1)** was mixed in equal volumes with a 20 mM solution of Tollens' reagent. The reaction was followed visually and compared to a control (20 mM Tollens' in water, to visually monitor colour changes in the ageing Tollens' solution) and a glucose reaction at the same concentration.

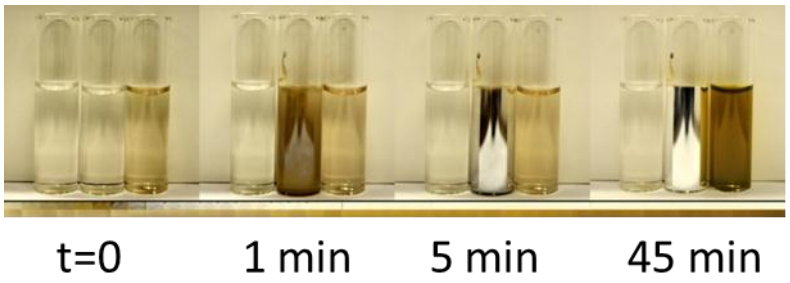

Figure 21: Colour progression of the Tollens' reaction with water (control, left), glucose (centre) and sugar (1, right) at room temperature.

The reaction was slower using **(1)** and resulted in the formation of a yellow colloidal suspension of AgNPs after 45 min. This lasted longer than in the corresponding reaction with glucose (5 min), where the nanoparticles formed but aggregated quickly to form "silver mirror".

The test was then repeated with more diluted solutions of Tollens' reagent with concentrations in the range of 0.1-1.0 mM. Out of 10 reaction attempts only 6 of the vials formed nanoparticles, with different concentrations and different onset times for the formation of the yellow colloids (between 50 mins to 4 hours). We were surprised to discover that sugar **(1)** formed nanoparticles efficiently in the

same “sweet spot” as glucose and only when the concentration of sugar was less than the concentration of silver (Table 2). If this ratio was switched, depending on the concentration, no silver nanoparticles were formed or silver mirror was the only product.

	Reaction time onset (min)	Reaction time completion (min)
1	5	45
2	10	180
3	10	235
4	10	55
5	5	40
6	10	200
7	10	200
8	10	70
9	10	150
10	10	160

Table 2: Variability of the onset and reaction completion time of ten AgNP formation attempts with sugar (1, 100μM) and Tollens' reagent (1 mM) in an open vial.

During the course of our studies, it was discovered that the acidity of the glass surface of the vials was retarding the formation of the AgNPs: Tollens' reagent $[Ag(NH_3)_2]^+$ is basic with a pH above 10 (depending on dilution)[116] due to the ammonium hydroxide and NaOH used during the preparation of the reagent. In highly diluted conditions (1 mM or less of Tollens' reagent), the ammonia and NaOH were insufficient to buffer the acidity of the glass vial, drastically reducing the reproducibility of the tests, as it's known that the Tollens' reaction works only in basic conditions.[117] Reactions were then conducted using plastic vials with a higher degree of reproducibility. Early attempts were also conducted by the addition of buffers and surfactants to the Tollens' reaction in the attempt to

improve the stability and quality of nanoparticles: classic surfactants like citrate and citric acid or aliphatic amines like DMEDA were tested (Figure 22).

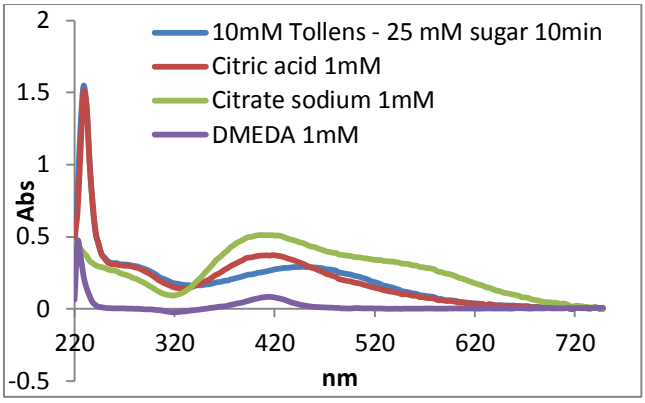

Figure 22: Variation of the UV-Vis spectrum by the addition of surfactants citric acid, citrate or DMEDA to AgNPs prepared with sugar (1).

While citric acid seemed to improve the colloid by reducing aggregation as noted by a 30 nm blue shift of the surface plasmon from 448nm to 418nm, sodium citrate instead increased aggregation with the formation of a secondary peak at 568nm. This was attributed to surface plasmon resonances corresponding to poly-aggregated particles.[118] Nitrogen ligands such as DMEDA resulted in the precipitation of the colloid. These results led us to conclude that the particles would be prepared without any additional surfactants.

2.3.4.2 Measure of a "sweet spot" for sugar (2)

Sugar **(2)** was tested initially in the same conditions as **(1)** and was found to form very little silver nanoparticles. The problem of this low yield was not understood at the beginning, however it was serendipitously discovered that **(2)** formed a stable silver colloid at much higher concentration of 10 mM. Starting at 10mM of Tollens' reagent (Table 3), which was ten times more concentrated than the

working “sweet spot” of **(1)** according to the formation of the surface plasmon peak. Nanoparticles were also more stable when the concentration of **(2)** was equal or higher than the concentration of the Tollens’ reagent, in contrast to the previous results made with **(1)**.

Compound	Tollens' reagent **(mM)**	Sugar **(mM)**	Result
(1)	1	1	AgNPs
(2)	1	1	no particles
(2)	10	1	AgNPs
(2)	10	10+	stable AgNPs

Table 3: Formation of AgNPs with sugar (1) and (2) at various Tollens’ and sugar concentrations showing a working reaction at 10+ mM of Tollens’ reagent.

The surface resonance plasmon peak of such prepared particles was also extremely sharp with a max peak at 419 nm, FWHM at 450 nm and <10% of max absorbance at 490 nm. These values indicated that the reaction produced a well dispersed, single population of silver nanoparticles colloid. Fluorescence spectroscopy (excitation at 325nm) showed a similar shape profile with a high intensity maximum emission at 462nm (Figure 23).

Early dynamic light scattering (DLS, see 2.3.5.3 for a short introduction) measurements showed also another property of the particles: there was a large difference in the reproducibility of the particle size when the Tollens’ reaction was conducted in open plastic vials versus the use of closed vials or nitrogen purged atmosphere.

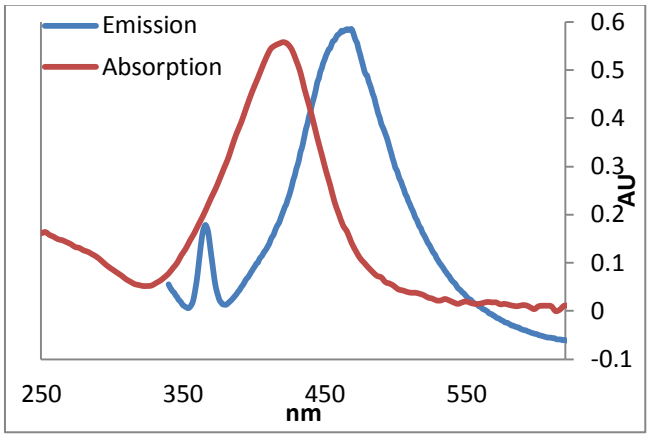

Figure 23: UV-Vis absorption of the AgNPs prepared with sugar (2) and fluorescence emission (excitation at 325 nm).

The open-vial DLS size distribution (Table 4) clearly showed the presence of aggregates and undesirable larger particles, which are not present when the reaction is prevented to come in contact with oxygen.

NANOPARTICLES SIZE DISTRIBUTION (nm)		Sugar2				
		10mM	1mM	100uM	10uM	1uM
Tollens	1mM	37.1	2.4	12.4	0.6	0.7
	10mM	2.4	12	1.5	3.5	38.9
	20mM	6.5	1.9	3370.3	128	-
	50mM	5	1511	-	-	-

	Sugar2				
	25mM	10mM	1mM	100uM	10uM
1mM	-	-	10.64	11.7	-
10mM	1.1	9.08	1.26	-	-
20mM	4.76	8.84	2.53	-	-
50mM	4.61	0.97	-	-	-

Table 4: DLS size distribution of AgNPs prepared with sugar (2) in an open vial (left) or in a closed vial (right).

The preparation of all the nanoparticles was then conducted in closed low-binding polymer 1.7 mL microcentrifuge tubes to avoid atmosphere contact. As a possible explanation of this observed behaviour, in the presence of oxygen, the AgNPs are coated with a thin layer of oxide that could promote spontaneous aggregation of the particles, leading to instability of the colloid. Oxygen instability of AgNPs was also noticed by Venkateswaran.[97]

In conclusion, a reproducible laboratory method for preparation of AgNPs with sugar triazoles was discovered. Sugars **(1)**, **(2)** and **(3)** were then tested with the Tollens' reagent in arrays at variable concentrations and results were analysed in details to determine the properties of the AgNPs formed.

2.3.5 AgNPs derived from sugar (1)

2.3.5.1 Preparation of (1) AgNP array

A AgNP array using compound **(1)** was constructed using a concentration range between 1 μM – 25 mM for sugar1 **(1)** and 10 μM – 50 mM for the Tollens' reagent. The prepared array was smaller than the previously described work with glucose (paragraph 2.3.4.1) as the outlying concentration values either formed a "silver mirror" or contained no particles and so unnecessary to this study.

Tollens	25mM	10mM	1mM	100uM	10uM	1uM
10uM	#1	#2	#3	#4	#5	#6
100uM	#7	#8	#9	#10	#11	#12
1mM	#13	#14	#15	#16	#17	#18
10mM	#19	#20	#21	#22	#23	#24
20mM	#25	#26	#27	#28	#29	#30
50mM	#31	#32	#33	#34	#35	#36

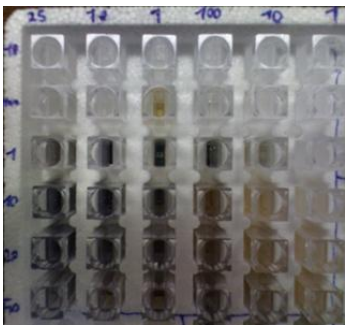

Figure 24: Schematic representation of the array used to investigate AgNP@(1) formation as function of [Tollens] and [(1)]. Photograph of the array after 24h showing the regions of formation of AgNPs.

Visual inspection of the array showed that some parts of the array were completely devoid of precipitate at 10 μM or less of Tollens' reagent. Conversely, all vials of 10 mM or more of Tollens' reagent resulted in the formation of a "silver mirror". Lastly, and more importantly, the array rows at 1 mM and 100

μM of Tollens' presented a yellow colour, which was indicative of a AgNPs colloid.

2.3.5.2 UV-Vis spectroscopy

All array cell mixtures were analysed over a period of 24h for reproducibility. Even if some cells presented yellow colloids and plasmon peaks at UV-Vis measurements before this time and later aggregated in silver mirrors, the work focused primarily on stable nanoparticles. It was found "as a rule of thumb" that if a Tollens' reaction had particles after 24 hours, those particles were stable enough to be preserved for weeks in a capped vial at 4°C for further analysis.

AgNP concentrations as measured by the intensity of the surface plasmon peak were distinctly located in 2 regions: **a low concentration region at the 100 μM Tollens' row, and a high concentration region at the 1 mM Tollens' row**, which was 15 times higher in concentration than the previous one (Figure 25).

Sugar1

Tollens	25mM	10mM	1mM	100uM	10uM	1uM
10uM	#1	#2	#3	#4	#5	#6
100uM	#7	#8	#9	#10	#11	#12
1mM	#13	#14	#15	#16	#17	#18
10mM	#19	#20	#21	#22	#23	#24
20mM	#25	#26	#27	#28	#29	#30
50mM	#31	#32	#33	#34	#35	#36

	25mM	10mM	1mM	100uM	10uM	1uM
10uM			412 0.01			
100uM	423 0.07	421 0.08	418 0.09	421 0.01		
1mM	412 0.86	407 1.09	413 1.41	434 1.31	413 0.18	

Figure 25: Array series for the preparation of AgNP@(1). On the left, white boxes represent no AgNP formation, yellow boxes represent AgNP formation and grey boxes represent silver mirror formation. On the right, detail of the array showing wavelength in nm and intensity in Abs units of the resonance plasmon peak of each sample.

Cell #15 showed the maximum concentration of AgNPs with an absorbance of 1.41 AU, while cell #16 (at the concentration of 1.31 AU) showed the maximum stability with no variability of the plasmon peak in 6 months at 4°C. While the frequency of the resonance plasmon peak of cells #13, #14, #15 and #16 seemed not to follow a specific pattern, each single cell was highly reproducible, indicating that the variability was due to different particle properties of each cell. As an example cell #16 was tested in quadruplicate resulting in a plasmon resonance at 421 ± 2 nm and an intensity variation of 1.31 ± 0.16 AU showing high reproducibility of the AgNPs wavelength and intensity of the resonance plasmon peak (Figure 26).

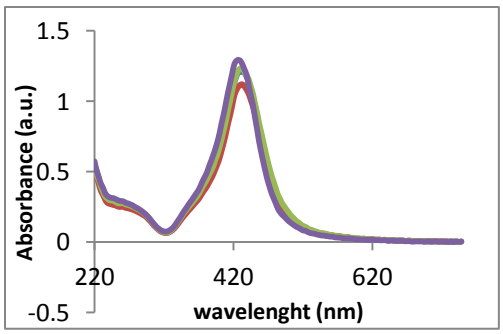

Figure 26: UV-Vis reproducibility in quadruplicate of AgNPs of cell #16.

However, as shown in Figure 25, such a variability of the plasmon peak frequency (27 nm between cell #14 and #16) cannot be accounted by the size of the particles, as predicted by Mie Theory.[119] In addition, it's unlikely that a red-shift of plasmon peaks due to the variations of the hydrodynamic range of the particles could give such a large shift and that would scale with the concentration of **(1)**. However, such a trend was not visible. A plausible explanation was that samples could be highly polydisperse, with multiple populations of particles with different sizes and

shapes coexisting in a cell. This was already evidenced by the work of Godet.[82] Consequently the observed plasmon peak maximum frequency would arise from the contribution of the dominant species of particles in each cell.

2.3.5.3 DLS

Dynamic light scattering (DLS) is a technique which can be applied to the study of colloids. DLS allows the analysis of the size distribution of small particles in suspension in a liquid in a non-destructive way. The size obtained from the technique for nanoparticles is the hydrodynamic range of the particles. This diameter includes both the metallic size of the particle and the size of the molecules in its solvation shell.

DLS was run on all the cells containing particles with a surface plasmon polariton to measure the hydrodynamic diameter and population distributions of the nanoparticles (Figure 27).

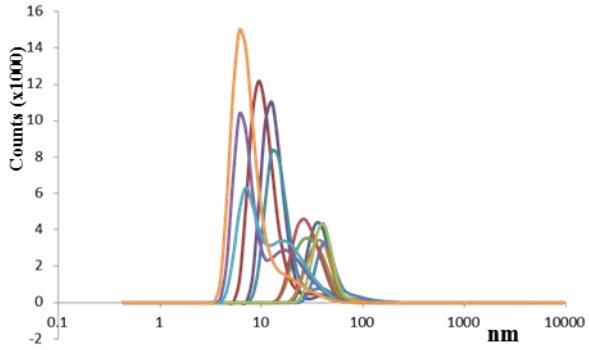

1mM	37.7	39.5	36.1	40.1	6.5	

Figure 27: DLS of reactions #13-17, showing the variability of particle sizes. Detail of the array (cells #13-17) reporting the average of the particle distribution.

Cells #13-16 showed size distributions with an average of size of ~40 nm for these particles. Cell #17 was different with particle sizes averaging at ~ 6.5 nm. By looking at DLS profiles however, it's evident that cells #13-16 contained at least 2 populations of particles, approximated by 2 Gaussian curves as shown in Figure 27. This result is consistent with theory describing growth of larger nanoparticles at the expense of smaller particles through an exponential autocatalytic process.[117] At low concentration of **(1)** (cell #17) small particles (6.5 nm average) are formed; due to the limited supply of reducing **(1)**, no more $Ag^{(0)}$ is available to promote particle growth and as a result they are quickly coated by carboxylic acids groups from the oxidised galactoses. At higher concentration of **(1)**, the $Ag^{(0)}$ nuclei are present for a longer time, resulting in the formation of larger ~40 nm particles. Such a process of "nano-soldering" has been proposed and observed before by Mallick.[120] Lastly, multiple populations of silver nanoparticles have been described during the synthesis with tannic acid (Figure 28).[121] As tannic acid concentration increased, the diameter of the AgNPs augmented in a similar fashion to sugar **(1)**, pointing to a similar mechanism of particle growth.

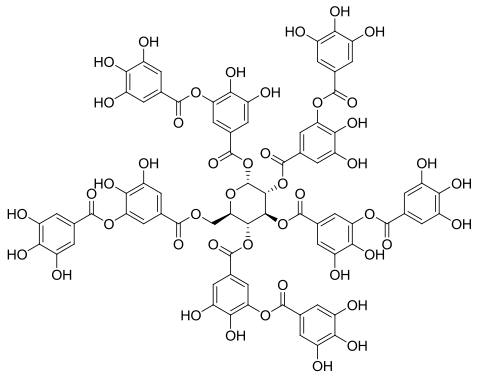

Figure 28: Structure of tannic acid.

As cells #13-16 contained both small and large silver nanoparticles in different ratios, it was possible that the observed behaviour was due to a non-complete "nano-soldering" process. To test this idea, a second smaller array was prepared with a finer concentration range between 100 μM and 10 μM of **(1)** and equivalent to the concentrations between cell #16 and #17 (Table 5).

	100uM	80uM	60uM	50uM	40uM	20uM	10uM		100	80	60	50	40	20	10
0.5mM								0.5		2.69	1.44	1.26	1.12	0.91	
0.75mM								0.75	43.20	43.51	39.90	40.25	43.82	1.68	3.52
1mM	**#16**						**#17**	1	41.47	43.15	43.63	5.37	4.39	3.29	1.66
1.5mM								1.5		46.12	44.35	41.74	44.86	39.91	

Table 5: Expanded array of AgNPs@(1) showing DLS particle distribution in nm in a region between cells #16 and #17.

This new array showed again two distinct groups of cells, with smaller nanoparticles at lower concentrations. However, a net trend was visible: the size of the small particles was directly proportional to the concentration of **(1)**. At a critical concentration of sugar and Tollens', larger particles appeared and became dominant.

2.3.5.4 Fluorescence spectroscopy

Samples #14-16 were tested for fluorescence (Figure 29). The intensity of the spectra showed a correlation with the concentration of the sugar **(1)**, which is directly linked to the final concentration of the particles for each sample. Cell #16 showed an interesting dual excitation wavelength at 340 nm and 490 nm that gave

rise to the same emission peak at 490 nm. This is unlikely to be direct excitation of multipolar plasmon optical excitations (Eg. Dipolar and quadrupolar plasmon resonances as by Mie theory), but it's probably due to simple scattering. Moreover all samples displayed the presence of multi-emission peaks, evidence supporting the presence of multiple populations or multi-shaped particles;[122] sample #15 showed well separated emission peaks at 471, 486 and 492 nm. Interestingly, samples #3, #7-#10 showed very weak emission peaks when excited at 325 nm, while showing no absorption bands in UV-Vis spectra. This is probably due to the higher light sensitivity of the fluorimeter used. Fluorescence spectroscopy is known to have much higher sensitivity that UV-Vis spectroscopy.[123]

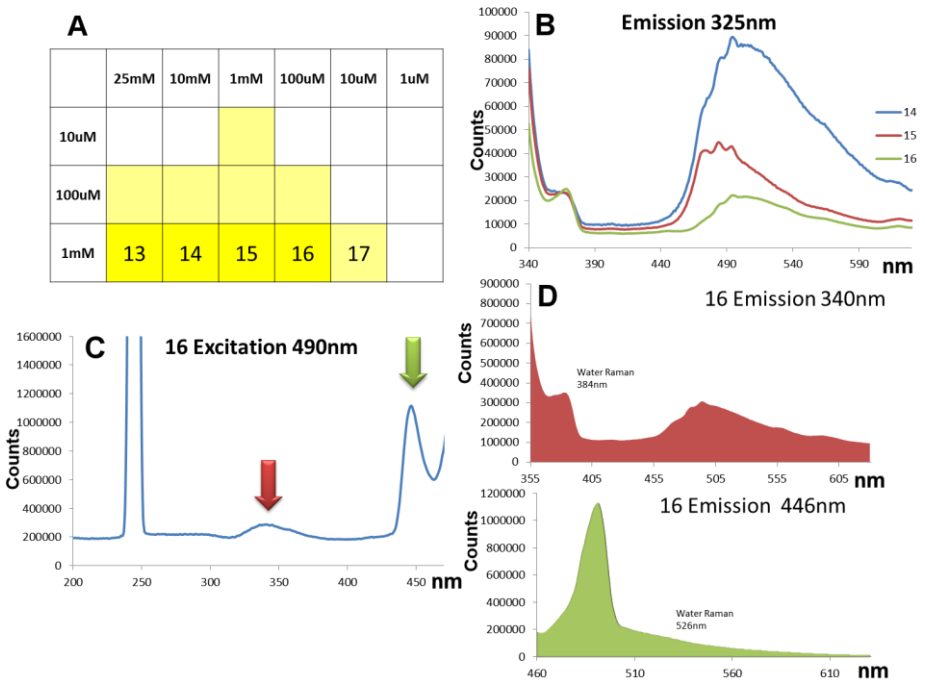

Figure 29: Emission and excitation spectra of samples #14-16. A. Visualisation of the analised samples in the array. B. Emission spectra of samples #14-16 (Excitation at 325 nm). C. Excitation spectrum of sample #16 (emission reading at 490 nm). D. Magnified and colour coded emission spectra of sample #16 corresponding to the excitation peaks at 340 nm (red arrow in C.) and 446 nm (green arrow in C.). Water raman peaks have been marked.

Sample #16 showed two excitation peaks at 340 nm and 446 nm that gave rise to two very different emission spectra (See green and red spectra in Figure 29). In particular the intense excitation at 446 nm with emission at 480 nm could be compatible with small silver nanoclusters.[124]

2.3.5.5 TEM

Initially, samples #15 and #16 was analysed with transmission electron microscopy, as they contained the highest concentration of particles. The dispersity of sample #16 showed an average diameter of 41.2 nm ± 25% (384 particles counted); values were in good agreement with the DLS data of 41.47 nm of averaged diameter (Figure 30). A difference of 0.27 nm was found and this value is consistent with known values of hydrodynamic ranges for nanoparticles coated with small organic molecules with carboxylic acids (such as citrate).[70]

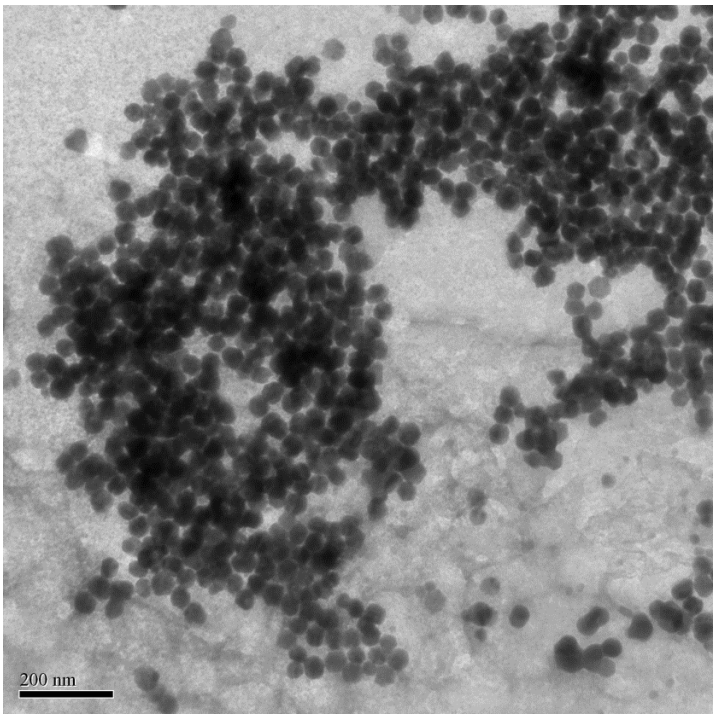

Figure 30: TEM image of AgNPs of sample #16.

While the particles of the sample were mainly spherical, a number of particles with different shapes were found, with the most common being icosahedral and hexagonal plates (Figure 31). Octahedral and triangular plates were also found but in far lower abundance. This is significant as multiple shapes were inferred by the fluorescence spectroscopy of the sample.

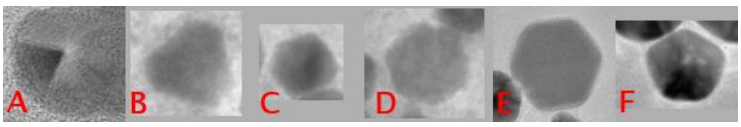

Figure 31: Selected polyhedra of AgNP@(1) formed using reaction condition #16: A. Rounded Icosahedron B. Truncated triangular plate C. Truncated octahedron D/E. Hexagonal plate F. Icosahedron.

High resolution TEM was taken on a single spheroid silver nanoparticle: fringe spacing which was measured to be 2.4 Å could be assigned to {111} reflection of face cubic centered silver crystal (fcc Ag). This is important as it showed that all particles were highly crystalline.

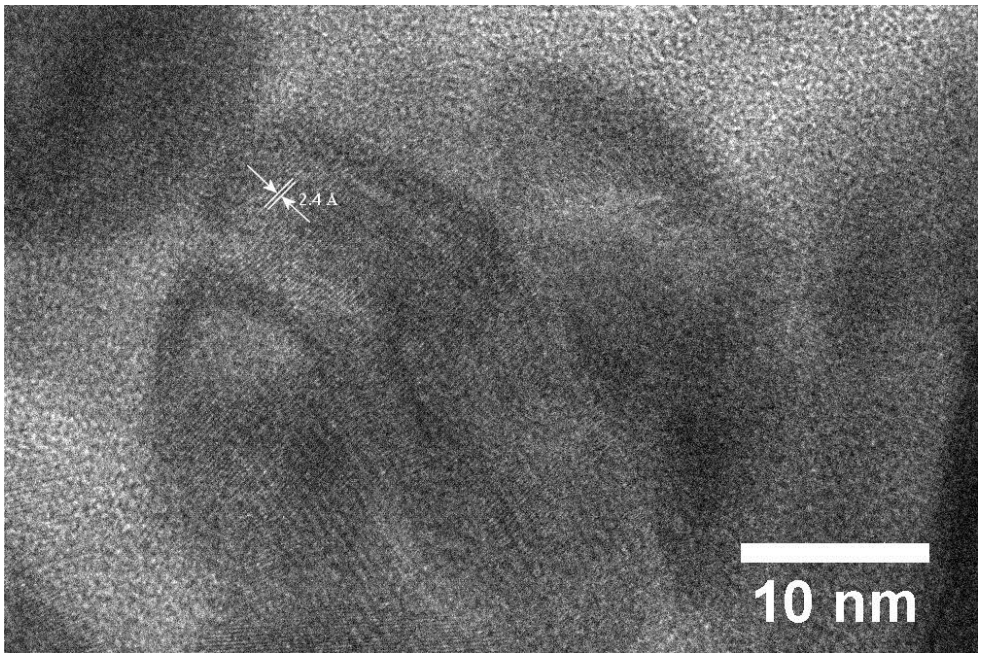

Figure 32: HR-TEM of a representative NP of the AgNP@(1) series derived from reaction condition #16.

Selected area electron diffraction (SAED) is a crystallographic experimental technique that can be carried out with a transmission electron microscope. SAED enables the observation of diffraction patterns of very small areas such as single particles and so gives information about the crystallinity and crystal defects. A SAED pattern shows a projection of the reciprocal lattice with lattice reflections showing as bright spots or circles. It can be used, when calibrated with a known sample, to directly measure lattice parameters and so identify crystal structures.

SAED confirmed the fcc nature of the particles where lines corresponding to {111}, {200}, {220}, {311} and {222} were clearly visible (Figure 33). Diameter of the {111} line was measured against crystalline standard sample of Al_2O_3 and found to be 0.24105 nm, in accordance of the fcc Ag nature of the nanoparticle.[f]

[f] International Center for Diffraction Data file no. 03-0931 for FCC silver metal

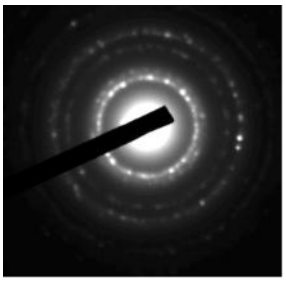

Figure 33: SAED of the particle shown in Figure 32.

Sample #15 was imaged and found to be highly polydisperse (Figure 34). Particles ranging from 1.5 nm to 60 nm were found, with an average of 39 nm ± 65%. The particles were also clumped together in small aggregates that were not visible at DLS, and so they were probably due to the preparation of the TEM grid itself. At even higher concentration of sugar, sample #14 showed an even more drastic polydispersity, with particles clearly divided in multiple populations.

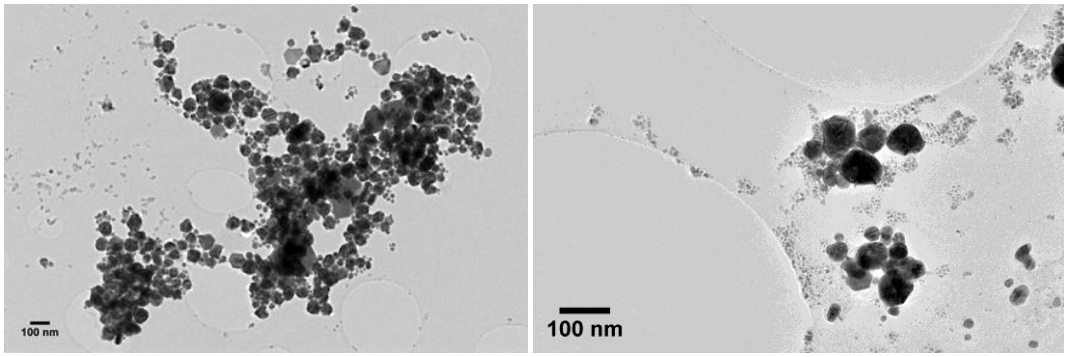

Figure 34: TEM image of AgNPs of sample #15 (left) and #14 (right).

On the contrary, at lower concentration of **(1)**, sample #17 showed the presence of <10 nm particles only, in accordance to the DLS data (Figure 35). The particles were also well separated, spherical with no signs of aggregation. Since these particles were supposed to be the "seeds" to the larger particles found in more

concentrated samples, it was quite surprising that we couldn't find any particle aggregate, *en route* to the larger particles.

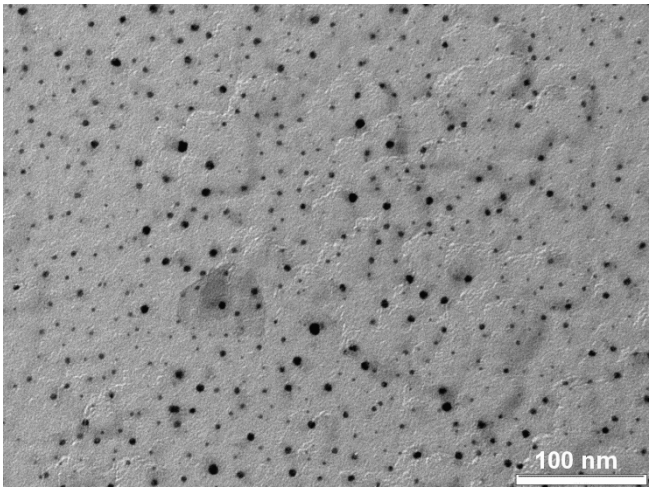

Figure 35: TEM image of AgNPs of sample #17.

In conclusion, 40 nm was found to be a critical size for silver nanoparticles prepared with the Tollens' reaction at 1 mM concentration when compound **(1)** is used as the reducing sugar. We therefore propose the following simple mechanism where particles could reach the critical 40 nm size. It is known that the surface curvature of nanoparticles of ~40 nm or more is locally similar to a flat plane,[125–127] we propose that this disfavours further growth of the particle thanks to the formation of a monolayer of oxidised galactoses forming an electrostatic repulsion barrier. However, at higher concentrations of **(1)**, smaller silver particles are still present forming a multi-population sample. At concentrations of **(1)** lower than the "sweet point", not enough silver is present to form a stable population of 40 nm particles. This effect can be macroscopically seen in samples #13-16 as the direct proportionality between polydispersity and concentration of **(1)** (Figure 36).

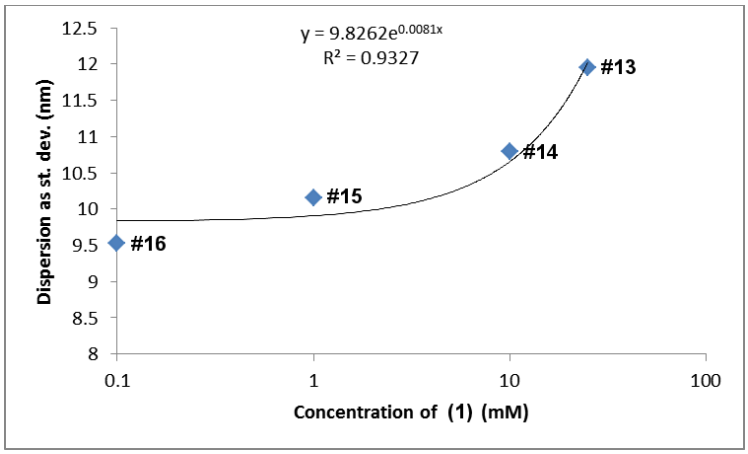

Figure 36: Relationship between the concentration of (1) and the standard deviation of Gaussian distribution of the AgNPs in samples #13-16 showing an exponential growth in dispersity at the increase of the (1)

Therefore, we conclude that in order to obtain stable AgNPs derived from **(1)**, the optimal conditions are 100 μM of **(1)** and 1 mM of Tollens' reagent.

2.3.6 AgNP derived from sugar (2)

2.3.6.1 Preparation of (2) AgNPs array

Figure 37 depicts the AgNPs array constructed over a concentration range between 10 μM – 25 mM for **(2)** and 100 μM – 50 mM for the Tollens' reagent.

Sugar2

Tollens	25mM	10mM	1mM	100uM	10uM
100uM	#1	#2	#3	#4	#5
1mM	#6	#7	#8	#9	#10
10mM	#11	#12	#13	#14	#15
20mM	#16	#17	#18	#19	#20
50mM	#21	#22	#23	#24	#25

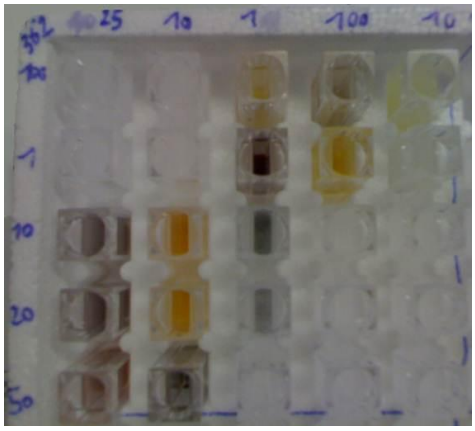

Figure 37: Schematic representation of the array used to investigate AgNP@(2) formation as function of [Tollens'] and [(2)]. Photograph of the array after 24h showing the regions of formation of AgNPs.

The particle distribution on the array of **(2)** was completely different from the particle distribution of **(1)**. One immediate difference was that no "silver mirror" was formed at high concentration of Tollens' reagent (Figure 37). Instead yellow colloidal solution was visible up to 50 mM of Tollens' reagent. At the concentration of 1 mM of Tollens' reagent little or no particles were formed (cells #6-10), while for **(1)** this was the only working range. At 10-50 mM of Tollens' reagent, the samples were strongly coloured due to the high concentration of AgNPs. Samples #21 and #22 showed as black solutions and reverted to a more common yellow colloid upon dilution.

2.3.6.2 UV-Vis spectroscopy

A striking difference of sugar **(2)** compared to **(1)** is that the array seemed subdivided into 3 regions (Figure 38): a region with a concentration range similar to **(1)** (1 mM Tollens', 10 uM – 1 mM sugar **(2)**), a high concentration region with particles 11 times more concentrated than typical AgNP@**(1)** and lastly a region at high concentration of **(2)** was showing AgNPs as a brown coloured colloid.

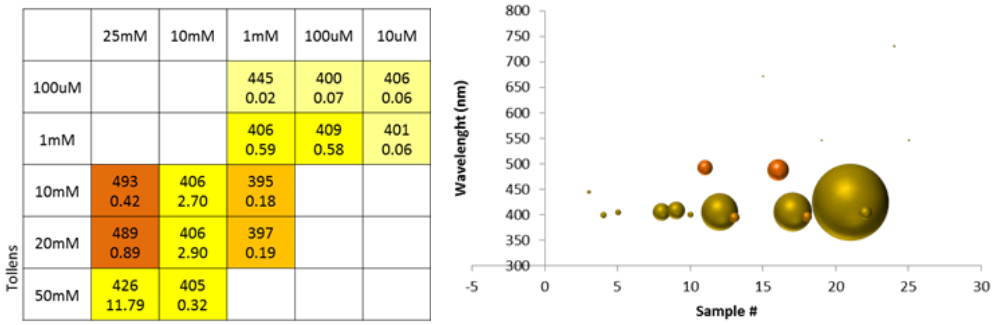

Figure 38: Array series for the preparation of AgNP@(2). White boxes represent no AgNP formation, Yellow boxes represent AgNP formation. Numbers are wavelength in nm and intensity as Abs units of the resonance plasmon peak. On the right a plot of the same data as relationship of cell number vs the wavelength of the plasmon peak (Size of the spheres indicated the intensity of the plasmon peak).

The surface plasmon peak resonances of the samples showed ordinary peaks centred at 406 nm and the intensity of the peaks correlated with the concentration of the sugar **(2)** (Figure 39). Samples #21 and #22 (high concentration Tollens') had particularly intense plasmon peaks and required dilution of 20 times to be measured by the UV-Vis spectrometer.

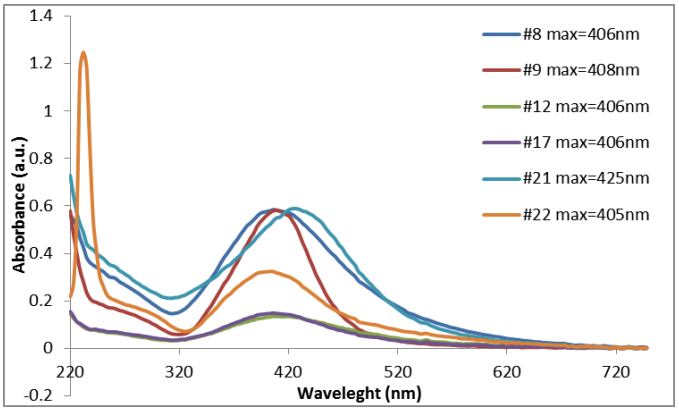

Figure 39: UV-vis spectra of reactions #8-9, 12, 17, 21-22 which formed AgNPs as observed by surface Plasmon peak. Samples #17-21-22 were diluted 1:20 prior the measurements. The peak at 223 nm is the absorbance of (2).

Samples #11 and #16 (brown colloid) had the surface plasmon resonance peak at 493 nm and 489 nm respectively (Figure 40). Such red-shift for silver nanoparticles is unusual, and has been described previously for small silver nanoclusters of 50 atoms or less (< 1 nm).[128,129]

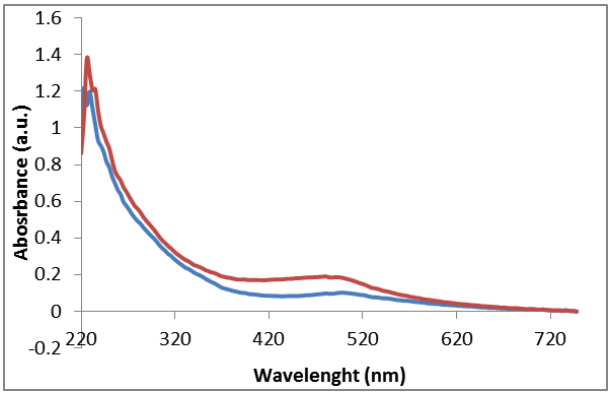

Figure 40: UV-vis spectra of reactions #11 and #16, showing absorption peaks at ~490 nm.

2.3.6.3 Dynamic Light Scattering analysis of AgNP@(2)

Cell #10 returned a non-reproducible result due to the low concentration of the sample (10 uM of **(2)** and 1 mM of Tollens') (Figure 41). Cells #8, #9, #11, #17, #21 and #22 revealed the presence of particles between 4 – 12 nm with high polydispersity up to 6.6 nm or 56% for sample #9 (100 uM **(2)** and 1 mM Tollens'). Samples #13 and #18 (1 mM **(2)**, 10 mM and 20 mM Tollens') showed the presence of multiple populations of particles, the value of dispersity for these samples was in fact higher than the average population size which was a physically impossible result and was due to the limitations of the DLS software.

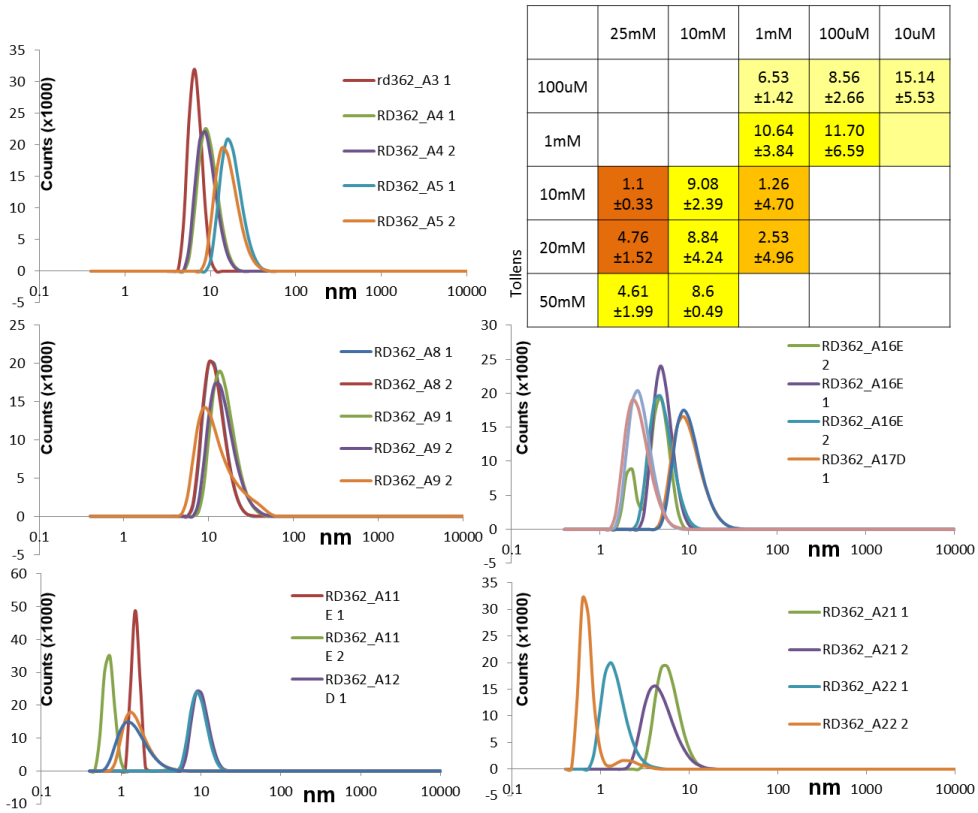

Figure 41: DLS of samples #3-5,8-9,11-12,16-17,21-22 which formed AgNPs colloids (indicated in the keys as A3, A4, etc. Samples marked with D are diluted 1:20. Samples marked with E are diluted 1:50). The array table shows the same data as average of the Gaussian distribution in nm and dispersity as st. dev. (± 1σ, in nm).

Samples #11 and #16 contained ultra-small particles (1.1 ±0.33 nm), with sample #11 showing sub-nanometre diameter particles and sample #16 containing 1-7 nm particles (Figure 41). Considering that ~1 nm diameter particles contain approximately 30 atoms, these colloids can be better described by the term "small silver nanoclusters". In conclusion, the size distribution of the AgNPs prepared with **(2)** showed large variations over the chemical space of the array. Even if a trend was not observed, particles were prepared in a reproducible way at the same concentration of Tollens' reagent and sugar **(2)**. Very noteworthy was the ability

of sugar **(2)** to stabilise small silver nanoclusters at the concentration of 25mM of sugar (Samples #11 and #16)

2.3.6.4 Fluorescence spectroscopy

Fluorescence of the majority of the samples of **(2)** emitted light with a peak maximum wavelength of 440 nm when excited at 325 nm (Figure 42).

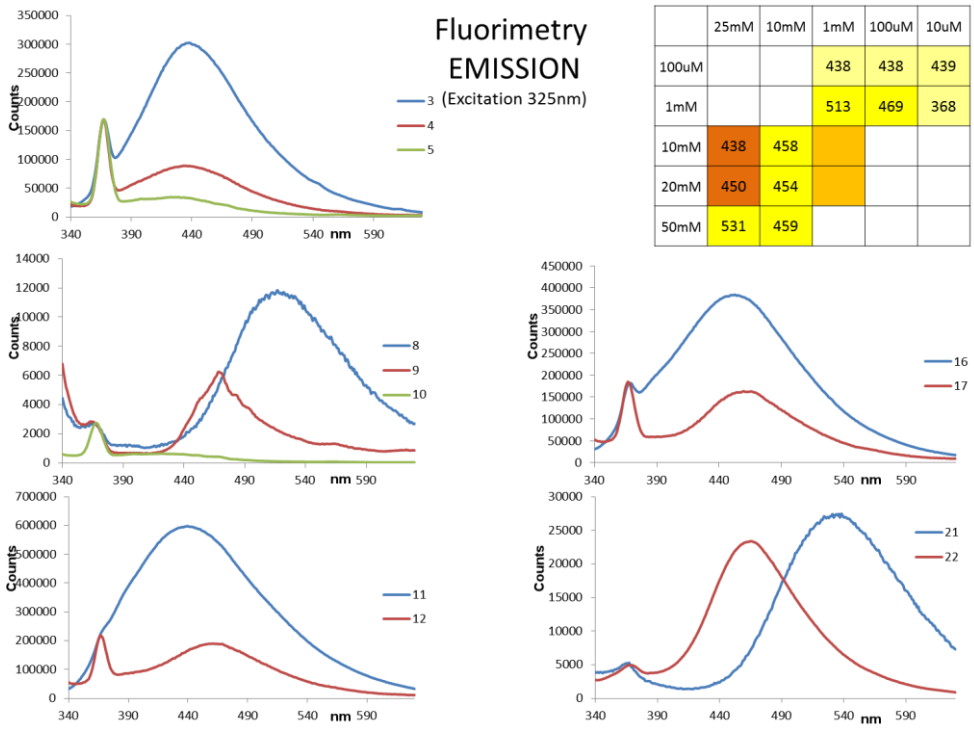

	25mM	10mM	1mM	100uM	10uM
100uM			438	438	439
1mM			513	469	368
10mM	438	458			
20mM	450	454			
50mM	531	459			

Figure 42: Emission fluorescence spectra of #3-5,8-9,11-12,16-17,21-22 recorded at the excitation of 325 nm. The array table reports the wavelength (nm) of the major emission peak.

Only sample #8 and #21 fluoresced at 513 nm and 531 nm respectively. Sample #9 showed a fluorescence profile similar to **(1)** AgNPs. The intensities of the emissions were inversely proportional to the particle size and were not correlating with the concentration of **(2)** or total concentration of silver used (Tollens' reagent). This is highly consistent with known theoretical results in literature

showing that AgNPs are highly fluorescent only with diameters of 10 nm or less (Figure 43).[130]

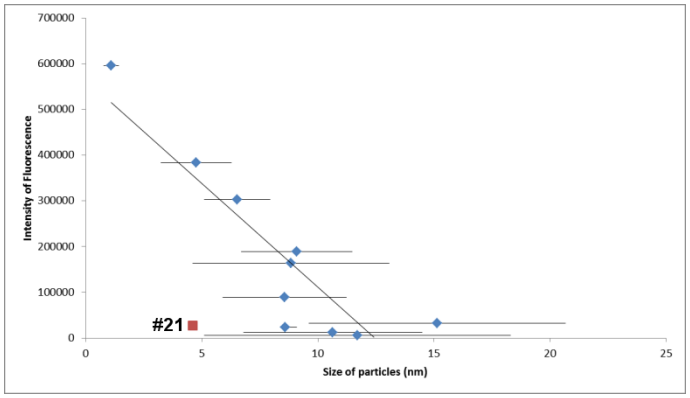

Figure 43: Plot showing the correlation between particle size (nm) and intensity of the fluorescence (Counts) of the AgNPs prepared with sugar (2).

Sample #21 (25 mM **(2)** and 50 mM Tollens', indicated as a red square in Figure 43) however deviated from this correlation, showing very low fluorescence intensity for the size of the particle measured. The excitation spectra intensity peaks of the samples were proportional to the emission intensity in the majority of the cases, in particular only sample #22 (10 mM **(2)** and 50 mM Tollens') showed a very intense excitation spectrum and a weak fluorescence (Figure 44).

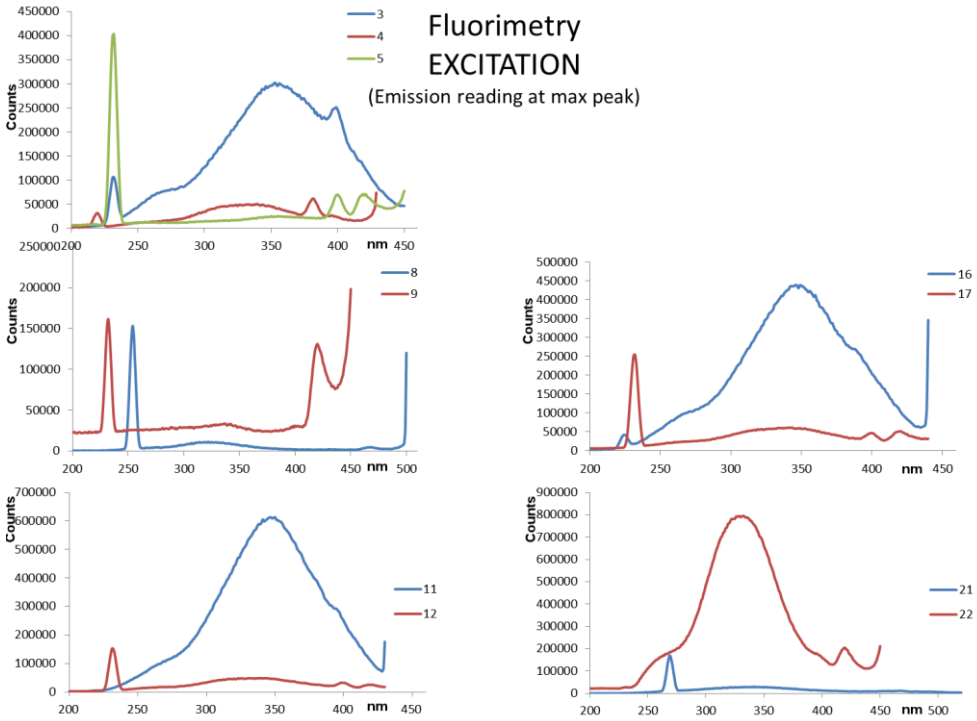

Figure 44: Excitation fluorescence spectra of samples #3-22 recorded at the maximum emission of the main peak.

2.3.6.5 TEM

Measured particles of sample #17 were an average of 7.9 nm ± 62% of dispersity (568 particles counted). Hydrodynamic radius was calculated at 0.94 nm; this value is ~3 times larger than the hydrodynamic radius measured for sugar **(1)** and is consistent with a larger molecule of **(2)** coating the particles (Figure 41).

Sample #11 showed only the presence of extremely small particles in the range of 0.6-1.2 nm as shown in Figure 45c.

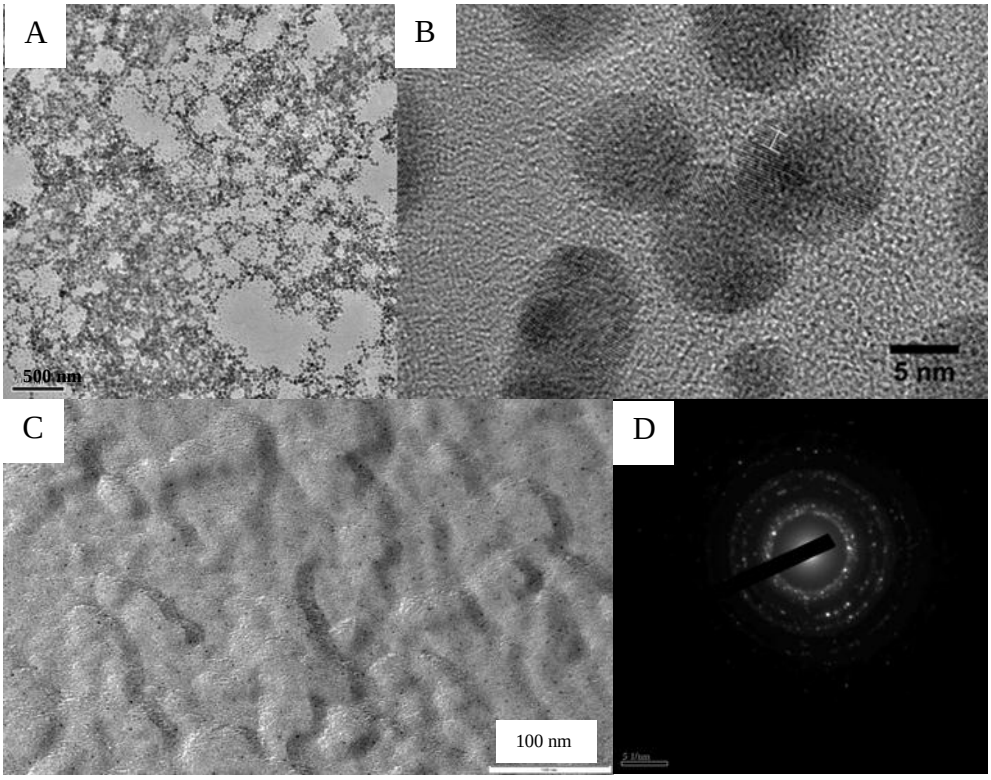

Figure 45: A. TEM image of sample #17; B. HR-TEM of sample #17; C. TEM image of sample #11; D. SAED of sample #17.

It is worth noting that particles of 0.6 nm of diameter are approximately 10-11 atom nanoclusters. This is important as small silver nanoclusters have been prepared before only in the presence of strong binding surfactants or gelling matrixes.[124,129,131] Analysis of SAED (Figure 45D) clearly showed intense reflections for {111}, {220}, {222}, {311} and {331},[82] pointing out that the nanoparticles made with sugar **(2)** were only spherical monocrystalline fcc. In contrast, samples made with glucose[117] or sugar **(1)** showed polycrystallinity or the formation of polyhedral shapes.

Samples #12 #18 #21 #22 were very similar to sample #17 (10 mM **(2)** and 20 mM Tollens'). Only sample #22 showed a distinct dual-population distribution

with clusters of 1-4 nm diameters being present together with larger 8-16 nm particles (Figure 46).

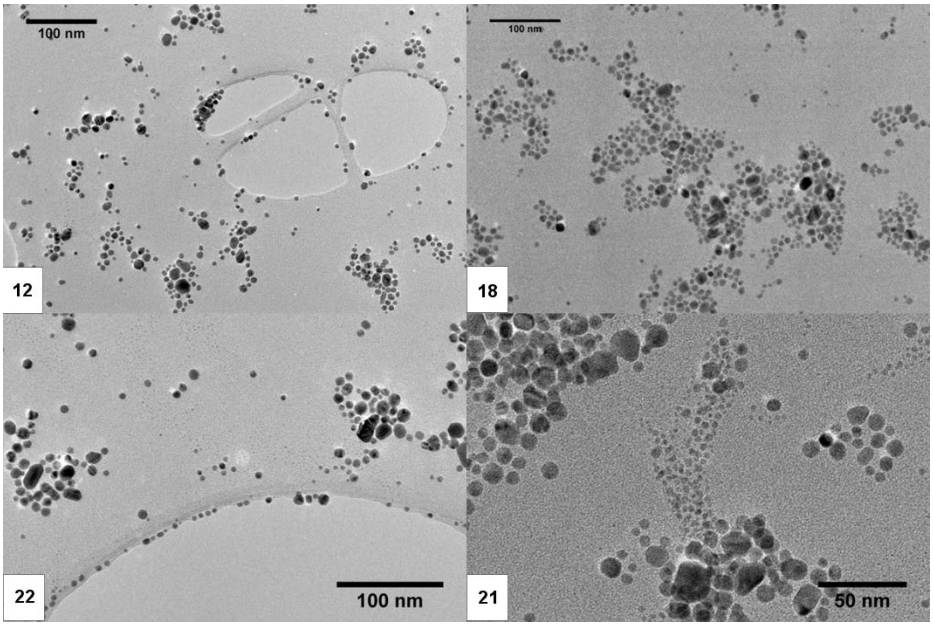

Figure 46: TEM images of samples #12,18,21 and #22.

In conclusion sugar **(2)** samples taken as a whole showed the formation of smaller AgNPs than those prepared with sugar **(1)** with an average of 7.9 nm ± 62% of dispersity.

2.3.7 AgNP derived from sugar (3)

2.3.7.1 Preparation of (3) AgNPs array

A AgNPs array derived from **(3)** was constructed in a concentration range between 1 μM – 5 mM for the sugar and 100 μM – 50 mM for the Tollens' reagent. It was not possible to obtain an array column for sugar **(3)** at 25 mM due to its lower solubility in water.

Sugar4

Tollens	5mM	1mM	100uM	10uM	1uM
100uM	#1	#2	#3	#4	#5
1mM	#6	#7	#8	#9	#10
10mM	#11	#12	#13	#14	#15
20mM	#16	#17	#18	#19	#20
50mM	#21	#22	#23	#24	#25

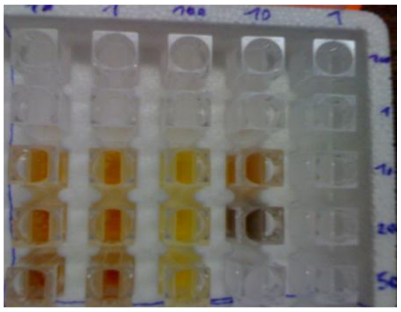

Figure 47: Schematic representation of the array used to investigate AgNP@(3) formation as function of [Tollens'] and [(3)]. Photograph of the array after 24h showing the regions of formation of AgNPs.

The formation of nanoparticles with **(3)** was confined in a region of high concentration of Tollens' solution; in fact all the samples up to 1 mM of Tollens' reagent had no traces of reduction of silver. This could indicate a different mechanism of formation of the nanoparticles than the one with sugar **(1)** and partially arising in sugar2 **(2)**. Conversely, at the highest concentrations of Tollens' reagent no signs of "silver mirror" were found, which was consistent with the observations of AgNPs formed using **(2)**. We therefore propose that a new mechanism is active in sugar **(3)** for the formation and stability of AgNPs which could involve the resorcinol ether core. (See Figure 67 paragraph 2.3.12 and 2.3.16 for more details on the proposed new mechanism)

2.3.7.2 UV-Vis spectroscopy

The particles in all the samples showed a high degree of uniformity with surface plasmon resonance peaks at 421 nm as average and FWHM at 451 nm resulting in sharp and narrow peaks (Figure 48). The intensity of the plasmon peaks showed correlation with the concentration of **(3)** (Figure 49); indeed the most concentrated

sample resulted #21 with 44.39 AU (~40 times more concentrated than sugar1 **(1)** AgNPs; the sample was diluted 20 times for the measurement, then the absorbance was calculated by considering a linear response to the Lambert-Beer law).

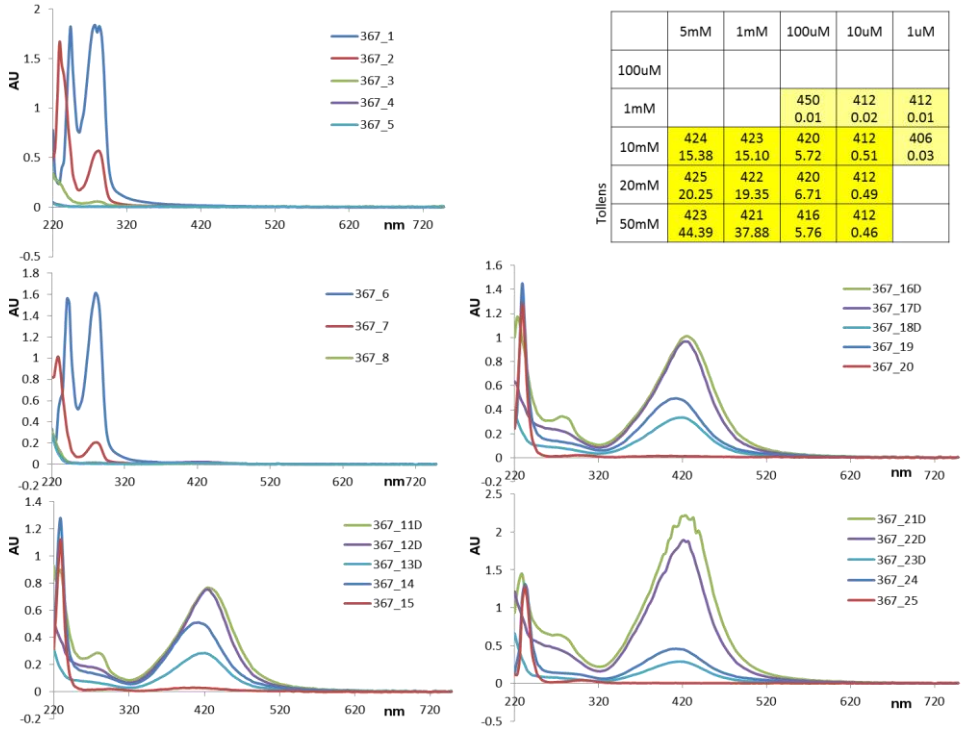

Tollens	5mM	1mM	100uM	10uM	1uM
100uM					
1mM			450 0.01	412 0.02	412 0.01
10mM	424 15.38	423 15.10	420 5.72	412 0.51	406 0.03
20mM	425 20.25	422 19.35	420 6.71	412 0.49	
50mM	423 44.39	421 37.88	416 5.76	412 0.46	

Figure 48: UV-vis spectra of samples #1-25. Samples #11-13,16-18,21-23 were diluted 1:20 prior the measurements. Absorption peaks in the range of 220-300 nm were due to sugar (3). The array table shows the same data: numbers are wavelength (nm) and intensity (in Abs units) of the resonance plasmon peak.

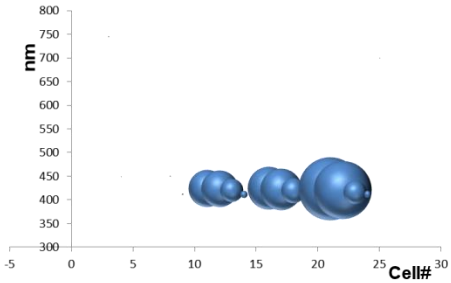

Figure 49: Relationship of cell # vs the wavelength (nm) of the plasmon resonance peak. Size of the spheres indicated the intensity.

2.3.7.3 DLS

Samples with an intense plasmon peak were measured using DLS.

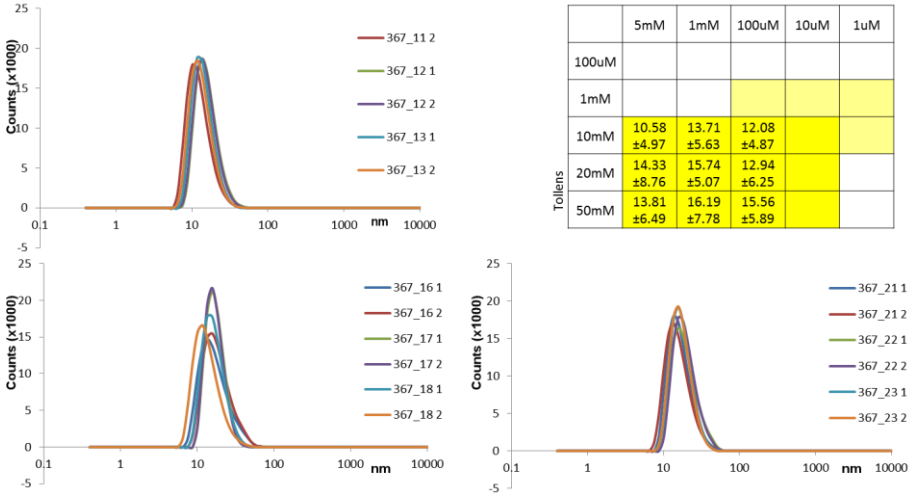

Tollens	5mM	1mM	100uM	10uM	1uM
100uM					
1mM					
10mM	10.58 ±4.97	13.71 ±5.63	12.08 ±4.87		
20mM	14.33 ±8.76	15.74 ±5.07	12.94 ±6.25		
50mM	13.81 ±6.49	16.19 ±7.78	15.56 ±5.89		

Figure 50: DLS of reactions #11-13,16-18,21-23 which formed AgNPs colloids. The table shows the average of diameter particle distribution (nm) and the dispersion as st. dev (1σ in nm).

All the samples showed a consistent 10-12 nm diameter maximum. Regions in light yellow in Figure 50 were non-reproducible due to low concentration of the particles (regions of 1-100 μM of **(3)**). Notably, the quality of the nanoparticles formed with sugar4 **(3)** were invariant of the concentration of Tollens' reagent and the concentration of sugar4 **(3)** itself. This is surprising as a similar behaviour has never been reported before and could be an important clue on the mechanism involved in the formation of the AgNPs.

2.3.7.4 Fluorescence spectroscopy

Fluorescence wavelength of AgNP@**(3)** is highly predictable and tuneable: higher concentration of sugar **(3)** makes more red-shifted particles (Figure 51).

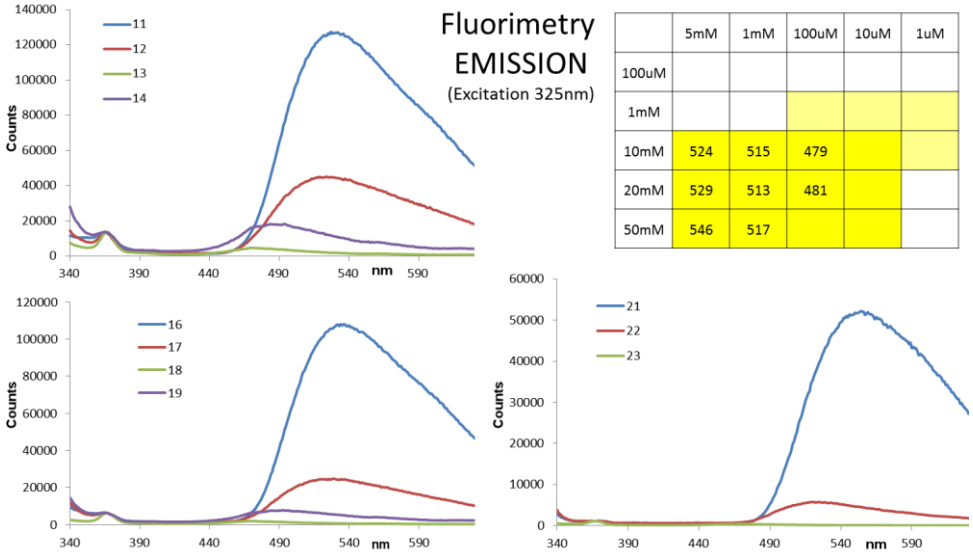

	5mM	1mM	100uM	10uM	1uM
100uM					
1mM					
10mM	524	515	479		
20mM	529	513	481		
50mM	546	517			

Figure 51: Emission fluorescence spectra of #11-23 recorded at the excitation of 325 nm. The array table reports the wavelength (nm) of the maximum of the emission peak.

Figure 52 highlighted that the fluorescence wavelength red-shift followed a logarithmic relationship with the concentration of the sugar **(3)**.

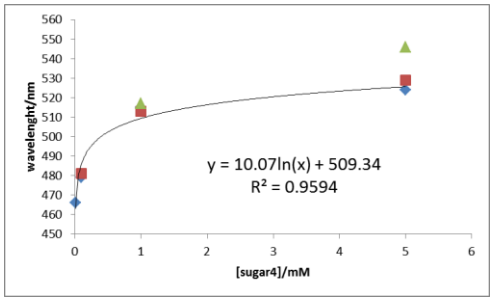

Figure 52: Logarithmic relationship between the concentration of (3) and the wavelength of the fluorescence emission peak showing a large shift at low concentration of sugar (3).

The red-shift is not an effect of partial energy dissipation due to particle-particle interactions caused by the high concentration of the samples, as dilution of the solution leaves the wavelength of the fluorescence unchanged (not shown). A proposed effect to the red-shift of the fluorescence of the particles is the interaction of the plasmon peak with the particle-bound **(3)** dendrimeric sugars. Interactions are known to red-shift the fluorescence of fluorophores bound to nano-objects[130,132,133] and could cause the same effect in the plasmon resonance.

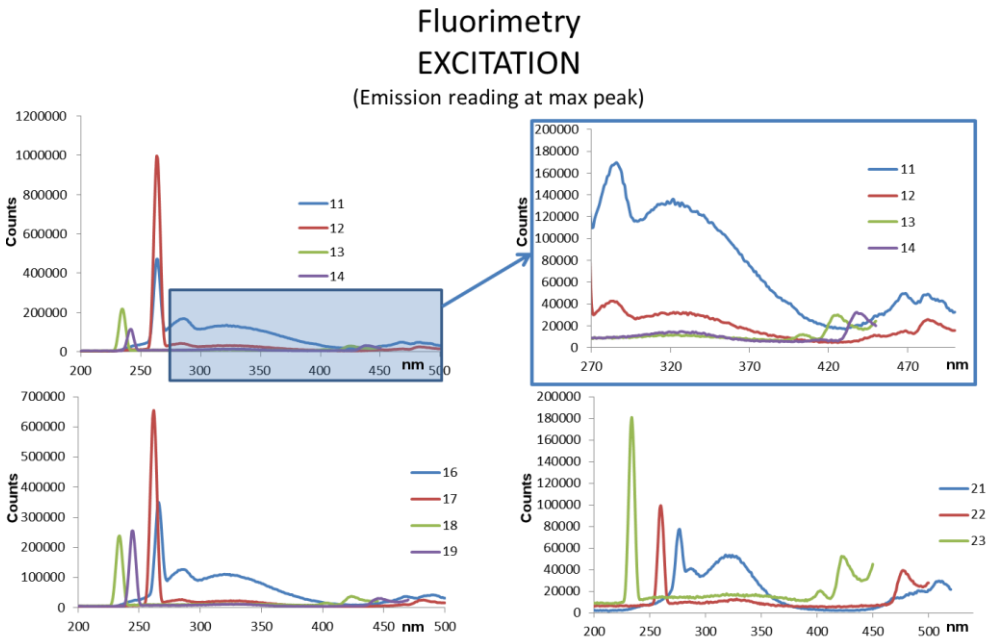

Figure 53: Excitation fluorescence spectra of samples #11-22 recorded at the emission maximum showing multiple excitation peaks.

Excitation fluorimetry of the sugar **(3)** AgNPs showed multiple excitation peaks (Figure 53). Multiple excitation peaks were already visible in AgNPs prepared with **(1)** and **(2)** but for sugar4 **(3)** this effect is more pronounced. No direct correlation was measured between the intensity of the emission peaks and the

corresponding excitation peak, inferring that the multiple excitation peaks are arising from different polyhedral shapes or different sizes of AgNPs.

2.3.7.5 TEM

Samples #12 and #17 were analysed at the electron microscope, in analogy with the analysed samples of **(2)**. Analysis of **(3)** AgNPs showed a predominance of spherical particles in both samples, similar to the results obtained with **(2)** (Figure 54). Sample #12 showed an average particle size of 9.7 nm and a dispersity of ±20% (160 particles counted). The solvation shell radius was calculated as the difference between the average hydrodynamic radius and the average particle size 13.71 - 9.7 = 4.01 nm. Such a large value is not compatible with a single layer of sugar4 molecules coating the AgNP. Sugar **(3)** has a calculated molecular volume of 1337.646 $Å^3$ (semi-empirical AM1[134]) and a spheroid-diameter of 1.367 nm. Consequently the hydrodynamic radius would be constituted by approximately 3 solvation shells of sugar **(3)** molecules. In contrast, the results with **(1)** and **(2)** showed only a single solvation shell (see paragraphs 2.3.5.5 and 2.3.6.5).

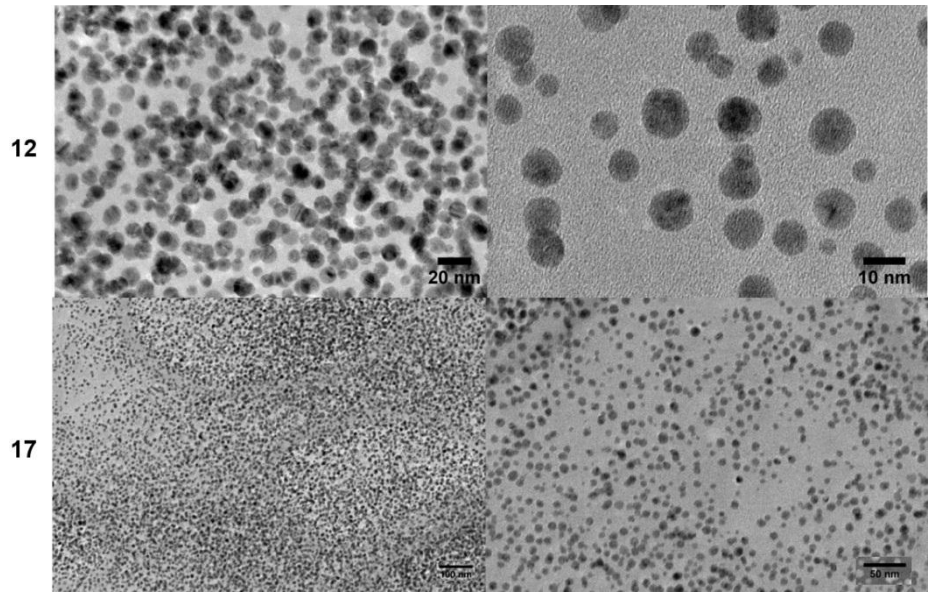

Figure 54: TEM images of sample #12 (top). TEM images of sample #17 (bottom).

HR-TEM revealed that not all the particles were spherical in shape, but a part of the population consisted of icosahedral nanoparticles (Figure 55). These particles had approximately the same average diameter and were difficult to distinguish from polycrystalline spherical particles, as opposed to mono-crystalline spherical, as shown in Figure 55.

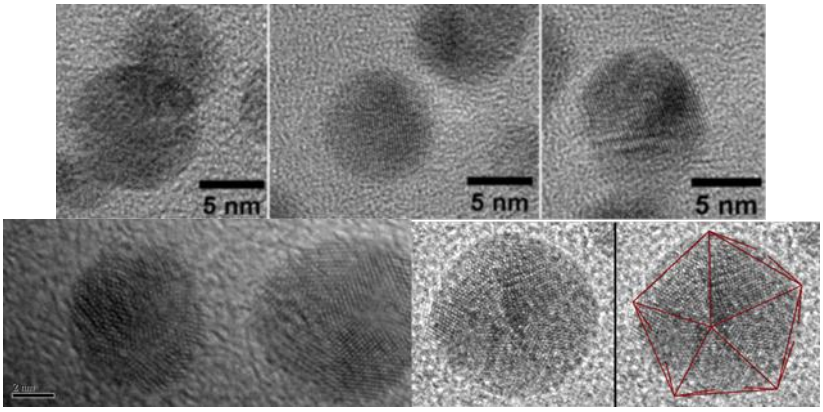

Figure 55: HR-TEM of selected spherical AgNP@(3) formed using reaction condition #12. In the bottom, example of icosahedral particle formed using reaction condition #12. On the right part of the image an overlay of the same particle with a wireframe regular icosahedron rotated to match the particle.

Figure 56 depicted the distribution analysis of AgNPs@**(3)**. The distribution analysis showed that the particles formed a single population of crystalline and mono-dispersed particles (20% dispersity).

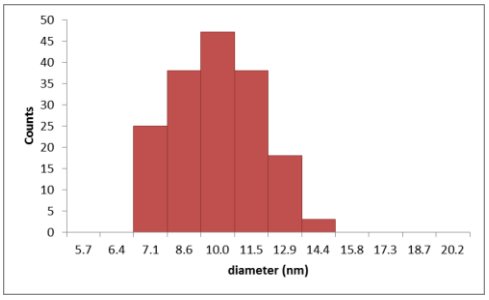

Figure 56: Dispersity of sample #12 showing an average of 9.7 nm ± 20% (160 particles counted).

2.3.8 Conclusions to AgNPs synthesis and properties.

AgNPs were prepared using sugar triazole ligands **(1)**, **(2)** and **(3)** via a mild and simple one-step process. Our novel synthetic strategy also provided AgNPs with an improved size and shape control with AgNPs@**(3)** providing monodispersed spherical particles for the first time for a Tollens' process.

2.3.9 Stability of AgNP to buffers and salts

One of the main aims of the project is to prepare AgNP that would resist aggregation in the presence of DNA, both in the cases of template synthesis of nanoparticles and the self-assembly of AgNP on DNA supramolecular structures. DNA is in fact stable only in the presence of buffers containing salts in amounts not-compatible to standard gold and silver nanoparticles. AgNP formed using **(1)**, **(2)** and **(3)** were tested for stability at 24 hours in the presence of NaCl and compared to commercially available citrate coated AgNP (Figure 57).

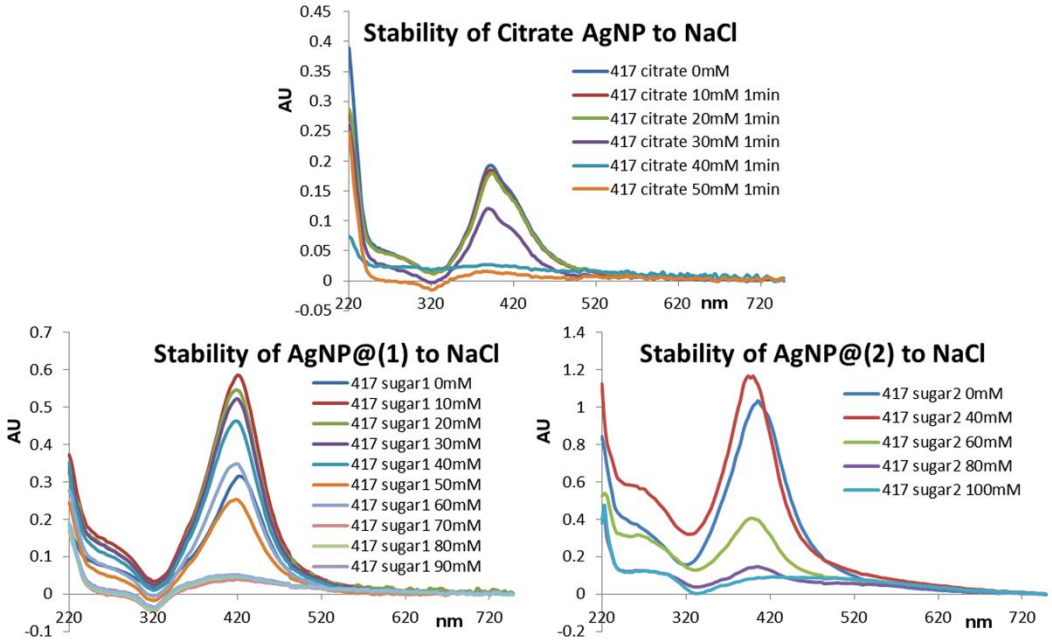

Figure 57: UV-Vis spectra were acquired at increased concentration of NaCl showing stability of AgNPs prepared with citrate, (1) and (2).

Aggregation of citrate coated AgNPs began at 30 mM NaCl and were completely aggregated at 40 mM NaCl. AgNPs@**(1)** started aggregating at 40mM NaCl and were completely aggregated at 60mM NaCl. AgNPs@**(2)** started aggregating at 40mM NaCl and were completely aggregated at 100mM NaCl. Despite a slight

increase in the stability of the particles going from citrate to **(1)** and **(2)**, none of these AgNPs exhibited adequate stability required for the use with biological macromolecules (Figure 57).

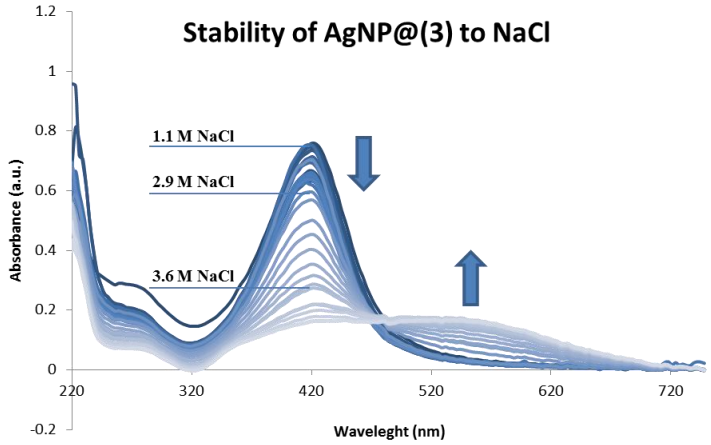

Figure 58: Stability of AgNPs@(3) sample #12 to increasing concentrations of NaCl: UV-Vis of #12 in the presence of 0 M NaCl, 0.1 M NaCl, 1.0-4.2 M at 0.1 M NaCl intervals (35 spectra in total). Spectra were registered after 24 hours incubation at 22°C. Particles started aggregating at 2.9M NaCl and were completely aggregated at 3.6M NaCl.

AgNP@**(3)** were tested in the same range of NaCl concentration used for **(1)** and **(2)** and were found to be stable up to 7 days (not shown). There are no reports in literature of AgNPs with such stability to NaCl. The concentration of NaCl was then increased in steps from 10mM to 4.2M and the stability of the particles was tested after 24 hours at room temperature (Figure 58). AgNP@**(3)** finally started aggregating at 2.9 M NaCl and were completely aggregated at 3.6 M NaCl. The particles were also tested for stability to a variety of solvents and reagents common to the preparation and manipulation of DNA. The nanoparticles were diluted 1:1 and left at 4°C for 6 months (Figure 59).

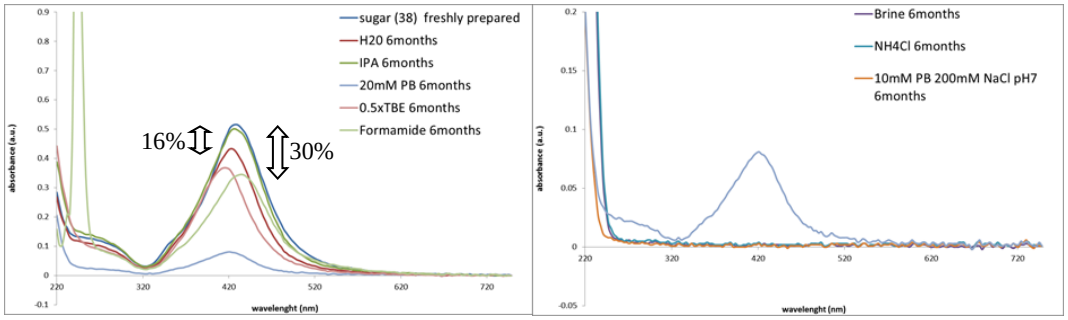

Figure 59: Stability of AgNPs@(3) to buffers (left) and high-salt buffers (right)

As expected, brine (3.45 M), NH_4Cl (2.45 M) and 10 mM phosphate buffer – 200 mM NaCl completely aggregated the particles (as denoted by the loss of the plasmon resonance peak in Figure 59), 20mM phosphate buffer partially aggregated the particles with 15.7% left of the original plasmon peak (Figure 59). Formamide and 0.5x TBE resulted in solutions that had lost 30% of the plasmon peak intensity. This result was still inferior to pure water with 16% loss of plasmon peak, however it showed that TBE 0.5x was a suitable buffer for AgNP made with **(3)**. Isopropyl alcohol preserved the AgNP better than pure water, with only a 3% loss of the plasmon peak after 6 months. In conclusion, AgNPs@**(3)** showed a remarkable stability in aqueous buffered solutions and preservation for longer periods (6 months at 4°C) similar to commercially available citrate coated AgNPs.

2.3.10 Necessity of sugar controls

The AgNPs prepared with **(2)** and **(3)** had a number of novel properties such as high resistance to salts, size and shape controls during synthesis. In particular, for the first time a Tollens' reagent formed silver nanoparticles consistently with a size of 1-10 nm, with a significant deviation from the known 40 nm glucose –

Tollens' particles. AgNP@**(3)** showed the most significant salt stability. As these results were thought to arise from the resorcinol ether core structure of **(2)** and **(3)**, a number of control molecules were synthesised to test this hypothesis (showcase of all the controls can be seen in Figure 61).

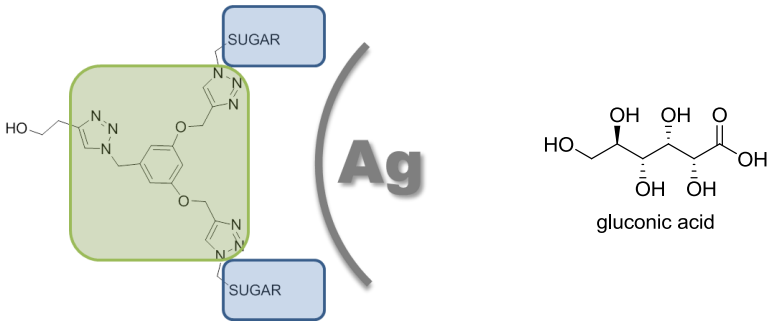

Figure 60: Schematic representation of sugar (2) binding on the surface of a silver nanoparticle. Blue boxes represent the sugar moieties, while the green box highlights the resorcinol ether core. On the right, schematic structure of gluconic acid.

In a classical Tollens' reaction with glucose, the "silver mirror" surface is coated with gluconic acid (Figure 60) and other carboxylic acids produced by the oxidation of the glucose itself.[70] Since sugars **(2)** and **(3)** contain 2 and 4 sugar moieties respectively, there were strong suggestions that these sugars could bind on the surface of a silver nanoparticle forming a much stronger monolayer by chelation effect (Figure 60).[135] Moreover, silver is known for its high affinity to nitrogen.[136] In particular, the triazole groups present in the skeleton of the sugars could potentially bind the silver surface, in a similar way to imidazoles binding gold surfaces.[137] If this binding occurs during AgNP synthesis, its effect would be detectable around the silver centres before the synthesis as chelation to Ag^{+} ions and after synthesis as binding on the surface of the $Ag^{(0)}$ of AgNPs. To test that, a

number of control molecules were prepared to determine the influence of sugar chelation and imidazole binding.

2.3.10.1 Synthesis of sugar controls

Scheme 7 depicts the preparation of sugar controls used to test whether AgNPs would form in the presence of Tollens'.

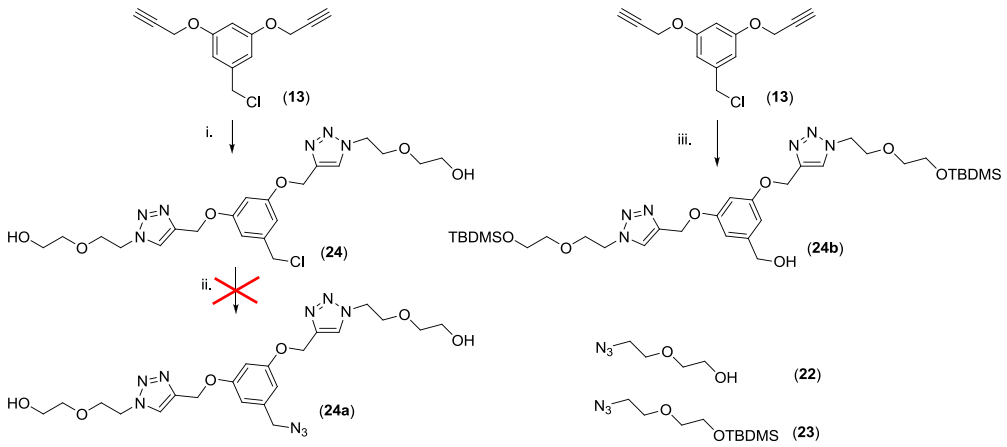

Scheme 7: unsuccessful synthetic strategy for the preparation of compounds (24a) and (24b): i. (22), $CuSO_4$-ascorbate ii. NaN_3, reflux iii. (23), $CuSO_4$-ascorbate, EtOH.

1-(chloromethyl)-3,5-bis(prop-2-ynyloxy)benzene **(13)** was reacted with azide **(22)** to afford the core **(24)** in 40 % yield. Compound **(24)** was reacted with NaN_3 in water/acetone, to produce an unknown dimer (MS: 959.19). As the dimer was thought to be produced by the reaction of the benzyl chloride with the ethylene glycol portion of the molecule, a second approach was investigated by the use of tert-butyl-dimethylsilyl (TBDMS) protecting group in the form of the azide **(23)**. The click-chemistry reaction was then attempted in various guises, but it always afforded the benzyl alcohol derivative **(24b)**. An additional effort was made to reconvert this last product to benzyl chloride with $SOCl_2$ without success. As the

preparation of additional sugars from the compound **(13)** core had synthetic problems, a simpler approach was devised based on the resorcinol unit.

The sugar controls prepared can be subdivided in 3 classes. The first investigated derivatives of resorcinol, a core that is roughly equivalent to **(2)**. This resorcinol core was prepared with two galactose **(6)** units, one galactose **(6)** unit, and one or two ethylene glycol moieties, derived from azide **(22)**, respectively (Scheme 8 and Scheme 9). The last one can act both as a templating test and as a negative control of the first two molecules. The second class includes two compounds containing 1-methoxy-galactose acetals **(32)** and would provide data on the chelation effect since acetal sugars are locked in a ring form and the aldehyde is not available for reactions with the Tollens' reagent. The third class contains the simple triazole-PEG molecule **(35)** that will be used as a negative control as this molecule contains no reducing sugars and a single triazole (Scheme 9).

Resorcinol **(25a)** was heated to reflux with propargyl-bromide **(17)** with K_2CO_3 in acetone over 24 hours whereas 1,3-bis(prop-2-ynyloxy)benzene **(25)** was obtained in 76% yield using column chromatography purification. Click-chemistry of this product with 0.65 eq (sub-stoichiometric) of sugar-azide **(6)** afforded a distribution of products between mono-clicked **(28)** and bis-clicked sugars **(27)** in 33% and 15% yield respectively. Compounds **(28)** and **(27)** were then reacted with TFA at 65°C for 3 hours to afford the deprotected sugars **(30)** and **(29)** with 99% and 21% yields respectively.

Both the 1,3-bis(prop-2-ynyloxy)benzene **(25)** and the mono clicked resorcinol **(30)** were reacted with 2-(2-azidoethoxy)ethanol **(22)** by click-chemistry to afford compounds **(26)** and **(31)** respectively.

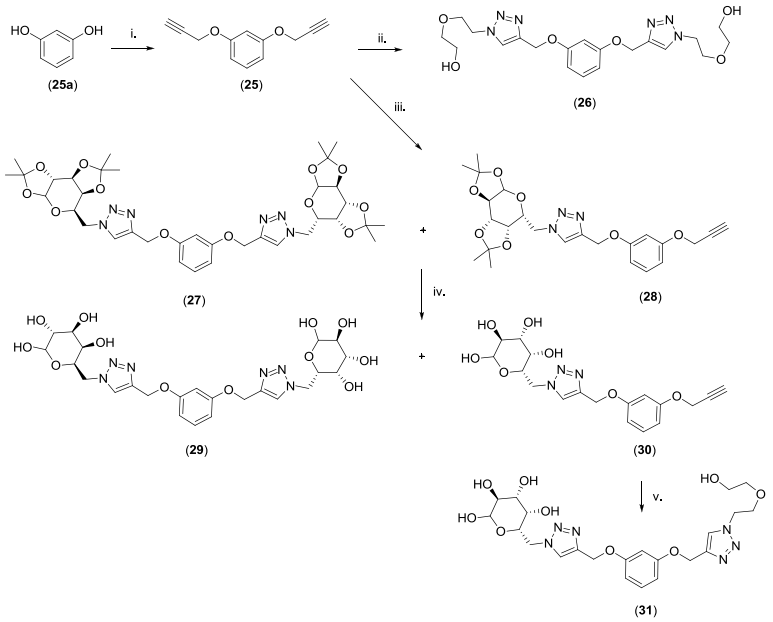

Scheme 8: Synthetic approach to the preparation of compounds (29), (31), and (26). i. (17), reflux, K_2CO_3, 24h, 76% ii. (22), $CuSO_4$-ascorbate iii. (6) 0.65eq, $CuSO_4$-ascorbate, 15% (27) and 33% (28) iv. TFA, 65°C, 3h, 21% (29) and 99% (30) v. (22), $CuSO_4$-ascorbate.

Sugar azide **(6)** was heated to reflux overnight in dry HCl/MeOH to afford the methoxy acetal azide **(32)** after recrystallization from ethyl acetate/MeOH in 86% yield. Methoxy acetal azide **(32)** was then reacted by click-chemistry with mono clicked resorcinol **(28)** and 3-butyn-1-ol **(9)** to afford compound **(33)** and compound **(34)** after purification by semi-preparative HPLC with 20% and 97% un-optimised yield respectively. The formation of triazole between 2-(2-azidoethoxy)ethanol **(22)** and 3-butyn-1-ol **(9)** in water with $CuSO_4$/ascorbate afforded the compound **(35)** after semi-preparative HPLC purification in 65% yield.

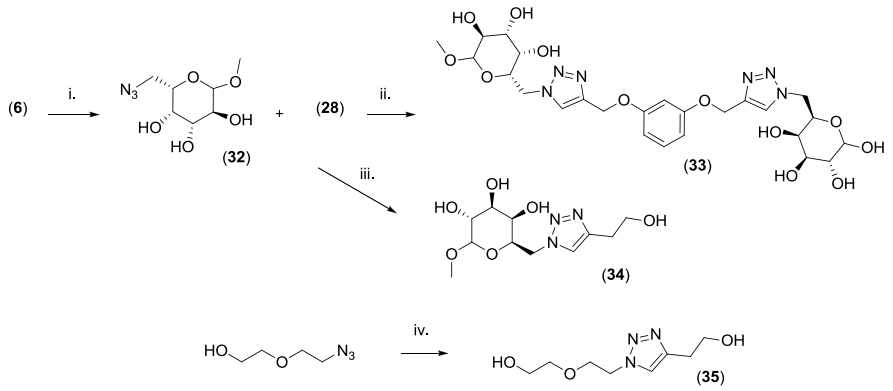

Scheme 9: Synthetic approach to the preparation of compounds (33), (35) and (34). i. HCl/MeOH, reflux, 18h, 86% ii. (28), $CuSO_4$-ascorbate, 20% iii. (9), $CuSO_4$-ascorbate, 97% iv. (9), $CuSO_4$-ascorbate, 65%.

2.3.10.2 Preparation of AgNP with sugar controls

Compounds **(29) (31) (26)**, including the negative controls **(33) (35) (34)**, could reduce the Tollens' reagent (Figure 61). Compound **(29)** failed to stabilise the nanoparticles that aggregated in large dark flakes or formed silver mirror. The same happened to compound **(31)** with the exception of cell #4, where a very weak plasmon peak of 0.02 AU was found. We also observed the importance of the third triazole in **(2)** as the lack of it completely changed the properties of the sugars by losing the ability to stabilise the particles. Compound **(26)** was actually able to form nanoparticles at high concentration (50 mM); since the compound lacks any reducing sugar, a mechanism where the ethylene glycols are oxidised could be responsible for the formation of the AgNPs. Abdul Kareem already exploited this in his AgNPs preparation.[74] Compounds **(33)** and **(34)** formed no stable colloids and silver mirror was present at high concentration of Tollens' reagent. Lastly, compound **(35)**, also behaved as a weak reducing agent and formed black aggregates of silver at the bottom of the vials. The behaviour only

appeared at a low concentration of sugar, in contrast to all the other tested compounds. This could be explained as an indirect oxidation by oxygen once all the molecules of compound **(35)** are oxidised: at higher concentration, the effect is not happening due to the large amount of the weakly reducing compound.

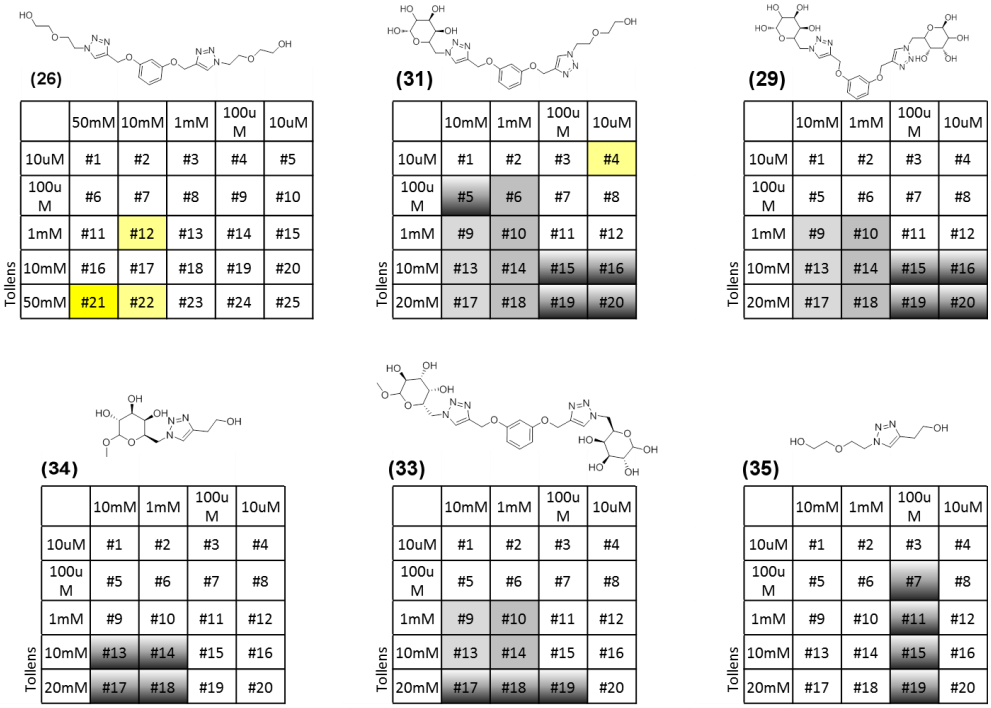

(26)	50mM	10mM	1mM	100uM	10uM
10uM	#1	#2	#3	#4	#5
100uM	#6	#7	#8	#9	#10
1mM	#11	#12	#13	#14	#15
10mM	#16	#17	#18	#19	#20
50mM	#21	#22	#23	#24	#25

(31)	10mM	1mM	100uM	10uM
10uM	#1	#2	#3	#4
100uM	#5	#6	#7	#8
1mM	#9	#10	#11	#12
10mM	#13	#14	#15	#16
20mM	#17	#18	#19	#20

(29)	10mM	1mM	100uM	10uM
10uM	#1	#2	#3	#4
100uM	#5	#6	#7	#8
1mM	#9	#10	#11	#12
10mM	#13	#14	#15	#16
20mM	#17	#18	#19	#20

(34)	10mM	1mM	100uM	10uM
10uM	#1	#2	#3	#4
100uM	#5	#6	#7	#8
1mM	#9	#10	#11	#12
10mM	#13	#14	#15	#16
20mM	#17	#18	#19	#20

(33)	10mM	1mM	100uM	10uM
10uM	#1	#2	#3	#4
100uM	#5	#6	#7	#8
1mM	#9	#10	#11	#12
10mM	#13	#14	#15	#16
20mM	#17	#18	#19	#20

(35)	10mM	1mM	100uM	10uM
10uM	#1	#2	#3	#4
100uM	#5	#6	#7	#8
1mM	#9	#10	#11	#12
10mM	#13	#14	#15	#16
20mM	#17	#18	#19	#20

Figure 61: Arrays for the preparation of AgNPs with the sugar controls (26), 29), (31), (33), (34) and (35). Yellow boxes represent AgNP formation and grey boxes represent silver mirror formation. Shaded grey boxes represent the formation of deposits of large micron-sized particles.

2.3.10.3 Rationalization of the results

All the compounds made as controls failed to stabilise silver nanoparticles, with the exception of compound **(26)**, which could stabilise AgNP at high concentrations. This effect could be explained with the ability of poly-ethoxilated compounds (like PEGs or PVP) to form sol-gel superlattice networks at high concentration and consequently stabilise the nanoparticles with a dual effect of

confinement and surfactant coating.[74] In all the other cases, this effect was not seen. However on the light of these negative results, a major role to the structure-activity relationship (SAR) of the third triazole was inferred (Figure 62).

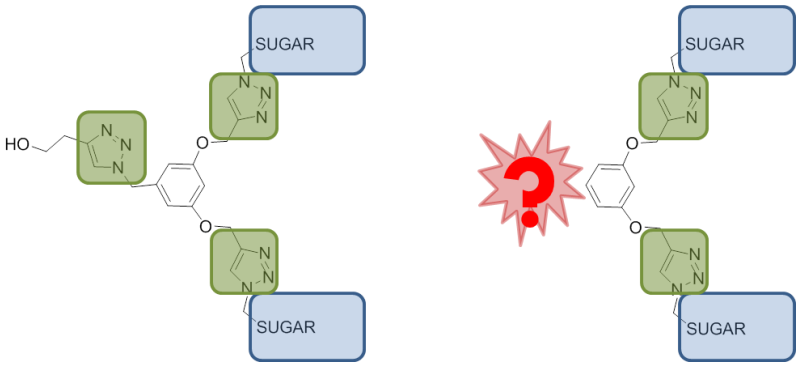

Figure 62: Schematic representation of sugars based on (2) (left) and on resorcinol (right); the absence of the third triazole is the key factor affecting the properties of the compounds.

Considering sugars **(3)** and in particular **(2)**, the addition of a third triazole on the aromatic ring could have a great effect on the stability of the resulting nanoparticles. If this is true, then such an effect should be detectable by spectroscopy. Surface enhanced Raman scattering (SERS) should return a strong enhancement to the nitrogen-nitrogen bonds if the triazoles are interacting with the surface of the silver nanoparticle. NMR should detect interactions of the triazoles with Ag^+ ions in the early stages of the silver oxidation and later after the formation of the particles, interaction with the silver surface. HR-MS spectroscopy would identify the formation of small silver nanoclusters, and the formation of chelates between silver ions and the sugars. All of these spectroscopic techniques will be discussed in the next paragraphs.

2.3.11 Time-resolved kinetic experiments

Kinetics experiments of AgNP formation were then conducted as a function of reducing sugar type (**1, 2, 3**) using the formation of the surface plasmon peak at ~400 nm as the diagnostic marker. For each of the sugar triazoles (**1, 2, 3**) investigated, an autocatalytic process was observed (Figure 63). The onset of AgNP@**(1)** formation was observed at ~ 2000 s with an endpoint at 2868 s using the optimised conditions (100 μM sugar **(1)**, 1 mM Tollens') for their formation. A significantly faster reaction rate [onset ~ 1000 s] was observed when D-galactose was used as the silver(I) reductant to form AgNP@D-galactose,[138] suggesting that the triazole unit in **(1)** is involved in the slower rate of AgNP@**(1)** formation (Figure 63).

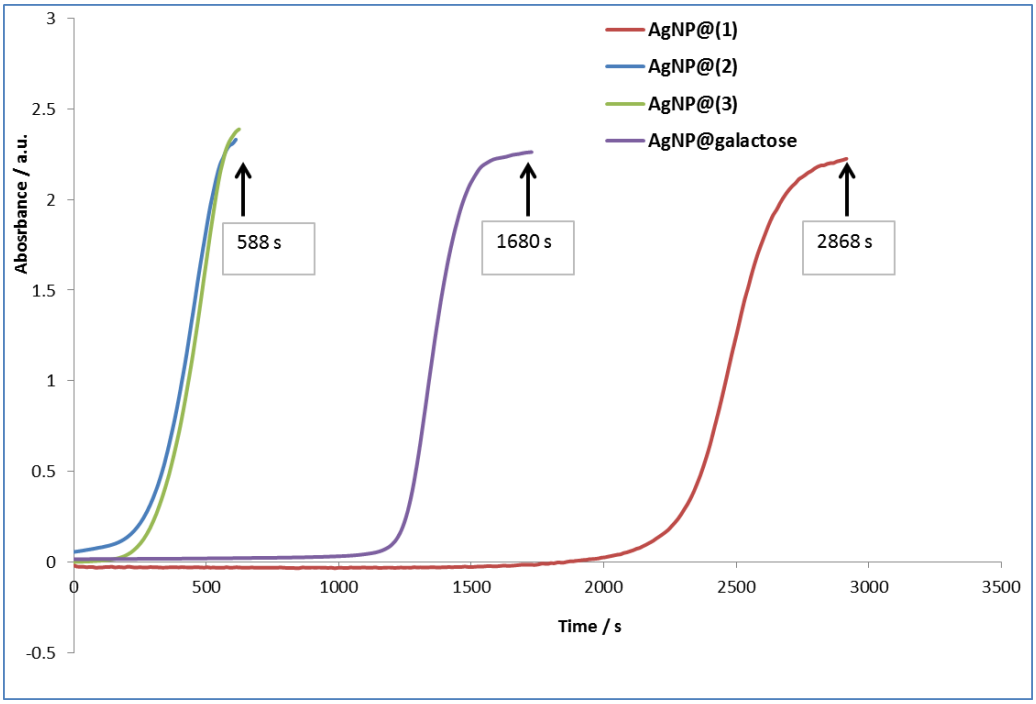

Figure 63: Kinetics of AgNP formation using sugar ligands (1, red), (2, blue), (3, green) and D-galactose (purple). AgNP formation was monitored by the formation of the surface Plasmon peak at 400 nm at the temperature of 20° C.

In contrast to the AgNP@**(1)** and AgNP@D-galactose systems, the reaction kinetics of both AgNP@**(2)** and AgNP@**(3)** were significantly faster (Figure 63). Intriguingly, the rate of onset (~ 120 s) and the end point (~ 588 s) of both AgNP@**(2)** and AgNP@**(3)** were virtually identical.[138] Thus, based on the kinetic data, an increase in the number of reducing sugars from one **(1)** to two **(2)** increased the rate of AgNP formation, however a further increase in the number of reducing sugars from two **(2)** to four **(3)** had little effect on the reaction rate. The similar reaction kinetics of AgNP@**(2)** and AgNP@**(3)** formation was also in line with the similarities in their particle sizes [AgNP@**(2)** ~8nm and AgNP@**(3)** ~ 10nm]. We also observed that the presence of the triazole unit in sugar **(1)** slowed the rate of AgNP@**(1)** formation relative to the rate of formation of AgNP@D-galactose. The rate of both AgNP@**(1)** and AgNP@D-galactose formation was significantly slower than AgNP@**(2)** and AgNP@**(3)**, resulting in the following trend: rate of AgNP formation AgNP**(2)** ≈AgNP**(3)** >> AgNP@D-galactose > AgNP@**(1)**. This trend cannot be rationalised by an increase in only the reducing sugar moieties, as based on this rationale the sugar **(3)** system should exhibit a considerably faster rate of AgNP formation relative to sugar **(2)**. Therefore, taken collectively with the TEM studies, we concluded that the resorcinol ether core structure of the sugar triazole **(2)** was a key determinant in the increased rate of the reaction kinetics relative to **(1)**.

2.3.12 NMR experiments

Natural silver occurs in two isotopic forms ^{107}Ag and ^{109}Ag. Both of them possess spin ½ and the NMR spectroscopic properties are similar. Silver is diamagnetic

and possesses very low NMR sensitivity and long relaxation times. These properties combined enable the acquisition of classical ^{1}H and ^{13}C NMR experiments in the presence of silver atoms without special optimizations of the acquisition parameters.[139] They also allow the detection of interacting organic molecules as chemical shift of NMR signals are displaced by complexation of silver atoms.[140] It was hinted in the previous paragraphs that sugars **(1)** and **(2)** could potentially chelate Ag^{+} ions and so pre-concentrate and stabilise early small silver nanoclusters formation. A series of NMR experiments were designed at increasing concentrations of $AgNO_3$ in the presence of sugars **(1)** or **(2)** and compared to D-galactose and sugar control **(29)** respectively (Figure 64).

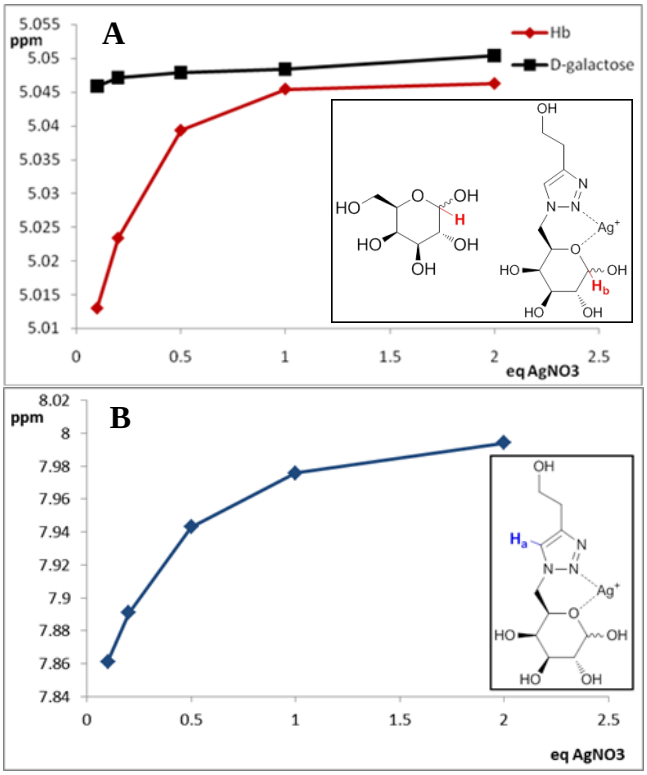

Figure 64: Plots of the ^{1}H-NMR titration of sugar (1) and D-galactose (4.2 mM) with $AgNO_3$ in D_2O (no data fitting was used). A. Plot of the anomeric proton. B. Plot of the aromatic proton.

The triazole proton (H_a, highlighted in blue, Figure 64B) and the anomeric sugar H1' (H_b highlighted in red, Figure 64A) of **(1)** were used as diagnostic markers for Ag^+ coordination. Titration of up to 1.0 equivalent of $AgNO_3$ resulted in a 0.2 ppm downfield shift of the triazole proton H_a using a concentration of 4.2 mM of **(1)**. This downfield shift reached a maximum at a 1 : 1 Ag^+ : **(1)** ratio (Figure 64). Concomitantly, a downfield shift (13 Hz, 0.026 ppm) of H_b was also observed, which, much akin to H_a, reached a maximum at a 1 : 1 Ag^+ : **(1)** stoichiometry, suggesting the formation of a Ag^+•**(1)** complex. Collectively these results pointed towards the formation of a complex such as **(36)**, which involved Ag^+ coordination to N2 of the triazole ring and the pyranosyl oxygen (Figure 65). We propose a coordination to the pyranosyl oxygen because this would lead to the 6-membered ring chelate but we cannot rule out coordination to the anomeric hydroxyl group, although this is less likely as this would lead to an 8-membered ring chelate. In contrast to the sugar triazole **(1)** titration experiment, a comparable titration of Ag^+ into an aqueous solution containing D-galactose did not afford a similar downfield shift of any of the sugar protons (Figure 64), highlighting the importance of the triazole unit in directing the coordination of Ag^+ towards the pyranosyl oxygen.

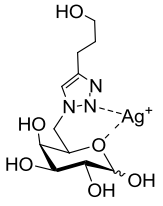

(36)

Figure 65: Structure of the proposed chelate (36) between sugar (1) and Ag^+

Surprisingly, very different behaviour was observed in the titration experiments when sugar **(2)** was used. In this example, triazole protons showed a similar downfield response [i.e. 0.2ppm or 100 Hz for H_c and 110Hz for H_d] to the addition of one equivalent of Ag^+ at a concentration of 2 mM. The downfield shift of H_d then reaches a maximum at a Ag^+ : **(2)** ratio of 1 : 1, whereas the downfield shift of H_c reaches maximum at a 2 : 1 Ag^+ : **(2)** ratio (Figure 66).

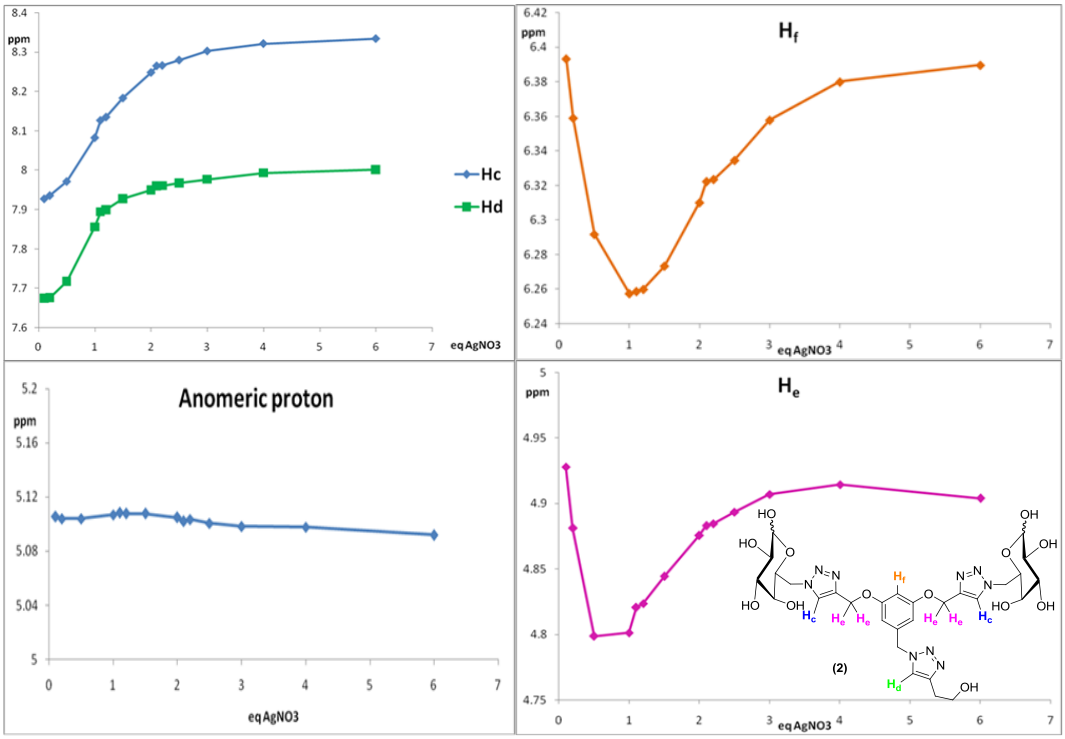

Figure 66: Plots of the ^{1}H-NMR titration of sugar (2) with $AgNO_3$ in D_2O (no data fitting was used).

This suggests that in the presence of one equivalent of Ag^+, all three triazole units work in concert to coordinate a single Ag^+ cation, resulting in the putative formation of a novel tridentate complex **(37)** (Figure 67).

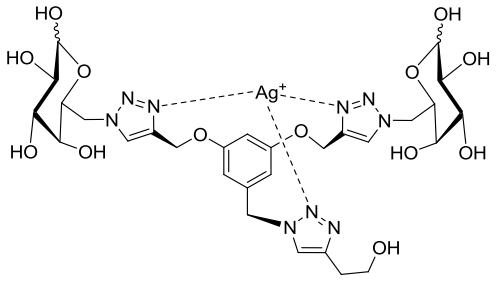

(37)

Figure 67: Structure of the proposed chelate (37) of sugar (2) with Ag^+

Consistent with the ability of the resorcinol ether core structure to provide an appropriate molecular framework to template the coordination of Ag^+, similar Ag^+-binding behaviour was also observed with sugar **(29)** (Figure 68), where in this respect, a concerted downfield shift of H_g protons was also observed.

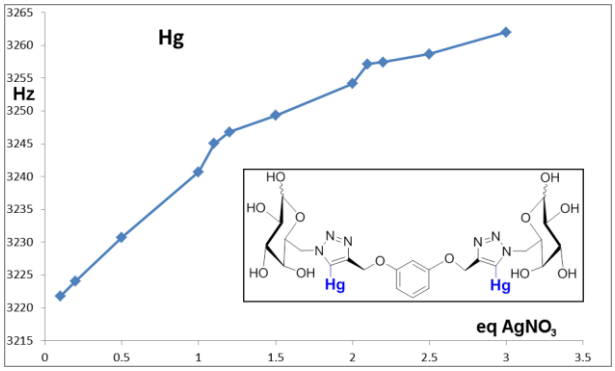

Figure 68: Plot of the ^{1}H-NMR titration of sugar control (29) with $AgNO_3$ in D_2O (no data fitting was used).

A significant deviation from the behaviour observed in the Ag^+•**(1)** complex was the lack of a downfield shift of the anomeric (H1') proton in Ag^+•**(2)** complexes, which was indicative of a fundamentally different coordinating behaviour and provides further support for the chelation of the Ag^+ by the triazoles rather than the utilization of the pyranosyl oxygen. This was also underpinned by an *upfield* shift observed for both H_e and H_f up to a 1 : 1 Ag^+ : **(2)** ratio. An upfield shift of

this kind has recently been observed in other triazole•Ag^+ complexes, in which the authors suggested the presence of face-to-face π-π stacking interactions (anisotropic effect caused by diamagnetic ring currents).[141] Beyond a 1 : 1 Ag^+ : **(2)** stoichiometry, resulted in a gradual return to a similar chemical shift position of H_e and H_f observed in the free ligand state after the addition of an excess amount of Ag^+ (i.e. > 3.0 equivalents). Taken collectively, these observations therefore suggested that sugar **(2)** coordinates one equivalent of Ag^+ via the three triazoles, resulting in the formation of a species such as **(37)** (Figure 67). Subsequent addition of Ag^+, resulted in the formation of multi-metal metallocyclic species.[141] Stability constants can be extracted from the NMR chemical shift data when in a system all the species are in rapid equilibrium in the experimental conditions. Usually, a large excess of one of the reagents is necessary to extract stability constants from NMR chemical shifts as in the common Benesi–Hildebrand approach.[142] More recently, non-linear fitting computer models allowed the extraction of data from interacting species with relatively similar concentrations.[142] The acquired NMR data of sugars **(1)**, **(2)** and **(29)** was then fed to WinEQNMR2[g] software[143] to extrapolate the stability constants as by the simple formula:

$$K_a = \frac{[Sugar \cdot Ag^+]}{[Sugar][Ag^+]}$$

[g] WinEQNMR2 Version 2.00 by Michael J. Hynes

The results were then plotted in the following table:

Compound	K_a (M^{-1})	Log K_a
Sugar1 **(1)**	483 ± 15	2.684 ± 1.177
Sugar2 **(2)**	72393 ± 2	4.859 ± 0.219
Sugar control **(29)**	160 ± 1	2.20433 ± 0.08854

Table 6: K_a and LogK_a values of sugar (1), (2) and (29) obtained by non-linear curve fitting of NMR chemical shift calculated by software WinEQNMR2g

At first glance, the K_a values of **(1)** and sugar control **(29)** can be considered as "weak" interactions.[142] However, although these values are considerably smaller than well-known association constants such as crown ethers with K_a ~10^5 M^{-1},[142] they are still much larger than solvent effect values of K_a= 0.1-1 M^{-1}.[144] Sugar control **(29)**, while possessing two sugar moieties and two triazoles, returned a K_a value ~3 times lower than **(1)**. Compound **(2)** K_a value was instead ~150 times greater than **(1)**. A trend was visible that mimicked the ability of the sugars to form and stabilise AgNPs: **(29)** formed little or no AgNPs, **(1)** formed ~40 nm particles and **(2)** stabilised smaller ~10 nm AgNPs. It is therefore proposed that, for sugars reacting with the Tollens' reaction, the association constant of silver ions with the sugars is an important factor for the successful formation of AgNPs. Even if this behaviour was already generally perceived in literature in an empirical way, this is the first example of calculated association constants applied to the formation of AgNPs. Moreover, this approach could lead to the prediction

of novel and optimised sugars for stabilisation of highly sought ultra-small AgNPs.

2.3.13 HR-MS spectra

Mass spectrometers using time of flight (TOF) detectors are known to return intense spectra of clusters of inorganic "charged particles". Small silver nanoclusters with a limited number of silver atoms can be detected and analysed by mass spectroscopy as inorganic ions with organic charged ligands on the surface (for example citrate or lipoic acid, Figure 69).

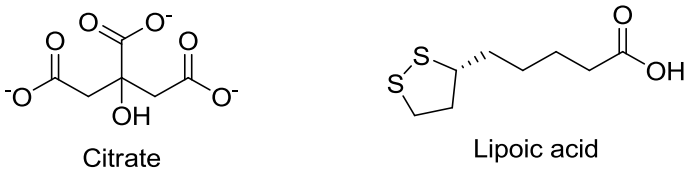

Figure 69: Structure of citrate ion and lipoic acid, two common surfactants uses with AgNPs.

The ionization method for the mass spectroscopy is also fundamental in the detection of clustering. One of the softest methods is matrix assisted laser desorption and ionization (MALDI), which is known to be able to avoid fragmentation of small silver nanoclusters. Rao *et al.* demonstrated the analysis of Ag_7 and Ag_8 nanoclusters by MALDI-TOF using DCTB (trans-2-[3-(4-tert-butylphenyl)-2-methyl-2-ropenyldidene]malononitrile, Figure 70).[128]

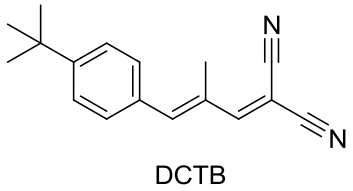

Figure 70: Structure of DCTB: a MALDI matrix used in the detection of metal clusters.

Using this technique, sample #11 of sugar **(2)** AgNP was analysed using DCTB as matrix and showed the presence of Ag_9 clusters that were previously reported by Henglein.[70]

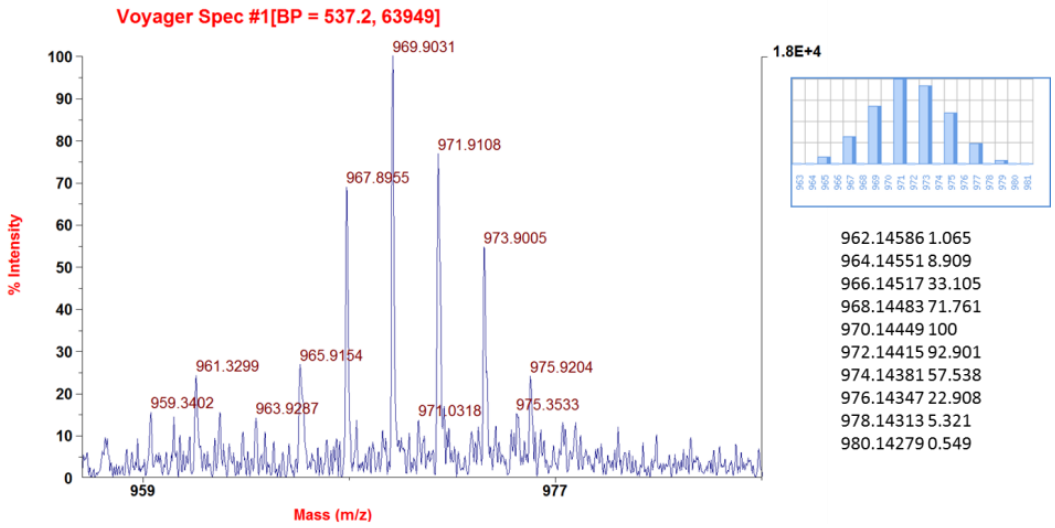

Figure 71: MALDI-TOF-MS spectrum of Ag_9 cluster. On the right theoretical calculation of the mass peaks and peak intensity for Ag_9

Unfortunately clustering with **(3)** was not detected in any sample, and no presence of smaller or larger nanoclusters was found (up to cluster of ~1.6nm, 125 Ag atoms, 13548 kDa). AgNPs@**(1)** from sample cell #17 were also analysed with no detectable peaks. Due to the characteristics of the MALDI-TOF MS spectrometer used and the necessary preparation of the sample, the nanoclusters could potentially aggregate or the sugars could dissociate from the surface due to their low binding strength (as found by NMR data in paragraph 2.3.12). Analysis of liquid samples using ESI-TOF could eventually return more data than with a MALDI. Samples of sugar **(1)**, **(2)** and **(3)** freshly prepared AgNPs were injected

through a custom peristaltic pump into an ESI-TOF MS spectrometer using water : MeOH 9:1 as carrier solution.

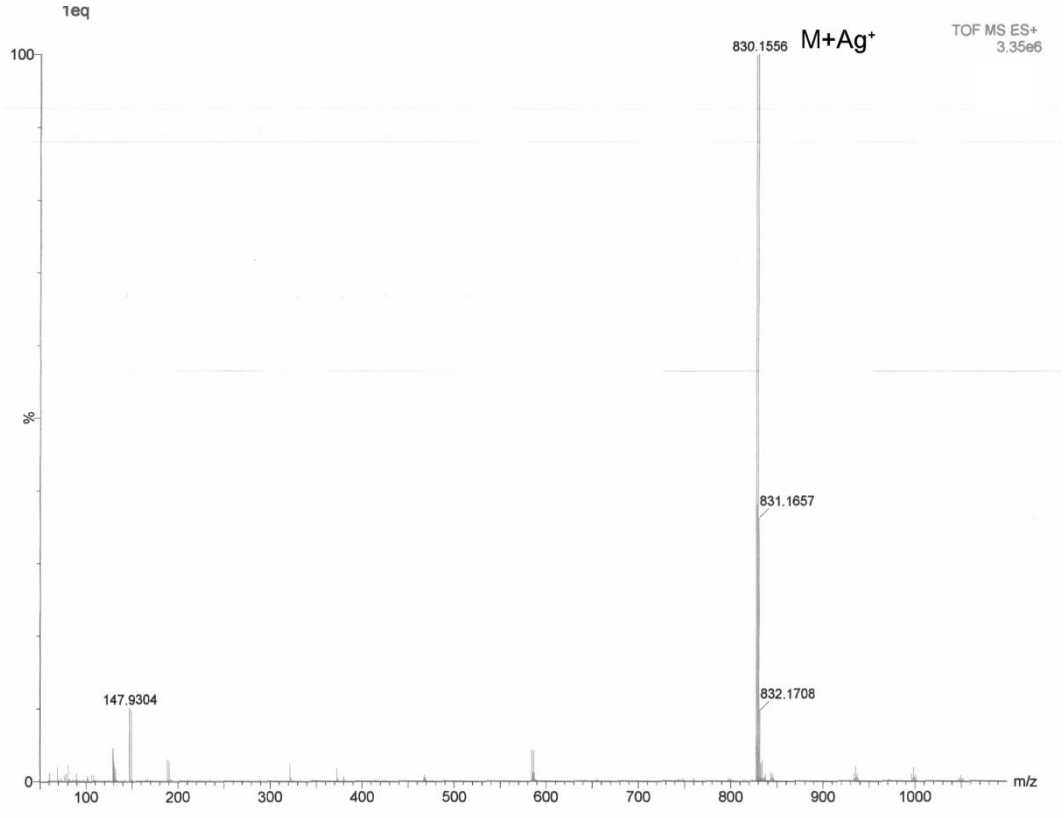

Figure 72: HRMS (ESI-TOF) of a solution of (2) with 1 eq of $AgNO_3$ in H_2O.

ESI-MS analysis of a Ag^+•**(2)** complex at a 1 : 1 Ag^+ : **(2)** ratio afforded the molecular ion *m/z* 828 (Figure 72) corresponding to the monomeric complex [**(2)**+Ag]$^+$ as the predominant species present, whereas in the presence 3 : 1 Ag^+ : **(2)** ratios, molecular ions corresponding to [**(2)**+2Ag]$^+$ and [**(2)**+3Ag]$^+$ begin to form over [**(2)**+Ag]$^+$ (Figure 72 and Figure 73).

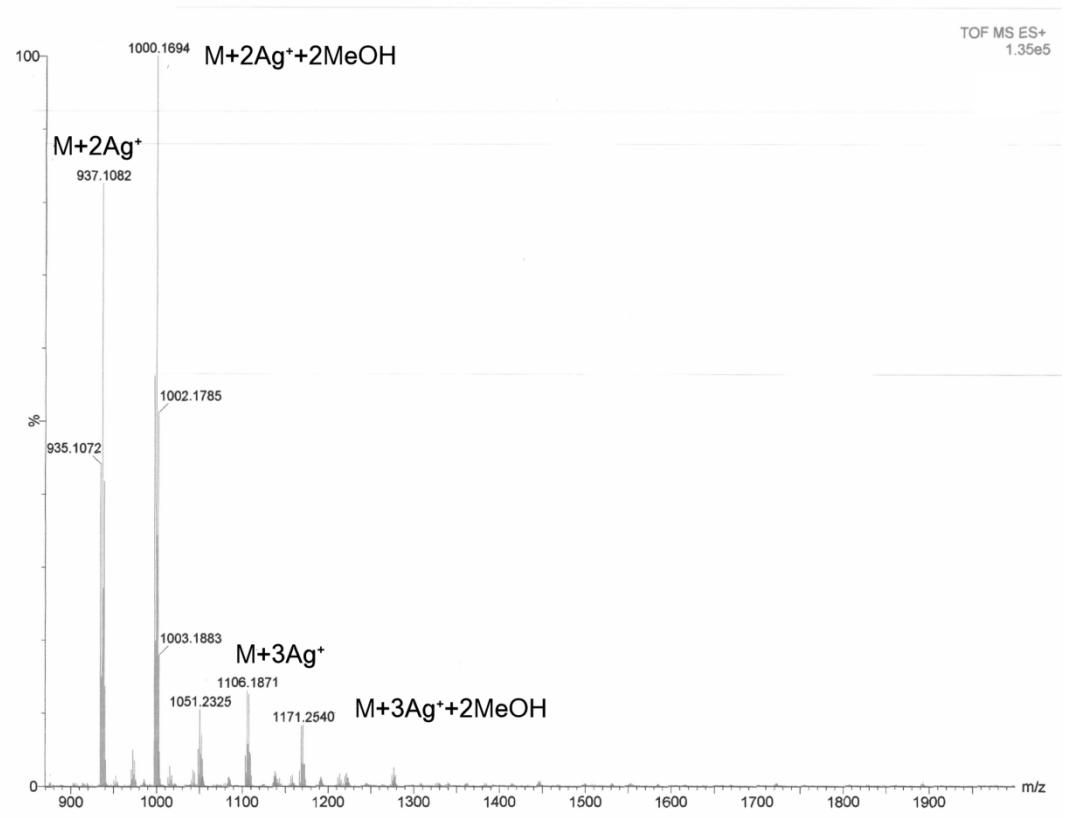

Figure 73: Selected areas of HRMS (ESI) of a solution of (2) with 3 eq of $AgNO_3$ in H_2O expanded x20 to show details of higher order cluster formation.

From these results we therefore conclude that sugars **(1)** and **(2)** complex Ag^+ in a fundamentally different manner. In Ag^+•**(1)** complexes, Ag^+ is coordinated to **(1)** in a 1 : 1 ratio via the triazole and most likely the pyranosyl oxygen to form a stable six-membered ring as highlighted in **(36)**. In contrast, a tridendate system **(37)** is formed when sugar **(2)** is used at 1 : 1 Ag^+ : **(2)** ratios, which crucially, *does not involve coordination with the pyranosyl oxygen but in fact coordination of* ***(2)*** *with* Ag^+ *is achieved via the three triazoles.*

2.3.14 X-Ray analysis of AgNP@(2)

A final confirmation of the clustering observed in NMR and MS spectroscopy would come from crystallographic data. Crystallization of sugar **(2)** was attempted in water, in solvent, with and without Ag+ ions, but without success. X-ray diffraction of a lyophilised crude AgNPs sample (Sugar **(2)** cell #17) was obtained (Figure 74).

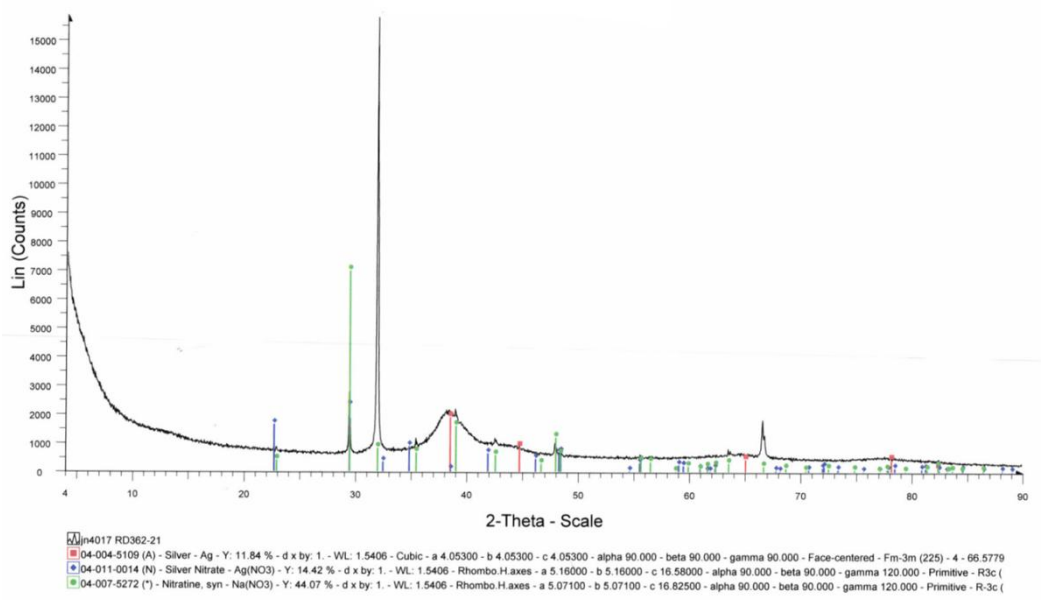

Figure 74: Powder diffraction spectrum of sample #17 AgNPs prepared with sugar (2) .

The spectrum was weak and contained $NaNO_3$ formed by the reaction between $AgNO_3$ and NaOH used to prepare the Tollens' reagent. The x-ray diffraction showed solely the presence of face-cubic-centered (fcc) Ag^0 as depicted by the 2θ peaks 38.1, 44.8, 65.0 and 78.2 deg,[145] confirming the electron microscopy results. The sample contained also Ag^+ ions, as $AgNO_3$ due to a non-complete reduction of the Tollens' reagent. The ratio between Ag+ salts and Ag^0 was 1.21 : 1, a significant result showing that less than 50% of the silver was actually

reduced to form silver nanoparticles in the crude sample. As the ratio of the Ag to sugar **(2)** of this sample is 2 : 1 (20mM Tollens', 10mM sugar), in light of this result it was possible to speculate that the Tollens' reaction occurs in a 1 : 1 apparent ratio for this particular compound instead of the supposed 4 : 1 (4 atoms of silver reduced by the 2 sugars of each molecule of **(2)**). From this ratio it was also possible to derive the concentration of the silver nanoparticles and consequently the absorption coefficient. The following formula could be used to calculate ε (absorption coefficient):

$$\varepsilon = \frac{(1 + 1.21)A}{cl} = \frac{2.9 * 2.21}{0.02 * 0.1} = 3200\ M^{-1}cm^{-1}$$

The relatively low value of the absorption coefficient denoted that the sample had poor optical absorbance, as AgNPs are known to have $\varepsilon > 10^7$ $M^{-1}cm^{-1}$.[146] However, the accuracy of the concentration value was limited by the quality of the x-ray spectrum. A more accurate value would be given by quantitative ICP-MS of a purified sample.

2.3.15 Raman Spectroscopic analysis of AgNPs

Raman spectroscopy could help to determine if sugar molecules are binding over the surface of the AgNP through the triazoles by looking for SERS effects as suggested in paragraph 2.3.10.3. Samples were initially lyophilised and analysed by Horiba LabRAM HR in powder form, however the intensity of the Raman signals was too weak to be distinguished from the background. Selected samples

were sent to Dr. Iain Larmour[h] for direct analysis of the liquid colloids. AgNP@**(1)** cell #16 showed significant SERS peaks (Figure 75): the main one at 1660 cm^{-1} clearly showed that the sugar **(1)** was bound on the surface of the nanoparticle through a CO bond. Similar peaks are known for citrate coated silver nanoparticles, showing that the carboxylates are interacting with the silver surface.[147]

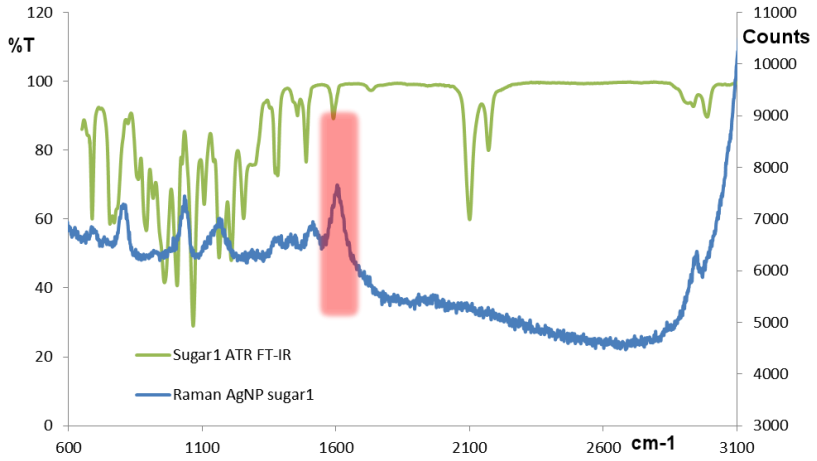

Figure 75: Overlay plot of a FT-IR spectrum of sugar (1, green) and a RAMAN spectrum of AgNPs prepared with (1, blue). The red box highlights a SERS signal of C=O of galactonic acid.

Sugar **(2)** sample cell #8 #12 #17 showed no detectable signals. Sample #16 could not be analysed as it showed a very high fluorescence. Sample #9 gave an interesting spectral fingerprint, in particular the peak at 1980 cm^{-1} which was not present in the FT-IR of the sugar **(2)** or AgNP@**(2)** and could evidence an interaction of the silver surface with the triazole (Figure 76).

[h] Centre of Molecular Nanometrology, University of Strathclyde, Glasgow

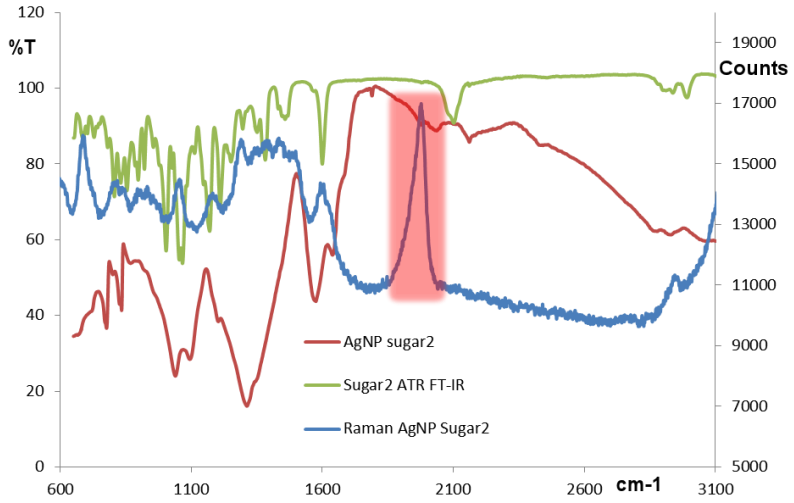

Figure 76: Overlay plot of a FT-IR spectrum of (2, green), a FT-IR spectrum of AgNPs prepared with (2, red) and a RAMAN spectrum of AgNPs prepared with (30, blue). The red box highlights a SERS signal of the triazoles of (2).

This discontinuous pattern of response SERS signals for AgNP@**(2)** could be due to their size distribution. It is known that SERS signals of AgNPs are highly size dependent with a maximum intensity with particles of ~50 nm.[148] AgNP@**(2)** are much smaller than this optimal diameter; sample #9, which showed high poly-dispersion and the largest average diameter, could potentially contain larger aggregates that are highly SERS responsive. Re-analysis of sample #9 by TEM showed the presence of ~80 nm polycrystalline aggregates that could be responsible for the high SERS signals (Figure 77).

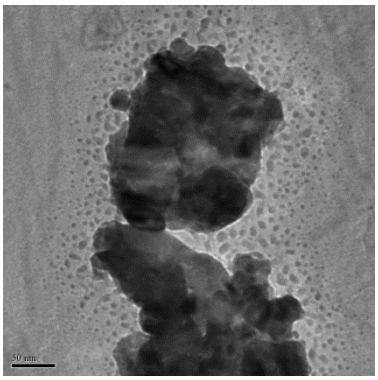

Figure 77: TEM image of sample #9 AgNPs prepared with (2) showing ~80 nm polycrystalline aggregates.

In conclusion, preliminary evidence of intense SERS signals could be detected for both AgNP@**(1)** and AgNP@**(2)**, however the sugars appeared to interact with the silver surface with two different modalities: AgNP@**(1)** appeared to interact predominantly with the carboxylates while AgNP@**(2)** results suggested an interaction with the triazoles.

2.3.16 Proposed mechanisms

2.3.16.1 AgNP surface stabilisation

Small charged molecules are known to prevent aggregation of nanoparticles mainly through an electrostatic repulsion mechanism. Such molecules can be negatively (citrate, tannic acid, ascorbate or oleic acid) or positively charged (CTAB, TOAB). The surface monolayer of adsorbed surfactants is known to be dynamic and it's widely exploited to exchange the coating of surfactants on nanoparticles (Figure 78).[149,150]

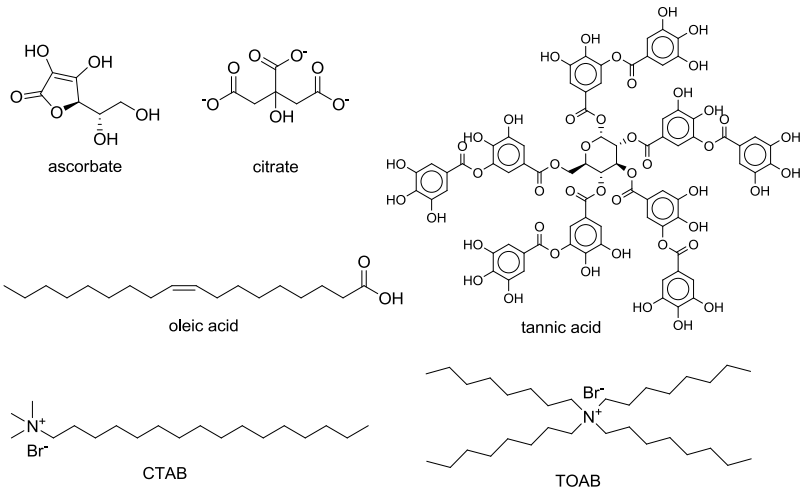

Figure 78: Structures of negatively (citrate, tannic acid, ascorbate or oleic acid) or positively charged (CTAB, TOAB) surfactants used in the preparation of AgNPs.

Therefore, it is proposed that this dynamic ligand exchange is also responsible for the size distribution of the mono-crystalline nanoparticles formed due to the following pieces of evidence. In order for the nanoparticle to increase in size and aggregate additional atoms on its surface, a molecule of surfactant must leave to create a vacant point on the surface for additional metal crystallisation (Figure 79).

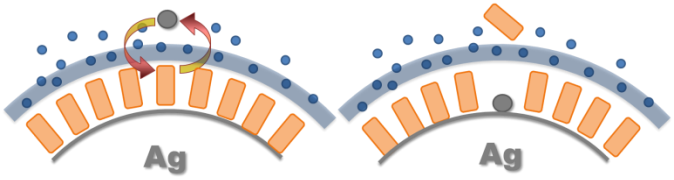

Figure 79: Schematic drawing of the proposed mechanism of ligand exchange on the surface of a AgNP allowing additional silver atoms to aggregate. A surfactant molecule exchange with a silver atom, the atom then can contribute to the growth of the particle.

This vacant point is then filled by an atom or multiple atoms, depending on the volume size of the gap left, resulting in an increase of NP size (Figure 79). As the

size of the nanoparticle increases, the curvature of the nanoparticles decreases. The properties of an adsorbed surfactant are highly dependent on the curvature of the surface, as described by Chad Mirkin.[125] The second assumption is that the stability of the surfactant binding on the surface of the nanoparticle is a function of the curvature. At a critical diameter, the curvature of the nanoparticle surface reaches a value where the kinetics of binding of the surfactants can be approximated to a local flat surface. This value is empirically recognised to be ~40 nm for silver nanoparticles coated with small negatively charged surfactants.[100] Surfactant loading is known to increase the density with smaller nanoparticles (smaller footprints) due to the deflection of the molecules caused by the curvature of the particle itself.[125–127,151] However, little is known on the stability of a surfactant monolayer as a function of the size of the nanoparticles, and consequently of the curvature. It can be assumed that multi-dentate ligands like **(2)** and **(3)** can bind to the surface more efficiently at higher values of the curvature and so the monolayer stability would be greater and growth of the AgNPs would be limited compared to **(1)**. Also, the probability of a multi-dentate ligand leaving the surface is smaller than a mono-dentate ligand at the same values of binding constant, due to a simple statistical distribution. For example, **(3)** could adsorb on a surface with up to 11 binding groups (Figure 80).

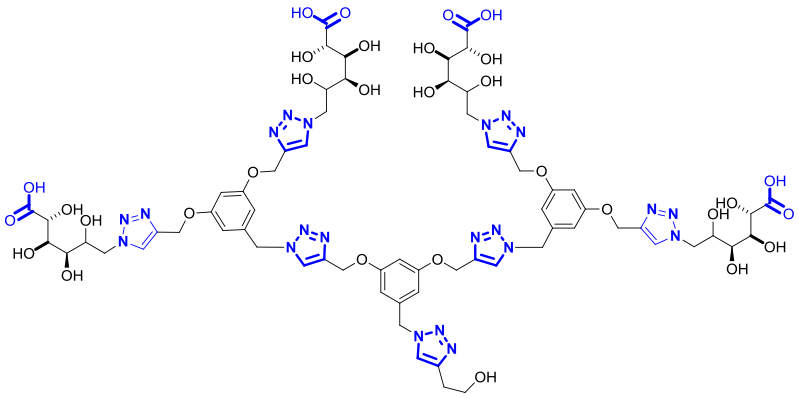

Figure 80: Putative molecule formed during reaction of (3) with Tollens' reagent, showing the formation of 4 galactonic acid residues.

In conclusion, it is proposed that negatively charged surfactants (such as **(1)**, **(2)**, **(3)**, galactonic acid or citrate) have a variable binding constant on the surface and this constant is inversely proportional to the surface curvature. At a critical particle diameter, ligand exchange is low enough to stop the growth of the particle. For **(1)** this critical diameter is equal to classical sugars like glucose or galactose (~40 nm) while sugars **(2)** and **(3)** can stabilise particles of much smaller diameter (8-10 nm).

2.3.16.2 Early mechanism Ag^+ ligand coordination

Triazoles are well known to coordinate to a variety of transition metals, including Ag^+.[141] In addition to surface stabilization as proposed in the previous paragraph 2.3.12, triazole sugars could influence the kinetics of the Tollens' reaction by chelating Ag^+ ions before the reduction steps. The slower kinetics of AgNP@**(1)** formation relative to AgNP@D-galactose suggests that the coordination of the Ag^+ to the pyranosyl oxygen in complex **(36)** hinders ring opening of the pyranose form of the D-galactose (Scheme 10)

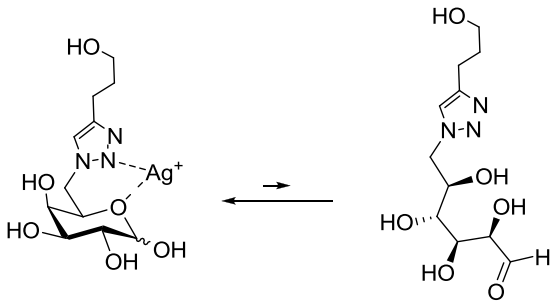

(36) **(36a)**

Scheme 10: Proposed mechanism that would explain the slower kinetics of (1) compared to D-galactose. Ag^+ ions chelates the pyranosyl oxygen of the pyranose form of (1) as in chelate (36), thus changing the equilibrium to form (36a)

Consequently, the equilibrium is shifted more to the pyranose form, which in turn reduces the amount of aldehyde (the reductant) present, subsequently slowing down the rate of AgNP@**(1)** formation. Both AgNP@**(1)** and AgNP@D-galactose produce AgNPs in the similar size regime despite their different reaction kinetics, which infers that, in these systems, the initial rate of Ag(I) reduction might not be the rate limiting step, but rather the downstream rates of nucleation and growth of the AgNP process are the controlling factors. The moderate size and shape control is also evident in these systems and is consistent with previous findings by Panacek *et al.*[152] and Kvitek *et al.*,[117] which also suggests that the presence of the triazole in **(1)** has little influence on size control. In contrast to AgNPs produced using **(1)** and D-galactose, AgNPs formed using either sugar **(2)** or **(3)** as the Ag(I) reductant results in significant faster rates of AgNP formation (Figure 63 in paragraph 2.3.11). In these systems, the increase in the rate of AgNP formation correlates with AgNPs of much smaller size than those produced using either **(1)** or D-galactose. Surprisingly, there is little difference in size regimes of

AgNP@**(2)** and AgNP@**(3)** as well as their rate of formation, which we surmise that the similar ligand cores of **(2)** and **(3)** relative to **(1)** is playing an influential and multi-faceted role in AgNP formation. According to ^{1}H NMR studies the ability to form AgNPs is directly associated with the unique capacity of the core of **(2)** and **(3)** to bind Ag(I) via a fundamentally different mechanism compared to **(1)**. Both sugars **(2)** and **(3)** contain the same resorcinol-ether triazole core, which pre-assembles a Ag(I) cation in close proximity to the sites of reduction (i.e. the D-galactose aldehyde). In 2006, Panigrahi *et al.* reported the preparation of AgNPs using resorcinol as a capping agent;[153] however to the best of our knowledge, there have been no reports highlighting the utility of resorcinol ethers facilitating the controlled syntheses of AgNPs. We therefore surmise that under our reaction conditions, the open chain form of the D-galactose units in **(2)** presents two aldehyde functionalities in close proximity to a Ag(I) cation held in place by three triazole units as putatively highlighted in **(37)**. This tridentate system is critical for size-controlled AgNP formation as typified by the complete lack of AgNP formation using the two-sugar-system **(29)** as the Ag(I) reductant. These results therefore highlight that the assembly of Ag^{+} within an appropriate tridentate ligand complex can be utilized for the preparation of size and shape-controlled AgNPs of significantly smaller size regimes than that of 40 nm as previously reported using readily available mono- and di-saccharides produced.[100,117,152]

Despite similar reaction kinetics there are significant differences between AgNPs formed in the presence of **(2)** and **(3)**. AgNPs derived from the use of ligand **(3)**

exhibit far superior size and shape-control and remarkable colloidal stability in high-salt aqueous buffers relative to AgNP@**(2)**. Although the molecular underpinnings of this are not completely understood at this point, we infer that the multiple resorcinol ether functionalities appears to facilitate not only size and shape control but also impart a vastly improved ability to passivate the AgNP surface. Panigrahi *et al.* reported a multi-functional role of resorcinol in the formation of highly stable AgNP suspensions in water albeit via a different mechanism to the one reported in this manuscript.[153] In this respect, the authors inferred that the improved water stability of the AgNPs was as a consequence of the OH groups of resorcinol forming a superlattice structure on the AgNP surface. Although there are no phenolic OH groups present in our ligands, it is feasible that the corresponding pendent sugars of **(2)** and **(3)** could also form a unique superlattice structure on the AgNP surface (Figure 81). In this respect the higher sugar density present in **(3)** would therefore provide a more extensive and stable superlattice network, thereby explaining the unique stability of AgNP@**(3)** in high salt aqueous buffers relative to AgNP@**(2)**.

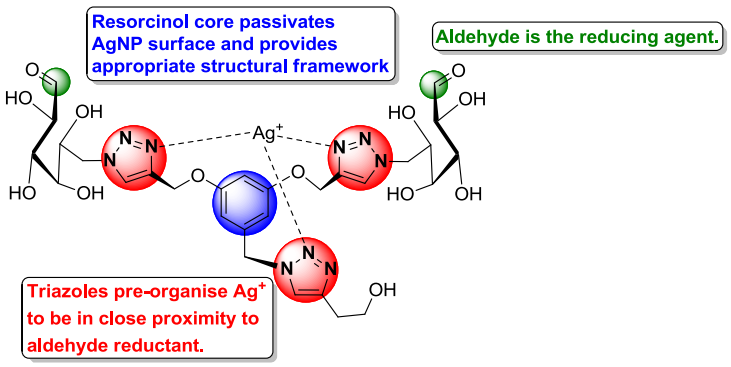

Figure 81: Proposed model for the formation of AgNPs using the template (2).

2.4 Conclusions

In conclusion, this chapter reports a novel synthetic strategy for the one-step synthesis of highly stable, size and shape-controlled AgNPs using sugar triazole ligands (**29, 30, 38**). The structure of the central resorcinol ether core in sugar **(2)** was critical for this control. By increasing the density of reducing sugars from two **(2)** to four **(3)**, the programmable synthesis of AgNPs with enhanced stability in high salt buffers was achieved. The availability of various derivatisation points in the central core of **(2)** enables tuneable and downstream derivatisation thus opening up new biomedical and material science-related opportunities for AgNPs where stability in aqueous buffered solutions and tuneable size control are critical parameters.

2.5 Experimental

Silver nitrate (99.9999%), NH_3 (28%) was purchased from Sigma Aldrich. UV-Vis measurements were taken with a Thermo-Scientific Nanodrop 1000. Time-course kinetics were acquired using a Perkin Elmer Lambda 35 fitted with a PTP6+6, a Varian Cary 50 Probe and a Shimadzu UV-2401PC. TEM images were acquired using a Jeol JEM 1400 with an Olympus Megaview III camera, a Jeol JEM 2100 with a GatanUltrascan 1000 camera and a Jeol JEM 2100F with a GatanOrius SC1000-2 high speed camera. TEM images were subsequently processed with ImageJ software (http://imagej.nih.gov). Mass spectra were obtained with a Waters AquityXevo and a Micromass Quattro LC. DLS data measurements were taken with a Malvern Instruments Zetasizer Nano S. GC-MS

spectra were taken with a Perkin Elmer Autosystem XL + Turbomass. Ultrapure water was generated by an Elgastat Option 4 water purifier. Powder X-ray diffraction was acquired with a Bruker D8 Advance. MALDI-TOF MS spectra were obtained with a Voyager DE-STR. Raman spectra were acquired with a Horiba Jobin-Yvon Lab Ram HR.

Purification of the sugars was accomplished by reverse phase HPLC: Sephadex C18; Mobile Phase: linear gradient, A: water and B: Acetonitrile, A:B from 90:10 to 70:30 in 15 min, maintain for 4 min; temperature: 22°C; flow rate: 1 mL/min Detector: PDA (220-400 nm) + 254 nm; Chromatogram: 0-22 minutes.

Synthesis of the PS-NHC-Cu(I)[110] **(42)** click-chemistry catalyst is detailed in the Appendix.

2.5.1 Synthesis of sugar (1)

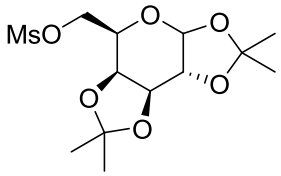

Synthesis of 1,2-3,4-diacetonide-6-mesyloxy-galactopyranose[154] **(5)**. To a stirred solution of 1,2-3,4-diacetonide-6-hydroxy-galactopyranose **(4)** (6.000 g, 23.5 mmol) in THF (200 mL) at 0°C was added mesyl chloride **(38)** (10.562 g, 92.2 mmol, 7.14 mL), DIEA (9.312 g, 92.2 mmol, 12.8 mL) dropwise. The mixture was stirred for 2h at 0°C followed by quenching by addition of cold water (300 mL) and ethyl acetate (300 mL). The organic phase was separated, washed with HCl 0.1 M (100 mL), $NaCO_3$ sat. (100 mL) and Brine

(100 mL), concentrated to a residue. This was then suspended in hexane (50 mL) and sonicated for 20 min until a fine white powder was obtained and filtered. Drying under vacuum overnight afforded 1,2-3,4-diacetonide-6-mesyloxy-galactopyranose **(5)** (10.925 g, 99% co-crystallized with 1eq of THF as calculated by NMR analysis). GC-MS (EI) *m/z:* [M^+] calc. for $C_{13}H_{22}O_8S$ 338.1035, found 338; m.p. 135-136°C; ^{1}H-NMR (300MHz , DMSO-d_6) δ 5.48 (d, *J* = 5.0 Hz, 1H), 4.63 (dd, *J* = 7.9, 2.3 Hz, 1H), 4.32 - 4.42 (m, 2H), 4.27 (d, *J* = 7.9 Hz, 1H), 4.07 - 4.20 (m, 1H), 3.97 (dd, *J* = 7.8, 1.9 Hz, 1H), 3.18 (s, 3H), 1.20 - 1.51 (m, 14H); ^{13}C-NMR (75 MHz, DMSO-d_6) δ 108.7 (Cq), 108.1 (Cq), 95.5 (C-1, CH), 70.0 (CH), 69.9 (CH), 69.5 (CH), 69.2 (C-6, CH_2), 66.0 (CH), 36.9 (CH_3-S), 25.8 (CH_3), 25.7 (CH_3), 24.8 (CH_3), 24.2 (CH_3)

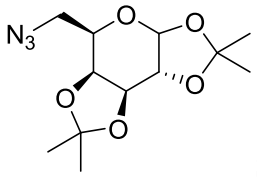

Synthesis of 1,2-3,4-diacetonide-6-azido-galactopyranose[154] **(6):** To a solution of 1,2-3,4-diacetonide-6-mesyloxy-galactopyranose **(5)** (10.925 g, 23.05 mmol) in DMF (200 mL) was added NaN_3 **(20)** (4.198 g, 64.58 mmol) followed by water (2 mL). The mixture was then heated to 120°C for 2 hours and concentrated at residue *in vacuo*. The residue was dissolved in ethyl acetate (200 mL) and extracted with brine (3x100 mL) then dried over $MgSO_4$ and concentrated to orange oil. This residue was purified by Si-60 column chromatography using hexane:ethyl acetate 90:10 as eluent to obtain 1,2-3,4-diacetonide-6-azido-galactopyranose **(6)** (7.034 g, 99%) as a clear oil. GC-MS (EI) *m/z*: [M^+] calc. for $C_{12}H_{19}N_3O_5$ 285.1325, found 285; FT-IR (ATR):

ν = 2104 cm^{-1} (m, ν_{as}(azide)); ^{1}H-NMR (300 MHz, $CDCl_3$) δ 5.48 (d, 1H, $J_{1\text{-}2}$ = 5.1 Hz, H_1), 4.56 (dd, 1H, $J_{2\text{-}3}$ = 2.4 Hz, $J_{3\text{-}4}$ = 7.9 Hz, H_3), 4.27 (dd, 1H, H_2), 4.13 (dd, 1H, $J_{4\text{-}5}$ = 1.9 Hz, H_4), 3.85 (ddd, 1H, $J_{5\text{-}6}$ = 7.7 Hz, $J_{5\text{-}6'}$ = 5.5 Hz, H_5), 3.44 (dd, $J_{6\text{-}6'}$ = 12.6 Hz, H_6), 3.29 (dd, 1H, $H_{6'}$), 1.48 (s, 3H, C-CH_3), 1.39 (s, 3H, C-**C**H_3), 1.27 (s, 6H, C-**C**H_3); ^{13}C-NMR (75.47 MHz, $CDCl_3$) δ 109.9 (Cq), 109.1 (Cq), 96.6 (C_1), 71.4 (C_4), 71.0 (C_3), 70.6 (C_2), 67.3 (C_5), 50.9 (C_6), 26.3 (C-**C**H_3), 26.2 (C-**C**H_3), 25.1 (C-**C**H_3), 24.7 (C-**C**H_3)

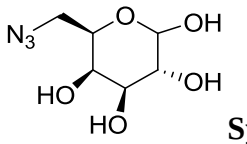

Synthesis of 1,2,3,4-hydroxy-6-azido-galactopyranose[154] **(7):** To a solution of 1,2-3,4-diacetonide-6-azido-galactopyranose **(6)** (1.000 g, 3.508 mmol) in water (15 mL) was added TFA (15 mL) and the mixture was heated to 50°C for 15 hours, cooled down and concentrated to a residue. This residue was then dissolved in water (10 mL) and freeze dried to obtain 1,2,3,4-hydroxy-6-azido-galactopyranose **(7)** (0.678 g, 94%) as a white powder. m.p. 152-154°C; ^{1}H-NMR (300 MHz, D_2O) δ 5.21 (d, 1H, $J_{1\text{-}2}$ = 3.6 Hz, H_1), 4.54 (d, 1H, $J_{1\text{-}2}$ = 7.7 Hz),4.14 (m, 1H), 3.89 (m, 1H), 3.83 (m, 1H), 3.83-3.70 (m, 1H), 3.62-3.29 (m, 1H); ^{13}C-NMR (75 MHz, D_2O) δ 96.7 (C_1), 92.6 (C_1), 73.7, 72.9, 69.9, 69.3, 69.2, 68.4, 51.1 (C_6), 50.9 (C_6)

2.5.2 Synthesis of sugar controls

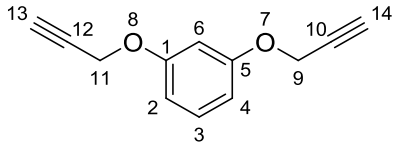

Preparation of 1,3-bis(prop-2-ynyloxy)benzene[155] **(25):** To a stirred solution of resorcinol (2.000 g, 18.2 mmol) in acetone (150 mL) was added propargyl bromide **(17)** (80% in Toluene, 4.3 g, 36.3 mmol), 18-crown-6 (0.02 g, 0.07 mmol), anhydrous and freshly ground potassium carbonate (2.760 g, 19.9 mmol) under a nitrogen atmosphere. The reaction mixture was heated to reflux for 24h followed by concentration *in vacuo*. The crude residue was then diluted with DCM (100 mL) and water (100 mL). The organic layer was separated, washed with brine (80 mL), dried with $MgSO_4$ and concentrated to a small volume. The concentrated solution was then purified by column chromatography over Si-60 using 100% DCM as eluent. 3-(prop-2-yn-1-yloxy)phenol **(39)** (0.417g, 17%) and **(25)** (2.586 g, 77%) were recovered as pale yellow oils. GC-MS (EI) *m/z:* [M^+] calc. for $C_{12}H_{10}O_2$ 186.0681, found 186; ^{1}H-NMR (300MHz, $CDCl_3$) δ 7.13 ppm (1H, m, H_3), 6.54 (3H, m, H_2, H_4, H_6), 4.59 (4H, d, J = 2.3Hz, H_9, H_{11}), 2.45 (2H, t, J = 2.3Hz, H_{13}, H_{14}); ^{13}C-NMR (75 MHz, $CDCl_3$) δ 158.9, 130.1, 108.0, 108.0, 78.6, 75.7, 56.0

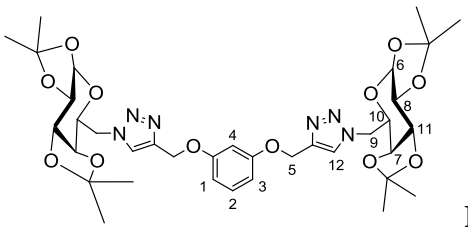

Preparation of (27):[156] To a stirred solution of **(25)** (0.550 g, 2.96 mmol) in EtOH (10 mL) was added **(6)** (0.551 g, 1.93

mmol), CuBr (0.061 g, 0.43 mmol), TBTA (0.190 g, 0.44 mmol) under a nitrogen atmosphere. The reaction mixture was stirred overnight at r.t. followed by concentration *in vacuo*, dilution with DCM (5 mL) and purification by column chromatography (Biotage 40L Si-60 column using Hexane:Acetate as eluents). Mono clicked product **(28)** (0.384 g, 33%), unreacted **(25)** (0.284 g, 52%) and **(27)** (0.330 g, 15%) were recovered. Compound **(27)**[156] ESI-MS (ES+) *m/z:* $[M+H]^+$ calc. for $C_{36}H_{48}N_6O_{12}$ 756.3330, found 756; m.p. 180-181°C; ^{1}H-NMR ($CDCl_3$, 300MHz, mixture of 4 diastereoisomers) δ 7.79 (2H, s, H_{12}), 7.20 (1H, m, H_2), 6.62 (3H, m, H_1, H_3, H_4), 5.52 (2H, d, J = 5.4 Hz, H_6), 5.20 (4H, s, H_5), 4.62 (4H, m, H_7, H_{11}), 4.46 (2H, m, H_{10}), 4.33 (2H, m, H_8), 4.19 (4H, m, H_9), 1.49 (6H, s, CH_3 isopropylidene), 1.39 (6H, s, CH_3 isopropylidene), 1.36 (6H, s, CH_3 isopropylidene), 1.30 (6H, s, CH_3 isopropylidene)

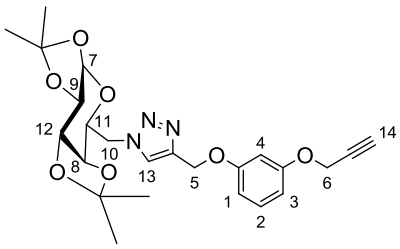

C**ompound (28):** ^{1}H NMR (300 MHz, $CDCl_3$, mixture of 2 diastereoisomers) δ 7.79 (s, 1H, H_{13}), 7.15 - 7.24 (m, 1H, H_2), 6.55 - 6.69 (m, 3H, H_1, H_3, H_4), 5.52 (d, J = 4.7 Hz, 1H, H_7), 5.20 (s, 2H, H_5), 4.59 - 4.70 (m, 4H, H_6, H_{11}, H_{12}), 4.40 - 4.55 (m, 1H, H_8), 4.33 (dd, J = 5.0, 2.6 Hz, 1H, H_9), 4.16 - 4.25 (m, 2H, H_{10}), 2.53 (t, J = 2.3 Hz, 1H, H_{14}), 1.28 - 1.52 (m, 14H, isopropylidenes); ^{13}C-NMR (75 MHz, $CDCl_3$, mixture of 2 diastereoisomers) δ 159.5, 158.8, 143.7, 129.9, 124.0, 109.9, 109.1, 107.9, 107.6, 102.3, 96.2, 71.1,

70.7, 70.3, 67.2, 62.1 (CH_2), 60.4, 55.9 (CH_2), 50.6 (CH_2), 26.0, 25.9, 24.9, 24.4, 14.1

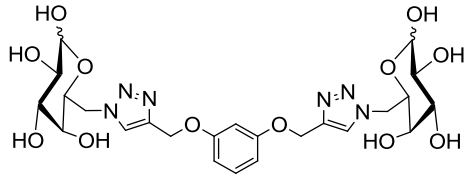

Preparation of (29): to a mixture of TFA : water (1 : 1, 10 mL) was added **(27)** (0.330 g, 0.44mmol.) under a nitrogen atmosphere. The reaction mixture was heated to 65 °C and followed by TLC until complete (3 hours). The mixture was then cooled, concentrated *in vacuo* to a small volume, diluted with water (1.5 mL) and purified by semi-preparative HPLC. **(29)** (55.2 mg, 21%) was recovered as a white powder after lyophilisation. UPLC-TOF (ESI) *m/z*: $[M+H]^+$ calc. for $C_{24}H_{33}N_6O_{12}$ 597.2151, found 597.2164; m.p. 182-184°C; ^{1}H-NMR (300MHz, DMSO-d_6, mixture of 4 diastereoisomers, see COSY-90 in Figure 82) δ 8.18 (m, triazoles C-H), 7.21 (m, aromatic ring), 6.74 (m, aromatic ring), 6.65 (m, aromatic ring + sugars anomeric protons), 6.24 (m, sugars anomeric protons), 5.25 (m, sugars), 5.11 (m, sugars + CH_2), 4.94 (m, sugars), 4.75 (m, sugars), 4.50 (m, sugars), 4.27 (m, sugars), 3.91 (m, sugars), 3.72 (m, sugars), 3.57 (m, sugars).

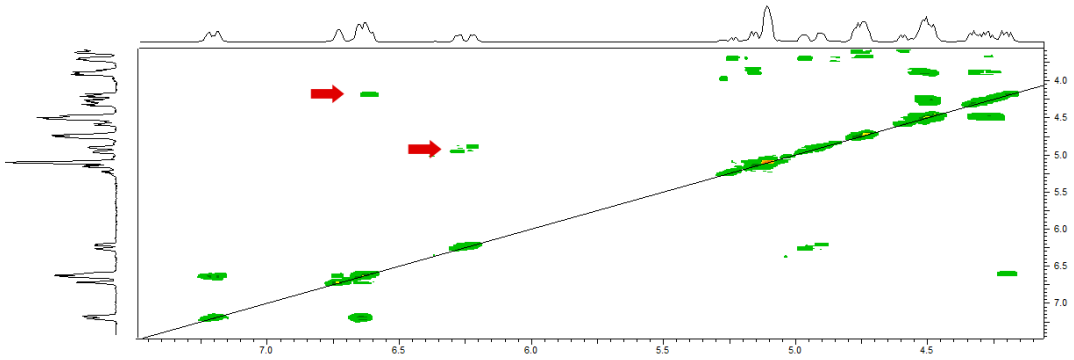

Figure 82: Selected area COSY-90 of sugar (29): red arrows highlight couplings of anomeric protons; the anomeric protons of the diastereoisomers show a difference of ~1 ppm in the chemical shift.

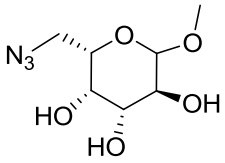

Synthesis of 2,3,4-hydroxy-1-methoxy-6-azido-galactopyranose (32): To a stirred suspension of sugar azide **(7)** (0.678 g, 2.376 mmol) in methanol (40 mL) was added dry HCl/MeOH 1.62 M (3 mL) and the mixture was heated to reflux overnight. The mixture was subsequently cooled and concentrated to residue, then re-crystallised from ethyl acetate:methanol 9:1 to obtain 2,3,4-hydroxy-1-methoxy-6-azido-galactopyranose **(32)** (0.612 g, 86% yield) as a white powder. UPLC-TOF (ESI) *m/z:* $[M-H]^-$ calc. for $C_7H_{12}N_3O_5$ 218.0782, found 218.0780; m.p. 154-156°C; ^{1}H-NMR (300 MHz, DMSO-d_6) δ 4.39 (br. s., 1H, OH), 4.57 (m, 1H), 3.69 - 3.77 (m, 1H), 3.36 - 3.65 (m, 5H), 3.26 - 3.32 (s, 3H, O-CH_3), 3.13 - 3.25 (m, 1H, C_1-H); ^{13}C-NMR (75 MHz, DMSO-d_6) δ 100.7, 70.2, 70.0, 69.6, 68.5, 55.0, 51.8 (CH_2)

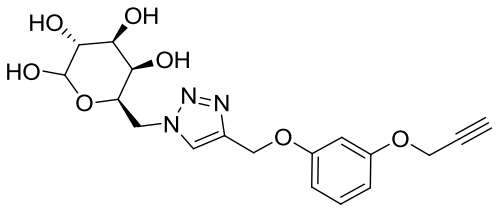

Synthesis of (30): To a stirred suspension of mono clicked **(28)** (0.384 g, 0.814 mmol) in water (5 mL) was added TFA (5 mL) and the mixture was heated at 65°C. The reaction was followed by TLC until completed, then cooled and concentrated to residue. This residue was azeotropically distilled using acetonitrile (2 x 50 mL) and toluene (2 x 50 mL) to afford **(30)** as a pale orange oil (0.150 g, 99%). UPLC-TOF (ESI) *m/z:* $[M+H]^+$ calc. for $C_{18}H_{22}N_3O_7$ 392.1452, found 392.1450; ^{1}H-NMR (300MHz, DMSO-d_6, mixture of 2 diastereoisomers) δ 8.13 - 8.25 (m, 1H), 7.61 - 7.74 (m, 1H), 7.10 - 7.26 (m, 1H), 6.51 - 6.71 (m, 2H), 5.09 (m, 2H), 4.94 - 4.99 (m, 1H), 4.90 (m, 1H), 4.76 (m, 2H), 4.43 - 4.55 (m, 2H), 4.08 - 4.32 (m, 2H), 3.82 - 3.94 (m, 1H), 3.48 - 3.74 (m, 2H), 3.22 - 3.36 (m, 1H); ^{13}C-NMR (75 MHz, DMSO-d_6, mixture of 2 diastereoisomers) *δ* 131.5, 129.9, 128.6, 125.2, 107.4, 101.8, 97.3, 92.6, 72.8, 71.5, 68.9, 67.4 (CH_2), 61.0 (CH_2), 55.4 (CH_2), 51.0 (CH_2), 38.0, 29.7 (CH_2), 28.30 (CH_2), 23.2, 22.3, 13.83, 10.8

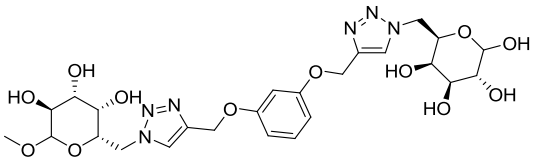

Synthesis of (33): to a stirred solution of **(30)** (0.150 g, 0.814 mmol) in DMSO (2 mL) were added 2,3,4-hydroxy-1-methoxy-6-azido-galactopyranose **(32)** (0.178 g, 0.814 mmol), water (3 mL), CuBr (0.0234 g, 0.1629 mmol), TP(OH)TA **(40)** (0.074 g, 0.171 mmol). The

reaction was followed by TLC (Al_2O_3, MeOH 100% as eluent, vanillin stain, R_f ~0.3) then concentrated to residue and the mixture was purified by semi-preparative HPLC. Compound **(33)** was recovered (0.099, 20% yield) as a white powder. UPLC-TOF (ESI) *m/z:* $[M+H]^+$ calc. for $C_{25}H_{35}N_6O_{12}$ 611.2307, found 611.2323; m.p. 181-183°C; ^{1}H-NMR (400 MHz, D_2O, mixture of 4 diastereoisomers) δ 7.90 - 8.06 (m, 2H), 7.15 (t, *J* = 8.3 Hz, 1H), 6.45 - 6.65 (m, 3H), 5.10 - 5.16 (m, 2H), 5.03 - 5.08 (m, 2H), 4.48 - 4.60 (m, 2H), 4.32 - 4.44 (m, 1H), 3.89 - 4.04 (m, 3H), 3.67 - 3.86 (m, 3H), 3.41 - 3.61 (m, 1H), 2.65 (d, *J* = 2.7 Hz, 2H); ^{13}C-NMR (100 MHz, D_2O, mixture of 4 diastereoisomers) *δ* 158.6, 158.3, 143.3, 143.1, 130.5, 125.9, 108.6, 108.4, 102.8, 99.2, 96.5, 92.3, 73.2, 72.6, 71.6, 69.3, 69.2, 67.9, 61.1, 60.9, 54.3, 51.1

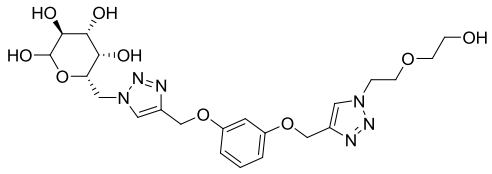

Synthesis of (31): To a stirred solution of **(30)** (0.050 g, 0.128 mmol) in water (1 mL) were added 2-(2-azidoethoxy)ethanol **(22)** (0.017 g, 0.128 mmol), $CuSO_4$ 0.26 M (98 uL, 0.0256 mmol), sodium ascorbate (0.028 g, 0.14 mmol). The reaction was stirred overnight at r.t. then concentrated to residue and the mixture was purified by semi-preparative HPLC. Sugar control **(31)** was recovered (0.0428, 64% yield) as a white powder. UPLC-TOF (ESI) *m/z:* $[M+H]^+$ calc. for $C_{22}H_{31}N_6O_9$ 523.2153, found 523.2145; m.p. 177-180°C; ^{1}H-NMR (400 MHz, D_2O) δ 8.03 (s, 2H), 7.18 - 7.25 (t, 1H), 6.59 - 6.69 (m, 3H), 5.14 (d, *J* = 12.1 Hz, 4H), 4.32 - 4.66 (m, 10H), 3.86 (s, 6H), 3.35 -

3.63 (m, 6H); ^{13}C-NMR (100 MHz, D_2O) δ 158.6, 158.5, 130.6, 108.8, 108.7, 103.1, 96.5, 92.4, 73.2, 72.7, 71.8, 69.1, 69.0, 68.8, 68.3, 61.3, 60.4, 50.8, 50.2

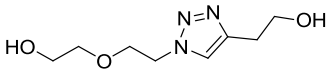

Synthesis of 1-(hydroxyethoxy)ethyl-4-hydroxyehtyl-triazole (35): To a stirred solution of 2-(2-azidoethoxy)ethanol **(22)** (0.060 g, 0.458 mmol) in water (1 mL) were added 3-butyn-1-ol **(9)** (0.032 g, 0.458 mmol), $CuSO_4$ 0.26 M (98 uL, 0.0256 mmol), sodium ascorbate (0.090 g, 0.458 mmol). The reaction was stirred overnight at r.t. then concentrated to a residue and the mixture was purified by semi-preparative HPLC. Sugar control **(35)** was recovered (0.060, 65% yield) as a white powder after lyophilisation. UPLC-TOF (ESI) *m/z:* $[M+H]^+$ calc. for $C_8H_{16}N_3O_3$ 202.1186, found 202.1185; m.p. 122-123°C; ^{1}H-NMR (400 MHz, D_2O) δ 7.78 - 7.99 (m, 1H), 6.11 - 6.64 (m, 2H), 3.91 (s, 4H), 3.46 - 3.69 (m, 6H), 2.79 - 2.97 (m, 3H); ^{13}C-NMR (100 MHz, D_2O) δ 71.7, 68.8, 60.7, 60.4, 50.0, 27.8

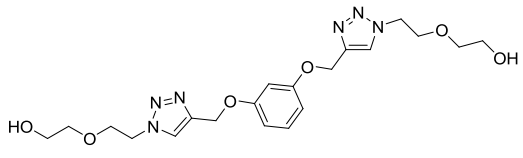

Synthesis of sugar control (26): To a stirred solution of 1,3-bis(prop-2-ynyloxy)benzene **(25)** (0.290 g, 1.561 mmol) in water (1 mL) was added 2-(2-azidoethoxy)ethanol **(22)** (0.408 g, 3.12 mmol), $CuSO_4$ 0.26 M (2.400 mL, 0.624 mmol), sodium ascorbate (0.679 g, 3.43 mmol) under a nitrogen atmosphere. The reaction mixture was stirred overnight at r.t. followed by concentration *in vacuo* and purification by semi-preparative HPLC.

Sugar control **(26)** (0.507 g, 73% yield) was recovered as a white powder. UPLC-TOF (ESI) m/z: $[M+H]^+$ calc. for $C_{20}H_{29}N_6O_6$ 449.2143, found 443.2146; m.p. 175-176°C; ^{1}H-NMR (400 MHz, DMSO-d_6) δ 8.22 (s, 2H), 7.20 (t, *J* = 8.2 Hz, 1H), 6.61 - 6.76 (m, 3H), 5.12 (s, 4H), 4.50 - 4.65 (m, 6H), 3.83 (t, *J* = 5.3 Hz, 4H), 3.40 - 3.50 (m, 8H); ^{13}C-NMR (100 MHz, DMSO-d_6) δ 159.3, 142.5, 129.9 (CH), 124.9 (CH), 107.2 (CH), 101.6 (CH), 72.0 (CH_2), 68.6 (CH_2), 61.1 (CH_2), 60.1 (CH_2), 49.4 (CH_2)

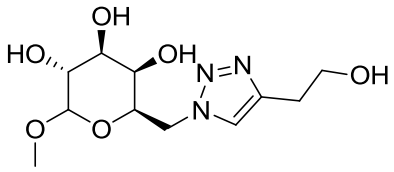

Synthesis of sugar control (34): To a solution of 2,3,4-hydroxy-1-methoxy-6-azido-galactopyranose **(32)** (0.100 g, 0.4566 mmol) in water (2 mL) were added 3-butyn-1-ol **(9)** (0.064 g, 0.9134 mmol), $CuSO_4$ 0.26 M (351 uL, 0.09132 mmol) and sodium ascorbate (0.100 g, 0.50226 mmol). The mixture was stirred at r.t. overnight under nitrogen atmosphere, concentrated *in vacuo* and the product was purified by semi-preparative HPLC. Sugar control **(34)** (0.128 g, 97%) was recovered as a white powder. UPLC-TOF (ESI) *m/z:* $[M+H]^+$ calc. for $C_{11}H_{20}N_3O_6$ 290.1347, found 290.1351; m.p. 168-170°C; ^{1}H-NMR (400MHz, D_2O, mixture of 2 diastereoisomers) δ 7.84 (s, 1H), 4.66 (d, *J* = 3.5 Hz, 1H), 4.47 - 4.58 (m, 2H), 4.05 - 4.15 (m, 1H), 3.96 (d, *J* = 2.5 Hz, 1H), 3.69 - 3.81 (m, 4H), 2.77 - 2.97 (m, 5H); ^{13}C-NMR (100 MHz, D_2O, mixture of 2 diastereoisomers) δ 124.7, 99.3, 69.4, 69.3, 69.2, 68.0, 60.5, 54.6, 50.9, 27.7

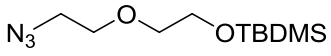

Synthesis of (2-(2-azidoethoxy)ethoxy)(tert-butyl)dimethylsilane (23): To a stirred solution of 2-(2-azidoethoxy)ethanol **(22)** (0.595 g, 4.54 mmol) in dry DMF (10 mL) were added TBDMS-Cl **(41)** (0.719 g, 4.77 mmol) and imidazole (0.325 g, 4.77 mmol). The mixture was stirred overnight at r.t. under a nitrogen atmosphere then diluted with ethyl acetate (100 mL) and washed with brine (4 x 100 mL), NH_4Cl sat. (2 x 100 mL), $NaHCO_3$ sat. (1 x 100 mL), dried over $MgSO_4$ and concentrated to residue to afford (2-(2-azidoethoxy)ethoxy)(tert-butyl)dimethylsilane **(23)** (0.785 g, 64% yield, contains 9.5% ethyl acetate) as a pale yellow oil. GC-MS (EI) *m/z*: [M^+] calc. for $C_{10}H_{23}N_3O_2Si$ 245.1560, found 245; ^{1}H-NMR (400 MHz, $CDCl_3$) δ 3.70 (m, 2H), 3.66 (m, 2H), 3.54 (m, 4H), 0.85 (m, 9H, Si-C(CH_3)$_3$), 0.03 (m, 6H, Si-CH_3); ^{13}C-NMR (100 MHz, $CDCl_3$) δ 72.8, 70.1, 62.8, 51.0, 25.9 (Si-C(CH_3)$_3$), -3.6 (Si-*C*(CH_3)$_3$), -5.3 (Si-CH_3)

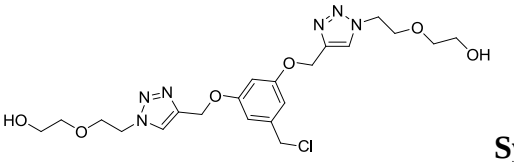

Synthesis of (24): To a stirred solution of 1-(chloromethyl)-3,5-bis(prop-2-ynyloxy)benzene **(13)** (0.261 g, 1.117 mmol) in THF (15 mL) were added 2-(2-azidoethoxy)ethanol **(22)** (0.261 g, 2.457 mmol) and PS-NHC-Cu(I) **(42)** 1.49mmol/g (0.750 g, 1.987 mmol) under a nitrogen atmosphere. The mixture was stirred overnight at r.t. then filtered, concentrated and purified by Si-60 column chromatography using ethyl acetate as eluent. Concentration of the fractions afforded **(24)** (0.220 g, 40% yield) as a light brown

solid. UPLC-TOF (ESI) *m/z*: $[M+H]^+$ calc. for $C_{21}H_{30}ClN_6O_6$ 497.1910, found 497.1934; m.p. 159-161°C; ^{1}H-NMR (300 MHz, DMSO-d_6) δ 8.21 (s, 2H), 6.59 (s, 3H), 5.03 - 5.18 (m, 4H), 4.36 - 4.67 (m, 4H), 3.82 (t, *J* = 5.3 Hz, 4H), 3.35 - 3.65 (m, 6H), 2.54 (s, 4H)

2.5.2.1 Synthesis of sugar triazole (1)

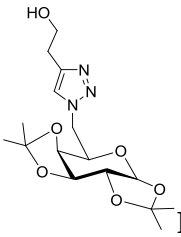

Preparation of (8): To a stirred solution of **(6)** (0.832 g, 2.9 mmol.) in DMSO (2 mL) was added 3-butyn-1-ol **(9)** (0.205 g, 2.92 mmol.), and PS-NHC-Cu(I)[110] **(42)** (1.49 mmol/g catalyst loading, 2.150 g, 3.20 mmol) under a nitrogen atmosphere. The reaction mixture was stirred overnight followed by quenching with brine (20 mL). The crude mixture was then filtered to remove the click-chemistry catalyst and extracted with ethyl acetate (3 x 20 mL). The combined organic layers were washed with brine (5 x 50 mL), 1.3% NH_3 (2 x 50 mL) and finally brine (50 mL). The organic layer was then dried (MgSO4), filtered and concentrated *in vacuo* to obtain **(8)** (0.693 g, 67%) as a pale yellow powder. UPLC-TOF (ESI) *m/z*: $[M+H]^+$ calc. for $C_{16}H_{26}N_3O_6$ 356.1816, found 356.1817; m.p. 161-162°C; ^{1}H-NMR (300 MHz, $CDCl_3$) δ 7.50 (s, 1H), 5.43 (d, 1H), 4.62 - 4.44 (m, 2H), 4.42 - 3.98 (m, 4H), 3.96 - 3.75 (m, 2H), 2.88 (s, 3H), 1.49 - 1.11 (m, 12H); ^{13}C-NMR (100 MHz, $CDCl_3$) δ 145.13, 122.85, 109.85,

109.04, 96.21, 71.17, 70.72, 70.31, 67.31, 61.71, 50.44, 28.72, 25.94, 25.88, 24.86, 24.39

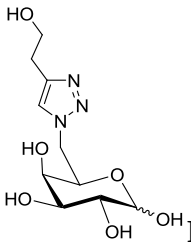

Preparation of (1): To a mixture of TFA : water (1 : 1, 10 mL) was added **(8)** (0.693 g, 1.946mmol) under a nitrogen atmosphere. The reaction mixture was heated to 70 °C and was followed by TLC until complete. The mixture was then cooled, concentrated *in vacuo* to a small volume, diluted with water (10 mL) and lyophilized overnight to afford **(1)** (0.322 g, 60 %) as a white powder. UPLC-TOF (ESI) *m/z*: $[M+H]^+$ calc. for $C_{10}H_{18}N_3O_6$ 276.1190, found 276.1193; m.p. 169-171°C; ^{1}H-NMR (500 MHz, D_2O, mixture of 2 diastereoisomers) δ 7.88 (s, 1H), 5.12 (d, 1H), 4.51-4.63 (m, 2H) 4.40 (m, 1H), 3.90-4.00 (m, 1H), 3.70-3.85 (m, 2H), 3.55 (m, 1H), 3.30-3.44 (m, 1H), 2.88 (t, 2H); ^{13}C-NMR (125 MHz, D_2O, mixture of 2 diastereoisomers) δ 96.4, 92.3, 73.1, 72.6, 71.6, 69.4, 69.0, 68.9, 68.1, 60.5, 51.0, 50.8, 27.8

2.5.2.2 Synthesis of sugar triazole (2)

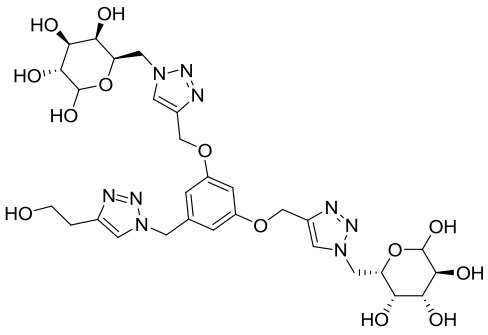

Preparation of compound (2). To a stirred solution of **(16)** (0.303 g, 0.465 mmol.) in DMSO (10 mL) was added butyn-3-ol **(9)** (32mg, 0.465 mmol.), and PS-NHC-Cu(I) **(42)** (1.49 mmol/g catalyst loading, 31 mg, 0.047 mmol) under a nitrogen atmosphere. The reaction mixture was stirred overnight then filtered with a 0.2 μm filter, the solid catalyst was washed with DMSO (1 mL) and the combined filtrate was concentrated to a small volume, diluted with water (1.5 mL) and purified by semi-preparative HPLC. Lyophilisation of selected fractions afforded **(2)** (0.310 g, 91%) as a pale yellow powder. UPLC-TOF (ESI) *m/z:* $[M+H]^+$ calc. for $C_{29}H_{40}N_9O_{13}$ 722.2740, found 722.2748; mp 178-180°C; ^{1}H-NMR (400 MHz, D_2O, mixture of 4 diastereoisomers) δ 7.95 (br. s.), 7.68 - 7.74 (m), 6.45 (br. s.), 5.35 (br. s.), 5.12 - 5.15 (m), 5.00 (br. s.), 4.48 - 4.63 (m), 4.40 (d, *J* = 7.8 Hz), 4.30 - 4.36 (m), 3.88 - 3.99 (m), 3.82 - 3.86 (m), 3.68 - 3.81 (m), 3.53 - 3.62 (m), 3.41 - 3.49 (m), 2.79 (s), 1.24 - 1.32 (m); ^{13}C-NMR (125 MHz, D_2O, mixture of 4 diastereoisomers) δ 158.9, 142.9, 137.8, 125.8, 107.9, 102.4, 96.5, 92.3, 73.2, 72.6, 72.6, 69.4, 69.0, 68.9, 68.7, 68.2, 61.2, 60.5, 53.4, 51.0,50.8, 27.8

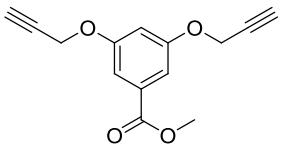

Synthesis of methyl 3,5-bis(prop-2-ynyloxy)benzoate[111] **(11):** To a stirred solution of methyl 3,5-dihydroxybenzoate **(10)** (4.000 g, 23.8 mmol) in acetone (71 mL) was added propargyl bromide **(17)** (80% in Toluene, 6.228 g, 52.36 mmol), 18-crown-6 (0.025 g, 0.095 mmol), anhydrous and freshly ground potassium carbonate (3.618 g, 26.18 mmol) under a nitrogen atmosphere. The reaction mixture was stirred 24h at reflux followed by concentration *in vacuo* to a small residue. The crude residue was then diluted with DCM (100 mL) and water (100 mL). The organic layer was separated, washed with brine (80 mL), dried with $MgSO_4$ and concentrated to a small volume. Methyl 3,5-bis(prop-2-ynyloxy)benzoate **(11)** was recovered as an orange solid (4.110 g, 70.78%) after re-crystallisation from MeOH. GC-MS (EI) *m/z*: [M^+] calc. for $C_{14}H_{12}O_4$ 244.0736, found 244; m.p. 80-81°C; ^{1}H-NMR (500 MHz, $CDCl_3$) δ 7.31 (s, o-Ar, 2H), 6.83 (s, p-Ar, 1H), 4.73 (d, J = 2.4 Hz, $CH_2C{\equiv}CH$, 4H), 3.92 (s, CH_3O, 3H), 2.55 (t, J = 2.4 Hz, $C{\equiv}CH$, 2H); ^{13}C-NMR (125 MHz, $CDCl_3$) δ 166.86 (s, $COOCH_3$, 1C), 158.90 (s, m-Ar, 2C), 132.54 (s, $CCOOCH_3$, 1C), 109.27 (s, o-Ar, 2C), 107.91 (s, p- Ar, 1C), 78.34 (s, $C{\equiv}CH$, 1C), 76.38 (s, $C{\equiv}CH$, 1C), 56.51 (s, $CH_2C{\equiv}CH$, 1C), 52.76 (s, CH_3O,1C)

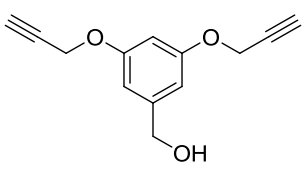

Synthesis of (3,5-bis(prop-2-ynyloxy)phenyl)methanol[111] **(12):** To a stirred solution of Methyl 3,5-bis(prop-2-ynyloxy)benzoate **(11)** (4.000 g, 16.39 mol) in anhydrous THF (150 mL) was

added LAH (6.228 g, 163.9 mmol) slowly in small portions. After 50 minutes the reaction was quenched by addition of ethyl acetate (50 mL) followed by water (50 mL). The heavy aluminium salts were filtered and the solution was concentrated to a small volume, diluted with DCM (250 mL) and washed with brine (150 mL). The organic phase was then concentrated to a small volume and hexane was slowly added (180 mL) to induce crystallization. (3,5-bis(prop-2-ynyloxy)phenyl)methanol **(12)** was recovered (3.035 g, 86%) as an off-white powder. GC-MS (EI) *m/z:* [M^+] calc. for $C_{13}H_{12}O_3$ 216.0786, found 216; m.p. 93-94°C; ^{1}H-NMR (500 MHz, $CDCl_3$) δ 6.56 (s, o-Ar, 2H), 6.46 (s, p-Ar, 1H), 4.61 (d, *J* = 2.4 Hz, $CH_2C{\equiv}CH$, 4H), 4.45 (s, CH_2OH, 2H), 2.46 (t, *J* = 2.4 Hz, C≡CH, 2H); ^{13}C-NMR (125 MHz, $CDCl_3$) δ 159.23 (s, m-Ar, 2C), 143.97 (s, CCH_2OH, 1C), 106.60 (s, o-Ar, 2C), 101.88 (s, p-Ar, 1C), 78.76 (s, C≡CH, 2C), 76.09 (s, C≡CH, 2C), 65.50 (s, CH_2OH, 1C), 56.30 (s, $CH_2C{\equiv}CH$, 1C)

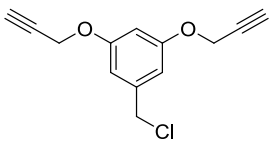

Synthesis of 1-(chloromethyl)-3,5-bis(prop-2-ynyloxy)benzene[111] **(13):** To a stirred solution of (3,5-bis(prop-2-ynyloxy)phenyl)methanol **(12)** (3.810 g, 17.72 mmol) in anhydrous DCM (51 mL) were added anhydrous pyridine (6.587 g, 83.28 mmol, 6.7 mL) and thionyl chloride (4.914 g, 41.64 mmol, 3.0 mL) dropwise in 1 hour while keeping the mixture at 0°C. The reaction was then heated to reflux for 2 hours, cooled and quenched with water (100 mL). The organic phase was separated and washed with water (50 mL), $NaHCO_3$ sat. (50 mL) brine (50 mL), dried with $MgSO_4$ and

concentrated to residue. This crude was then purified over a Si-60 chromatographic column using n-hexane:ethyl acetate. 1-(chloromethyl)-3,5-bis(prop-2-ynyloxy)benzene **(13)** was recovered (1.592 g, 39%) as a pale cream solid. GC-MS (EI) *m/z*: [M^+] calc. for $C_{13}H_{11}ClO_2$ 234.0448, found 234; m.p. 68-70°C; ^{1}H-NMR (300 MHz, $CDCl_3$) δ 6.58 (d, 1H, ArH), 6.52 (t, 2H, ArH), 4.61 (d, 4H, CH_2O, J = 2.3 Hz), 4.45 (s, 2H, CH_2Cl), 2.47 (t, 2H, ≡CH, J = 2.3 Hz); ^{13}C-NMR (75 MHz, $CDCl_3$) δ 158.9, 108.1 (CH), 103.1 (CH), 71.1 (CH_2), 56.0 (CH_2), 38.5 (≡**C**H)

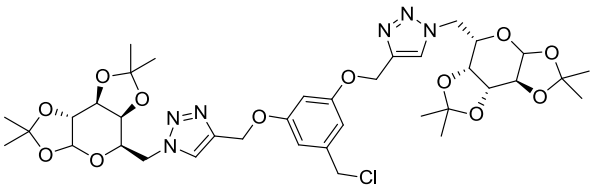

Synthesis of (14):[105] To a solution of 1-(chloromethyl)-3,5-bis(prop-2-ynyloxy)benzene[105] **(13)** (0.576 g, 2.47 mmol) in THF (6 mL) were added 1,2-3,4-diacetonide-6-azido-galactopyranose **(6)** (1.400 g, 4.91 mmol), $CuSO_4$ 0.26M (0.02 g, 476 uL) and a solution of sodium ascorbate (0.0486 g, 0.245 mmol) in water (2 mL). The mixture was stirred for 48 hours at r.t. then diluted with water (60 mL) followed by NH_3 29% (2 mL) and stirred for 10 minutes. The mixture turned cloudy and blue and was then extracted with DCM (6 x 50 mL); the combined organic phases were washed with brine (50 mL), dried over $MgSO_4$ and concentrated to give **(14)** (2.117 g, 96%, as a DCM solvate) as a white crystalline solid. ESI-MS (ES+) *m/z:* [M+H]$^+$ calc. for $C_{37}H_{50}ClN_6O_{12}$ 805.3170, found 806; m.p. 184-185°C; ^{1}H-NMR (400

MHz, $CDCl_3$) δ 7.79 (s, 2H, C=CH-), 6.64 (d, 2H, *J* = 1.8 Hz, Ar-H), 6.59 (t, 1H, *J* = 1.8 Hz, Ar-H), 5.51 (d, 2H, *J* = 4.8 Hz), 5.18 (s, 4H, -CH_2-), 4.64 (m, 2H), 4.62 (m, 2H), 4.50 (s, 2H, -CH_2-), 4.46 (dd, 2H, *J* = 14.4, 8.4 Hz), 4.32 (dd, 2H, *J* = 4.8, 2.4 Hz), 4.19 (m, 4H), 1.49 (s, 6H, C-CH_3), 1.38 (s, 6H, C-CH_3), 1.35 (s, 6H, C-CH_3), 1.29 (s, 6H, C-CH_3); ^{13}C-NMR(100 MHz, $CDCl_3$) δ 160.0, 143.4, 139.6, 124.0 (C=CH), 110.0, 109.1, 107.9, 102.0 (Ar-CH), 96.0, 70.9, 70.5, 70.1, 67.0, 62.2 (Ar-CH_2-), 50.6, 46.1 (CH_2-), 26.0 (C-CH_3), 25.9 (C-CH_3), 24.7 (C-CH_3), 24.4 (C-CH_3)

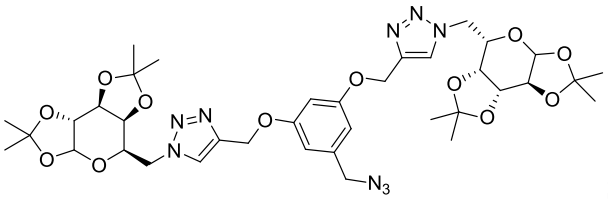

Synthesis of (15):[105] To a solution of **(14)** (0.153 g, 0.19 mmol) in acetone (8 mL) and water (2 mL) was added NaN_3 **(20)** (0.018 g, 0.285 mmol) under nitrogen. The mixture was then heated at reflux for 3 hours, cooled and diluted with water (100 mL) and ethyl acetate (100 mL); the organic phase was separated, dried over $MgSO_4$ and concentrated to give SG1-N_3 **(15)** (0.093 g, 60%) as a white powder. UPLC-TOF (ESI) *m/z:* $[M+H]^+$ calc. for $C_{37}H_{50}N_9O_{12}$ 812.3573, found 812.3474; m.p. 181-183°C; ^{1}H-NMR (400 MHz, Acetone-d_6) δ 8.07 (s, 2H, C=C-H), 6.73 (m, 3H, Ar-H), 5.47 (d, 2H, *J* = 4.8 Hz), 5.20 (s, 4H, -CH_2-), 4.70 (dd, 2H, *J* = 7.6, 2.4 Hz), 4.64 (s, 2H, -CH_2), 4.61 (d, 2H, *J* = 3.6 Hz), 4.39 (dd, 2H, *J* = 4.8, 2.4 Hz), 4.36 (dd, 2H, *J* = 7.6, 1.6 Hz), 4.32 (dd, 2H, *J* = 3.2, 1.6 Hz), 4.30 (dd, 2H, *J* = 3.6, 2.0 Hz), 1.44 (s, 6H, C-CH_3), 1.36 (s, 6H, C-CH_3), 1.35 (s, 6H, C-CH_3), 1.28 (s, 6H, C-CH_3); ^{13}C-NMR

(100 MHz, Acetone-d_6) δ 161.8, 144.8, 141.9, 126.3 (C=CH), 111.2, 110.4, 109.9 (Ar-CH), 103.3 (Ar- CH), 98.2, 72.9, 72.5, 72.0, 68.8, 63.4 (Ar-CH2-), 52.0, 47.6 (CH_2-), 27.4 (C-CH_3), 27.2 (C-CH_3), 26.1 (C-CH_3), 25.7 (C- CH_3)

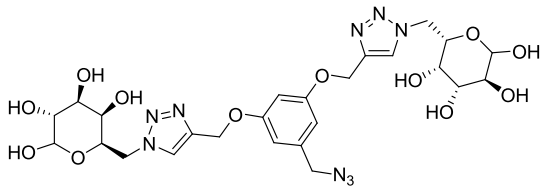

Synthesis of (16)[105]: To a stirred suspension of **(15)** (640 mg, 0.79 mmol) in water (10 mL) was added TFA (10 mL) and the mixture was heated at 80°C for 2 hours. The mixture was then concentrated to a residue. Precipitation of the product by the addition of acetone afforded the product as a fine white powder. The mixture was centrifuged, the supernatant decanted and the solids were dissolved in water and freeze dried to afford **(16)** (0.303 g, 59%) as a white powder. UPLC-TOF (ESI) *m/z:* $[M+H]^+$ calc. for $C_{25}H_{34}N_9O_{12}$ 652.2321, found 652.2332; m.p. 185-186°C; ^{1}H-NMR (400 MHz, DMSO-d_6) δ 8.20 (s, 2H), 6.60 - 6.81 (m, 3H), 5.43 (d, J = 4.9 Hz, 2H), 5.16 (s, 4H), 4.19 - 4.76 (m, 15H); ^{13}C-NMR (100 MHz, DMSO-d_6) δ 159.4, 142.2, 137.8, 125.0, 108.8, 108.1, 107.4, 101.0, 95.5, 68.8, 61.2, 53.5, 50.1

2.5.2.3 Synthesis of sugar triazole (3)

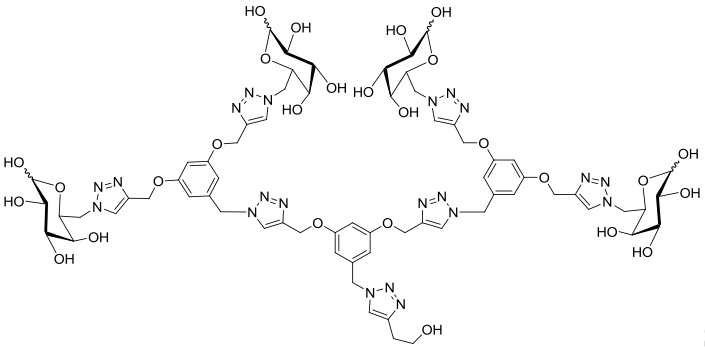

Synthesis of (3): To a stirred solution of **(21)** (0.057 g, 0.037mmol.) in DMSO (3 mL) was added 3-butyn-1-ol **(9)** (2.6mg, 0.037mmol.), and PS-NHC-Cu(I) **(42)** (1.49 mmol/g catalyst loading, 3.7 mg, 0.006mmol) under a nitrogen atmosphere. The reaction mixture was stirred overnight then filtered with a 0.2 μm filter, the solid catalyst was washed with DMSO (1 mL) and the combined filtrate was concentrated to a small volume, diluted with water (1.5 mL) and purified by semi-preparative HPLC. Lyophilisation of selected fractions afforded **(3)** (0.053 g, 92%) as a pale yellow powder. UPLC-TOF (ESI) *m/z:* $[M+H]^+$ calc. for $C_{67}H_{84}N_{21}O_{27}$ 1614.5840, found 1614.5908; m.p. 168-169°C

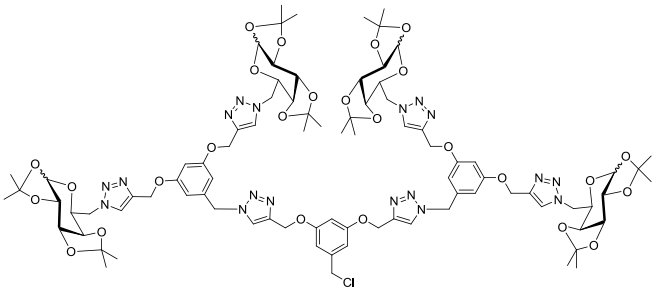

Synthesis of (18):[105] To a stirred solution of 1-(chloromethyl)-3,5-bis(prop-2-ynyloxy)benzene **(13)** (0.014 g, 0.0615 mmol) in THF (20 mL) was added **(15)** (0.100 g, 0.123 mmol),

CuOTf.benzene complex (0.031 g, 0.0615 mmol) and sodium ascorbate (0.012 g, 0.0615 mmol) under a nitrogen atmosphere. The mixture was stirred for 24 hours and then concentrated to residue. This was diluted with DCM (50 mL), washed with water (3 x 10 mL), NH_3 0.8 M (10 mL) and brine (10 mL), dried with $MgSO_4$ and concentrated to afford **(18)** (0.045 g, 20% yield) as a pale cream powder. ESI-MS (ES+) *m/z:* $[M+H]^+$ calc. for $C_{87}H_{110}ClN_{18}O_{26}$ 1857.7522, found 1859; m.p. 172-174°C; ^{1}H-NMR (400 MHz, $CDCl_3$) δ 7.78 (s, 4H, C=CH-), 7.59 (s, 2H, C=CH-), 6.61 (m, 2H, Ar-H), 6.58 (m, 1H, Ar-H), 6.55 (m, 2H, Ar-H), 6.50 (m, 4H, Ar-H), 5.49 (bd, 4H, *J* = 4.8 Hz), 5.40 (s, 4H, -CH_2-), 5.15 (s, 4H, -CH_2-), 5.12 (s, 8H, -CH_2-), 4.64 (m, 4H), 4.62 (m, 4H), 4.47 (s, 2H, -CH_2-), 4.46 (m, 4H), 4.32 (m, 4H), 4.19 (m, 8H), 1.48 (s, 6H, C-CH_3), 1.35 (s, 12H, C-CH_3), 1.34 (s, 12H, C-CH_3), 1.27 (s, 6H, C-CH_3), 1.26 (s, 12H, C-CH_3); ^{13}C-NMR (100 MHz, $CDCl_3$) δ 160.0, 159.5, 144.1, 143.2, 140.0, 136.7, 124.2, 122.9, 109.9, 109.0, 108.0, 107.2, 101.7, 101.6, 96.1, 71.1, 70.5, 70.1, 67.0, 61.9 (Ar-CH_2-), 61.8 (Ar-CH_2-), 53.9 (Ar-CH_2-), 50.4, 45.9 (CH_2-), 26.0 (C-CH_3), 25.9 (C-CH_3), 24.9 (C-CH_3), 24.4 (C-CH_3)

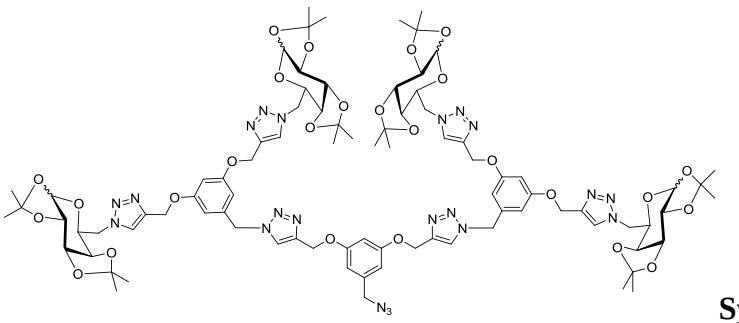

Synthesis of (19)[105]*:* To a stirred solution of **(18)** (0.045 g, 0.0242 mmol) in dioxane (5 mL) and water (5

mL) was added NaN_3 **(20)** (0.039 g, 0.605 mmol) under a nitrogen atmosphere. The mixture was heated at reflux for 4 hours then cooled, diluted with DCM (10 mL), washed with water (3 x 10 mL), brine (10 mL), dried over $MgSO_4$ and concentrated to afford **(19)** (0.041 g, 91% yield) as a pale cream powder. ESI-MS (ES+) *m/z:* $[M+H]^+$ calc. for $C_{87}H_{110}N_{21}O_{26}$ 1864.7925 , found 1865; UPLC-TOF (ESI) *m/z*: $[M+Na]^+$ calc. for $C_{87}H_{109}N_{21}NaO_{26}$ 1886.7745, found 1887.7862; m.p. 171-172°C; ^{1}H-NMR (400 MHz, $CDCl_3$) δ 7.79 (s, 4H, C=CH-), 7.78 (s, 2H, C=CH-), 6.60 (m, 2H, Ar-H), 6.58 (m, 1H, Ar-H), 6.55 (m, 4H, Ar-H), 6.50 (m, 2H, Ar- H), 5.49 (bd, 4H, *J* = 4.8 Hz), 5.43 (s, 4H, -CH_2-), 5.18 (s, 8H, -CH_2-), 5.12 (s, 4H, -CH_2-), 4.64 (m, 4H), 4.62 (m, 4H), 4.46 (dd, 4H, *J* = 13.8, 8.4 Hz), 4.32 (m, 4H), 4.24 (s, 2H, -CH_2-), 4.19 (m, 8H), 1.48 (s, 12H, C-CH_3), 1.37 (s, 12H, C-CH_3), 1.34 (s, 12H, C-CH_3), 1.27 (s, 12H, C-CH_3); ^{13}C-NMR (100 MHz, $CDCl_3$) δ 159.9, 159.7, 144.1, 143.4, 143.1, 137.8, 124.2, 124.0, 109.9, 109.0, 107.7, 107.4, 101.8, 101.7, 96.2, 71.1, 70.7, 70.3, 67.1, 62.1 (Ar-CH_2-), 62.0 (Ar-CH_2-), 54.6 (Ar-CH_2-), 50.4, 45.9 (CH_2-), 25.9 (C-CH_3), 25.8(C-CH_3), 24.8 (C-CH_3), 24.4 (C-CH_3)

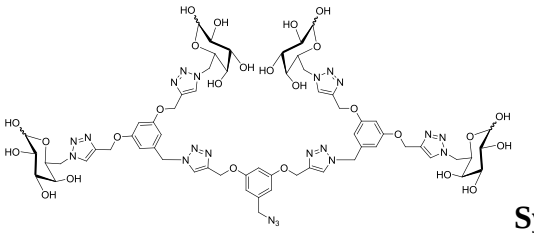

Synthesis of (21)[105]*:* To a mixture of TFA : water (1 : 1, 10 mL) was added **(19)** (0.040 g, 0.021 mmol.) under a nitrogen atmosphere. The reaction mixture was heated to 65 °C for 6 hours. The mixture was then cooled, concentrated *in vacuo* to a small volume, diluted with

water (1.5 mL) and purified by semi-preparative HPLC. **(21)**[105] (0.016 g, 48% yield) was recovered as a white powder after lyophilisation. ESI-MS (ES+) *m/z:* $[M+H]^+$ calc. for $C_{63}H_{78}N_{21}O_{26}$ 1544.5421, found 1545; m.p. 177-179°C

2.5.3 Silver Nanoparticle (AgNP) formation

Preparation of sugar stock solutions: Sugars **(1)** and **(2)** were dissolved in ultrapure water and diluted as necessary with ultrapure water for the preparation of the arrays. Sugar **(3)** is relatively less soluble; the concentrated (10 mM) stock solution in ultrapure water was warmed at 40°C for 15 minutes prior to use. All the sugars stock solutions were preserved at 4°C.

Preparation of Tollens stock solutions: Tollens stock solutions were prepared fresh on a daily basis from 3 equivalent recipes and diluted as necessary for the nanoparticle arrays:

Protocol 1. 100 mM Tollens: to 1.790 mL H_2O was added $AgNO_3$ (0.5 M, 500 uL), followed by NaOH (3 M, 100 uL) and finally NH_4OH (28%, 110 uL).

Protocol 2. 20 mM Tollens: to 4059.2 mL H_2O was added $AgNO_3$ (0.5 M, 278.4 uL), followed by NaOH (3 M, 55.7 uL) and finally NH_4OH (28%, 61.25 uL)

Protocol 3. 3 mM Tollens: to 9.915 mL H_2O was added $AgNO_3$ (0.5 M, 60 uL), followed by NaOH (3 M, 12 ul) and finally NH_4OH (28%, 13.2 ul)

General procedure for the preparation of AgNPs: 300uL of Tollens stock solution and 300uL of sugar stock solution were mixed in disposable plastic Eppendorf. The solution was briefly shaken and left in the dark for 24 hours. The mixture was then centrifuged for 20 secs to remove occasional micrometre sized

particles, then collection of surnatant afforded the AgNP colloid without any further purification.

Procedure for the preparation of NMR plots: Sugars were dissolved in 600 μL D_2O at concentrations specified below and spectra were recorded after the addition of increasing aliquots of a stock solution of $AgNO_3$ 978.38 mM dissolved in D_2O. Volume variations were small enough to be ignored in calculations.

The recorded spectra are shown in Appendix and ordered from bottom to top:

5 ^{1}H-NMR (400 MHz, D_2O) of D-galactose 144.56 mM with 0.1, 0.2, 0.5, 1.0, 2.0 eq $AgNO_3$

5 ^{1}H-NMR (500 MHz, D_2O) of **(1)** 88.69 mM with 0.1, 0.2, 0.5, 1.0, 2.0 eq $AgNO_3$

14 ^{1}H-NMR (500 MHz, D_2O) of **(2)** 22.30 mM with 0.1, 0.2, 0.5, 1.0, 1.1, 1.2, 1.5, 2.0, 2.1, 2.2, 2.5, 3, 4, 6 eq $AgNO_3$

12 ^{1}H-NMR (400 MHz, D_2O) of **(29)** 20.00 mM with 0.1, 0.2, 0.5, 1.0, 1.1, 1.2, 1.5, 2.0, 2.1, 2.2, 2.5, 3 eq $AgNO_3$

CHAPTER 3: SYNTHESIS OF SUGAR-MODIFIED DNA-BINDING PAs

3.1 Pyrrole-Imidazole (Py-Im) polyamides (PAs) introduction

A standard first generation Py-Im PAs contains three main motifs: a "tail", a "loop" and two short oligomers of pyrrole (Py) and imidazoles (Im), similar to distamycin (Figure 83). The "loop" joins the oligomers and it is usually an aliphatic gamma amino acid, while the "tail" is due to the solid phase synthesis used to prepare the PA and contains a beta alanine and a terminal tertiary amine. (Figure 83) All of these motifs have an important role on the binding of the PAs to DNA sequences.

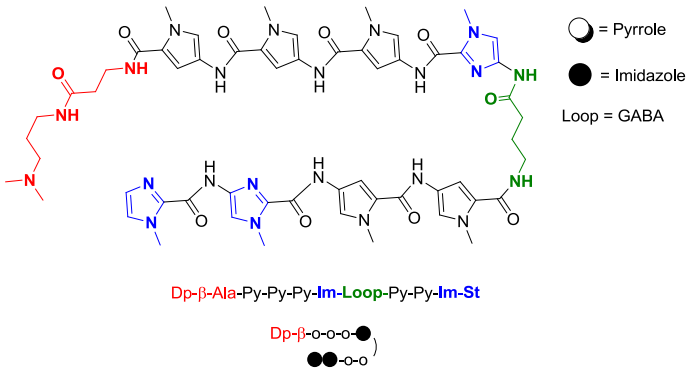

Figure 83: Schematic representation of a typical Py-Im PA. At the bottom, examples of short nomenclature for the drawn PA. For clarity, the "loop" (green), the "tail" (red) and the heterocyclic rings (blue and black) have been colour coded.

An eight-ring PA can be programmed to potentially bind any sequence of 6-8 DNA base pairs with affinities and specificities in the nanomolar and subnanomolar range.[157] These binding affinities surpass many endogenous transcription factors which bind to similar target sequences.[158] Sequence recognition is achieved by the molecular recognition of the hydrogen-bond landscape arising from the Watson-Crick hydrogen-bond donor and acceptor

moieties and the PA functional groups. As in distamycin (Figure 84), pyrrole pairs selectively recognise A/T sequences.

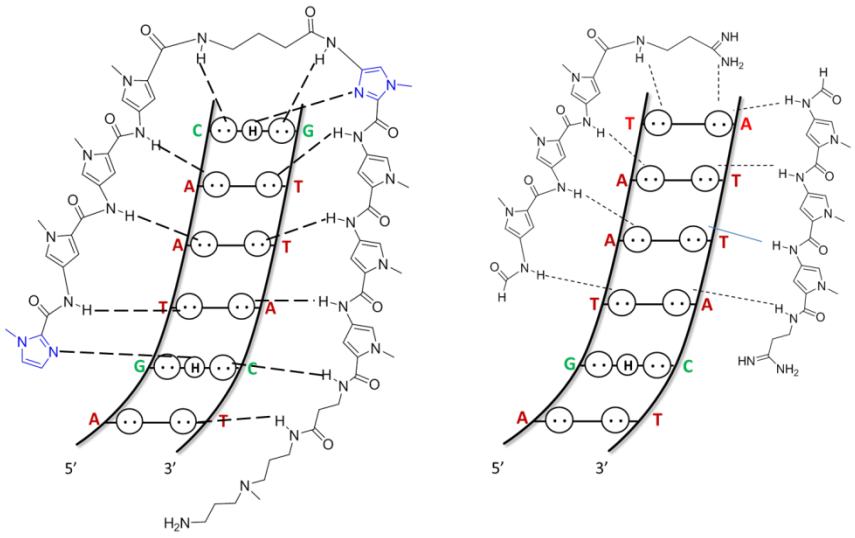

Figure 84: Molecular recognition of DNA by a Py-Im PA (left) and two molecules of distamycin (right). In blue highlighted the selective recognition of guanines by imidazoles in the Py-Im PA.

Replacing a pyrrole with an imidazole unit, introduces a lone pair that can accept an additional H-bond from a guanine, altering the sequence specificity from A/T to G/C (Figure 84). This fundamental discovery was first reported by William Lown while researching derivatives of distamycin in the attempt to vary the sequence specificity.[159] Second generation PAs by the Dervan group introduced the hydroxypyrrole (Hp) unit, which can form an additional H-bond with T, allowing the pair Hp/Py to break the degeneracy and distinguish T/A from A/T (Figure 85).[160]

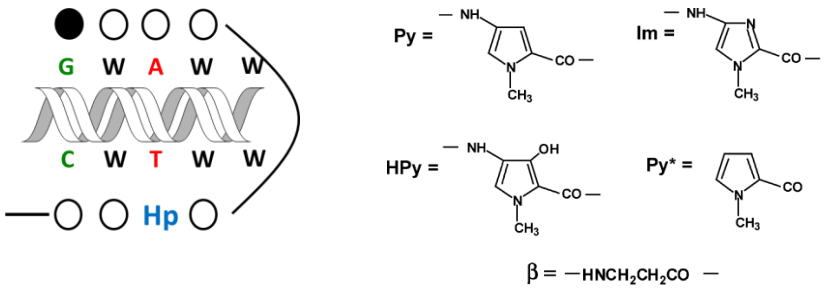

Figure 85: Schematic representation of a Py-Im PA binding DNA, with highlighted the preferential binding of Im (black sphere) to guanine (25) and hydroxylpyrrole (Hp, blue) binding thymine (9). On the right, structure of Py, Im and HydroxyPyrrole (HPy or HP) (image reproduced from Ref.[161])

Charged turn units using ammonium functional groups increase the binding affinity by additional charge interactions with the DNA phosphates, without any increase in specificity.[162] Charged amino turns are also inherently chiral and the two chiral forms (R,S) have different binding affinity when used in polyamides.[162] A number of other 5-membered heterocycles (such as thiophene) have been studied by Dervan in an attempt to increase the binding affinities by studying the angle constraints of the rings in order to adjust the winding geometry of the PA in the minor groove of DNA.[163] The outcome of this last study was an increase in specificity with a general decrease in the binding affinity and a much higher synthetic challenge. Lastly, macrocyclic PAs were devised as a method to increase the cell-permeability of PAs.[164] The study also speculated that by closing the hairpin of the PAs yielding a cyclic structure would enhance the binding affinity to DNA.[165]

3.1.1 Advantages of Pyrrole-Imidazole PAs over other DNA binders

The main advantage of Py-Im PAs is the inherent programmability to virtually bind any short DNA sequence of 6-8 base pairs with high selectivity. Py-Im PA synthesis is comparably simpler than cyclic and additional heterocycle PA synthesis, while retaining high specificity in the binding of short DNA sequences. The second advantage of PAs allows them to be modified to deliver any desired functional material to the selected DNA site. The three previously described motifs ("loop", "tail" and heterocycle) (Figure 83) can be modified to carry additional functional groups without major impact on the ability of the PA to selectively bind DNA. The unique properties of molecular recognition and programmability of PAs are highly promising for their use in DNA nanotechnology. For example, Py-Im PAs can recruit tethered molecular components such as proteins and position them onto DNA nanostructures.[166–168]

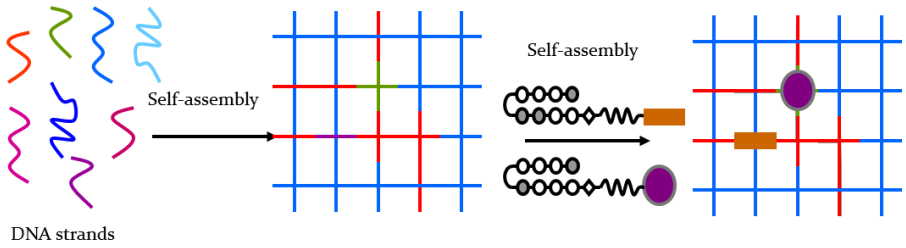

Figure 86: Schematic representation of a self-assembled construction of a DNA sensor/electronic device by sequence specific self-assembly of Py-Im PAs tethered to molecular components.

3.1.2 Applications of Py-Im PAs in bionanotechnology

PA applications can be divided in 3 groups: (i) functionalization of PAs for biosensing applications, (ii) up- or down-regulation of gene transcription; and (iii) DNA nanotechnology. PAs tethered to a thiazole orange have been used to detect

specific double stranded DNA sequences. Fluorescence is observed by the binding of the PA to its matched double stranded target sequence. A decrease in fluorescence up to 40% was observed for one-base-pair mismatched, thus demonstrating the selectivity of these compounds for their target sequence.[169] Covalently bound fluorescein has been used as a sensor for detecting DNA nanoarchitectures[170] or to detect the internalisation of the PA inside the cell nucleus.[171–173] The advantage of these techniques is that it is possible to follow the internalisation of a PA in the cell cytoplasm and into the nucleus by confocal microscopy. However, tethered PAs have demonstrated an erratic behaviour during internalisation as the tethered fluorophores drastically modified the ability of the PA to pass through nuclear membranes.[172]

3.1.2.1 Applications of PAs in the manipulation of gene expression

Direct influence of gene transcription is a very important biochemical field for the implication of development of new cures of genetic disorders.[174] PAs showed promising results as a mean to down-regulate the expression of various genes including vascular endothelial growth factor (VEGF),[175,176] hypoxia-inducible factor (HIF),[177] androgen receptor-mediated gene expression,[178] glucocorticoid receptor-mediated gene expression,[179] topoisomerase IIa expression,[180] human Aurora kinase gene expression[181] in *in-vitro* assays. PAs have also been demonstrated to work as activators of gene expression by working as cell-permeable artificial transcription factors.[182,183]

3.1.2.2 Application of PAs in DNA nanotechnology.

PAs have demonstrated the ability to be used as a construction element in nano-assembly. Thorsten and Heckel have shown that the binding strength of a PA is high enough to be used as a "strut" to bind two DNA plasmids. This is quite a significant achievement as the molecular weight of these plasmids is a hundred times the weight of the PA itself.[184]

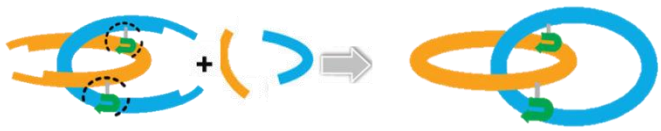

Figure 87: Schematic representation of the formation of DNA catenanes by self-assembling of PAs. (Image reproduced from ref. [185])

The Heckel group also showed that PAs can be functionalised and self-assembled to form DNA nanoring catenanes (Figure 87).[185] Cohen and Dervan broadened the use of PAs to DNA origami, showing that a 2D origami tile can be specifically targeted and single molecules, such as biotin-streptavidin, can assemble over a 120 nm surface area. This effectively opened the possibility of directed self-assembly of proteins using the duplex structure of DNA rather than ssDNA sequences as in conventional approaches.[168] This approach was then expanded with the use of multiple PAs targeting selectively DNA origami sites allowing the multi-patterning of unmodified DNA templates.[166]

In conclusion, Py-Im PAs have shown to be highly efficient DNA binders with a high selectivity towards selected DNA *loci*. Their properties have been exploited as a molecular tool in both biology and nanotechnology. In a further step towards a more widespread use of this important class of molecules, PAs should be tested

as tools for templated DNA metallisation. As analysed in the previous chapters, templated techniques for the assembly of DNA and metallic nanoparticles with high precision are required.[59] It was surmised that by combining the use of sugar-modified Py-Im PAs in conjunction with the mild generation of silver nanoparticles via the use of the Tollens' reagent, one could confine the growth of silver nanostructures along DNA architecture with superior control over current methods.

3.2 Aims of this chapter

The aim of this chapter is to synthesise sugar functionalised PAs. Such PAs could be used, together with the optimized Tollens' reaction (Chapter 2) to metallise natural DNA, both for the production of metallic nanowires through selective coating of the DNA and for the templated deposition of silver nanoparticles in a sequence specific fashion. This chapter will focus on interfacing Py-Im PAs with sugars using "click chemistry" to fuse each component together.

3.3 Results

The synthesis of PAs is divided in two parts: i) preparation of the heterocyclic monomers and ii) solid phase synthesis of PAs. Web of Knowledge returns 441 papers related to the use of Py-Im PAs from 1997-2011, however the most authoritative publication remains the solid phase synthesis of PAs by Baird and Dervan in 1996.[161] Despite their apparent ease of synthesis, these compounds are challenging to prepare and result in moderate yields which were prohibitive for

our research programme. For these reasons, the preparation of Py-Im PAs was optimized.

3.3.1 Synthesis of PA monomers

3.3.1.1 Preparation of pyrrole monomer (45)

Boc-Py-COOH **(45)** was prepared from the commercially available nitropyrrole ester **(43)** in 2 steps: **(43)** was reduced using a *nickel boride* (catalytic, prepared *in situ*) reaction using excess $NaBH_4$ and Boc protected in a single step in MeOH at -20ºC to afford **(44)** in 73% yield. The catalytic activity of nickel salts reduced with excess $NaBH_4$ was already known to Cornelius.[186] Caddick[187] established that this type of catalysts could be used for the reduction of nitriles to amines and Boc protection in one step. This modified protocol first devised by Caddick *et al.* employed the same preparation of the *nickel boride* and showed an excellent reactivity towards nitro groups.

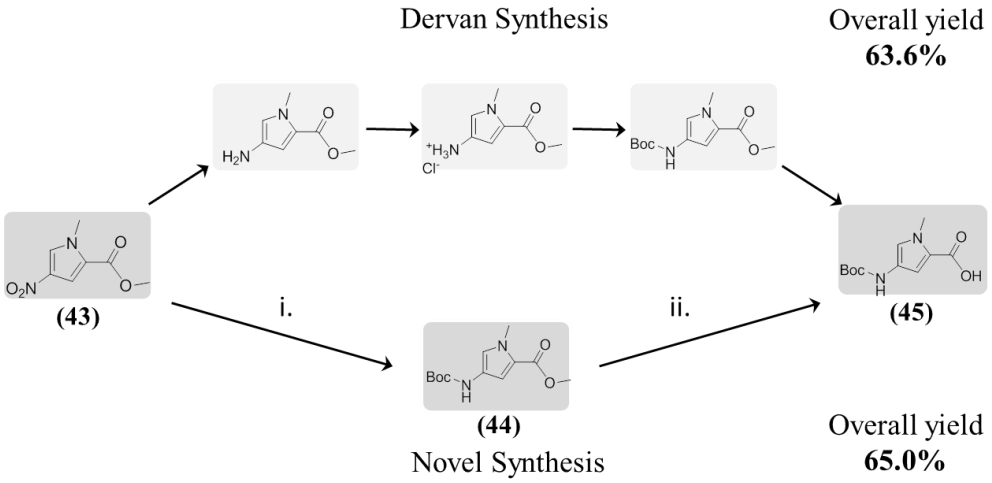

Scheme 11: Optimised synthesis of Py monomer (45). i. $NiCl_2 \cdot 6H_2O$, $NaBH_4$, Boc_2O (58), -20°C, 73% ii. NaOH, MeOH/H_2O, 60°C, 12h, 89%

The mechanism of nickel boride reductions is still a matter of speculation; however we noticed that the yield of **(44)** varied significantly with the reaction temperature (Table 7).

Entry	Temperature (°C)	Yield (%)
1.	22	30
2.	0	50
3.	-20	73
4.	-40	74

Table 7: Table showing the dependence of the yields of the nickel boride reduction to the temperature of the reaction.

The nickel boride catalyst is formed *in situ* by the addition of $NaBH_4$ to a solution of $NiCl_2 \cdot 6H_2O$ in MeOH, forming a black suspension of particles. The exact ratio between nickel and boron in the particles is still up to discussion in literature and has been reported as Ni_2B, Ni_3B or NiB.[188–193] However, it is suggested that the size of the particles have a strong dependence to the temperature of the preparation, with smaller particles forming at lower temperatures.[194,195] This result could then be explained simply by an increase of catalytic activity by the increase of surface area of the particles at low temperature. Lastly, the ester **(44)** was then hydrolysed using aqueous NaOH in MeOH at 60ºC for 12 hours to afford **(45)** in 89% yield. In conclusion, this protocol was superior to Dervan's synthesis. It is two steps shorter and avoids a high pressure hydrogenation while maintaining the same yields.

3.3.1.2 Preparation of the Imidazole monomer (51)

The preparation of the imidazole monomer **(51)** was performed from 1-methylimidazole **(46)** due to a lack of a commercial supplier of the nitro precursor **(49)**.

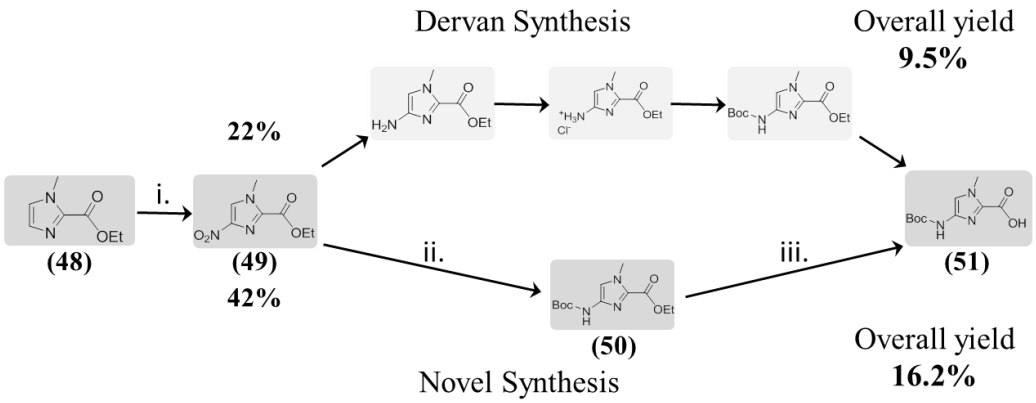

Scheme 12: Optimised synthesis of Im monomer (51). i. 99% HNO_3, 98% H_2SO_4, 90°C, 50min, 42% ii. Boc_2O (58), H_2, 10% Pd/C, MeOH, 88% iii. LiOH 1M, MeOH, 22°C, 2h, 42%

1-methylimidazole **(46)** was reacted with ethylchloroformate **(47)** at 0°C for 18 hours to afford **(48)** in 42% yield. Nitration of **(48)** using 99% HNO_3 and 98% H_2SO_4 was achieved without the use of an additional solvent at 90°C for 50 minutes. These extreme conditions afforded a mixture of 4-nitro **(49)**, 5-nitro **(49a)** and 4,5-dinitro **(49b)** imidazoles as described by Bailly.[46]

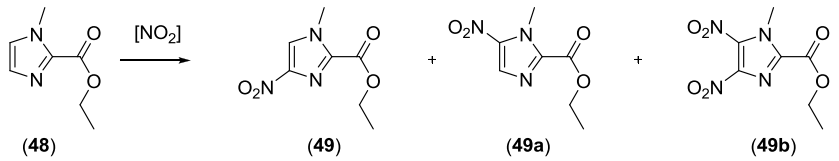

Scheme 13: Product distribution of nitration of compound (48)

This complex mixture was purified by preferential re-crystallisation of the 4-nitro-isomer **(49)** from CCl_4:EtOH in 22% yield, using a protocol described by Dervan *et al.*[161] By screening solvents it was discovered that it was possible to selectively purify the 4-nitroimidazole **(49)** by re-crystallisation using $CHCl_3$:diethyl ether at 0°C in 42% yield, nearly doubling the yields of the previous report. Furthermore, concentration of the mother liquor and subsequent re-dilution with ethyl acetate induced selective crystallisation of the 5-nitroimidazole **(49a)** in 21% yield.

Reduction of the nitro group of **(49)** posed additional problems. The hydrogenation reaction conducted at 1 atm was slow with less than 30% conversion after 48h. Additionally, the putative product 4-amino-2-carboethoxy-1-methylimidazole **(49c)** was not stable under these reaction conditions and tended to oligomerise over a few hours as observed visually by the darkening of the reaction solution and by TLC; moisture was a factor speeding up this side reaction as tests conducted in anhydrous MeOH significantly reduced the oligomerisation.

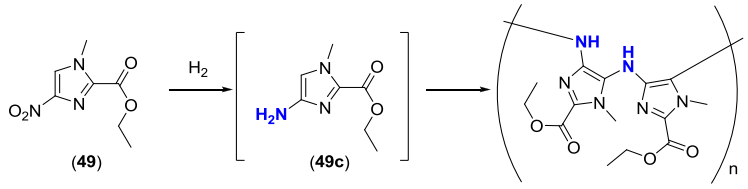

Scheme 14: Proposed mechanism and structure of oligomers of compound (49) during hydrogenation

Dervan *et al.*[161] resolved the problem by conducting the hydrogenation at high pressure in a high polarity anhydrous solvent such as DMF (500 psi of H_2, 10% Pd/C) and then quenching the reaction with gaseous HCl to trap the product as the

stable hydrochloride salt. Due to the unavailability of high-pressure hydrogenation devices in the laboratory, it was decided to re-optimise the reaction. It was noted that hydrogenation in MeOH using a constant stream of hydrogen was considerably faster and concluded in 24 hours. Boc_2O added in the reaction resulted in reduction and Boc-protection in a single step and prevented oligomerisation. Moreover when highly anhydrous MeOH was used (dried overnight with $CaCl_2$ then cannula distilled over 3Å molecular sieves) oligomerisation was further reduced. All of these factors combined afforded a one-pot, single step hydrogenation and Boc protection with 88% yield to **(50)**. Finally **(50)** was saponified using 1M LiOH in MeOH at room temperature for 2 hours to afford **(51)** in 44% yield and an overall yield of 16.2% (1.7 times higher than previously reported yield[161]).

3.3.2 Solid phase synthesis (SPS) of PAs

Py-Im PAs and PA conjugates have been prepared using a variety of protocols over the last 2 decades.

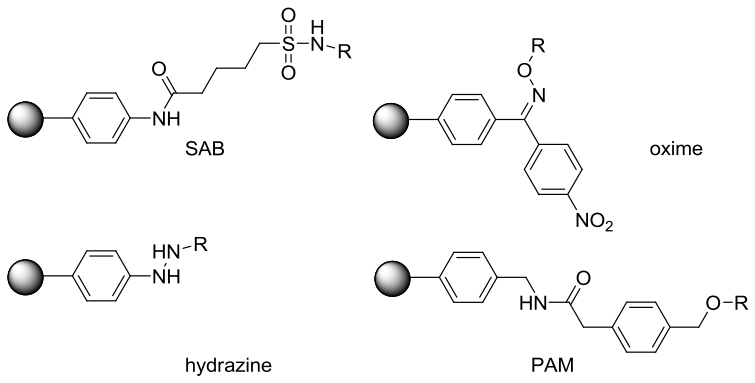

Figure 88: Structures of SPS resins: SAB, oxime, PAM resins and hydrazine.

Both Boc[161] and Fmoc[196] protocols have been used to prepare PAs in analytical quantities (0.1-5 mg) using a variety of solid supports such as PAM resin,[197] oxime resin,[198] sulfonamidobutyryl (SAB) resin[199] and hydrazine safety catch resin (Figure 88).[200]

Methods were also developed to increase the speed of the SPS[197] or to automate it.[196] Py-Im PAs synthesis however has been plagued by yields as low as 0.1% as a consequence of truncated products.[201] Studies have determined the following major factors impacting on the final yield of a Py-Im PA: i) the number of Im units, ii) the use of DABA or GABA loops (Figure 89) and iii) the coupling of the terminal Im unit **(52)** can all cause drastic reduction of the yield.

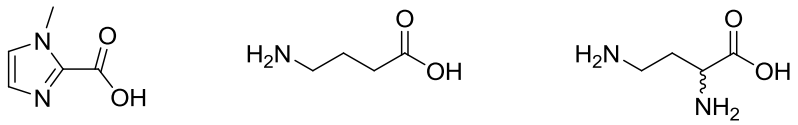

(52) GABA (**53**) DABA (**54**)

Figure 89: Structure of GABA (53) and DABA (54) loops and 1-methylimidazole-2-carboxylic acid used in SPS of PAs

The introduction of the Im units causes reduction of the yield because of the inherent electronic properties of the species involved. There is a low electronic driving force in the reaction of a Py monomer coupling to the growing PA chain immobilised on a solid support ending in an Im-NH_2, since the Py monomer is behaving like an electron-rich electrophile and the Im is an electron-poor nucleophile. The loop classically used in the synthesis of Py-Im PAs is gamma-aminobutyric acid (GABA) **(53)** and generally is associated with good yields. When the loop is replaced with a charged molecule such as di-aminobutyric acid (DABA) **(54)**, a notable reduction in the yield can be attributed to the reduced

stability of the PA and of the necessary orthogonal protecting groups[202] (such as Fmoc or Cbz) at the conditions of the SPS. Lastly, the introduction of the final ring of a PA, usually 1-methylimidazole-2-carboxylic acid **(52)** is known to be a difficult step with classical coupling agents like HATU or HBTU giving only poor yields (<10%) while DCC/HOAt performs better with average yields (10-40%). Dervan's group devised an alternative strategy to the coupling of **(52)** by using trichloroketones (Figure 90) in the presence of Hunig's base at 50°C in 18h with good yields for some PA sequences,[161] while Sugiyama's group preferred to completely avoid the step and couple an additional Im monomer **(51)**.

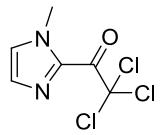

N-methyl imidazole trichloromethyl ketone

Figure 90: Structure of N-methyl imidazole trichloromethl ketone used by Dervan to couple the terminal Im of PAs during SPS.

3.3.2.1 General protocol and reagents for the Boc SPS of PAs

The original method for Boc-based SPS relies on Boc protected heterocyclic monomers **(45)**, **(51)** and **(53)** of the PA sequentially coupled onto PAM resin using HATU or HBTU as coupling agents[161] and four-fold excess of monomer. Next, the Boc group is removed with a strong acid, such as TFA in the presence of 2.5% water and 5% phenol that act as scavengers of the tert-butyl cations formed during the deprotection (TPW solution). The deprotected amino group is then coupled and the cycle is repeated. Multiple DMF washes are performed to remove the unreacted reagents. NMP is sometimes used to wash the resin to remove

"clumping" caused by impurities, mainly uronium salts, which are more soluble in this solvent. Additionally, DCM washes are necessary to re-swell the resin and allow better access to all the reactive sites and so improving the yields and purity of the final PA. Thus, the generalised protocol for a synthesis of an 8-ring PA consists of no-less than 5 different multistep operations to be repeated 9 times (8 rings + loop) as summarised in Scheme 15.

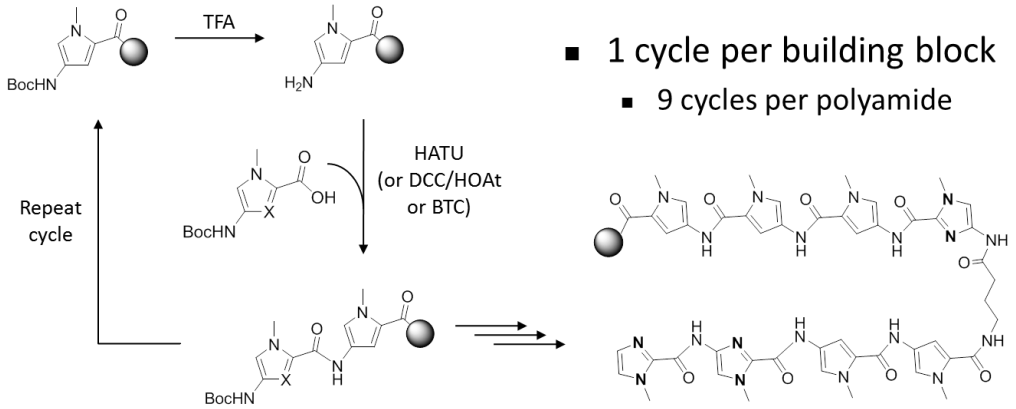

Scheme 15: General protocol for the solid phase synthesis (SPS) of Py-Im PAs, highlighting deprotection with TFA and coupling of a Py or Im.

Upon completion of the synthesis, the resin is washed and shrinked with MeOH to purge it from solvents and impurities, then dried under vacuum. The PA is cleaved using an amine at 50°C for 12-18 hours.

Amines such as di-methylaminopropylamine **(55)** (Dp) and bis-(3-aminopropyl)-methylamine **(56)** are commonly used (Scheme 16), the latter if post-synthetic modification of the PA are necessary.

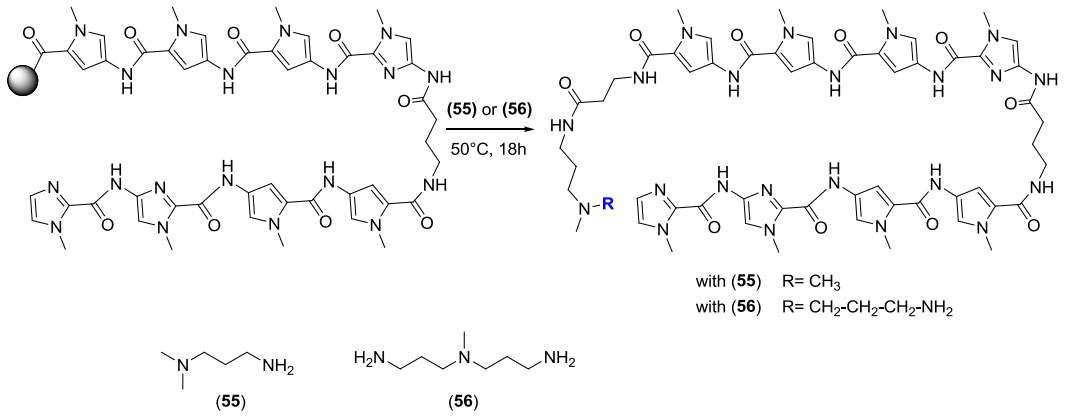

Scheme 16: Cleavage and amidation of Py-Im PA. Structure of cleaving amines (55) and (56).

3.3.2.2 Novel triphosgene (BTC) SPS coupling method

The coupling of the electron-rich pyrrole monomer **(45)** with the electron deficient amine imidazole **(51)** is known to be difficult with only 5-8% yield.[203] Modi Wetzler of the Wemmer's group prepared dimers of pyrrole and imidazole ready to be used in the SPS,[204] as well as Dervan's circumvented the low yielding coupling by the same strategy.[196] While this viable method achieved average yields, it required the preparation of all the permutation dimers necessary to get any desired sequence of Py-Im PAs. Moreover the dimers showed limited solubility in typical coupling solvents (DMF, NMP, DMSO). To address these limitations, our group developed a novel coupling strategy with the use of triphosgene (BTC) as coupling agent (Scheme 17).

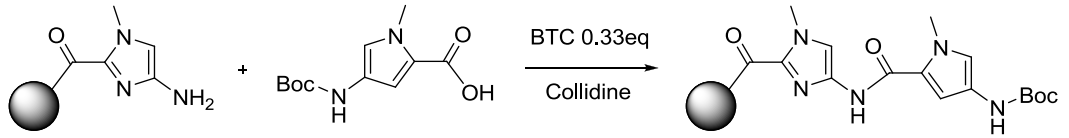

Scheme 17: Novel BTC protocol for difficult coupling in Py-Im PAs

BTC is an extremely reactive reagent that forms mixed anhydrides (Scheme 18) with the desired carboxylic acid with greater electrophilicities than standard benzotriazole activation.[205]

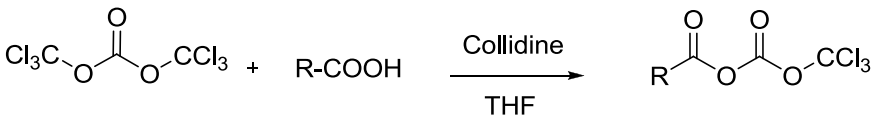

Scheme 18: Structure of the highly reactive mixed anhydride formed with BTC and a carboxylic acid.

Due to the extreme sensitivity to bases, DMF cannot be used as a solvent. Dry THF was chosen (with dry diglyme being an alternative because of similar solubility profiles for these compounds). 2,4,6-collidine was chosen as optimal base for catalysis, it has a pKa of 7.5, more basic than pyridine (pKa = 5.25) and so able to efficiently catalyse the reaction but mild enough to control it; we found that even catalytic quantities of DMF (pKa ~ 9.5) were too basic to control the reaction without run-away exothermicity resulting in decomposition of the mixed anhydride. Traces of TFA were detrimental as they could react with the triphosgene and cap the resin to form triflic amides. It was found that a single additional wash with DMF/Hunig's base, prior to the couplings with BTC, was sufficient to completely remove the TFA traces. The whole protocol has been summarised in Scheme 19.

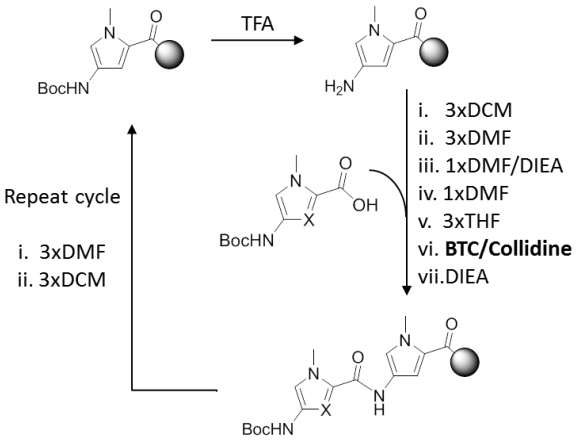

Scheme 19: Step-by-step scheme of the novel BTC protocol, that includes extensive washes after the deprotection, solvent exchange to THF, coupling with BTC/Collidine/DIEA and finally washing of the resin to remove excess reagents.

The new protocol showed complete couplings of the difficult Resin-Im-NH_2/BocPyOH coupling (Table 8).

Amide bond	HATU (%)	DCC/HOAt (%)	BTC (%)
BocPyOH -> H_2N-Im-Resin	5	8	>98
BocPyOH -> H_2N-Py-Resin	95	95	>98
BocImOH -> H_2N-Im-Resin	12	>98	>98

Table 8: Yields of formation of amide bonds between Py and Im at the variation of the coupling agents HATU, DCC/HOAt and BTC.

We chose to investigate the synthesis of the challenging PA **(57)** (Figure 91) in order to assess the scope of the methodology.

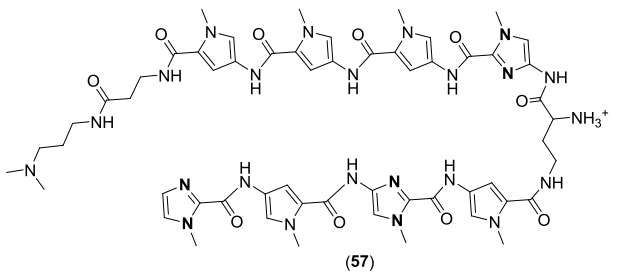

Figure 91: Structure of PA (57).

PA **(57)** targets the DNA sequence 5′-WWGWGCW-3′ (where W is either A or T) with nanomolar affinity.[201] Compound **(57)** was prepared in only 0.1% reported yield using the PAM resin via a traditional Boc-chemistry protocol by Dervan *et al*.[206] This PA sequence also comprises other typical coupling sequences such as Py-Py, Py-Im, and Im-aliphatic couplings which enabled us to ascertain the scope of the BTC coupling methodology. Using Boc-based chemistry and exclusively our BTC protocol, we prepared PA **(57)** in 33% yield after CBz deprotection of the γ-turn motif (CBz was deprotected using a mixture of trifluoromethanesulfonic acid : TFA 10:90 for 1 minute at -40°C[203]). This constitutes a 330-fold increase in isolated yield for **(57)** using this BTC coupling protocol.

3.3.3 Convergent solution phase and solid phase synthesis of PAs

The synthesis of Py-Im PAs could be improved even further if one could adopt a more convergent approach for both upscaling and library synthesis. Based on the experience on the optimisation of SPS of PAs, a significant drop in isolated yields after the 6th coupling was observed. This effect was detected even with the highly efficient BTC coupling described in *section 3.3.2.2*. With natural peptides, manually conducted SPS has noticeable reduction in yields between the 6th to the 24th residues.[207] We surmised that the drop in isolated yield is due to the build-up of truncated sequences. Recently the Dervan's group showed a solution phase synthesis of PAs.[208] The synthesis is achieved by a convergent synthesis of the two requisite halves of the PA (Scheme 20).

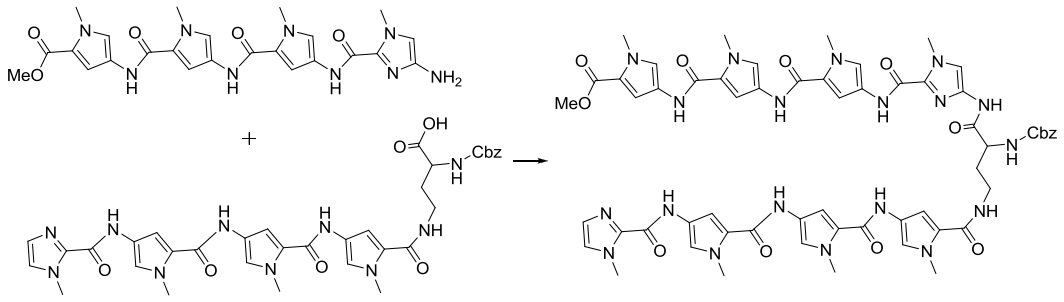

Scheme 20: Dervan's approach to a solution phase synthesis of Py-Im PAs

This protocol enables multi-gram synthesis of PAs; however, it suffers from low isolated yield attributed to impurities associated with the stoichiometric use of coupling reagents and the use of precipitation as the only means of purification for each step. Nevertheless, the yields are excellent up to the formation of the tetramers (four heterocyclic rings). By taking these observations into account, our group envisioned a convergent method for the preparation of the Py-Im PAs that combined the advantages of the SPS (i.e. facile preparation, highly pure final product) with a solution synthesis (i.e. large scale synthesis) approach.

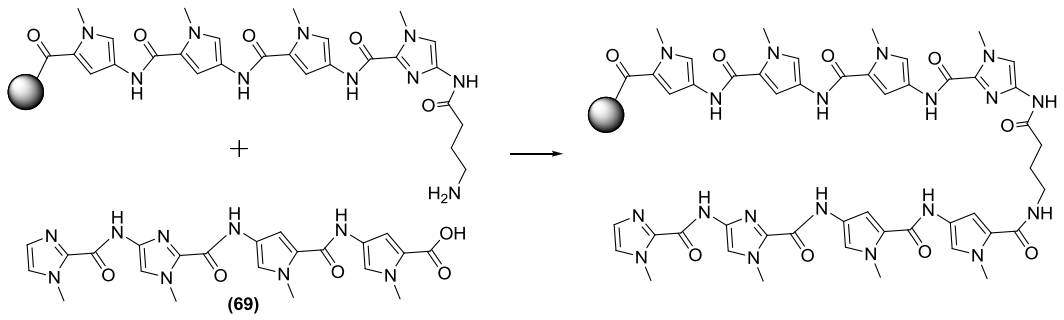

Scheme 21: Mixed solution phase-solid phase synthesis of Py-Im PAs

We envisaged that the tetramer approach would allow the synthesis of PAs with unprecedented speed, diversification and yields.

3.3.3.1 Solution phase synthesis of PA tetramers

Compound **(60)** was prepared with the same one-pot procedure described by Cenoweth[208] and is highlighted in Scheme 22. Tetramer **(61)** was then prepared by click-chemistry between sugar azide **(6)** and compound **(60)** (details are found in paragraph 3.3.4.1). Compound **(61)** was then subjected to hydrolysis with 1M LiOH in MeOH at 50°C.

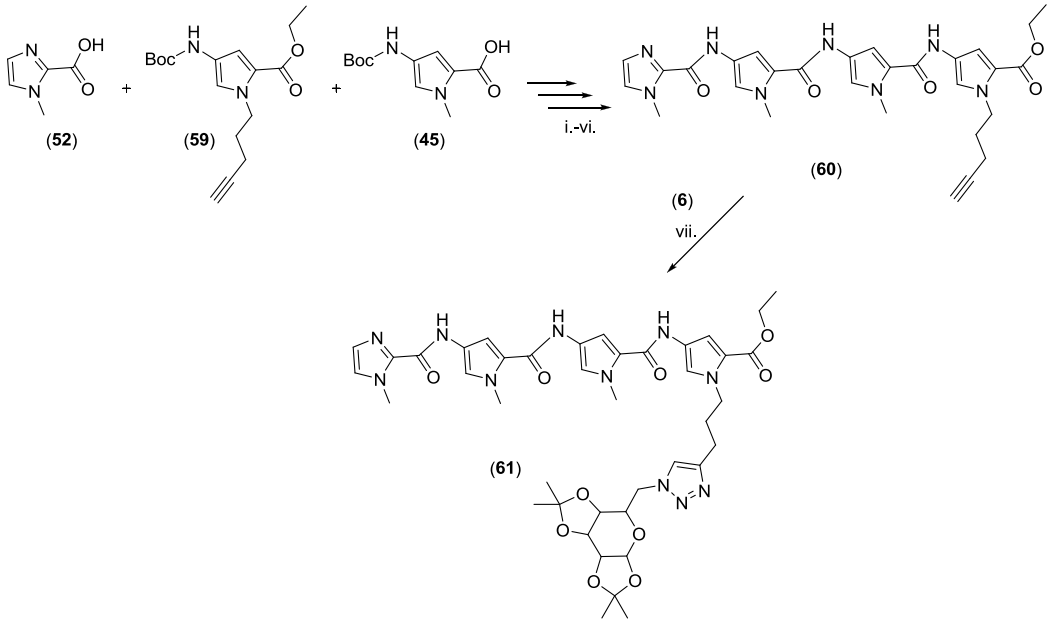

Scheme 22: Preparation of compound (61). i. (59), TFA ii. (45), HATU iii. TFA iv. (45), HATU v. TFA vi. (52), DCC/HOAt vii. (6), $CuSO_4$, ascorbate

Surprisingly, no product was detected after 18h by HPLC. This instability of Py-Im PA derivatives to basic conditions was unexpected as this was not observed by Chenoweth and Dervan. There are no reports in literature that would have pointed out the instability to basic conditions of this class of compounds. A screening of reaction conditions was then designed in the attempt to optimise this last critical step.

As noted by Table 9, no suitable reactions conditions were found that could cope with the instability of the tetramer. This unexpected instability to basic conditions pointed us to reconsider the protecting groups involved in the synthesis.

The simplest non-acid and non-base labile protecting group for carboxylic acids is a benzyl ester, which can be deprotected under hydrogenation conditions.

Boc-Py-OH **(45)** was coupled with benzyl alcohol **(62)** in the presence of EDC/DMAP in DCM for 30 minutes to afford Boc-Py-OBz **(63)** with 99% yield. Deprotection of the Boc group of **(63)** with TFA at room temperature overnight afforded NH2-Py-OBz **(64)** in 80% yield after lyophilisation. Boc-Py-OH **(45)** was coupled to **(64)** in DMF using HATU as coupling agent to afford the dimer **(65)** in 99% yield. Acidic deprotection of the Boc group of **(66)** using TFA (2 hours) at room temperature afforded **(66)** in 98% yield.

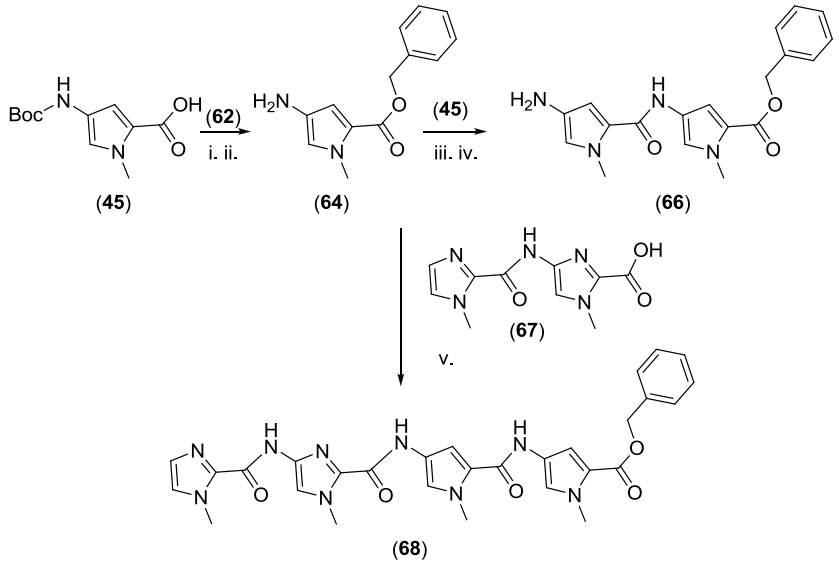

Scheme 23: Preparation of the tetramer benzyl ester (68). i. (62), DCC/DMAP, 99% ii. TFA, 80% iii. (45), HATU, 99% iv. TFA, 98% v. (67), DCC/HOBt, then re-precipitation in MeOH 48%

Entry	Conditions	Temperature (°C)	Results
1	LiOH/MeOH	22	Degradation
2	CsOH/THF	22	No reaction
3	CsOH/DMF	22	Degradation
4	CsOH/MeOH	22	Degradation
5	CsOH/Dioxane	22	No reaction
6	KOH/THF	22	Degradation
7	KOH/DMF	22	<5% product
8	KOH/MeOH	22	Degradation
9	KOH/Dioxane	22	Degradation
10	K_2CO_3/THF	40	Degradation
11	K_2CO_3/DMF	40	No reaction
12	K_2CO_3/MeOH	40	<5% product
13	K_2CO_3/Dioxane	40	Degradation

Table 9: Screening of reaction conditions for the attempted hydrolysis of compound (61)

Lastly, commercially available Im-COOH **(52)** was preactivated with DCC/HOAt for 1.5 hours in DMF and then added to a solution of NH2-Im-COOEt **(89)** in DMF in the presence of Hunig's base overnight to form the dimer Im-Im-COOEt, which was not isolated. Saponification of the ester using LiOH (1M) and subsequent acidification (pH 3) afforded **(67)** in 54% yield after extraction in ethyl acetate and lyophilisation. Dimer **(67)** was then pre-activated with DCC/HOBt for 24 hours then added to a mixture containing dimer **(66)** and Hunig's base in DMF and reacted for 2 hours to afford the tetramer **(68)** in 48% yield after re-precipitation (Scheme 23).

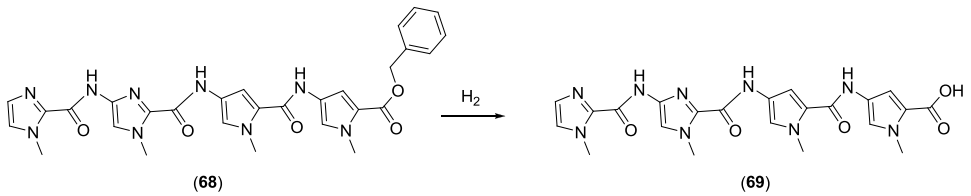

(**68**) (**69**)

Scheme 24: Preparation of compound (69) by hydrogenation

Hydrogenation was then attempted using a range of conditions (Table 10).

Entry	Conditions (1 atm H_2, MeOH)	Conversion (% HPLC, 24h)
1	5% Pd/C	9.6
2	10% Pd/C	21
3	20% $Pd(OH)_2$/C	64
4	20% $Pd(OH)_2$/C, 1.7eq HCl	100

Table 10: Screening of reaction conditions for the preparation of compound (69)

Higher catalytic activity was necessary to push the reaction to completion so the hydrogenation was conducted with 20% $Pd(OH)_2$/C (Pearlman's catalyst) in MeOH and 1.7 eq of HCl in the presence of 1 atm of H_2 for 24 hours. These conditions afforded complete conversion of the tetramer to the carboxylic acid **(69)** in an isolated yield of 69% and in a purity of 93.34%.

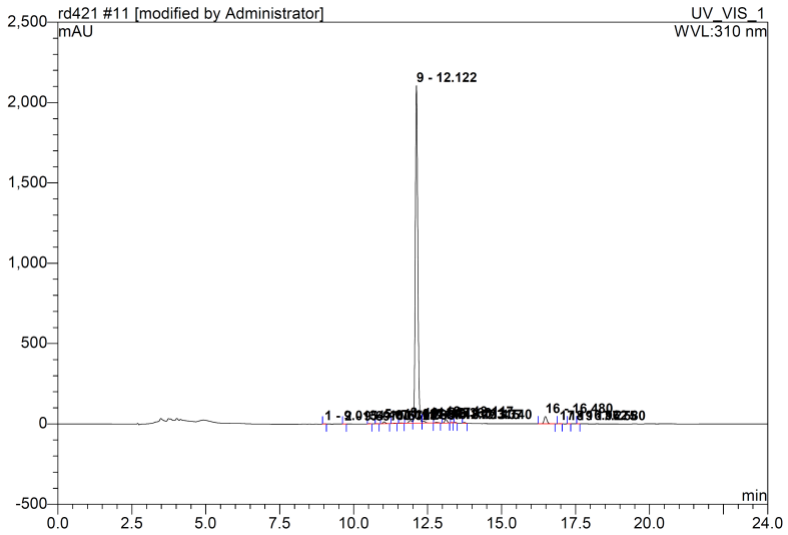

Figure 92: HPLC of a sample of tetramer (69) showing a purity of 93.34%

In summary, for this 7-step convergent synthesis of tetramer **(69)** no chromatographic purifications were necessary. A single precipitation was used to obtain a Py-Im PA tetramer **(69)** with an overall yield of 25% and a purity of 93.34%.

3.3.3.2 Preparation of PA (70) using the convergent solution phase and solid phase synthesis

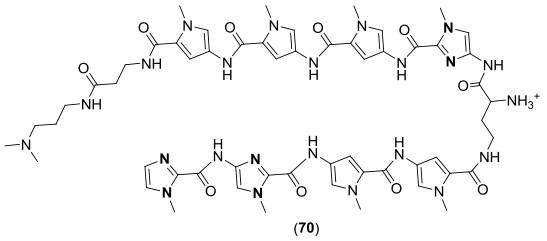

Figure 93: Structure of PA (70) consisting of 5 pyrrole and 3 imidazole heterocycles

PA **(70)** was chosen as an example to be prepared by this novel method for the following reasons: it contains an imidazole in the first half of the PA which can be

addressed by using the BTC protocol, it presents a charged DABA loop that is known to be synthetically challenging.[i] The preparation commenced by coupling 3 pyrrole **(45)** monomers using the HATU protocol (Scheme 25).

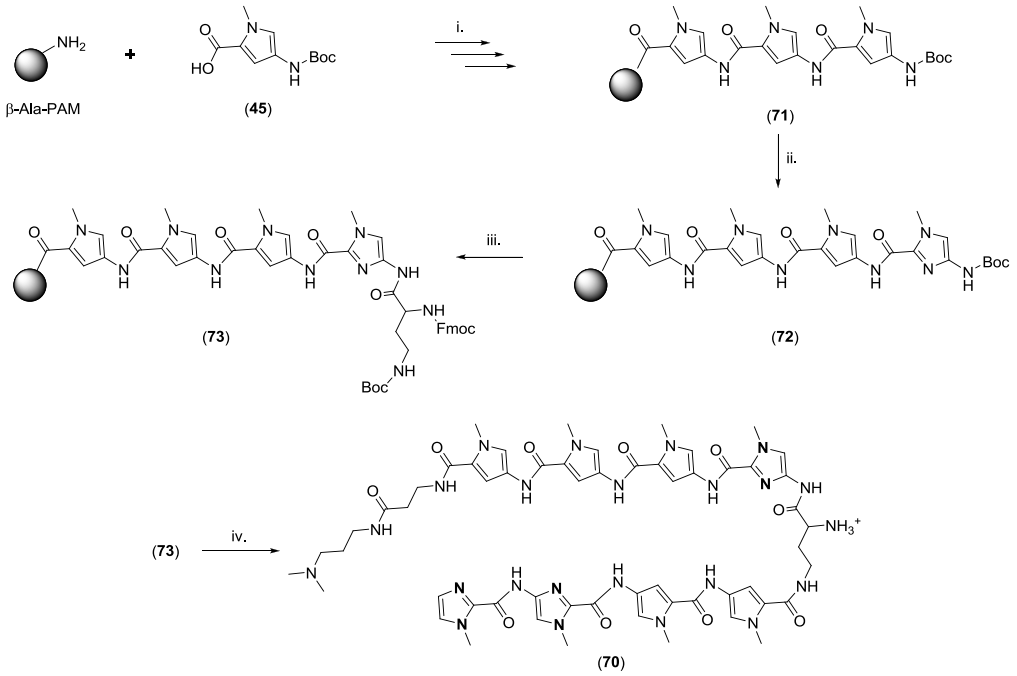

Scheme 25: Preparation of the solid phase synthesis part of PA (70). i. (45), HATU then TPW, repeat x3 ii. (51), BTC/Collidine, then TPW iii. Fmoc-DABA-OH, DCC/HOAt iv. TPW, then tetramer (69), HATU, DMF, 14h, then piperidine/DMF.

The Im monomer **(51)** was then coupled by the application of the BTC protocol to afford **(72)**. Commercially available Fmoc-DABA-OH **(54)** was coupled to **(72)** using the DCC/HOAt protocol (see experimental paragraph 3.6.1). The Boc-group of **(73)** was then deprotected using TPW and carefully rinsed with an extensive washing method consisting of 3x2 mL of DCM, 3x2 mL of DMF, 3x2 mL of NMP, 1x2 mL of DMF/DIEA, 1x2mL of DMF. The DCM was necessary to wash

[i] The reported yield by SPS is 0.1%.[307]

out the TPW solution and re-swell the PAM resin. The DMF and NMP washings were used to rinse the resin from impurities, reduce clumping and prepare it for the coupling. The DMF/DIEA wash was used to remove TFA salts and so improving the purity of the successive coupling. Subsequently 1.2 eq of tetramer **(69)** was pre-activated with 1.08 eq HATU in DMF and 12 eq of DIEA. The mixture was added to the resin and shaken for 14 hours. The resin was washed with 6x2 mL of DMF. Deprotection of the Fmoc group of **(70a)** with 3x2 mL of Piperidine/DMF afforded **(70b)**. Finally cleavage of **(70b)** using Dp **(55)** afforded crude **(70)**. The compound was then purified by semi-preparative HPLC and lyophilised to afford pure PA **(70)** (18.4 mg, 57% yield) with a purity of 97.1%

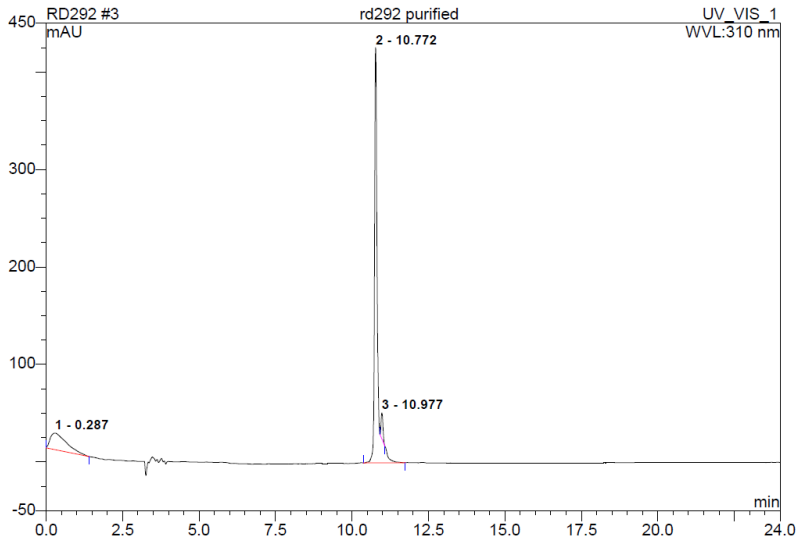

Figure 94: HPLC of PA (70)

In conclusion, a convergent approach for the synthesis of PAs was developed. This method ameliorates current problems in the preparation of PAs. For compound **(70)**, a 570-fold increase of the isolated yield was observed.

3.3.4 Functionalization of Py-Im PAs

Py-Im PAs have been functionalised with a variety of groups and functional molecules ranging from fluorophores,[209] anti-cancer intercalators[210] and alkylators.[211,212] Such modifications have been tethered to PAs via a linkage using classical coupling agents such as uronium salts and carbodiimides.

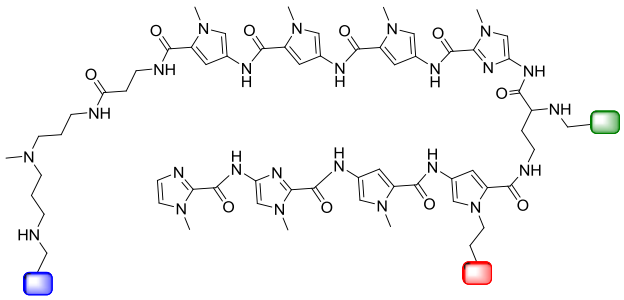

Figure 95: Example of PA showing possible modification sites which are not interfering with their DNA binding properties. Modifications shown are on the "tail" (blue), "loop" (green) and on a heterocycle (red).

Py-Im PAs would greatly benefit from novel functionalization methods and protocols that would reduce the burden of further chemical modifications and purifications of these compounds. Click chemistry methods are good candidates due to the greater compatibility and bio-orthogonality with DNA and biological substrates. With this in mind, bio-conjugation protocols based on Huisgen (3+2) cycloaddition and thiol-ene click chemistry with an appropriate PA-based reaction partner were tested.

3.3.4.1 PA CuAAC click chemistry

PA (**74**, Figure 96)[161] was prepared using the previously described protocols (see paragraph 3.3.2 and experimental section 3.6.1).

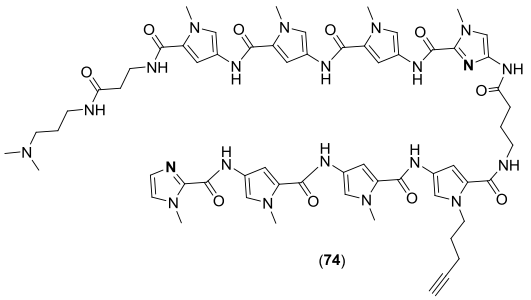

(74)

Figure 96: Structure of PA (74)

CuAAC protocols proceeds poorly in aqueous acidic conditions.[213] Since acidity conditions are required for the dissolution of the PA **(74)** in water, it was decided to attempt the click-chemistry in non-aqueous conditions. In an eppendorf vial PA **(74)** was dissolved in DMSO:tBuOH 75:25. A $CuSO_4$ (0.1M) solution was then added, followed by sugar azide **(6)** and sodium L-ascorbate. The vial was then capped, and shaken in a thermomixer at 25°C, 900 rpm. The HPLC showed only the presence of starting materials, so a series of tests were conducted at increasing concentrations of copper and azide, as shown by Table 11. Under a variety of conditions, no product was observed.

Copper source	Cu (eq)	Sugar azide **(7)** (eq)	T (°C)	Yield
$CuSO_4$	0.1	5	25	0%
$CuSO_4$	1	50	25	0%
$CuSO_4$	10	50	25	0%
$CuSO_4$	10	50	45	<1%
$CuSO_4$	100	50	45	Degradation
CuBr.TBTA	100	50	45	Degradation
Cu-benzene triflate	100	50	45	Degradation

Table 11: Screening of reaction conditions for the attempted "click chemistry" between sugar (7) and PA (74)

Such an unexpected negative result led us to surmise that the PA **(74)** could bind the copper and inhibit reaction. Increasing the number of equivalents of copper, increasing the temperature, or the use of the TBTA ligand or different species of copper did not improve the yield beyond the formation of **(75)** in trace quantities. The click chemistry was then attempted on the tetramer **(60)**, homologue of the PA **(74)**.

Tetramer **(60)** was reacted with 1eq $CuSO_4$, 2eq sugar azide **(6)** and 4eq sodium L-ascorbate in DMSO:tBuOH 75:25 for 18h. Complete conversion was observed, and after quenching of the reaction with water and work-up, clicked crude tetramer **(61)** was recovered with 79% yield and a purity of 57% (Figure 97).

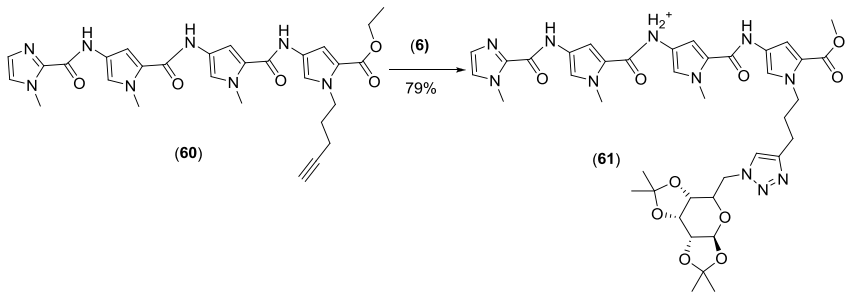

Scheme 26: Preparation of tetramer (61) by click-chemistry with sugar (6): $CuSO_4$, sugar azide (6), sodium L-ascorbate, DMSO:tBuOH, 18h r.t., 79%

The result of PA **(74)** versus the homologous tetramer **(60)** was unclear. While all the reagents were handled in the same way for both reactions, it was noted that the click-chemistry reactions conducted with PA **(74)** weren't developing the classical yellow colour of the formation of Cu^I species. If this was the case, then, hypothetically, PA **(74)** was able to chelate and sequester the copper ions at low concentration, effectively inhibiting the reaction. Many nitrogen ligands are

known to have a negative effect on the click-chemistry reaction.[214] At high concentration of copper (100 eq), PA **(74)** was unstable to the reaction conditions.

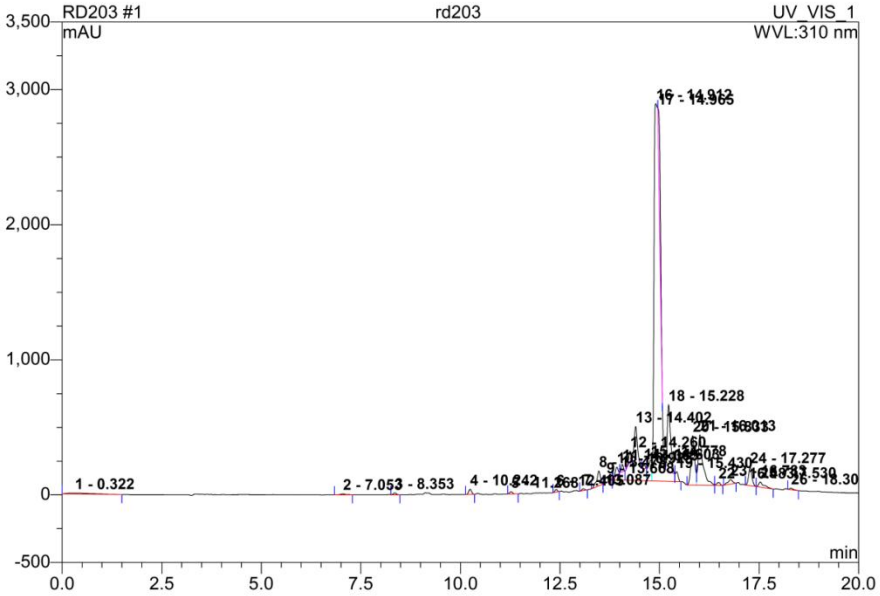

Figure 97: HPLC of crude tetramer (61) showing a purity of 57%

In conclusion, overall the synthesis showed positive results as working conditions were found for the use of CuAAC click-chemistry with Py-Im tetramers. However the clicked tetramer **(61)** was incompatible to saponification (as described in paragraph 3.3.3.1), that would have made the compound useful for the preparation of PAs with pendant functional groups. As a consequence of these issues, other reactions which could provide a more general method of bio-conjugation were investigated.

3.3.4.2 Thiol-ene click chemistry.

Thiol-ene is a photochemical bio-compatible conjugation reaction between and alkene and a thiol (Scheme 27).

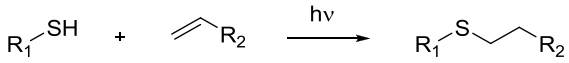

Scheme 27: General reaction scheme of thiol-ene click chemistry between a thiol and an alkene.

It has been shown to work on proteins by using 254 nm mercury UV lamps.[215] Thiol-ene click-chemistry is non-metal catalysed, and thus it could overcome the limitations observed with CuAAC. The potential of this reaction was initially tested on a single Py monomer **(81)**. Alkylation of Boc-Py(H)-OEt **(80)**[216] with 6-bromo-hex-1-ene **(90)** in diglyme afforded compound **(81)** in 41% yield. **(81)** was then used to test for compatibility with the thiol-ene reaction. A general solution for irradiation of **(81)** and cysteine methyl ester **(91)** was prepared. The solution was added to a Pyrex tube, degassed with argon for 10 minutes and irradiated at 366 nm using 48 W (6 x 8 W lamps) of UV light for 18 hours. HPLC analysis showed a complete conversion of the Py monomer (Figure 98). MS confirmed the formation of the desired product **(92)** with an m/z peak at 472 corresponding to the $[M+H]^+$ ion.

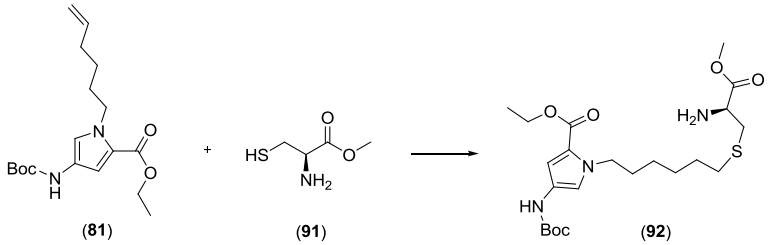

Scheme 28: Thiol-ene click-chemistry between compound (81) and cysteine methyl ester (91)

This promising result showed that the thiol-ene reaction was compatible with soft-UV light at 366 nm. The use of a photoinitiator as a strategy for thiol-ene click

chemistry has been explored by Fiore.[215] However, in the absence of photoinitiator, such a reaction can only be considered if the Py monomer itself is behaving as a photochemical initiator. The chromophore-initiator consists of the pyrrole carboxylic acid part of **(81)** absorbing weakly at 366 nm. The excited diradical can then initiate a radical cascade by hydrogen abstraction from a thiol, as shown in a putative mechanism in Scheme 29. The cysteine radical **(91a)** can then react with the alkene by free radical addition following an anti Markovnikov's rule. The resulting radical **(91b)** can then hydrogen-abstract another cysteine molecule, closing the radical cycle.

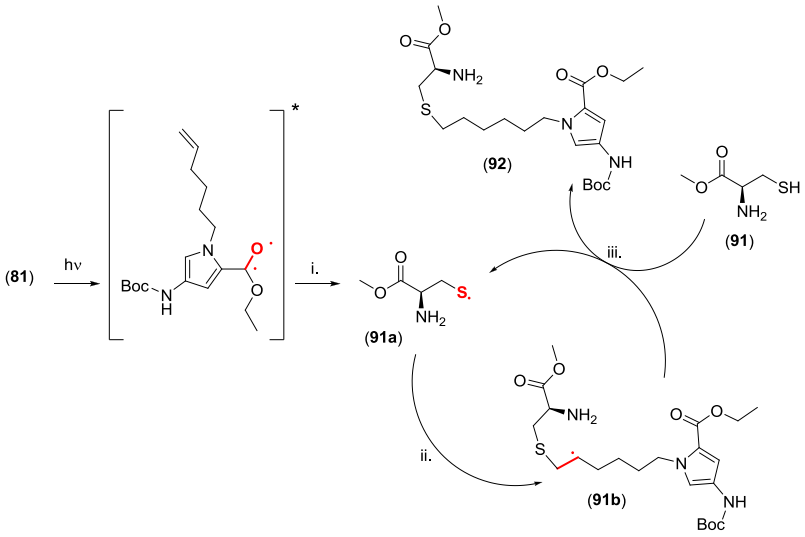

Scheme 29: Proposed mechanism of the observed thiol-ene click-chemistry. i. radical initiation ii. Free radical addition (anti Markovnikov's) iii. Hydrogen abstraction

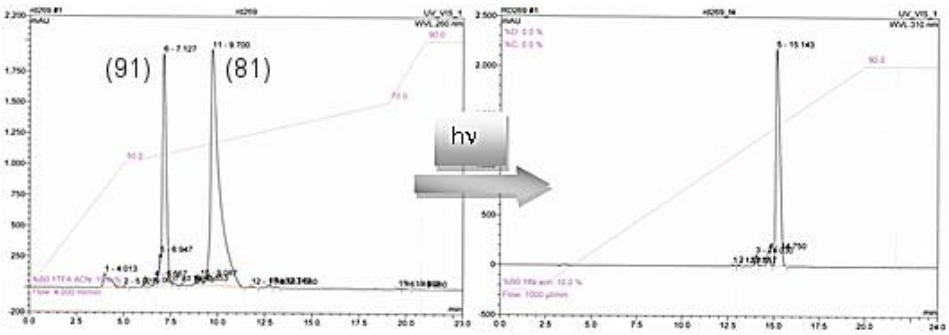

Figure 98: HPL chromatogram traces of compound (81) and cysteine methyl ester (91) before irradiation (left) and after irradiation (right) showing complete conversion to compound (92).

The thiol-ene click-chemistry was then applied to a full PA. PA **(93)** was reacted with pent-4-enoic acid **(94)** using HATU as coupling agent in DMF at r.t. overnight to afford PA-alkene **(95)** with 8.4% yield after purification by semi-preparative HPLC.

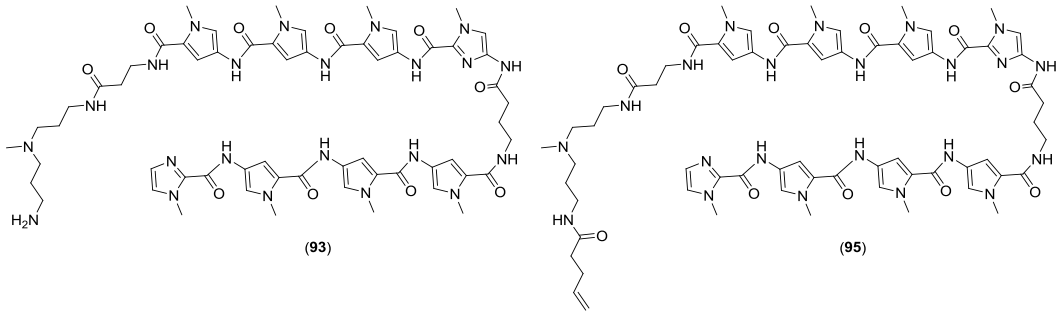

Figure 99: Structure of PA (93) and PA (95)

PA **(95)** was then dissolved in MeOH together with a large excess of cysteine methyl ester **(91)** in a Pyrex tube (pseudo-first order reaction conditions), degassed with argon, then irradiated with 366 nm UV light using 48 W (6 x 8 W lamps). A second tube was prepared without cysteine methyl ester as a control reaction. The reactions were then sampled at regular intervals to monitor the progress of the photochemical reaction by HPLC.

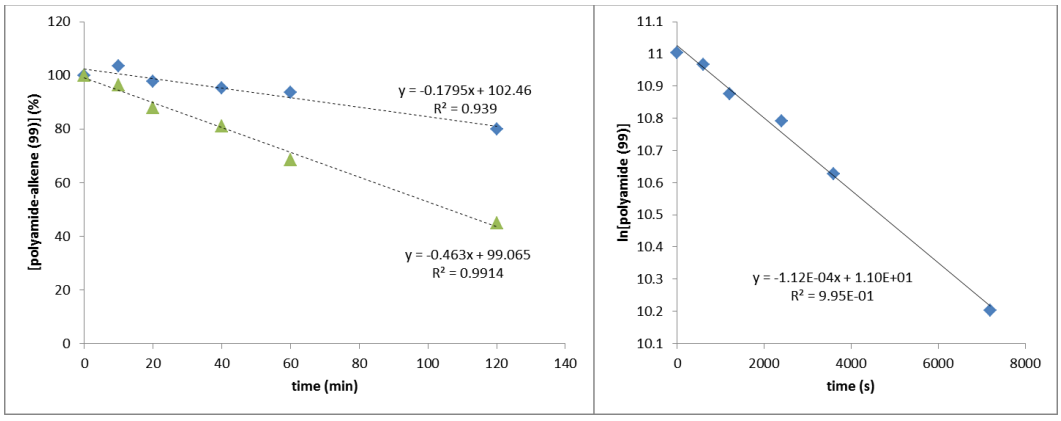

Figure 100: Plot of the photochemical reactions of A. PA-alkene (95) in MeOH (blue) and in the presence of cysteine (98, green) showing a strong photobleaching of the starting material. B. plot fitting of the ln[PA (95)] vs time.

The results showed photodegradation of PA, as the control reaction showed degradation of **(95)** as monitored by the disappearance of the HPLC peak at 310 nm (Figure 100, blue diamonds). Photodegradation of **(95)** is an important side reaction that is highly competitive with the thiol-ene click chemistry (Figure 100, green triangles). The reaction control showed a zero-order of reaction, consistent with a photobleaching process (Figure 100, right). The rate was calculated to be 0.1795 mol L^{-1} s^{-1} by plot fitting the time of the reaction and the logarithm of the concentration of **(95)** (Figure 100, right). The reaction with cysteine methyl ester **(91)** fitted a pseudo-first order reaction rate with a calculated constant of 1.12 x 10^{-4} s^{-1}. However, this last rate constant is in reality a combination of the zero-rate photobleaching reaction and pseudo-first order thiol-ene click chemistry, as shown by the formula:

$$[A] = [A_0]e^{-(k1[A]^0 + k2[A])} = [A_0]e^{-(k1 + k2[A])}$$

In conclusion, although the thiol-ene click-chemistry was efficient, the protocol was not feasible to be used due to large photobleaching of the Py-Im PA. Further tests with the use of a photoactivator could eventually allow the development of a successful click-chemistry method for PAs by avoiding the photobleaching.

3.3.4.3 Preparation of PAs amenable for further conjugation

Both thiol-ene and CuAAC were incompatible bio-conjugation reactions to interface PAs with desired functional groups. The use of isothiocyanates (NCS) PA was then attempted to obtain linked molecules without the need of coupling agents and/or purification (required if using HATU or DCC).

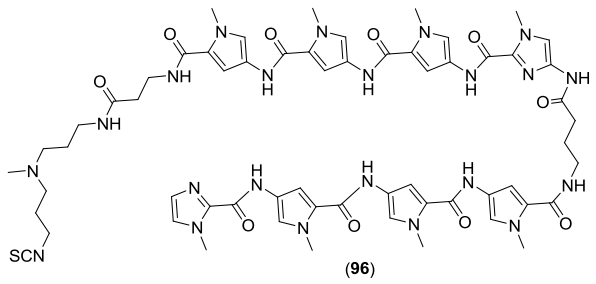

(**96**)

Figure 101: Structure of PA (96)

This is important as the preparation of easily derivatisable compounds could greatly simplify the synthesis and increase the diversity of the compounds prepared. PA **(93)** was reacted with carbon disulfide (CS_2) in the presence of DIEA for 40 minutes in DMF. The mixture was then treated with ethyl chloroformate **(47)** for 35 minutes and then was directly injected and purified by semi-preparative HPLC to afford PA isothiocyanate **(96)** in 1.3% yield. The mechanism of the reaction is assumed to proceed via a two-step one-pot process: the amine is converted to a dithiocarbamate (Scheme 28) by reacting with CS_2 in

the presence of a base, then ethyl chloroformate (or in alternative a carbodiimide such as DCC) acts as a desulfurylating agent (Scheme 30). A similar method has been used by Thorsten to prepare tethers for PAs.[185]

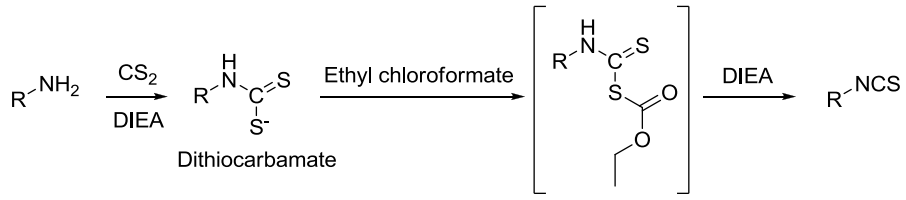

Scheme 30: General reaction scheme of the preparation of an isothiocyanate using a mild CS_2 protocol.

In conclusion, PA isothiocyanates have been successfully prepared. This facile and mild preparation can be used to prepare isothiocyanates of PAs cleaved using bis-(3-aminopropyl)-methylamine **(56)**.

3.4 Conclusions

PAs have been prepared for their application as silver nucleating sites along DNA duplexes with natural DNA and sugars for the preparation of supramolecular self-assembling systems for the sequence specific metallisation of DNA.[217] The potential of PA-sugar systems as silver directing groups is described in Chapter 4. New methods of PAs synthesis have been developed: the novel BTC coupling strategy and the half solution phase, half solid phase synthesis were successfully deployed and afforded PAs with unprecedented yields. Regarding click-chemistry approaches to PAs, CuAAC and thiol-ene were incompatible with functionalising PA scaffolds, the first due to the substrates inhibiting the click-chemistry reaction, the second due to the instability of the PA to the reaction conditions. However, a

novel “tail”-NCS functionalisation of PA has been developed and poses as an alternative to PA tethering.

3.5 Future Studies

Ru-catalysed click-chemistry[218] is a recently developed methodology to react azides and alkynes together to form 1,5-triazoles (as opposed to CuAAC that forms exclusively 1,4-triazoles). This novel reaction could overcome the problems such as copper binding and enable full PA click-chemistry.

3.6 Experimental

3.6.1 Solid phase synthesis of PAs

Solid phase synthesis was performed using established protocols and protocols developed in our laboratories. All the PAs have been characterised by HRMS (ESI) and HPLC and UV/Vis. When HRMS is not available, EIMS main peaks are reported. The following reagents were prepared as stock solutions:

TPW: 92.5 mL TFA, 5 g phenol and 2.5 mL water.

p-Chloranil test reagent: 5g p-Chloranil in 25 mL of Toluene

Solid phase synthesis was conducted using β-Ala-PAM resin (0.26 mmol/g) in glass vials adapted with a glass sintered frit using a custom-built oscillator shaker. For a typical amount of resin (100-125 mg), the following protocols were employed:

A. Resin preparation and swelling: 6 mL DCM, 3h; 2 mL TPW, 2 min; 2 mL TPW, 2 min; 2 mL TPW, 15 min; 3x2 mL DCM, 2 min; 3x2 mL DMF, 2 min
B. Pyrrole monomer **(45)** coupling procedure: 4 eq **(45)**, 3.6 eq HATU, 12 eq DIEA, 30 min; 3x2 mL DMF, 2 min; 3x2 mL DCM, 2 min; 2 mL TPW, 1 min; 2 mL TPW, 2 min; 2 mL TPW, 5 min; 3x2 mL DCM, 2 min; 3x2 mL DMF, 2 min
C. Imidazole monomer **(51)** coupling procedure (Novel BTC protocol): 3x2 mL NMP, 2 min; 12 eq DIEA, 2 mL DMF, 2 min; 3x2 mL THF, 2 min; 4 eq **(51)**, 1.2 eq BTC, 12 eq collidine, 2 mL THF, 10 min then 12 eq DIEA, 30 min; 3x2 mL DMF, 2 min; 3x2 mL DCM, 2 min; 2 mL TPW, 1 min; 2 mL TPW, 15 min; 2 mL TPW, 15 min; 3x2 mL DCM, 2 min; 3x2 mL DMF, 2 min
D. GABA **(53)** and DABA **(54)** coupling procedure: 4 eq **(53)** or **(54)**, 3.6 eq DCC, 4 eq HOAt, 1.5 h then DIEA, 1 h; 3x2 mL DMF, 2 min; 3x2 mL DCM, 3h; 2 mL TPW, 2 min; 2 mL TPW, 2 min; 2 mL TPW, 15 min; 3x2 mL DCM, 2 min; 3x2 mL DMF, 2 min
E. Terminal imidazole **(52)** coupling procedure: 4 eq **(52)**, 3.6 eq DCC, 4 eq HOAt, 1.5 h then DIEA, 1 h; 6x2 mL DMF, 2 min
F. Resin washing and cleaving procedure: 3x2 mL DMF, 2 min; 3x2 mL NMP, 2 min; 3x2 mL DCM, 2 min; 6x2 mL MeOH, 2 min; nitrogen flushing and drying, 5 min; 4 mL of amine **(55)** or **(56)**, 55°C, 18 h

Cleavage conditions: After cleaving from the resin (protocol F), PAs were precipitated using Et_2O 10 mL and centrifuged at 4200 rpm for 10 min, re-suspended in Et_2O 10 mL and centrifuged again at 4200 rpm for 10 min. The crude PA was then dissolved in H_2O 0.1% TFA and purified by semi-preparative HPLC with the following method:

Reverse Phase HPLC: Sephadex C18; Mobile Phase: linear gradient, *A:* water 0.1% TFA and *B:* Acetonitrile 0.1% TFA, *A:B* from 90:10 to 10:90 in 18 min, maintain for 4 min; temperature: 22°C; flow rate: 1 mL/min Detector: PDA (220-400 nm) + 310 nm; Chromatogram: 0-22 minutes, PAs have retention times between 11-14 min.

3.6.1.1 Synthesis of polyamides

Polyamides have been prepared by application of the previously described protocols (Es. A = Protocol A)

Polyamide **(73)**: PAM resin-β-Ala-Py-Py-Py-Im-DABA(Fmoc)-Boc

Synthesis: A, Bx3, C, D using Boc-DABA(Fmoc)-OH

Polyamide **(74)**: Dp-β-Ala-Py-Py-Py-Im-GABA-Py(Alkyne)-Py-Py-Py-Im

Synthesis: A, Bx3, C, D using GABA, B using **(59)**, Bx2, E, F using **(55)**

Polyamide **(93)**: Dp-β-Ala-Py-Py-Py-Im-GABA-Py-Py-Py-Im

Synthesis: A, Bx3, C, D using GABA, Bx3, E, F using **(56)**

3.6.1.2 M_r characterisation of polyamides and polyamide tetramers

Polyamides have been characterised by MALDI-TOF-MS, UPLC-TOF or ESI-MS.

(57):[203] ESI-MS *m/z* (%): $[M+H]^+$ calc. for $C_{57}H_{72}N_{23}O_{10}$ 1239.3291; found 1239 (100)

(93): ESI-MS *m/z* (%): $[M+H]^+$ calc. for $C_{60}H_{77}N_{22}O_{10}$ 1265.6188; found 1266 (100), 584 (80), 460 (45)

(70): UPLC-TOF (ESI) *m/z:* $[M+H]^+$ calc. for $C_{57}H_{72}N_{23}O_{10}$ 1239.3291; found 1239.5991

(74): MALDI-TOF *m/z*: $[M]^+$ calc. for $C_{62}H_{75}N_{21}O_{10}$ 1273.6006; found 1273.5945

(60): UPLC-TOF (ESI) *m/z:* $[M]^+$ calc. for $C_{29}H_{32}N_8O_5$ 572.2496; found 572.2283

(61): UPLC-TOF (ESI) *m/z:* $[M+H]^+$ calc. for $C_{40}H_{50}N_{11}O_{10}$ 844.3737; found 844.3734

(95): UPLC-TOF (ESI) *m/z:* $[M+H]^+$ calc. for $C_{65}H_{83}N_{22}O_{11}$ 1347.6612; found 1347.6635

(96): UPLC-TOF (ESI) *m/z:* $[M+H]^+$ calc. for $C_{61}H_{74}N_{22}O_{10}S$ 1307.5752; found 1307.5961

(109) ESI-MS m/z (%): $[M\text{-Sugar}+2H]^{2+}$ calc. for $C_{61}H_{78}N_{24}O_{11}$ 661.3141; found *m/z* (%): 659 (50). UPLC-TOF (ESI) *m/z:* $[M+4H+O]^{4+}$ calc. for $C_{70}H_{87}N_{25}O_{18}$, 391.4165; found 391.2876

3.6.2 Synthesis of PA monomers

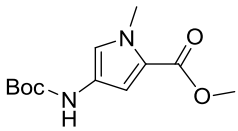

Synthesis of Boc-Py-COOMe (44).[161] To a solution of NO_2-Py-COOMe **(43)** (10 g, 54 mmol) in MeOH (300 mL) at -20°C was added $NiCl_2.6H_2O$ (1.29 g, 5.43 mmol) and Boc anhydride **(58)** (23.7 g, 108.68 mmol). $NaBH_4$ (14.37 g, 380mmol) was slowly added in batches to the mixture. At the end of the addition the mixture was allowed to warm to 0°C and left stirring overnight. The reaction was quenched with ethyl acetate (300 mL) and H_2O (100 mL), filtered over celite and concentrated *in vacuo*. Ethyl Acetate (200 mL) was added and the mixture washed with $NaHCO_3$ (200 mL), brine (200 mL), 1% aqueous diethylenetriamine (3x200 mL) and brine (200 mL). The solution was concentrated *in vacuo*, dissolved in DCM (19 mL) and precipitated with n-hexane (250 mL) to afford Boc-Py-COOMe **(44)** (9.97 g, 73%) as a white powder. UPLC-TOF (ESI) *m/z:* $[M+H]^+$ calc. for $C_{12}H_{19}N_2O_4$ 255.1339, found 255.135; m.p. 139-140°C; ^{1}H-NMR (400 MHz, DMSO-d_6) δ 9.10 (s, 1H), 7.10 (s, 1H), 6.63 (s, 1H), 3.79 (s, 3H), 3.71 (s,

3H), 1.45 (s, 9H); ^{13}C-NMR (100 MHz, DMSO-d_6) δ 160.7, 152.7, 123.1, 119.2, 118.6, 107.3, 78.4, 50.8, 36.0, 28.1

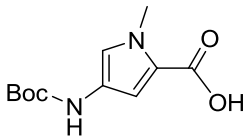

Synthesis of Boc-Py-COOH (45).[161] To a solution of NO_2-Py-COOMe **(44)** (9.97 g, 39.40 mmol) in MeOH (300 mL) was added NaOH (35mL, 3M). The reaction mixture was heated to reflux for 12 hours. The mixture was concentrated *in vacuo* to give a yellow oil. HCl (250 mL, 0.1M) was added to pH 3 and the aqueous layer was extracted using ethyl acetate (4x150 mL). The combined organic layers were washed with brine (50 mL), dried with $MgSO_4$ and then concentrated *in vacuo*. The pure compound was precipitated in DCM/n-hexane to afford Boc-Py-COOH **(45)** (8.40 g, 89%) as an off-white powder. UPLC-TOF (ESI) *m/z:* $[M+H]^+$ calc. for $C_{11}H_{17}N_2O_4$ 241.119, found 241.119; m.p. 164-165°C; ^{1}H-NMR (400 MHz, DMSO-d_6) δ 12.07 (s, 1H), 9.04 (s, 1H), 7.04 (s, 1H), 6.58 (s, 1H), 3.77(s, 3H), 1.44 (s, 9H); ^{13}C-NMR (100 MHz, DMSO-d_6) δ 161.8, 152.7, 122.8, 119.6, 118.7, 107.5, 78.4, 36.0, 28.1

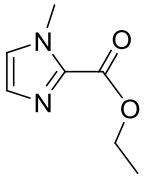

Synthesis of Im-COOEt (48).[161] N-methylimidazole **(46)** (8.21 g, 100 mmol) neat was added to Et_3N (30 mL, 152.3 mmol) at 0°C. Ethyl chloroformate **(47)** (11.5 mL, 38.81 mmol) was added dropwise over 30 mins. The reaction mixture was stirred at 0°C for a further 2hrs and then allowed to warm to room temperature and stirred overnight. The mixture was then filtered; the filtrate was diluted with water (100 mL) and then extracted with chloroform (3x100 mL). The organic layer was washed with brine (100 mL),

dried over Na_2SO_4 and concentrated *in vacuo* to give an orange residue. The residue was diluted in ethyl acetate (150 mL) and filtered over a plug of Si-60 to afford Im-COOEt **(48)** (6.592 g, 42%) as an orange solid. UPLC-TOF (ESI) *m/z:* $[M+H]^+$ calc. for $C_7H_{10}N_2O_2$ 155.078, found 155.082; m.p. 84-85°C; ^{1}H-NMR (400 MHz, DMSO-d_6) δ 7.48 (s. br., 1H), 7.09 (d, J = 0.9 Hz, 1H), 4.32 (q, J = 7.1 Hz, 2H), 3.95 (s, 3H), 1.33 (t, J = 7.1 Hz, 3H); ^{13}C-NMR (100 MHz, DMSO-d_6) δ 158.7, 136, 128.5, 127.2, 60.5, 35.4, 14.0

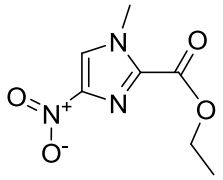

Synthesis of NO_2-Im-COOEt (49).[219] Im-COOEt **(48)** (6.59 g, 42.79 mmol) neat was added H_2SO_4 98% (20 mL) and cooled at 0°C. HNO_3 100% (20 mL) was added dropwise and stirred at 0°C for 10 mins. The mixture was heated to 95°C and allowed to stir at this temperature for 50 mins. After cooling to r.t., the mixture was quenched by pouring over ice chips (300 mL) and extracted with DCM (4x150 mL). The organic phase was washed with saturated $NaHCO_3$ solution (2x100 mL), brine (100 mL), dried over $MgSO_4$ and evaporated *in vacuo* to give a bright yellow solid. The solid was dissolved in chloroform (20 mL) and quickly added to diethyl ether (300 mL). The mixture was cooled down to 0°C for 1 hour to allow precipitation and then filtered to afford NO_2-Im-COOEt **(49)** (3.58 g, 42%) as a white powder. UPLC-TOF (ESI) *m/z:* $[M+H]^+$ calc. for $C_7H_{10}N_3O_4$ 200.068, found obs. 200.067; m.p. 104-105°C; ^{1}H-NMR (400 MHz, DMSO-*d6*) δ 8.63 (s, 1H), 4.35 (q, J = 7.1 Hz, 2H), 3.99 (s, 3H), 1.34 (t, J = 7.1 Hz, 3H); ^{13}C-NMR (100 MHz, DMSO-*d6*) δ 157.7, 144.9, 134.8, 126.8, 61.7, 36.7, 13.9

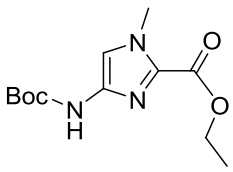

Synthesis of Boc-Im-COOEt (50).[219] A solution of NO_2-Im-COOEt **(49)** (3.67 g, 18.44 mmol), Boc anhydride **(58)** (5 g, 229 mmol) and Pd/C (10%) (0.035 g) in anhydrous methanol (150 mL) was placed under a 1 atm stream of H_2 for 24 hrs. The solid catalyst was then filtered, petroleum ether 40-60 (220 mL) was added and the mixture sonicated for 20 mins. The precipitate was isolated by suction filtration to a residual powder. The powder was dissolved in ethyl acetate and filtered over a Si-60 plug (20 g) to afford Boc-Im-COOEt **(50)** (4.37 g, 88%) as a white powder. UPLC-TOF (ESI) *m/z:* $[M+H]^+$ calc. for $C_{12}H_{20}N_3O_4$ 270.148, found 270.145; m.p. 134-135°C; ^{1}H-NMR (400 MHz, DMSO-*d6*) δ 9.68 (s, 1H), 7.30 (s, 1H), 4.26 (q, J = 7.1 Hz, 2H), 3.89 (s, 3H), 1.44 (s, 9H), 1.29 (t, J = 7.1 Hz, 3H); ^{13}C-NMR (100 MHz, DMSO-d_6) δ 158.4, 138.0, 130.8, 113.7, 60.4, 35.4, 28.0, 14.1

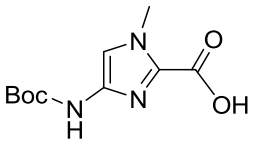

Synthesis of BOC-Im-COOH (51).[219] To a solution of Boc-Im-COOEt **(50)** (1.0 g, 3.72 mmol) in MeOH (6 mL) was added to a solution of 1M LiOH (3.72 mmol, 3.72 mL). The reaction mixture was stirred at room temperature for 2 hrs. The mixture was then diluted with water (20 mL), acidified to pH 3 using 1M HCl and extracted with ethyl acetate (5x20 mL). The solution was then concentrated *in vacuo* to afford BOC-Im-COOH **(51)** (0.400 g, 44%) as a white powder. ESI-MS *m/z:* $[M+H]^+$ calc. for $C_{10}H_{16}N_3O_4$ 242.1135, found 242; m.p. 173-174°C; ^{1}H-NMR (400 MHz, DMSO-d_6) δ 9.60 (s, 1H), 7.20 (s, 1H), 5.60-5.65 (s br), 3.85 (s, 3H),

1.40 (s, 9H, CH_3); ^{13}C-NMR (100 MHz, DMSO-d_6) δ 159.8, 152.7, 137.4, 132.0, 113.4, 78.9, 35.4, 28.1

3.6.3 Solution phase synthesis of PA tetramers

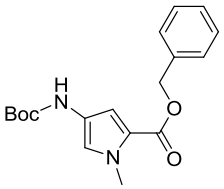

Synthesis of (63).[220–223] To a solution of **(45)** (331 mg, 1.38 mmol) in anhydrous DCM (25 ml) was added benzyl alcohol **(62)** (373.1 mg, 357 uL, 3.45 mmol), DMAP (168 mg, 1.38 mmol) and EDC (264 mg, 1.38 mmol) under a nitrogen atmosphere. The reaction mixture was stirred at r.t. for 30 min and checked for completion by TLC (n-hexane:ethyl acetate 6:4, stain green bromocresol then ninhydrin). The mixture was then diluted with DCM (75mL) and washed with water (50 mL), HCl 0.1M (50mL), $NaHCO_3$ sat (50mL) and finally brine (50mL). The organic phase was then dried (MgSO4), filtered and concentrated *in vacuo* to obtain **(63)** (511 mg, 99%) as a pale yellow oil. ESI-MS *m/z:* $[M+H]^+$ calc. for $C_{18}H_{22}N_2O_4$ 330, found 330; m.p. 151-152°C; ^{1}H-NMR (300 MHz, $CDCl_3$) δ 7.05 - 7.40 (m, 7H), 4.63 (br. s., 2H), 3.74 - 3.89 (br. s., 3H), 1.28 (s, 9H); ^{13}C-NMR (100 MHz, DMSO-d_6) δ 159.2, 135.8, 135.2, 129.6, 128.4, 127.9, 122.5, 111.8, 65.8, 37.4

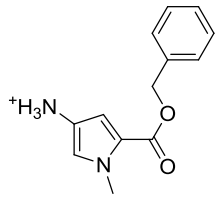

Synthesis of (64).[223] To a suspension of **(63)** (1.02 g, 3.08 mmol) suspended in water (10 mL) was added TFA (25 mL). The resultant solution was stirred at r.t. overnight and then concentrated *in vacuo* to an oily residue. Water was added (5 mL) and lyophilized overnight to afford **(64)**[223] (827 mg, 80% as TFA salt) as white powder. ESI-MS

m/z: $[M+H]^+$ calc. for $C_{13}H_{15}N_2O_2$ 231, found 231; m.p. 181-183°C; ^{1}H-NMR (400 MHz, DMSO-d_6) δ 9.69 - 10.20 (m, NH_3^+), 7.19 - 7.47 (m, 7H), 5.27 (s, 2H), 3.88 (s, 3H); ^{13}C-NMR (100 MHz, DMSO-d_6) δ 159.5, 136.2, 128.4, 127.8, 123.8, 114.5, 111.5, 65.2, 36.6

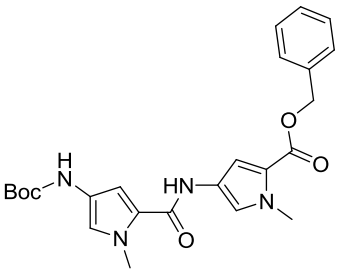

Synthesis of (65).[223] To a solution of **(64)** (827 mg, 2.47 mmol) in peptide grade DMF (10 mL) was added DIPEA (1.2 mL, 8.028 mmol). In a separated flask a solution of **(45)** (593 mg, 2.47 mmol) in DMF (5 mL) was preactivated with HATU (939 mg, 2.47 mmol) and DIPEA (0.8 mL, 5.352 mmol) for 2 minutes then added to the solution containing **(64)**. The reaction mixture was stirred under nitrogen for 1.5 h at room temperature, then quenched with HCl 0.1 M (35 mL). The suspension was centrifuged at 15 kRPM (0°C) for 15 min, and the supernatant decanted. The solid was re-suspended in water (50 mL) and centrifuged again. After decanting the supernatant, the solid was lyophilized overnight to afford **(65)**[223] (1.12 g, 99%) as a pale brown powder. ESI-MS (ES+) *m/z:* $[M+H]^+$ calc. for $C_{24}H_{28}N_4O_5$ 453, found 453; m.p. 180-181°C; ^{1}H-NMR (400 MHz, DMSO-d_6) δ 9.82 (s, 1H), 9.09 (br. s., 1H), 7.26 - 7.58 (m, 6H), 6.71 - 7.03 (m, 3H), 5.25 (s, 5H), 5.12 - 5.37 (m, 2H), 3.70 - 3.98 (m, 6H), 1.36 - 1.64 (m, 9H); ^{13}C-NMR (100 MHz, DMSO-d_6) δ 160.1, 158.3, 152.8, 136.6, 128.4, 129.8, 123.0, 122.4, 120.9. 118.4, 117.2, 108.6, 103.8, 78.3, 64.8, 36.1, 36.0, 28.2

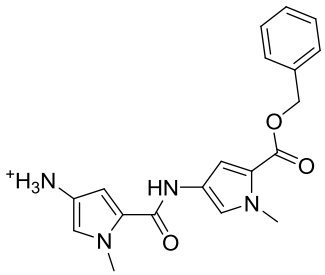

Synthesis of (66). To a suspension of **(65)** (1.11 g, 2.453 mmol) in water (5 mL) was added TFA (25 mL). The solution was then stirred at r.t. for 2h and concentrated *in vacuo*. The residue was then azeotropically distilled with toluene (5x50 mL), dissolved in water (5 mL) and lyophilized overnight to afford the TFA salt of **(66)** (1.126 g, 98%) as a pale brown powder. UPLC-TOF (ESI) *m/z:* $[M+H]^+$ calc. for $C_{19}H_{21}N_4O_3$ 353.1614, found 353.1616; m.p. 187-188°C; ^{1}H-NMR (400 MHz, DMSO-d_6) δ 9.66 - 10.38 (br. s., NH_3^+), 6.88 - 7.59 (m, 9H), 5.25 (s, 2H), 3.80 - 3.99 (m, 6H); ^{13}C-NMR (100 MHz, DMSO-d_6) δ 160.0, 157.6, 136.5, 128.4, 127.8, 124.7, 122.6, 121.7, 121.0, 118.6, 113.2, 108.6, 107.0, 64.9, 36.5, 36.1

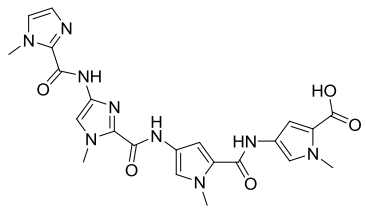

Synthesis of (69). To a solution of **(66)** (572 mg, 1.22 mmol) in peptide grade DMF (5 mL) was added DIPEA (0.4296 mL, 2.44 mmol). To a solution of **(67)** (304 mg, 1.22 mmol) was added DCC (251 mg, 1.22 mmol), HOBt (166 mg, 1.22 mmol) and DMF (5 mL) and stirred for 24 hours. The preactivated solution of **(67)** was added to the mixture of **(66)**. The resulting mixture was stirred at r.t. under nitrogen for 2h and the reaction quenched with HCl 0.1 M (10 mL). The suspension was centrifuged at 15 kRPM, 0°C, 15 min, decanted, the solid re-suspended in water (50 mL) and centrifuged again. After decanting, the solid was re-crystallized from MeOH to afford **(68)** (343 mg, 48%) as a pale grey solid. UPLC-TOF (ESI) *m/z:* $[M+H]^+$ calc. for $C_{29}H_{30}N_9O_5$

584.2357, found 584.2370; m.p. 213-214°C. To a solution of **(68)** (340 mg, 0.585 mmol) in MeOH (100 mL) was added HCl 1M (1 mL) followed by 20% $Pd(OH)_2/C$ (87 mg). The mixture was stirred for 24h at r.t. under H_2 1 atm. The reaction was checked for completion by HPLC and then filtered over celite. DMSO (2 mL) was added and the mixture was concentrated to a small volume. Compound **(69)** was precipitated by the addition of water (25 mL) followed by centrifugation and decanting of the supernatant to afford **(69)** (200 mg, 69%) as a cream coloured powder. UPLC-TOF (ESI) *m/z:* $[M+H]^+$ calc. for $C_{22}H_{24}N_9O_5$ 494.1892, found 494.1895; m.p. 241-242°C; ^{1}H-NMR (400 MHz, DMSO-d_6) δ 10.18 - 10.36 (m, 2H), 9.95 (s, 1H), 7.59 - 7.64 (m, 2H), 7.43 (d, *J* = 1.8 Hz, 1H), 7.33 (d, *J* = 0.8 Hz, 1H), 7.29 (d, *J* = 1.8 Hz, 1H), 7.18 (d, *J* = 1.8 Hz, 1H), 6.87 (d, *J* = 1.8 Hz, 1H), 3.98 - 4.10 (m, 6H), 3.86 (s, 3H), 3.83 (s, 3H); ^{13}C-NMR (100MHz, CDCl3) *δ* 187.2, 161.9, 158.3, 156.6, 155.5, 154.2, 137.0, 134.6, 134.4, 126.9, 122.9, 121.3, 119.5, 118.7, 114.5, 108.4, 104.9, 47.5, 45.8, 36.1, 35.2, 33.3, 25.3, 24.4, 13.8

3.6.4 Synthesis of modified monomers

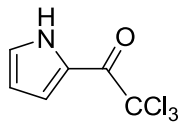

Synthesis of Py-COCCl$_3$ (77).[224–226] To a solution of pyrrole (10 mL, 144.13 mmol, ρ = 0.967) in diethyl ether (80 mL) was added dropwise to a solution of trichloroacetyl chloride **(76)** (16.5 mL, 147 mmol, ρ = 1.62) in diethyl ether (20 mL) over a 3 hour period. The mixture was allowed to stir for 4 hours until the solution turned purple. K_2CO_3 (12.5 g) in water (50

mL) was added and stirred until the solution turned red. The organic phase was separated, washed with brine (50 mL), treated with activated carbon and dried over $MgSO_4$. It was then evaporated *in vacuo* to afford **(77)** (13.19 g, 43%) as a grey powder. ESI-MS (ES-) *m/z* (%): $[M-H+ACN]^-$ calc. for $C_8H_6Cl_3N_2O$ 250.9551, found 249 (8), $[2M-2H+Na]^-$ calc. for $C_{12}H_6Cl_6N_2NaO_2$ 442.8464, found 442 (5); m.p. 72-73°C; ^{1}H-NMR (300 MHz, DMSO-d_6) δ ppm 12.42 (br. s., 1H), 7.22 - 7.40 (m, 2H), 6.27 - 6.42 (m, 1H)

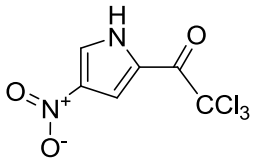

Synthesis of NO_2-Py-$COCCl_3$ (78).[227] To a cooled (-30°C) solution of Py-$COCCl_3$ **(77)** (13.19 g, 62 mmol) in acetyl anhydride (200 mL) was added dropwise HNO_3 100% (4.6 mL, 110.45 mmol, ρ = 1.513). The reaction mixture was allowed to warm to 5°C and stirred for 4 hrs. The solution was cooled down again to -30°C and water (200 mL) was added until a brown precipitate formed. The reaction mixture was allowed to stir overnight. The precipitate was isolated by suction filtration and dried under high vacuum for 3 hrs to afford a crude mixture of 4-nitro, 5-nitro and 4,5-dinitro. Selective crystallisation from boiling toluene and subsequent washing of the solid with petroleum ether 40-60 afforded NO_2-Py-$COCCl_3$ **(78)** (7.00 g, 44%) as a beige powder. ESI-MS (ES+) *m/z:* $[M+H]^+$ calc. for $C_6H_4Cl_3N_2O_3$ 256.9282, found 257; m.p. 159-160°C; ^{1}H-NMR (400 MHz, DMSO-d_6) δ 12.87 - 13.57 (br. s., 1H), 7.90 (d, *J* = 1.6 Hz, 1H), 7.61 - 7.69 (d, *J* = 1.6 Hz, 1H); ^{13}C-NMR (100MHz, DMSO-*d6*) δ 172.8, 137.1, 126.0, 121.5, 114.2, 93.8

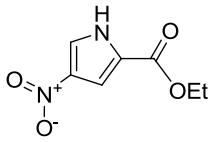

Synthesis of NO_2-Py-COOEt (79).[228,229] Sodium Hydride 60% (0.312 g) was dissolved in Ethanol (70 mL) and NO_2-Py-$COCCl_3$ **(78)** (1.57 g, 60.98 mmol) was added to the solution in a single portion. The reaction was carried out at room temperature for 18 hrs. The mixture was added to a solution of HCl (350 mL, 0.1M). The product precipitated as a white solid and was filtered by suction. The crude product was re-precipitated in DCM : n-hexane and dried to afford **(79)** (1.14 g, 100%) as a white powder. ESI-MS (ES+) *m/z:* $[M+H]^+$ calc. for $C_7H_9N_2O_4$ 185.0557, found 185; m.p. 146-147°C; ^{1}H-NMR (300 MHz, DMSO-d_6) δ 13.12 (br. s., 1H), 8.06 (d, *J* = 1.8 Hz, 1H), 7.25 (d, *J* = 1.8 Hz, 1H), 4.28 (q, *J* = 7.0 Hz, 2H), 1.28 (t, *J* = 7.0 Hz, 3H)

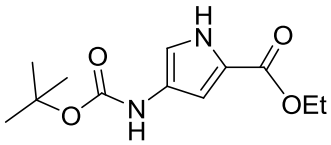

Synthesis of BOC-Py(H)-COOEt (80).[216] To a solution of NO_2-Py-COOEt **(79)** (1.14 g, 6.19 mmol) in freshly dried MeOH (350 mL) was added Pd/C (10%) (0.110 g). A steady stream of H_2 was bubbled through the mixture for 14 hrs. Boc anhydride **(58)** (1.6 g, 7.43 mmol) was then added to the H_2 streamed solution and the reaction stirred out for a further 22 hrs. The mixture was filtered through celite and concentrated *in vacuo* to a black oil. The oil was dissolved in DCM (200 mL), washed with saturated $NaHCO_3$ solution (100 mL), brine (100 mL), HCl 0.1M (100 mL) and brine (100 mL). The organic phase was evaporated *in vacuo* and the product precipitated from hexane to afford **(80)** (0.616 g, 39.9%) as a brown powder. ESI-MS (ES+) *m/z:* $[M+H]^+$ calc. for $C_{12}H_{19}N_2O_4$ 255.1339,

found 255; m.p. 138-140°C; ^{1}H-NMR (300 MHz, $CDCl_3$) δ 8.79 - 9.00 (br. s., 1H), 7.10 (br. s., 1H), 6.54 - 6.65 (br, 1H), 6.25 (br, 1H), 4.23 (q, *J* = 7.2 Hz, 2H), 1.43 (s, 9H), 1.27 (t, *J* = 7.2 Hz, 3H); ^{13}C-NMR (75 MHz, $CDCl_3$) *δ* 124.6, 120.7, 112.8, 106.0, 60.4, 28.4, 27.5, 14.4

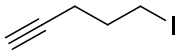

Synthesis of 5-Iodo-Pent-1-yne (82).[230] To a solution of PPh_3 (21.83 g, 83.22 mmol) in DCM (250 mL) was added imidazole (5.67 g, 83.22 mmol) and iodine (21.13 g, 83.22 mmol) in a single batch. After 30 mins at room temperature, a solution of pent-4-yn-1-ol **(97)** (5.023 g, 59.4 mmol) in DCM (5 mL) was added and stirred for 48 hrs. A saturated solution of Na_2SO_3 (250 mL) was added, and the reaction mixture stirred for a further 15 mins and then separated. The organic phase was washed with brine (100 mL) and concentrated *in vacuo*. Petroleum ether 40/60 (400 mL) was added and the residual solid filtered. The solution was then purified by Si-60 column chromatography and eluted with petroleum ether 40/60. The combined fractions containing the product were evaporated *in vacuo* to afford **(82)** (7.35 g, 63.7%) as a pale yellow oil.[230] GC-MS (EI) *m/z:* 194 [M^+]; ^{1}H-NMR (300 MHz, $CDCl_3$) δ 3.32 (t, *J* = 6.7 Hz, 2H), 2.30 - 2.38 (m, 2H), 1.95 - 2.08 (m, 3H); ^{13}C-NMR (75 MHz, $CDCl_3$) *δ* 69.5, 31.8, 29.1, 19.5, 5.1

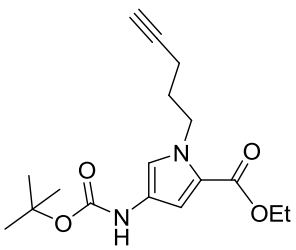

Synthesis of BOC-Py(alkyne)-COOEt (83). To a solution of **(80)** (0.81 g, 3.19 mmol) in DMF (5 mL) was added 5-iodo-pent-1-yne **(82)** (1.86 g, 9.6 mmol) and

K_2CO_3 (1.32 g, 9.6 mmol). The reaction was heated to 115°C for 72 hrs. The mixture was cooled and ethyl acetate (250 mL) added. The organic layer was washed with brine (5x150 mL), dried over $MgSO_4$ and concentrated *in vacuo*. The crude residue was purified by Si-60 column chromatography using DCM: ethyl acetate to afford **(83)** (0.65 g, 63%) as an orange oil. ESI-MS *m/z:* $[M+H]^+$ calc. for $C_{17}H_{25}N_2O_4$ 321.1809, found 321; ^{1}H-NMR (300 MHz, DMSO-d_6) δ 9.19 (br. s, 1H), 7.18 (br. s, 1H), 6.72 (br. s, 1H), 4.15 - 4.41 (m, 4H), 2.91 (t, J = 1.0 Hz, 1H), 2.09 - 2.26 (m, 2H), 1.79 - 1.94 (m, 2H), 1.51 (s, 9H), 1.32 (t, J = 7.2 Hz, 3H); ^{13}C-NMR (75 MHz, DMSO-d_6) δ 153.1, 123.7, 118.7, 83.6, 72.2, 29.9, 28.6, 15.4, 14.7

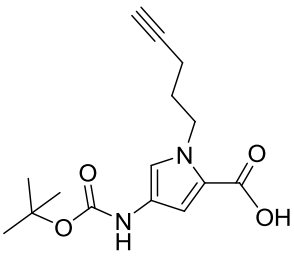

Synthesis of BOC-Py(alkyne)-COOH (59). To a solution of BOC-Py(alkyne)-COOEt **(83)** (0.65 g, 2.03 mmol) in MeOH (15 mL), THF (3 mL) and water (10 mL) was added LiOH (0.18 g, 2.64 mmol). The reaction mixture was heated at 65°C for 18 hrs. The solution was then concentrated *in vacuo* to 10 mL. Water (5 mL) was added followed by a dropwise addition of HCl 1M to reach pH ~2 resulting in the formation of a white precipitate. The precipitate was isolated by suction filtration to afford **(59)** (0.548 g, 92.4%) as a white powder. ESI-MS (ES+) *m/z (%):* $[M+H]^+$ calc. for $C_{15}H_{21}N_2O_4$ 293.1496, found 293 (60), (ES-) *m/z (%):* $[M-H]^-$ calc. for $C_{15}H_{19}N_2O_4$ 291.1350, found 291 (100), $[2M-H]^-$ calc. for $C_{30}H_{39}N_4O_8$ 583.2773, found 583 (40); m.p. 145-146ºC; ^{1}H-NMR (300 MHz, DMSO-d_6) δ 12.11 (br. s., 1H), 9.08 (s, 1H), 7.07 (br. s, 1H),

6.60 (d, *J* = 1.5 Hz, 1H), 4.25 (t, *J* = 6.9 Hz, 2H), 2.82 (t, *J* = 2.5 Hz, 1H), 2.06 (td, *J* = 6.9, 2.6 Hz, 2H), 1.81 (q, *J* = 6.9 Hz, 2H), 1.43 (s, 9H); ^{13}C-NMR (75 MHz, DMSO-d_6) δ 153.1, 123.4, 119.4, 118.3, 83.9, 72.2, 47.4, 30.4, 28.6, 15.4

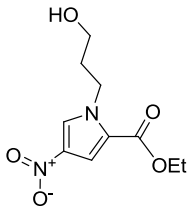

Synthesis of NO_2-Py(OH)-COOEt (84). To a solution of NO_2-Py-COOEt **(79)** (5 g, 27.2 mmol) in acetone (200 mL) was added anhydrous and freshly ground K_2CO_3 (11.2 g, 164.7 mmol). The reaction mixture was stirred at room temperature for 2 hours, then heated to 65°C. 3-iodopropanol **(82)** (4.56 g, 109.8 mmol) was added dropwise over 15 mins and the reaction was left overnight. The solution was cooled and then concentrated *in vacuo*. Water (200 mL), ethyl acetate (300 mL) and HCl (10 mL, 32%) were added until the aqueous phase turned colourless. The organic phase was separated, washed with HCl 0.1M (100 mL), brine (100 mL), dried over $MgSO_4$ and concentrated *in vacuo*. The crude product was purified with Si-60 column chromatography using DCM: ethyl acetate to afford pure **(84)** (3.16 g, 48%) as a yellow oil. ESI-MS (ES+) *m/z:* $[M+Na]^+$ calc. for $C_{10}H_{14}N_2NaO_5$ 265.0800, found 265, $[2M+Na]^+$ calc. for $C_{20}H_{28}N_4NaO_{10}$ 507.1703, found 507; ^{1}H-NMR (300 MHz, DMSO-d_6) δ 8.24 (d, *J* = 1.5 Hz, 1H), 7.32 (d, *J* = 1.5 Hz, 1H), 4.60 (m, 2H), 4.40 (t, 2H), 4.25 (q, *J* = 7.0 Hz, 2H), 1.87 (m, 2H), 1.29 (t, *J* = 7.0 Hz, 3H); ^{13}C-NMR (100MHz ,$CDCl_3$) δ 162.7, 134.0, 133.6, 124.4, 107.1, 57.9, 56.8, 44.8, 35.7, 34.4

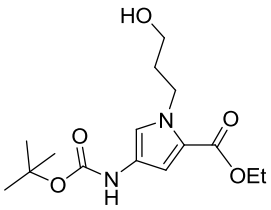

Synthesis of Boc-Py(OH)-COOEt (85).[231] To a cooled (-20°C) solution of NO_2-Py(OH)-COOEt **(84)** (3.16 g, 13.06 mmol) in MeOH (95 mL) was added $NiCl_2.6H_2O$ (0.31 g, 1.31 mmol) and Boc anhydride **(58)** (5.7 g, 26.12 mmol). $NaBH_4$ (3.46 g, 91.42 mmol) was slowly added in batches to the mixture. At the end of the addition the mixture was allowed to warm to 0°C and left stirring overnight. The reaction was quenched with ethyl acetate (100 mL) and H_2O (30 mL), filtered over celite and concentrated *in vacuo*. Ethyl acetate (80 mL) was added and the mixture washed with $NaHCO_3$ (80 mL), brine (80 mL), 1% aqueous diethylenetriamine (3x80 mL) and brine (80 mL). The solution was concentrated *in vacuo* to afford **(85)** (3.52 g, 86.7%) as a pink oil. ESI-MS (ES+) *m/z:* $[M+H]^+$ calc. for $C_{15}H_{25}N_2O_5$ 313.1758, found 313; ^{1}H-NMR (300MHz, DMSO-d_6) δ 9.10 (s, 1H, NH), 7.10 (s, 1H, C-H aromatic), 6.65 (s, 1H, CH aromatic), 4.50 (t, 2H, CH_2), 4.22 (t, 2H, N-CH_2), 4.15 (q, 2H, CH_2), 1.75 (quin, 2H, CH_2), 1.50 (d, 9H, -C(CH_3)$_3$)), 1.25 (t, 3H, CH_3)

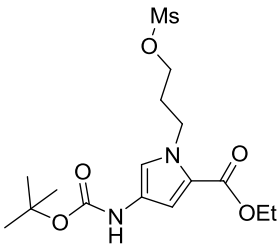

Synthesis of BOC-Py(OMs)-COOEt (86). To a stirred solution of Boc-Py(OH)-COOEt **(85)** (3.52 g, 11.32 mmol) in anhydrous DCM (220 mL) at 0°C, was added a solution of mesyl chloride **(38)** (2.12 g, 18.5 mmol, 1.43 mL) and DIPEA (2.386 g, 18.5 mmol, 3.16 mL) dropwise over 30 minutes. The reaction mixture was stirred for 2h at 0°C and then at room temperature overnight. The reaction was quenched by addition of cold water (300 mL) and ethyl acetate (300 mL). The organic phase was separated, washed with HCl 0.1 M (100 mL),

$NaHCO_3$ sat. (100 mL) and brine (100 mL) and concentrated *in vacuo* to give a brown-orange oil. The crude oil was dissolved in DCM and purified through a Si-60 chromatography column. The product was recovered from the column with DCM: ethyl acetate 50:50 to afford BOC-Py(OMs)-COOEt **(86)** (4.4 g, 100%) as a bright-yellow oil. UPLC-TOF (ESI) *m/z:* $[M\text{-}Boc+H]^+$ calc. for $C_{11}H_{19}N_2O_5S$ 291.1009, found 291.1054; ^{1}H-NMR (DMSO-d, 300MHz) δ 9.12 (s, 1H, N*H*), 7.12 (s, 1H, C-H aromatic), 6.65 (s, 1H, CH aromatic), 4.3 (t, 2H, CH_2), 4.1-4.2 (m, 4H), 3.16 (s, 3H, CH_3), 2.05 (m, 2H, CH_2), 1.44 (d, 9H, -C(CH_3)$_3$)), 1.25 (t, 3H, CH_3)

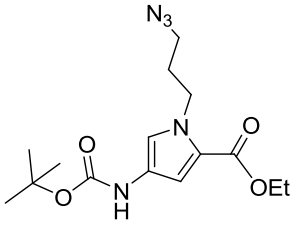

Synthesis of BOC-Py(N_3)-COOEt (87). To a solution of BOC-Py(OMs)-COOEt **(86)** (4.4 g, 11.3 mmol) in dioxane (50 mL) was added NaN_3 **(20)** (1.83 g, 28.24 mmol), K_2CO_3 (0.194 g, 1.41 mmol) and water (50 mL) were added and the mixture was heated under reflux overnight, then concentrated *in vacuo*. The residue was dissolved in ethyl acetate (200 mL), washed with HCl 0.1M (50 mL), $NaHCO_3$ (sat.) (50 mL) and brine (50 mL), then dried over $MgSO_4$ and concentrated *in vacuo*. The oily residue was purified by Si-60 column chromatography using n-hexane: ethyl acetate to afford **(87)** (3.36 g, 88.5%) as an orange oil. UPLC-TOF (ESI) *m/z:* $[M+H]^+$ calc. for $C_{15}H_{24}N_5O_4$ 338.1823, found 338.34; ATR-FTIR: ν = 2069 cm^{-1} (s; ν_{as}(azide)); ^{1}H-NMR (300 MHz, DMSO-d_6) δ 9.13 (s, 1H), 7.12 (s, 1H), 6.66 (d, *J* = 1.2 Hz, 1H), 4.27 (t, *J* = 6.9 Hz, 2H), 4.18 (q, *J* = 7.0 Hz, 7H), 3.27 (t, *J* = 6.7 Hz, 2H), 1.89 (m, 2H), 1.44 (s, 9H), 1.25

(t, J = 7.0 Hz, 3H); ^{13}C-NMR (75 MHz, $CDCl_3$) δ 160.5, 153.1, 123.8, 118.7, 108.3, 79.0, 59.9, 48.4, 46.0, 30.6, 28.6, 14.7

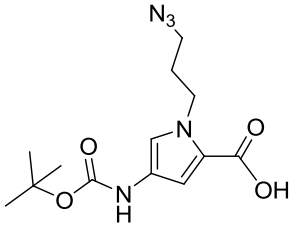

Synthesis of BOC-Py(N_3)-COOH (88). To a mixture of BOC-Py(N_3)-COOEt **(87)** (3.36 g, 10 mmol) in MeOH (100 mL) was added LiOH (1.17 g, 28 mmol) and water (100 mL). The reaction mixture was heated to 65°C for 18 hrs. The solution was then concentrated *in vacuo* to 100 mL and HCl 1M was added to reach pH ~3. The aqueous phase was extracted with ethyl acetate (3x100 mL). The combined organic layers were dried over $MgSO_4$ and evaporated *in vacuo*. The residue was precipitated from 1:10 DCM: petroleum ether 40/60 to afford **(88)** (1.76 g, 57%) as a brown powder. ESI-MS (ES-) *m/z:* $[M-H]^-$ calc. for $C_{13}H_{18}N_5O_4$ 308.1364, found 309; ^{1}H-NMR (300MHz, DMSO-d_6) δ9.05 (s, 1H, N*H*), 7.1 (s, 1H, C-H aromatic), 6.6 (s, 1H, C-H aromatic), 4.25 (t, 2H,CH_2), 3.25 (t, 2H, CH_2), 1.9 (quin, 2H, CH_2), 1.4 (d, 9H, -C(CH_3)$_3$)); ^{13}C-NMR (100MHz, DMSO-d_6) δ 161.59 (CO), 152.63 (CO), 123.05 (quaternary), 118.91 (quaternary), 117.78 (C*H*), 107.98 (C*H*), 78.41 (quaternary), 47.90 (CH_2), 45.30 (CH_2), 30.15 (CH_2), 28.11 (CH_3)

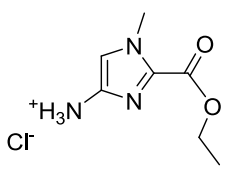

Synthesis of NH_3^+-Im-COOEt (89).[219] Boc-Im-COOEt **(50)** (0.720 g, 0.268 mmol) was added to a solution of dry HCl 1M in dioxane (10 mL, 1.2M). The reaction was stirred at room temperature for 2 hrs and then concentrated *in vacuo*. The residue was

diluted with water and lyophilised to afford **(89)** (0.594 g, 74% as a dioxane solvate) as a white powder. ESI-MS (ES+) *m/z:* $[M+H]^+$ calc. for $C_7H_{12}N_3O_2$ 170.0924, found 170; m.p. 173-174°C; ^{1}H-NMR (400 MHz, DMSO-d_6) δ 9.74 (br. s, 1H), 7.49 (s, 1H), 4.23 - 4.45 (m, 2H), 4.00 (s, 3H), 1.26 - 1.44 (m, 3H); ^{13}C-NMR (100 MHz, DMSO-d_6) δ 157.0, 137.9, 132.2, 116.6, 61.3, 36.0, 13.9

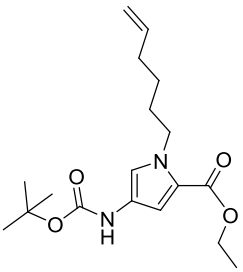

Synthesis of BOC-Py(alkene)-COOEt (81). To a solution of **(80)** (0.100 g, 0.394 mmol) in diglyme (15 mL) was added 6-bromo-hex-1-ene **(80)** (0.300 g, 1.84 mmol) and K_2CO_3 (1.32 g, 9.6 mmol). The reaction was sealed in a high pressure vessel and heated to 175°C for 18 hrs. The mixture was cooled and ethyl acetate (150 mL) added. The organic layer was washed with brine (3x150 mL), dried over $MgSO_4$ and concentrated *in vacuo*. The crude residue was purified by Si-60 column chromatography using DCM: ethyl acetate to afford **(81)** (0.062 g, 47%) as a yellow oil. ESI-MS *m/z:* $[M+H]^+$ calc. for $C_{18}H_{29}N_2O_4$ 337.2122, found 337; ^{1}H-NMR (300 MHz, $CDCl_3$) δ 9.66 - 9.87 (m), 7.13 - 7.24 (m), 6.75 - 6.89 (m), 6.30 - 6.46 (m), 5.35 - 5.61 (m), 4.53 - 4.83 (m), 3.82 - 4.04 (m), 3.41 - 3.62 (m), 1.68 - 1.89 (m), 1.44 - 1.65 (m), 1.13 - 1.32 (m), 0.90 - 1.09 (m); ^{13}C-NMR (125 MHz, DMSO-d_6) δ 165.3, 138.5, 138.4, 132.5, 131.6, 128.6, 116.4, 115.0, 114.8, 67.4, 61.7, 32.8, 32.6, 29.8, 13.9, 10.8

CHAPTER 4: SITE-SPECIFIC METALLISATION OF DNA

4.1 Introduction

DNA is an excellent framework for the creation of ordered nanostructures, due to its ability to self-assemble in a predictable and reproducible manner and the availability of restriction enzymes to modify it (Chapter 1). This chapter will focus on addressing a major unmet challenge in the application of DNA nanotechnology to the field of nanoelectronics: the low inherent conductivity of DNA. In an attempt to address this limitation, a number of groups around the world have tried to convert DNA structures into conductors by metallisation. Methods to initiate nucleation and growth of metals along DNA templates have been developed and have produced defined metallised architectures; however, the current methods lack the capacity to confine metallisation to specific regions along DNA architectures (Figure 102).

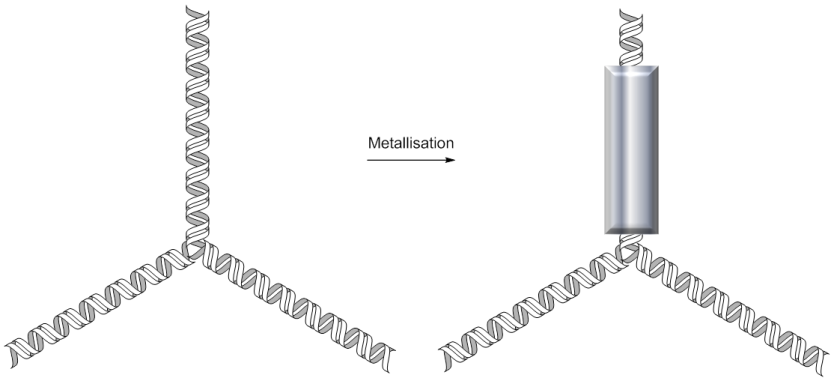

Figure 102: Schematic representation of a confined metallisation of a DNA architecture (T-junction used as an example in this figure)

4.1.1 Synopsis of previous methods of DNA metallisation

Methods which metallise DNA can be divided in two major groups: 1) interfacing pre-formed metal nanostructures such as metal nanoparticles with DNA; and 2) DNA-templated growth of metal nanostructures. Both of the techniques have

advantages and disadvantages and these will be outlined in sections 4.1.1.1 and 4.1.1.2.

4.1.1.1 Assembly of pre-formed metal nanostructures using DNA

Nanoparticle assembled DNA starts with Chad Mirkin who in 1996 developed the first DNA coated gold nanoparticles.[232] Thiol DNA with sticky-ends (Figure 103) was prepared and used to coat AuNP, leading to uncontrolled aggregation that was thermally reversible.

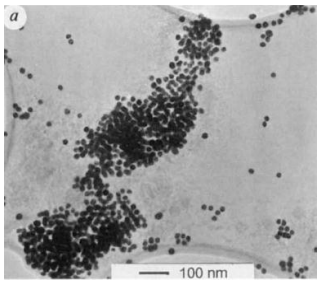

Figure 103: Sticky-ends DNA coated gold nanoparticles prepared by Chad Mirkin (Reproduced from Ref.[232])

Since this seminal discovery, the programmed assembly of metal nanostructures has rapidly developed. The development of synthetic Holliday junctions (Chapter 1 Figure 7), for example, allowed Seeman and Turberfield to construct novel branched supramolecular structures such as cubes, tetrahedrons and bipyramids (Figure 104).[233,234] Paul Alivisatos and co-workers exploited this method for the assembly of four different nanoparticles at the edges of a regular DNA tetrahedron, forming a putative chiral nanocrystal.[235]

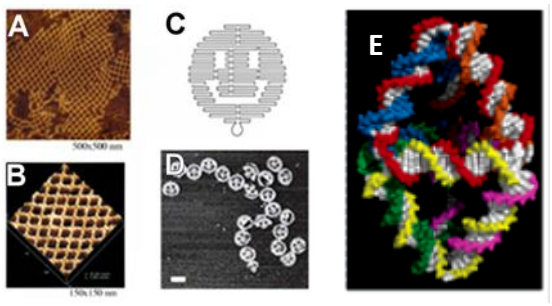

Figure 104: A-B. Examples of self-assembling Holliday junctions (Ref.[236,237]) C-D. DNA Origami (Ref.[38]) E. DNA double tetrahedron made by Turberfield (Ref.[234]).

Aldaye pushed the field of structural DNA nanotechnology with the construction of large arrays of shapes such as dodecahedrons bearing AuNPs.[37,238–240] A breakthrough event was the discovery and development of "DNA origami" by Rothemund in 2003.[38] DNA origami methods revolutionised the DNA supramolecular field as challenging nanostructures were now available to the chemist through the use of short synthetic DNA "staples" used to shape a large viral DNA template 7 kbases in length in any possible desired way (Chapter 1).

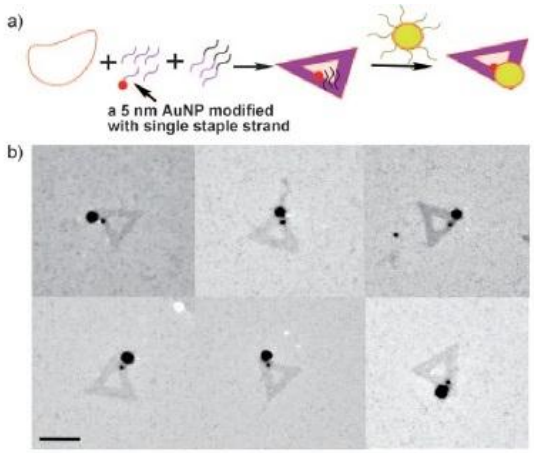

Figure 105: Metallised DNA-triangle origami prepared by the Yan group. (reproduced from Ref.[241])

The use of DNA origami allowed Hao Yan and his group to build highly ordered self-assembled silver and gold nanoparticles in two-dimensions using a DNA triangle origami[241,242] (Figure 105).

The current drawback of this technique is the need of highly functionalised DNA scaffolds which can require significant optimisation at the self-assembly process. This limits the scope and applicability of the technique.

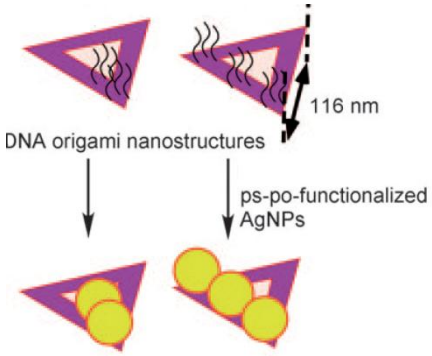

Highly functionalised DNA scaffolds, requiring a large amount of optimisation.

Confined DNA metallisation

Figure 106: Metallisation of a DNA triangle origami made by Yan (reproduced from Ref.[241]) The DNA origami with a highly functionalised scaffold with DNA staples required a significant amount of optimisation.

Reviews of the current approaches to modified DNA as a supramolecular scaffold towards the creation of functional molecules have been recently published by Stulz[243,244] and Mirkin.[59] Challenges in templated self-assembly of nanoparticles and DNA have been recently reviewed by Yan,[245] as a follow up of LaBean review of 2007 in DNA structural nanotechnology.[246]

4.1.1.2 DNA-templated metal growth of metal nanostructures

DNA-templated metal growth methods can use any type of DNA scaffold, including natural DNA, and so are potentially better suited for the global metallisation of DNA duplexes. The main techniques that have been used for

metal growth using DNA scaffolds are: 1) photochemical and 2) chemical reduction processes. The photochemical method generally involves mixing DNA and Ag^+ ions in a suitable buffer, then irradiating with UV light to start the photo-induced metal reduction. Electrostatic interactions between the negatively charged DNA and the positive Ag^+ ions result in a selective deposition of native metal along the DNA, effectively creating a nanowire[247] (Figure 107)

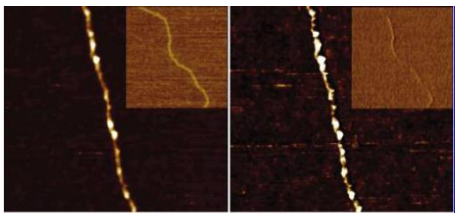

Figure 107: Silver coated DNA nanowire created by UV irradiation (reproduced from Ref.[247]).

Jacopo Samson of the Drain group showed how it's possible to photochemically deposit silver onto a toroidal DNA plasmid creating silver nanorings.[248] This is important as it shows how it is possible to use a DNA template to grow silver nanostructures.

Chemical reduction methods generally involve the use of metal ions and aldehyde-modified DNA.[105]

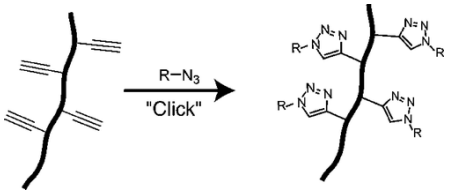

Figure 108: Schematic representation of functionalisation of alkyne-modified oligodeoxyribonucleotides with sugar azides. (reproduced from Ref.[105])

A modified DNA is constructed using unnatural bases bearing desired functional groups, like the alkyne in this example (Figure 108). DNA is pre-treated with glutaraldehyde as disclosed by Braun,[249] then the metal is added and the solution is heated or photo-irradiated to initiate nucleation. This highly successful method has been exploited for the creation of Ag nanowires by LaBean,[250] Au[251] and Co[252] by Gu, Pd by Richter,[253] Pt[254] and Cu[255] by Woolley's group and Ni by Bagkar.[256] The drawback is that metal is deposited along the whole DNA duplex and the rate of growth is difficult to control. In order to confine the metallisation process to specific DNA strands, Carell *et al*. developed a new click and metallisation method by using Tollens' reagent and aldehyde modified DNA to induce metallisation to only regions of the DNA bearing the aldehydes (Figure 108).[105]

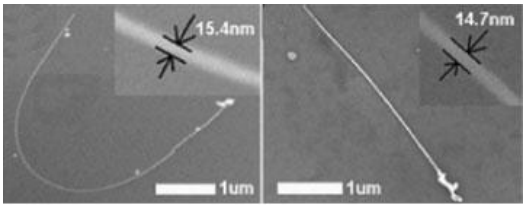

Figure 109: Silver DNA nanowire prepared by Carell's group. (reproduced from Ref.[105]).

Despite its potential to confine metallisation to specific DNA duplexes, this method suffers from a lack of control of the metallisation process to defined regions within nanostructures.[105,257] DNA nanostructures created with unnatural DNA can be even more difficult to optimise and control.

4.1.2 AIM

The aim of this chapter and the primary aim of this thesis is to develop a new infrastructure of methods to template functional materials at specific sites in a DNA architecture using molecular recognition of specific DNA duplexes. The project focused on the use of naturally occurring duplex DNA and the Tollens' reaction as a mild source of metal amenable to reduction in the presence of aldehyde functional groups. The advantages of this choice are:

1) the use of naturally-occurring DNA increases modularity;

2) the Tollens' reagent acts as a mild selective metallising reagent that enables the reduction of metal ions at specific sites along DNA. Molecules such as polyamides (PAs) prepared in Chapter 3 were tested to determine whether selective metallisation of DNA nano-architectures can be achieved by confining the nucleation and growth of silver nanostructures to defined regions along a DNA duplex.

4.2 Results

4.2.1 Stability of DNA to silver salts

The stability of duplex DNA has been assessed in a variety of physiological conditions; depurination,[258] cytosine deamination[259] and strand breakage[260] are the most common reactions occurring in both double stranded and single stranded DNA. During metallisation events, DNA is treated with highly electropositive metals (i.e. Ag^{+} and Au^{3+}) and at non-physiological conditions such as elevated pH.[40] It was surprising to discover that besides studies of the well-known role of

Cu in strand breakage,[261] only studies of alkaline denaturation[262] and cobalt[263] induced conformational changes are well assessed in literature. Therefore stability studies of DNA in the presence of Ag^+ were conducted.

4.2.1.1 Studies of stability of duplex DNA in the presence of Ag^+ ions

Double stranded DNA **(98)** (dsDNA) of an exemplar duplex sequence 5'-CGATGTTCAAGC-3' was prepared in stock solutions at 1 μM in both cacodylate buffer (sodium dimethylarsinate is a common buffer used for *DNA* sequencing, recombinant *DNA* procedures and for the preparation and fixation of TEM samples), and phosphate buffer. The dsDNA was then tested for stability by isothermal melting in the presence of $AgNO_3$ at a concentration of 1 eq of Ag^+ for each C-G base pair of the DNA (6 eq in total). This was chosen, as G oxidation to 8-hydroxyguanine is the most abundant lesion of DNA oxidative stress.[264] As Ag^+ is a high electropositive ion, the most likely lesion caused would be the oxidation of G. Moreover, silver atoms have been shown to oxidise G by Karadeniz.[265] However, DNA under these conditions showed no variation in the melting point. As concentration of Ag^+ increased, the DNA duplex was shown to be stable up to 10 eq $AgNO_3$ for each G (60 eq of Ag^+ / dsDNA), but at 100 eq $AgNO_3$ (600 eq of Ag^+ / dsDNA) DNA was completely degraded as shown by a loss of the characteristic UV-Vis absorption peak at 260 nm and by gel-electrophoresis.

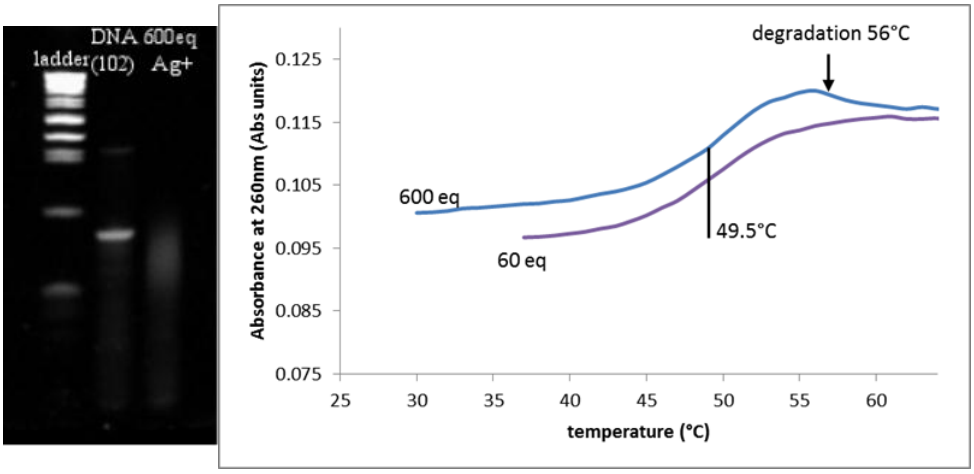

Figure 110: GEL-electrophoresis of a sample of DNA (98) and the same sample after isothermal melting in the presence of 600 eq of Ag^+ showing degradation of the DNA. Isothermal melting spectra of DNA (98) in the presence of 60 eq Ag^+ and 600 eq Ag^+ showing a melting temperature of 49.5 °C and a degradation temperature of 56 °C in the presence of 600 eq of Ag^+.

In conclusion, short dsDNA was shown to be stable during isothermal melting with up to 60eq of Ag^+ ions. At higher concentration (600 eq Ag^+) DNA degraded, probably due to strand breakage and oxidations as shown by the smear in the gel-electrophoresis (Figure 110). This test was important to assess if DNA nanostructures could be manipulated or assembled by annealing in the presence of silver ions. However, these measurements did not evaluate the room temperature stability of the DNA duplex in the presence of Ag^+ ions.

4.2.1.2 Melting point studies of duplex DNA- polyamide complexes in the presence of Ag^+ ions

As a further step in the preparation of metallised DNA using natural DNA, Py-Im polyamides and silver, DNA was tested in the presence of both the polyamide and Ag^+ ions. Possibly, the binding affinity of polyamides could be perturbed by the

presence of Ag^+ ions. Polyamide **(93)** (Figure 99) was then tested by melting point with DNA **(98)** in sodium cacodylate buffer with and without the presence of $AgNO_3$ at the concentration of 10 eq of $AgNO_3$ for each G (60 eq of of Ag^+ / dsDNA), as previously disclosed in paragraph 4.2.1.1.

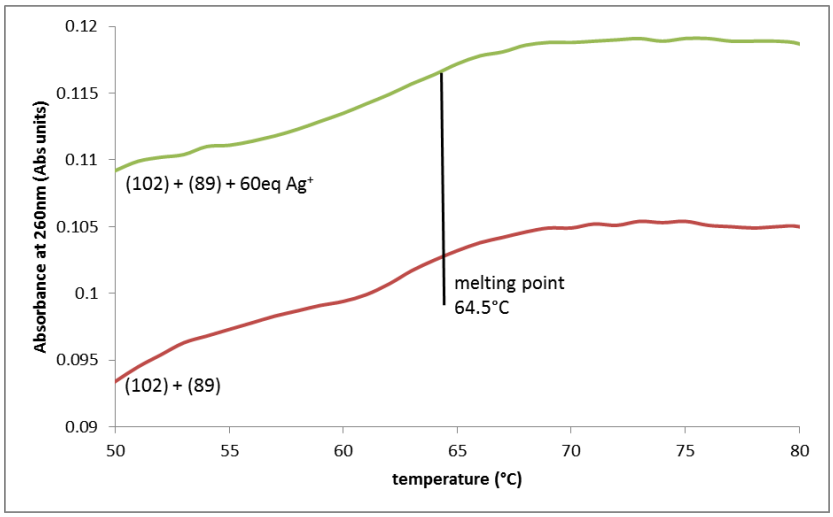

Figure 111: Isothermal melting spectra of DNA (98) + polyamide (93) with and without Ag^+ ions showing the same melting point at 64.5°C (Reported 64°C by ref. [266])

In conclusion, results showed that the binding affinity of the polyamide is unaffected by silver salts up to the tested concentration of 60 eq $AgNO_3$ for each C-G pair.

4.2.2 Stability of gold and silver colloids to the presence of Py-Im PAs

The stability of the metallised system is a fundamental factor for the success of this metallisation approach as explained in the aims (paragraph 4.1.2). Both the templated metal and the polyamides involved in the DNA templating process must be stable to the metallisation conditions. In addition, the dsDNA-PA complex must also withstand the metallisation and nucleation conditions. The

following paragraph describes tests conducted to assess the concentration ranges at which the metallised systems are stable.

4.2.2.1 Preparation of Py-Im polyamide dimers as polyamide-NP stability probes.

PAs are multifunctional molecules that can hypothetically bind on the surface of a metal nanoparticle through their nitrogen heteroatoms. Imidazoles binding to silver atoms have been previously exploited for the construction of supramolecular scaffolds.[267] Two-ring polyamides are the smallest prototypes for probing the binding properties and stability with metal nanoparticle colloids.

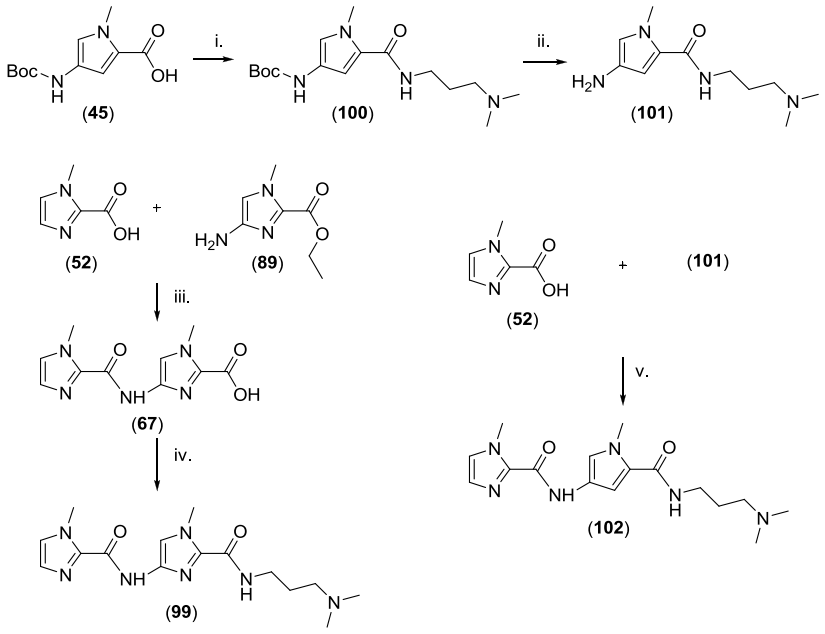

Scheme 31: Preparation of compound (102) and (99). i. (55), HATU, 2h, 64% ii. TFA, 6h, 97% iii. EDC/HOBt then LiOH, 54% iv. (55), HATU, DMF, 26% v. (52), HATU, DMF, 22%

Boc-Py-OH **(45)** was coupled with di-methylaminopropylamine **(55)** in DMF in the presence of HATU and DIEA for 2 hours to afford Boc-Py-ODp **(100)** in 64%

yield. Boc deprotection of **(100)** was achieved using TFA at 35°C for 6 hours to obtain NH2-Py-ODp **(101)** in 97% yield. Compound **(101)** was then coupled with Im-OH **(52)** using HATU/DIEA to afford the first dimer Im-Py-ODp **(102)** in 22% yield. The second dimer was prepared by coupling Im-Im-OH **(67)** (synthesis is described in Chapter 3.3.3.1) with di-methylaminopropylamine **(55)** using HATU/DIEA as coupling agent to afford **(99)** in 26% yield after purification by semi-preparative HPLC. Low yields were attributable to the low coupling efficiency of **(52)** with HATU. The two polyamide probes were then tested with silver and gold colloids.

4.2.2.2 Stability of gold and silver nanoparticles to aggregation induced by (102) and (99)

Polyamides contain a number of residues, in particular nitrogen atoms, which can bind to the surface of silver and gold colloids.[137] This behaviour is undesirable as it could cause a destabilisation of the colloid and aggregation.

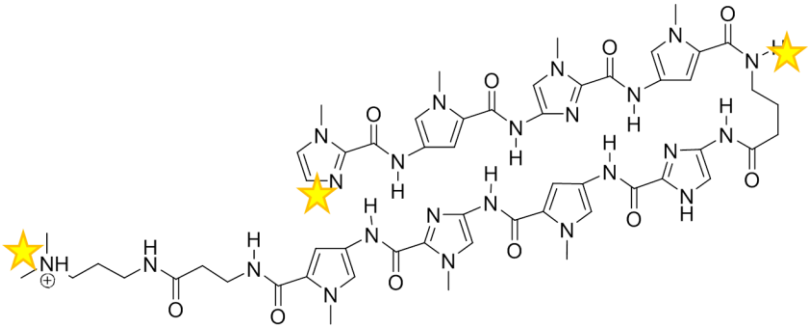

Figure 112: Scheme of a generic polyamide with marked types of nitrogens (yellow stars mark exemplars of aromatic, amides, ammonium nitrogens) that could possibly bind metal surfaces.[267]

Primary amine residues are known to bind the surface of silver and gold colloids but not to cause spontaneous aggregation events.[268] Imidazoles are known to

cause aggregation in gold nanoparticles.[137,269] The effect is due to the binding of two nanoparticle surfaces to each imidazole. If that is the case, then aggregation should not scale linearly with the number of imidazoles in a polyamide, as each polyamide could potentially bind only two nanoparticles due to the large difference in sizes and steric hindrances. In order to test this, **(102)** and **(99)** were dissolved in water as 20 μM stock solutions and added to a stock solution of a 15 nm diameter, 10 nM phosphine coated AuNPs. The AuNPs were prepared by ligand exchange of commercially available citrate coated AuNPs (preparation is described in the Experimental section). Increasing the concentration of the dimers resulted in a decrease of the plasmon peak at 520 nm. A concomitant formation of absorption at 720 nm was observed, indicating aggregated clusters (Figure 113).

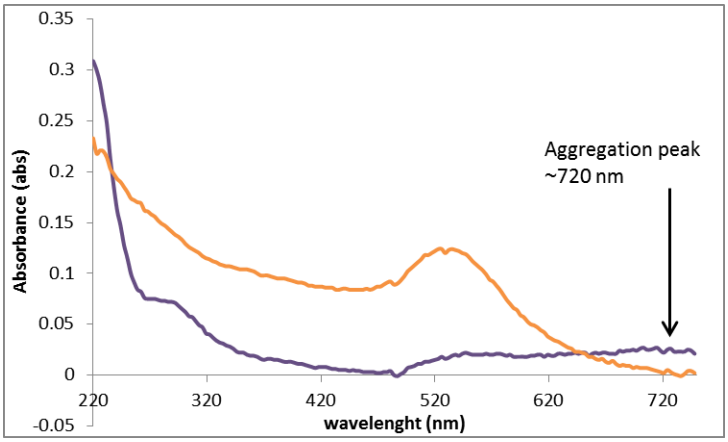

Figure 113: UV-Vis spectra of 15nm phosphine-coated gold nanoparticles (orange) and the same solution after the addition of 8 μM (102) showing aggregation and the formation of a peak at ~720 nm (blue).

Visually, the colloid turned progressively from bright red to blue. The critical concentration at which aggregation was observed was at 1.95 μM of dimer **(102)**

for a 10 nM solution of AuNPs. Aggregation was complete at 6 μM of **(102)**. We therefore infer that the imidazole group induces aggregation of gold colloids.

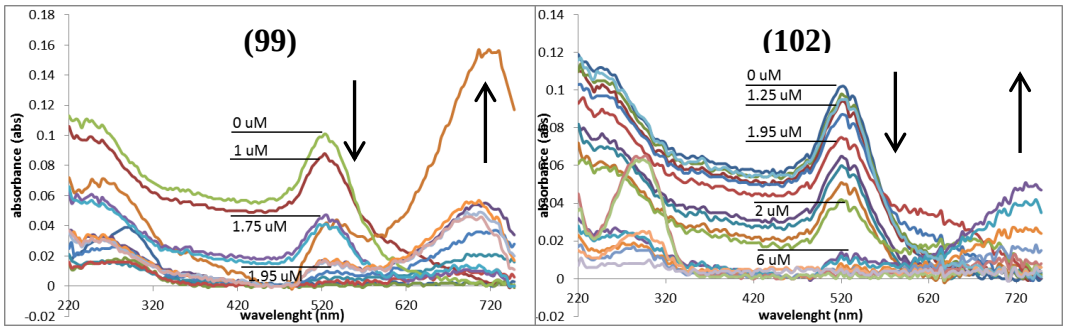

Figure 114: UV-Vis absorbance of a 10 nm gold nanoparticles colloid at the increasing concentration of compound (99) and (102).

Compound **(99)** showed a similar aggregation profile to **(102)**, however the aggregation was more pronounced and the GNP colloid completely aggregated at a concentration of 1.75 μM. This could be due to the presence of the second imidazole in compound **(99)**.

Silver nanoparticles prepared from sugar (**1**, Chapter 2) gave similar results, pointing to the same binding mechanism of polyamides to gold and silver surfaces. However the necessary concentration for aggregating AgNP@**(1)** was much higher than the one required for phosphine coated gold nanoparticles. In particular, the addition of compound **(102)** to AgNP@**(1)** resulted in 52 % aggregation at a concentration of 500 μM as measured by the decrease of UV-Vis absorbance of the surface plasmon peak (Figure 115). Dimer **(99)** was found to induce a broadening of the resonance plasmon peak and aggregate the AgNP@**(1)** only by 24% at the concentration of 500 μM (Figure 115). This effect was not noticed for compound **(102)** or in the test series with gold nanoparticles.

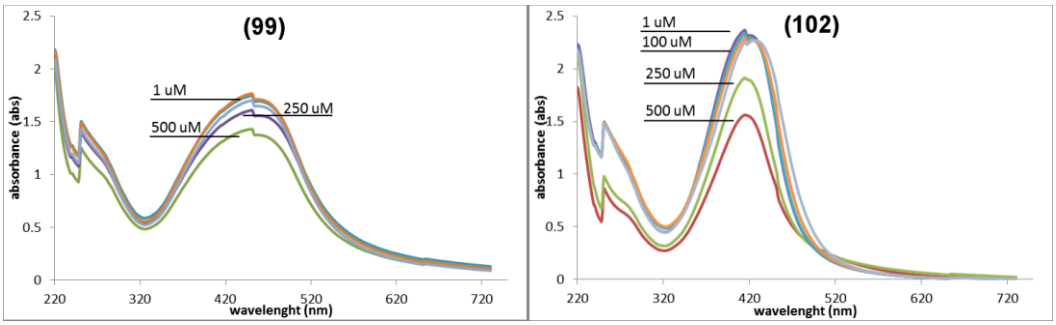

Figure 115: UV-Vis absorbance of AgNP@(1) at the increasing concentration of compound (99) and (102).

This is important, as by these results, it seemed that AgNPs prepared with the Tollens' reagent are more stable to aggregation induced by polyamides than widely used phosphine coated gold nanoparticles.

The dimers **(99)** and **(102)** were then tested during the growth of 5 nm citrate coated AuNP with a synthesis adapted from a published method by Martin of the Sang-Kee Eah group.[270] A gold chloride stock solution was prepared with 50 mM $HAuCl_4$ and 50 mM HCl. A stock solution of borohydride was prepared with 50 mM $NaBH_4$ and 50 mM NaOH. An additional stock solution of sodium citrate 50 mM was prepared. 100 μL of gold solution was diluted in a glass vial with 10 ml of water, and then 50 μL of citrate solution was added while the solution was strongly vortexed, followed by 166 μL of borohydride solution. In a matter of seconds, the solution acquired a deep purple-red colour, sign of the formation of gold nanoparticles. This simple protocol was modified with the addition of increasing quantities of compound **(99)** and **(102)** to test an inhibition of the formation of a stable gold colloid. This test was undertaken in order to determine

the concentration parameters that were then used for the DNA-PA-Tollens' system.

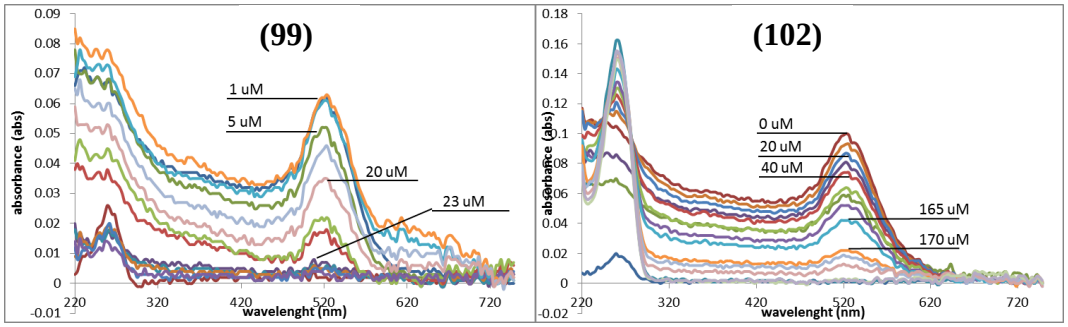

Figure 116: UV-Vis absorbance of a AuNPs colloid formed in the presence of an increasing concentration of compound (99) and (102).

The results showed that Im-Py-Dp dimer **(102)** can interfere in the formation of a AuNP colloid only at a concentration greater than 165 µM, while Im-Im dimer **(99)** was causing aggregation of the forming colloid already at 22 µM, showing that the presence of two consecutive imidazole had a great effect on the stability of the nanoparticles.

In conclusion, a strong implication of the Im heterocycle in the destabilisation of the colloids was observed and a maximum concentration of Py-Im polyamides for further experiments was determined. Moreover, these tests showed that the presence of two consecutive imidazoles were strongly detrimental on the stability of the gold colloids. Consequently, it was decided to choose a polyamide for DNA metallisation that did not possess this moiety.

4.2.3 Preparation of biotin-sugar, Tollens' metallisation and attempted aggregation with streptavidin

The properties of the surface of silver nanoparticles formed with Tollens' reagent are an area of research still under scrutiny. Sugars, such as galactose are known to bind the surface of the AgNPs as galactonic acid.[147] Sugars can then be exploited, if tethered with ligands, to form bonds and anchor a AgNP onto DNA or any desired surface, without the need of additional surfactants specific for this role. An experiment in which a biotin molecule is tethered to a sugar could potentially probe the application of this strategy in a simple way that could be detected by UV-Vis spectroscopy. The biotin-streptavidin couple is widely used in bionanotechnology due to the couple possessing one of the strongest non-covalent interactions in the natural world. The affinity of biotin to streptavidin is of the order of 10^{-14} mol/L,[271] and it is resistant to solvents and to surfactants like sodium dodecylsulphate (SDS). The preparation of biotin-AgNPs would give an indication of the strength and availability of binding sites over the surface of AgNPs. Biotin-alkyne **(103)** was prepared by following a protocol of Mattoussi's group[272] (Scheme 32).

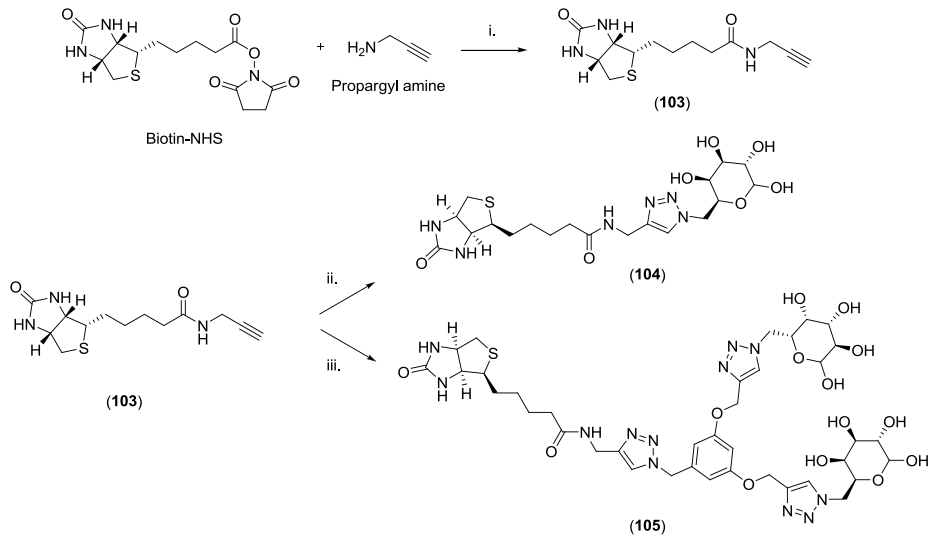

Scheme 32: Synthetic route for the preparation of biotin sugars (104) and (105). i. TEA, DMF, r.t., 18h, 47% ii. (7), (42), DMSO, 18h, 26% iii. (15), (42), DMSO, 18h then TFA, 80°C, 2h, 8%

Commercially available Biotin-NHS was coupled to propargylamine in DMF at room temperature to afford compound **(103)** with 47% yield. Compound **(103)** was then reacted with sugar azide **(7)** and sugar azide **(15)** in the presence of PS-NHC-Cu(I) **(42)** in DMSO at room temperature overnight to afford biotin-sugars **(104)** and **(105)** in 26% and 8% yield respectively after deprotection using TFA.

The biotin-sugars **(104)** and **(105)** were then dissolved in a metallisation buffer composed of TBE 0.5x and SDS. Two arrays were used to dose the concentration of Tollens' reagent, sugar and SDS.

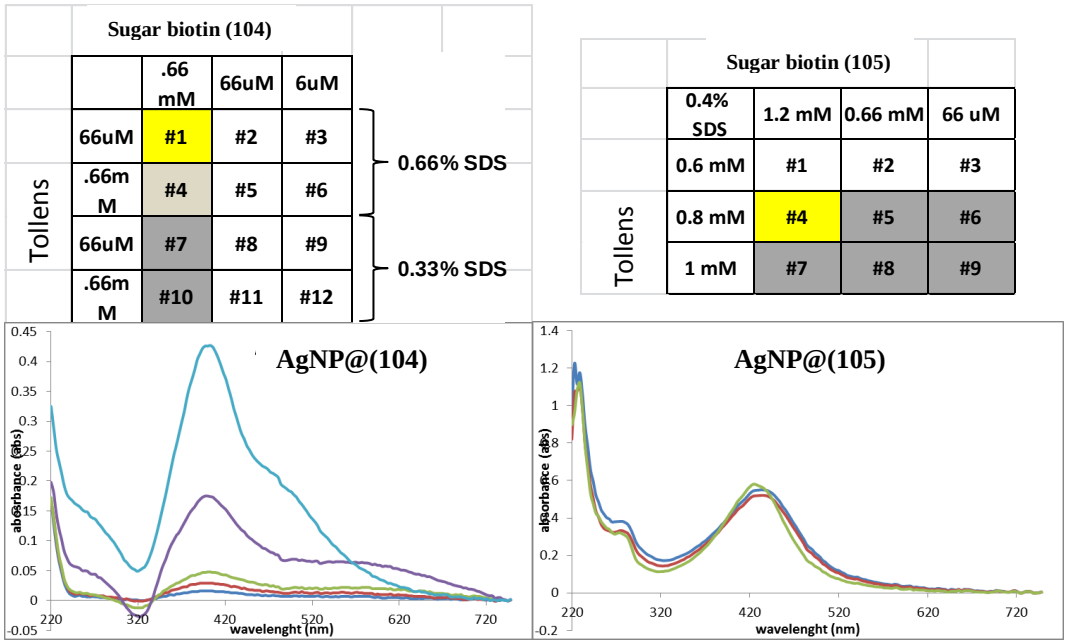

Figure 117: Array series for the preparation of AgNP@(104) and AgNP@(105). White boxes represent no AgNP formation, grey boxes represent "silver mirror" and yellow boxes represent AgNP formation. UV-Vis spectra of samples of AgNP@(104) and AgNP@(105) that formed a stable AgNP colloid after 24h (repeated experiments).

The optimal concentration for the formation of biotin-sugar **(104)** AgNP was determined to be 0.66 mM sugar, 0.66 mM Tollens' and a minimum concentration of 0.66% of SDS. Sugar2-biotin **(105)** optimal concentrations were determined to be 1.2 mM sugar, 0.8 mM Tollens' and a minimum concentration of 0.4% SDS. The nanoparticles formed were then purified by passing them through a Sephadex G-25 pre-packed column, eluting with 0.5x TBE buffer / 0.2% SDS and collecting only the fractions containing AgNPs. Streptavidin (1 uL of 947 nM) was then added to 10 uL of the desalted and concentrated particles in an Eppendorf tube. UV-Vis analysis showed no significant shift in the plasmon resonance peak of the particles, indicating no aggregation (Figure 118). The test was then repeated with the addition of 1 μL of 0.1 M NaCl, since streptavidin requires a certain amount

of salts to bind successfully the biotin, however even in this case no binding was visible to UV-Vis (Figure 118).

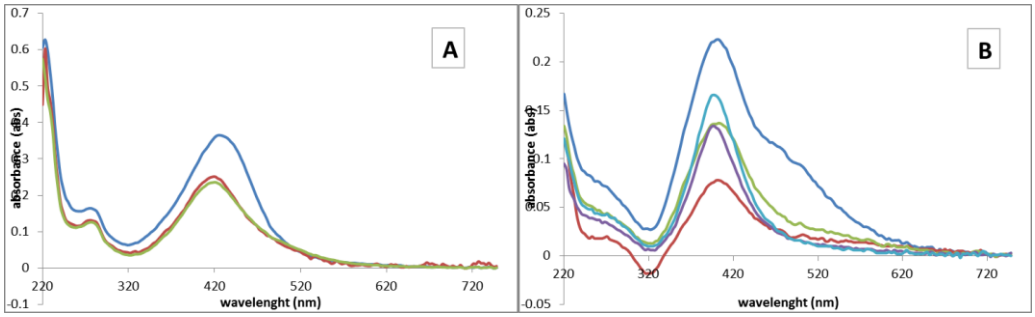

Figure 118: UV-Vis spectra of A. AgNP@(105) treated with streptavidin B. AgNP@(104) treated with streptavidin

As the concentration of the streptavidin used is much lower than the concentration of the particles, it is assumed that the number of particles aggregated was too little to be determined by absorption analysis. A sample of the streptavidin treated AgNP@**(105)** was then loaded onto a carbon coated copper grid and imaged by TEM.

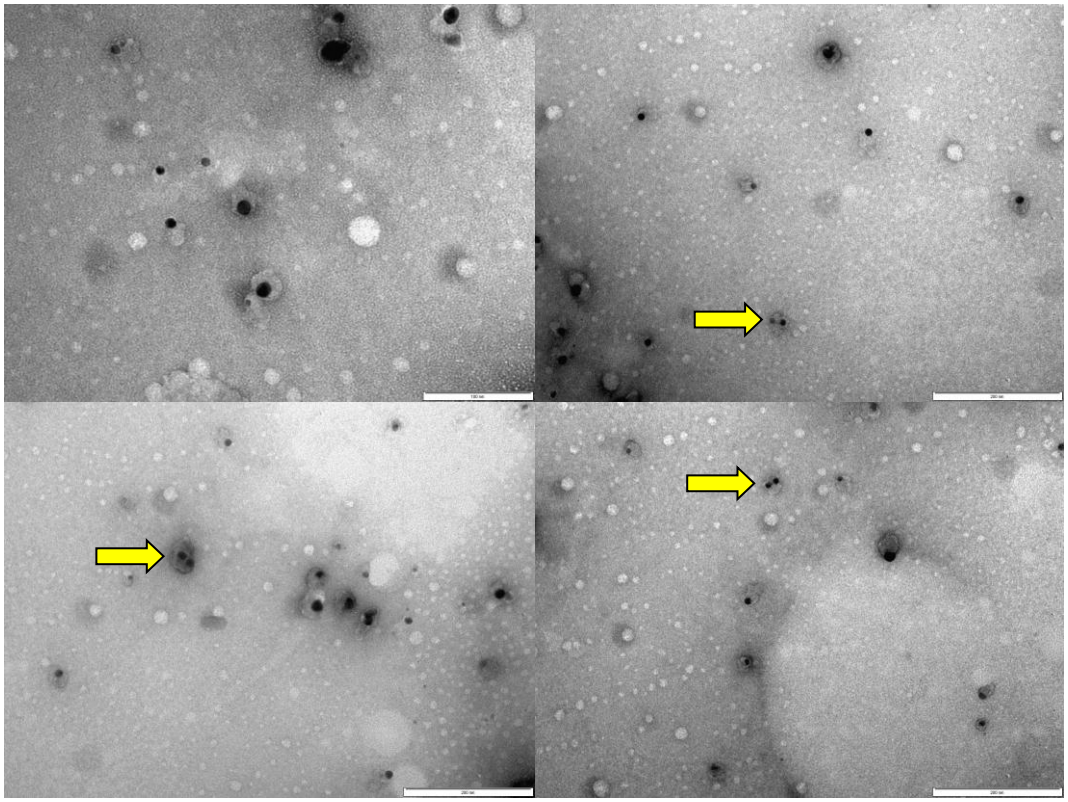

Figure 119: TEM images of streptavidin treated AgNP@(105), showing only sparse metallisation of the streptavidin. Yellow arrows highlight streptavidins metallised with two AgNPs.

Streptavidin was recognized as dark oval shadows by comparing the images with the work of Naik Rajesh[273] and Velev's ferritin-metallised liposomes.[274] These dark shadows are mostly non metallised. Some of them contain one AgNP, rarely two particles are aggregated together. The low propensity of aggregation explains the lack of shift of the UV-Vis plasmon resonance peak, (Figure 118) as most of the particles are still well dispersed in the solution.

In conclusion, even if most of the particles are aggregated with a streptavidin, it does not prove that the biotin is presented on the surface of the AgNP and it's available to form complexes with streptavidin. In fact it's largely possible that the aggregation observed is caused by electrostatic interaction between negatively

charged AgNPs and positively charged streptavidin.[275] In these conditions, also no self-assembled fiberlike structures between biotin and silver were formed as previously reported by Sudhir Kapoor.[276] These results hinted to the possibility that the biotin was not present on the surface of the nanoparticles or that in general the biotin molecules were not available to form bonds. Multiple reasons can be conjectured: 1) biotins are not bound on the surface of the silver with a strong enough bond to actually cause aggregation 2) biotin is chemically modified (Eg. oxidation to sulfoxide is known to increase dissociation[277]) during the Tollens' reaction and its binding to streptavidin is compromised.

Additional techniques could be used to determine which process is occurring on the surface of the particles. For example, secondary electron images from Auger electron spectroscopy (AES) and secondary ion mass spectroscopy-time of flight (SIMS-TOF) could give hints of the composition of the surfaces as explained by Baer.[278]

4.2.4 Direct metallisation of "*switch*SENSE"

4.2.4.1 Introduction to the technique

Molecular sensing is a branch of supramolecular analytical chemistry that exploits the classical host-guest chemistry to produce a spectroscopical signal able to detect the guest with high sensitivity (with single molecule detection being the ultimate objective). DNA sensing is a branch of molecular sensing that focuses on the detection of DNA binding events such as protein or small molecules. Numerous approaches to DNA electrochemical detection have been developed,

relying on direct or indirect electrochemistry, redox couples or charge transports.[279,280] However, current methods involve many development steps to prepare the sensor, the destruction of the sample and the non-reusability of the sensor.[279] The development of a new lab-on-a-chip sensor with simple techniques and reusability would enable the construction of large, multiplexed arrays.[279] Ulrich Rant and his group developed a novel DNA sensing technology called "*switch*SENSE". A short oligonucleotide strand is tethered onto a surface of gold. DNA can be easily modified at one end to bear groups (thiols) and grafting it onto the gold surface. Since DNA is a charged macromolecule, it is possible to electrically manipulate it using the electric field formed between the gold surface, acting as an electrode, and a Pt reference electrode.[281] The intrinsic molecular properties of DNA, such as molecular weight, size and charge can influence the behaviour of the strand. DNA, in fact, acts as a bio-electromechanical system.

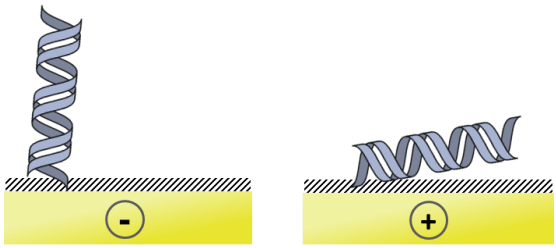

Figure 120: Schematic representation of a dsDNA bound on the surface of gold and the behaviour of DNA when the surface is charged positively or negatively.

When a negative potential is applied to the gold surface, the DNA is repelled and tends to orthogonally align itself on the gold surface. When a positive potential is applied, DNA is attracted to the surface (Figure 120) The technology has been

assessed first on gold electrodes in 2004 by Ulrich Rant and Shunsaku Takeishi.[282,283]

The system has consolidated potential as a biosensing platform for the detection of protein interactions and nucleic acids. When proteins binds to the DNA strands, an increase of the hydrodynamic drag is detectable as the switching behaviour slows down. This allows the determination of both DNA binding events and the size of the protein involved without any labelling of the analysed sample.[284]

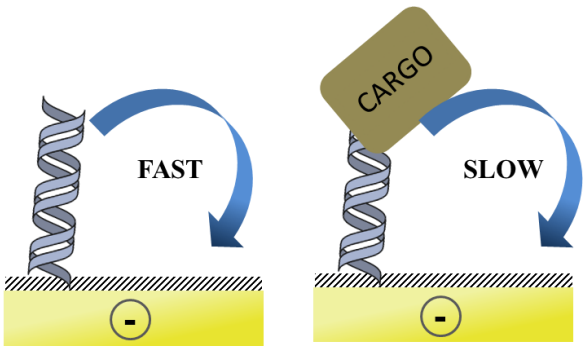

Figure 121: Schematic representation of the dynamics of the binding of a cargo molecule (protein, nanoparticle) onto the free end of the dsDNA, slowing down the switching behaviour.

More recently, this technology matured into a bio-electro-optical system. By loading the free end of the DNA with a fluorophore, fluorescence is detectable only when a negative charge is applied to the gold surface. When a positive charge is applied, fluorescence cannot happen as the excitation is dissipated non-radiatively by the gold surface.

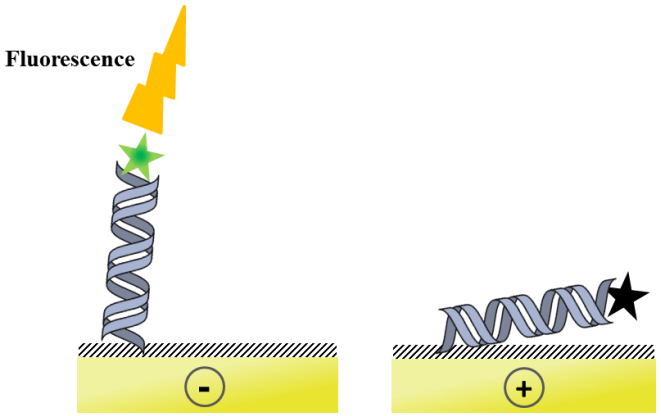

Figure 122: Schematic representation of a *"switch*SENSE" layer with a DNA-fluorophore conjugate. The fluorophore has detectable fluorescence only when the surface is negatively charged.

The sensitivity of the optical part of "*switch*SENSE" is directly proportional to the coefficient of extinction of the fluorophore used.

4.2.4.2 Proposal and rationale

Silver nanoparticles have the highest coefficient of extinction between metal nanoparticles and organic dyes.[146] A "*switch*SENSE" bio-sensor formed using a DNA probe end-modified with a AgNP would increase the optical detection limit of the system. However the preparation of mono-functionalised AgNPs is a considerable challenge as explained by Mirkin.[285] An alternative is to test whether a AgNP can be grown on the end of a sugar-modified DNA probe and determine whether these probes can be applied to "*switch*SENSE" biosensing applications. The successful metallisation of the free end of the dsDNA would directly validate the metallisation challenge as described in the aims of this chapter (paragraph 4.1.2).

4.2.4.3 Preparation of the sugar-modified DNA probes

The initial approach to the problem was the preparation of a sugar end-modified ssDNA that could be used for the "*switch*SENSE" platform. The silver nanoparticles, to be efficiently used with the "*switch*SENSE" technology should be relatively small of approximately 10 nm of diameter. Since the surface detection of the particles would rely on dark-field microscopy and fluorescence, AgNPs of this size are well suited as they possess both high scattering power and high fluorescence. Sugar **(16)** reliably afforded AgNPs of 6-10 nm diameter, and so it was chosen as a good candidate for DNA conjugation. The ssDNA required for "*switch*SENSE" technology must have particular properties too. In particular, linearity, non-self-complementarity of the sequence and avoidance of sequences forming loops are important for the successful operation of the DNA switching. A 48-mer ssDNA **(106)** of sequence 3' ATC AGC GTT CGA TGC TTC CGA CTA ATC AGC CAT ATC AGC TTA CGA CTA-alkyne was chosen for its propensity to not form secondary structure as tested by *OligoCalc* and *mfold* web DNA calculators.[286,287]

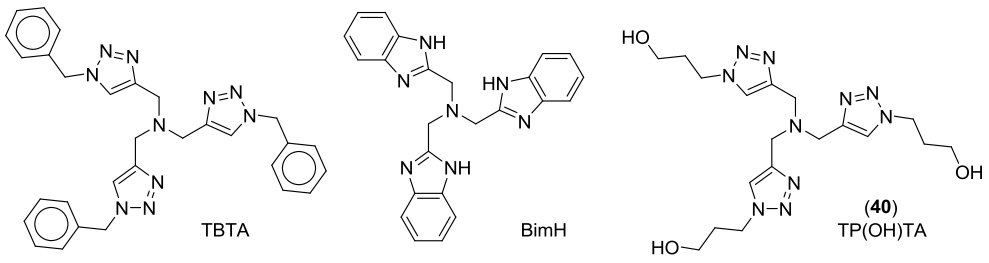

Scheme 33: Structure of click-chemistry ligands TBTA, BimH and TP(OH)TA (40)

The ssDNA **(106)** was prepared on a DNA synthesiser using commercially available phosphoramidites. Subsequently click-chemistry was conducted to link sugar azide **(16)** to the 5' end of the DNA.

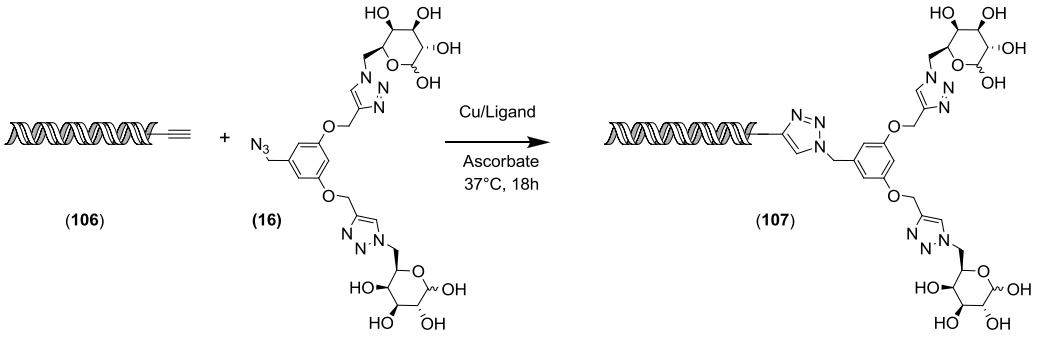

Scheme 34: Preparation of DNA-sugar (107)

Click-chemistry is a widely used technique to modify nucleic acids due to its high efficiency and bio-orthogonality.[288,289] However, the use of click-chemistry on oligonucleotides is not a straightforward process: DNA is known to be unstable in the presence of Cu^{2+} ions as by classical Fenton's reagent chemistry.[261] To prevent premature degradation, the copper must be kept complexed so that it will not damage the DNA. Ligands that were designed for enhanced catalytic activity, such as the widely used BimH and TBTA[290] can have a secondary role in preventing the copper to degrade the DNA (Scheme 33). However, commonly used ligands in click-chemistry are less useful when used with DNA, as they are highly hydrophobic and not soluble in water. TP(OH)TA[291] **(40)** a less known but water soluble click-chemistry ligand, closely related to the TBTA ligand, was chosen following El-Sagheer's indications.[289] The click-chemistry reaction was then designed and screened for copper source: $CuSO_4$, CuBr and Cu-triflate benzene complex. The efficiency of the click-chemistry is sometimes influenced

by factors like solvent polarity and copper source, so a screening was deemed necessary.[292]

Entry	Cu source	Ligand
1	$CuSO_4$	TBTA
2	$CuSO_4$	TP(OH)TA
3	CuBr	TBTA
4	CuBr	TP(OH)TA
5	CuOTf	TBTA
6	CuOTf	BimH
7	CuOTf	TP(OH)TA

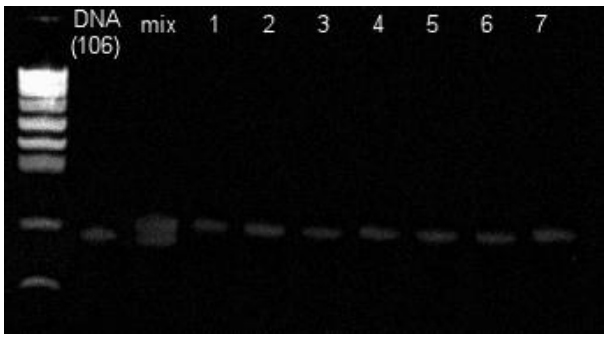

Table 12: Reaction conditions tested for the click-chemistry between ssDNA (106) and sugar (16) and gel electrophoresis of the reaction mixtures after 18h at 37°C.

For a complete conversion of the DNA strand 100 eq of the sugar azide **(16)** along 50 eq of Cu/Ligand **(40)** complex and 100 eq of sodium L-ascorbate were incubated at 37°C for 18 hours to afford sugar-DNA **(107)**. Sugar-DNA **(107)** was then purified by semi-preparative HPLC.

In conclusion, for the sugar-DNA **(107)** the source of Cu had no influence in the reaction outcome. It was necessary to prepare separately the copper-ligand system and then add the mixture to the DNA and sugar solution, implying that the reaction was kinetically driven by the formation of the catalytic copper-ligand system. This effect was particularly visible when CuBr was used, due to its low solubility in water.

4.2.4.4 Metallisation comparison of "*switch*SENSE"

Metallisation tests were conducted by Markus Shuster using the synthesised DNA-sugar **(107)**, commercially available DNA-Cy3 and the DNA 48-mer

without any modification. Unmodified DNA was used as a control reaction. Cy3 is known to be sensitive to oxidants, a property that is considered a nuisance during its use in microarrays.[293] However, this property can be exploited and Cy3 can effectively act as a reducing agent for mild oxidants (such as Tollens' reagent), as well as being a fluorophore with a high extinction coefficient. These properties make DNA-Cy3 a good candidate for its comparison with DNA-sugar **(107)** in metallisation tests. The gold surface was first treated with the commercially available complementary 48-mer strand modified with a thiol group dissolved in 10 mM Tris buffer. Concentration was adjusted as previously reported to have evenly spaced DNA strands.[281] The gold surface was then passivated with mercaptohexanol (MCH) by formation of a mixed DNA/MCH monolayer. Specific portions of the surface were then hybridized with DNA **(107)**, DNA-Cy3 and the DNA 48-mer. For the hybridisation, the surface was exposed to an excess of the ssDNA strands in a buffer of 1M NaCl and 10 mM Tris at room temperature for 2 hours.[281] The surface was then washed with a modified Tris buffer containing 100 mM $NaNO_3$ instead of NaCl, due to the incompatibility of Cl^- ions with the Tollens' reagent as AgCl, that would form, is not soluble in water. 1 mM Tollens' reagent was then flushed onto the surface for 30 minutes. Detection of the particles was done on an optical bench fitted with a dark-field microscope. Since silver nanoparticles have very large light scattering intensity, they are easily detected as bright spots on the dark background. The colour of the spots also gives an indication of the diameter of the particles, since the wavelength dependent scattering angle is highly influenced by the size of the

silver particle. As a comparison, unmodified DNA and Cy3-DNA were used in parallel metallisations.

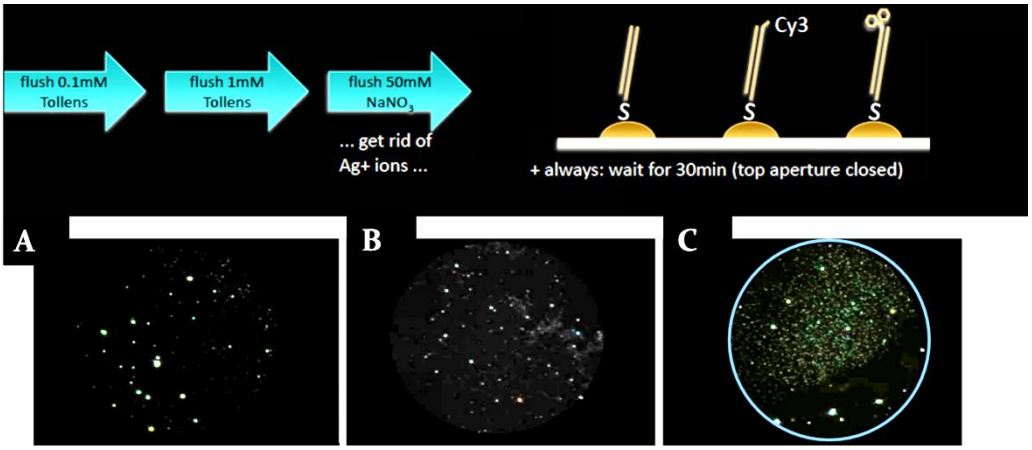

Figure 123: Schematic representation of the metallisation process of a *"switch*SENSE" DNA surface. A. Dark-field image of metallised unmodified DNA B. Dark-field image of metallised Cy3-DNA C. Dark-field image of metallised Sugar-DNA (107)

As shown by Figure 123-C, Sugar-DNA **(107)** formed a uniformly distributed, high density and even sized AgNPs over the gold surface. In contrast, Cy3-DNA (Figure 123-B) did not have an appreciable contribution to the formation of nanoparticles compared to DNA only (Figure 123-A). The faint and uniform blue colour of the particles indicated that they were approximately monodisperse and of the same size. It is known that polydisperse samples of silver nanoparticles appear multi-coloured under a dark-field microscope.[294]

In conclusion, the technology of the sugars developed in Chapter 2, when applied to "*switch*SENSE", showed a high degree of control in the formation of the AgNPs, and it's a promising candidate for the direct metallisation and growth of a AgNP-DNA bio-sensor.

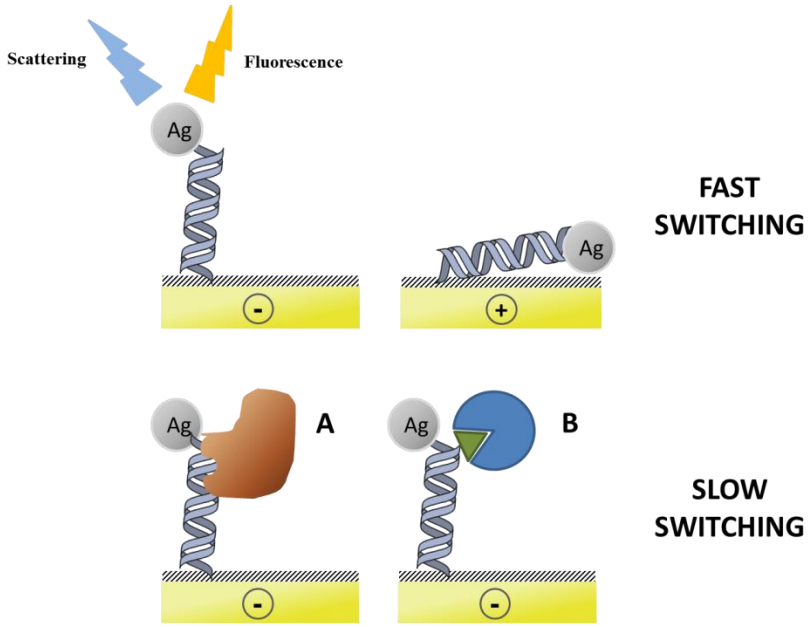

Figure 124: Schematic representation of a "*switch*SENSE" layer with a DNA-AgNP conjugate. The AgNPs have detectable scattering and fluorescence only when the surface is negatively charged. A. Detection of a direct DNA-binding protein B. Detection of an antigen-binding protein by using antigen-DNA conjugates.

The high fluorescence of silver nanoparticles would allow the direct single event detection of a switching DNA and consequently the detection of binding molecules with two modalities: 1) detection of DNA binding proteins and 2) detection of antigen binding proteins (for antigen DNA bio-sensors). In conclusion, the metallisation of the "*switch*SENSE" technology was a viable proof of concept of surface-anchored DNA metallisation. The development of AgNPs "*switch*SENSE" technology would improve the single-molecule detection sensitivity compared to any fluorophores.

4.2.5 Plasmid DNA metallisation

The metallisation of free-floating dsDNA, such as a plasmid, would provide additional data to determine the behaviour of the Tollens' reaction. In solution, the 3D environment provides an additional challenge, as the newly formed nanoparticles are free to interact with multiple plasmids.

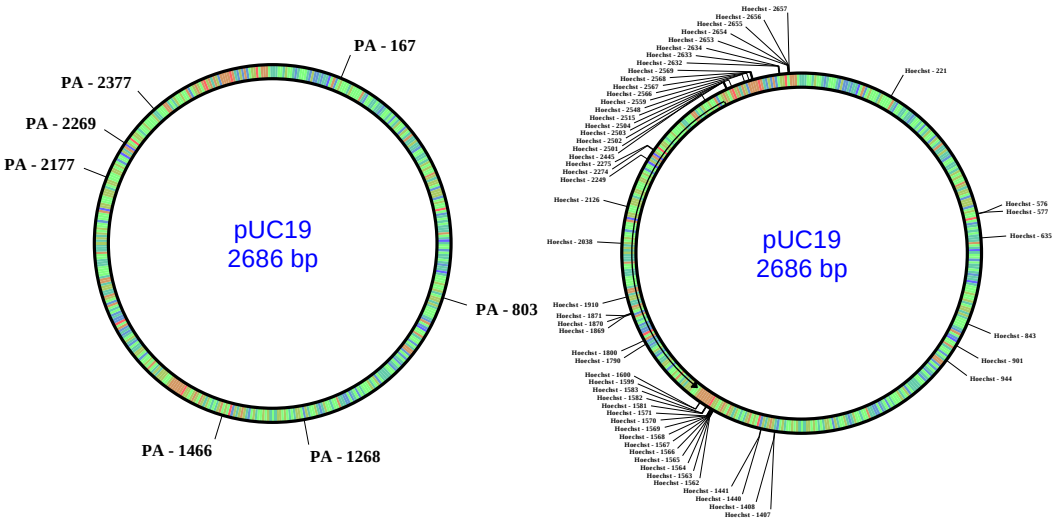

Figure 125: Analysis of the binding sites of pUC19 conducted with pDRAW32 for polyamide (109, left, label PA marks PA binding sequence WGWWCW where W=A/T) and Hoechst 33258 (right, label Hoechst marks binding sequences WWWWWW where W=A/T).

This complex environment is usually avoided by conducting the metallisation directly over TEM grids[295] or mica surfaces[296] of the AFM, thus circumventing undesirable supramolecular aggregations. Plasmid pUC19 was chosen as the template for the selective metallisation of DNA through the use of minor groove binders Py-Im polyamide **(109)** and Hoechst 33258. pUC19 is a 2686 bp plasmid cloning vector created by Messing.[297] It's widely available and used in biological experiments. The sequence of the plasmid was analysed with the software

pDRAW32[298] to find all the potential binding sites of polyamide **(109)** and Hoechst 33258.

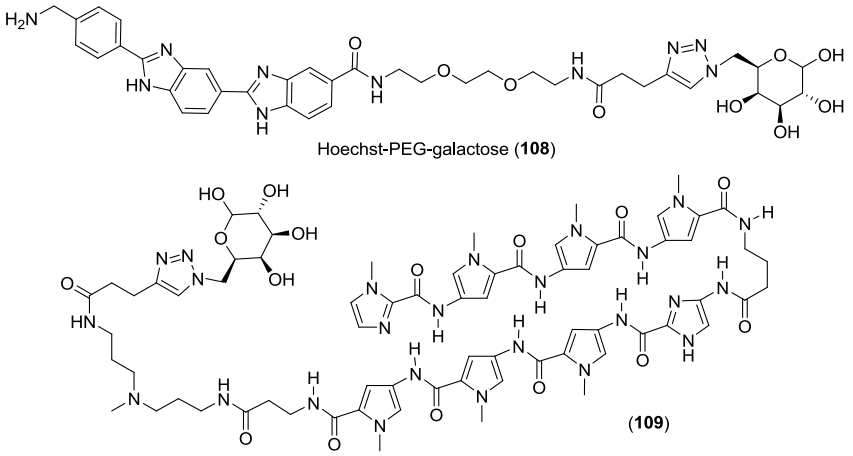

Scheme 35: Structures of Hoechst-PEG-galactose (108) and polyamide-sugar (109).

Polyamide **(109)** returned 7 potential binding sites of sequence 5'-WGWWCW in plasmid pUC19 (where W stands for A/T). Hoechst 33258 returned 57 potential binding sites of sequence 5'-WWWWWW (binding equilibrium constant is ~$3x10^5$ M^{-1})[299]. The discovered loci mark the metallisation pattern of these two molecules and would help in their analysis. In particular, the limited binding sites for polyamide **(109)** would return restricted metallisation areas, while the Hoechst 33258 would probably show extended metallisation of the whole plasmid. For these reasons, plasmid pUC19 was identified as an ideal candidate for DNA metallisation.

4.2.5.1 Preparation of polyamide-sugar (109) and metallisation with Tollens'

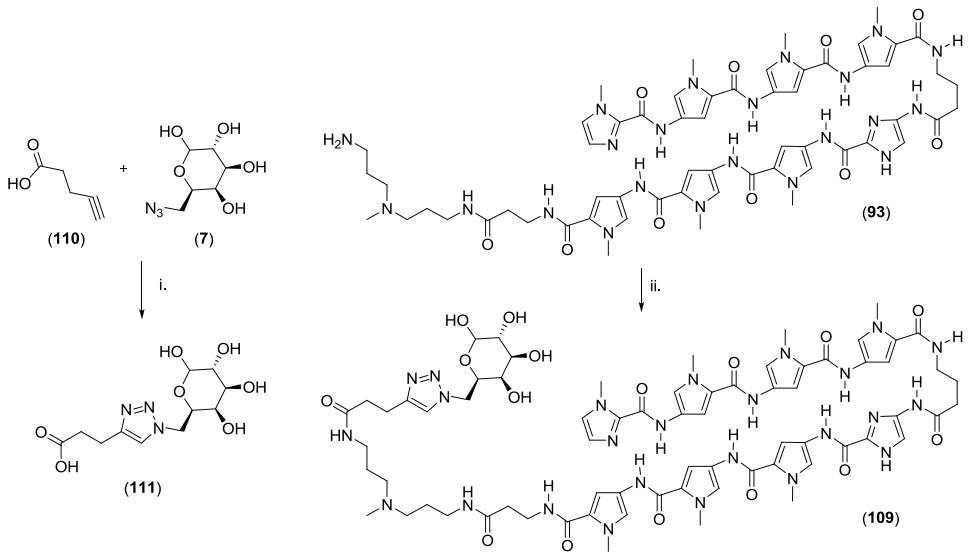

Scheme 36: Preparation of compound (109) i. $CuSO_4$, ascorbate, r.t., 18h ii. (111), HCTU, DMF/DIEA, 18h, 16%

Sugar azide **(7)** was reacted with pent-4-ynoic acid **(110)** in the presence of $CuSO_4$ and sodium L-ascorbate at room temperature overnight to afford sugar-acid **(111)**. Polyamide sugar **(109)** was prepared by HCTU coupling between sugar acid **(111)** and polyamide **(93)** in DMF/DIEA overnight with 16% yield. It was subsequently dissolved in 100 uL of water to prepare a stock solution at 6 ug/uL (ε_{310nm} = 69200 $M^{-1}cm^{-1}$, 4.728 mM). Two metallisation buffers were prepared as based on the results of paragraph 4.2.3.

Buffer A: 0.5xTBE, 0.02% SDS and 78.5 mM $NaNO_3$.

Buffer B: 0.5xTBE, 0.02% SDS.

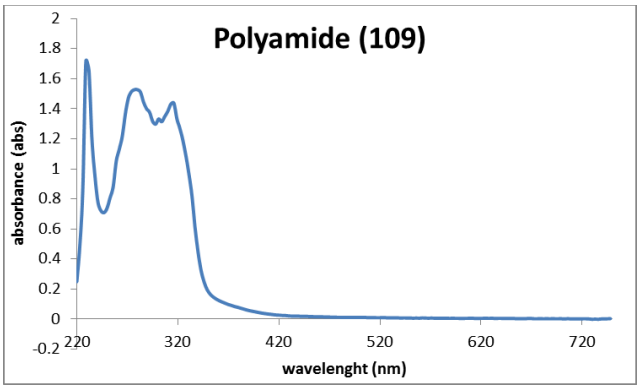

Figure 126: UV-Vis trace of polyamide (109).

The buffers have been planned to prevent both the nanoparticles to aggregate and the DNA from denaturing (TBE buffer is a widely used buffer in DNA nanotechnology;[242] sodium ions, usually as NaCl are used to counter balance the negative charge of DNA; $NaNO_3$ is here used as Cl^- ions are not compatible with Tollens' reagent; SDS is a widely used surfactant for the preservation of nanoparticles[300,301]). A high concentration Tollens' reagent stock solution at 374 mM was prepared for the metallisation tests, thus allowing the use of very small volumes. Plasmid pUC19 was used from the commercial 20 ng/uL (~10.54 nM) solution without further dilutions. An array summarised in Table 13 was designed to determine the dilution that the reaction mixture could sustain, allowing the formation of nanoparticles and reducing at the minimum the denaturation or the formation of silver mirrors. The reagents were mixed and allowed to stand in the dark for 24 hours at room temperature. Sample 12 showed the highest formation of particles by UV-Vis, however the peak at 260 nm of the DNA showed degradation.

Sample	Polyamide Sugar **(109)**	Tollens' reagent	Buffers	Plasmid	Comments
1	1 uL galactose	2 uL	-	-	Positive control
2	-	2 uL	2 uL	-	Negative control
3	2 uL	2 uL	-	-	Positive control
4	2 uL	2 uL	2 uL A	-	
5	2 uL	2 uL	4 uL A	-	
6	2 uL	2 uL	8 uL A	-	Buffer
7	2 uL	2 uL	16 uL A	-	optimisation
8	2 uL	2 uL	4 uL B	-	controls
9	2 uL	2 uL	8 uL B	-	
10	2 uL	2 uL	16 uL B	-	
11	2 uL	2 uL	4 uL H_2O	1 uL	Metallisation
12	2 uL	4 uL	-	1 uL	Metallisation
13	2 uL	2 uL	4 uL A	1 uL	Metallisation
14	2 uL	2 uL	4 uL B	1 uL	Metallisation

Table 13: optimisation of the reaction conditions and metallisation tests conducted with pUC19 and polyamide (109).

Sample 13 and 14 showed reduced formation of particles, but with better preservation of the DNA as shown by Figure 127.

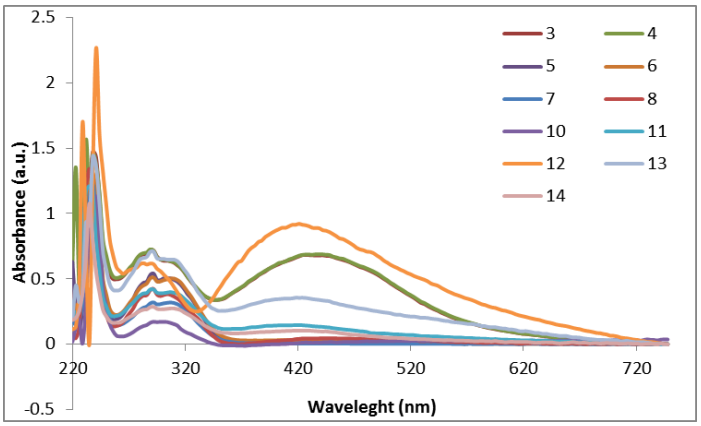

Figure 127: UV-Vis traces of the samples shown in Table 13. The samples showed a variable formation of AgNPs as denoted by the intensity of resonance plasmon peak ~420 nm and a variable stability of the DNA as showed by the reduction in intensity of peak at ~260nm.

Sample 13 was then analysed by TEM, pictures showed dense bundles with a high concentration of silver particles and a lower visible amount of DNA. The shapes of these bundles were mostly irregular; however hexagonal plates of 500 nm diameter were identified.

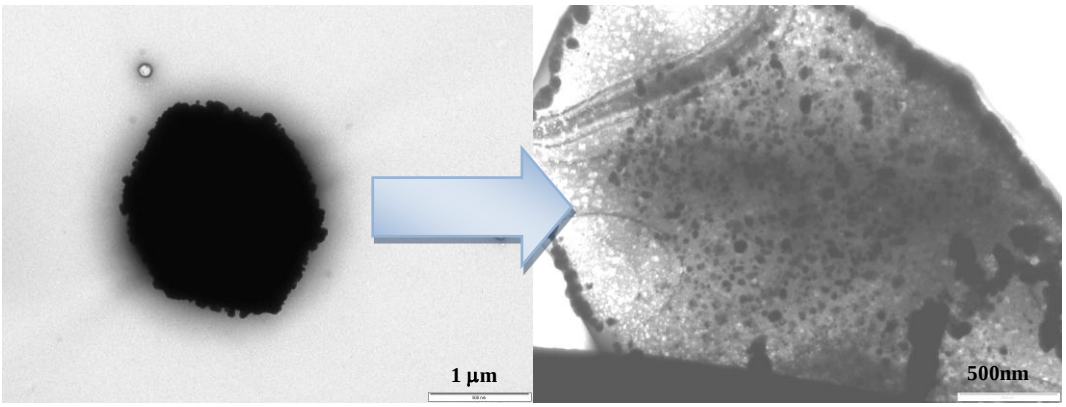

Figure 128: TEM images of sample 13 showing aggregated silver nanoparticles as hexagonal hollow plates.

The plates were initially considered as densely packed silver nanoparticles, however with greater magnification and by refocusing the beam contrast it was revealed that the bundles contained cavities and filamentous structures that can be attributed to a DNA templated formation. The similar formation of hollow DNA templated shells was also discovered by Dai-Wen Pang and co-workers by using charged CTAB quantum-dots and lambda DNA.[302]

Sample 14 was then analysed by TEM. In contrast to sample 13, no large aggregated nanoparticle formations were detected and DNA was much better preserved. Since the difference between the two samples consisted only in the presence of $NaNO_3$ as a buffer component, it was suggested that this was the cause of the large aggregations of sample 13. The AgNPs formed in sample 14 were in the range of 9.5-32 nm, forming small clusters. However, some of them

showed proximity to the DNA, suggesting binding events were taking place (Figure 129).

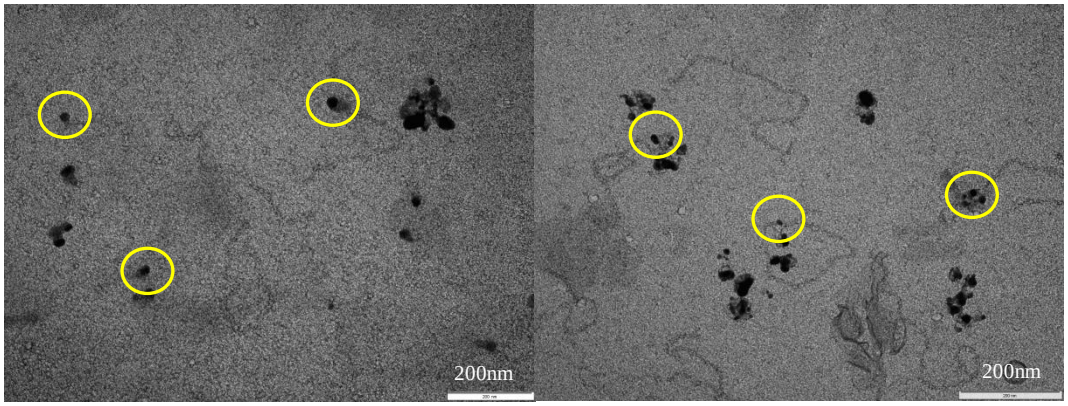

Figure 129: TEM images of sample 14, showing better preservation of DNA than sample 13. Highlighted with yellow circles are possible binding events of AgNPs to DNA.

In conclusion, a simple protocol was developed to metallised DNA consisting in mixing the polyamide sugar **(109)**, the DNA and the Tollens' reagent at room temperature for 24h.

4.2.5.2 Metallisation of pUC19 using Hoechst-PEG-galactose (108)

Hoechst-PEG-galactose **(108)** was prepared by Glenn Burley for DNA metallisation (synthesis is reported in the Appendix).

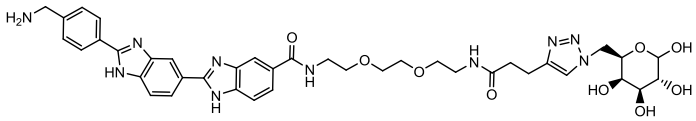

Scheme 37: Structure of Hoechst-PEG-galactose (108).

The Hoechst-PEG-galactose **(108)** was dissolved in water at the concentration of 4.7 mM. Buffer A, Tollens' reagent and plasmid were prepared as described earlier in this chapter (paragraph 4.2.5.1). 2 uL of Hoechst-PEG-galactose **(108)**, 2

uL of Tollens' reagent, 4 uL of Buffer A and 1 uL of plasmid were mixed and allowed to stand for 24 hours at room temperature. Metallisation was visually confirmed by the formation of a yellow solution and by UV-Vis measurements (Figure 130).

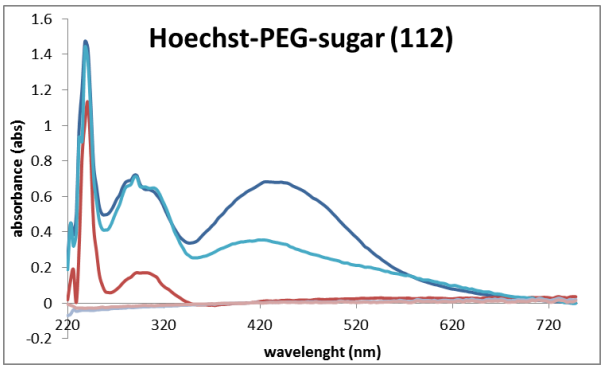

Figure 130: Hoechst-PEG-galactose (108) metallisation with Tollens' reagent in the presence of DNA.

Considering the large number of loci in pUC19 plasmid that can bind the Hoechst, it was expected that a metallisation attempt would mostly coat the DNA and form silver nanowires. Analysis of the samples by TEM showed instead the formation of ~40 nm diameter AgNPs that were surrounded by DNA. Fragmentation of the plasmids was also visible. The particular DNA bundling around the AgNPs (Figure 131) could have formed by the early assembling of silver nano-clusters to form larger nanoparticles; this behaviour would have pulled multiple plasmids and multiple loops of the same plasmid together in close proximity forming a *"spaghetti with meatballs"* appearance.

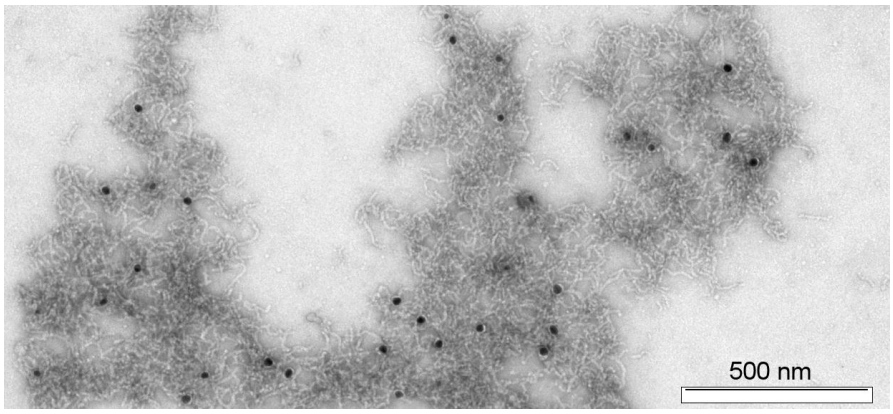

Figure 131: TEM image of metallisation of DNA conducted with Hoechst-PEG-galactose (108) and Tollens' reagent showing DNA bundling around the nanoparticles.

Such an encapsulation effect has not been seen before by metal particles and DNA. A less dramatic but similar binding behaviour has been seen by Ross Inman with gold labelled antibodies and Z-DNA plasmids.[303] Such technology would become Immunogold™ commercial labelling kits.

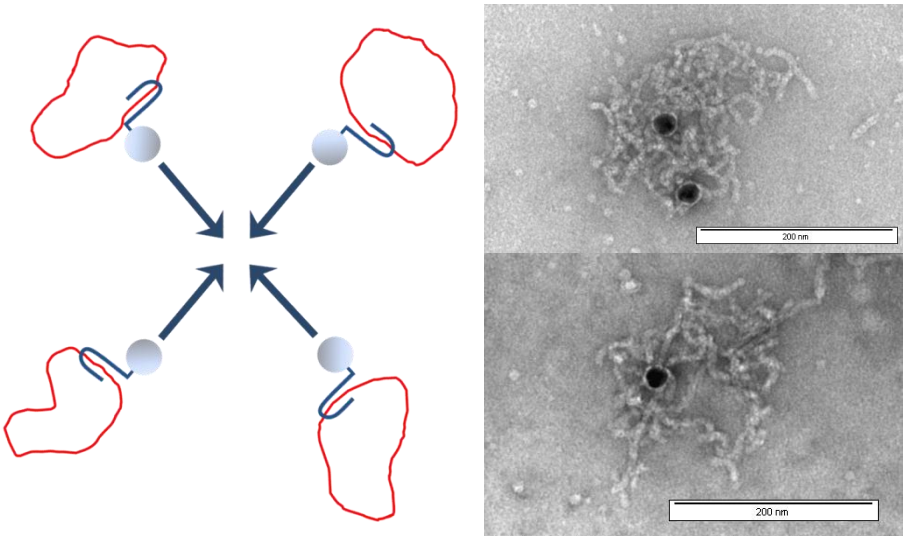

Figure 132: Schematic representation of the possible mechanism for the formation of DNA bundles around AgNP@(108) by condensation of small silver nanoclusters during early metallisation. On the right TEM images of AgNP@(108) clearly showing multiple loops of the DNA around a single nanoparticle.

This hypothesis was supported by the analysis of short DNA fragments. Isolated fragments showed binding of a single AgNP to the DNA (Figure 133). This behaviour was only possible if the Hoechst-PEG-galactose **(108)** tethered the DNA to the AgNP.

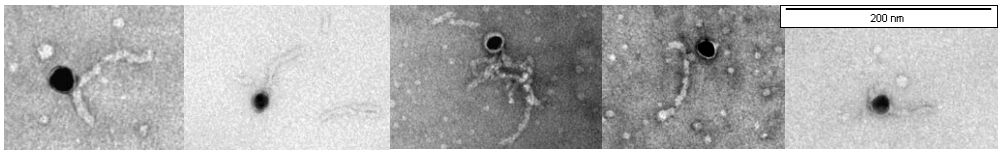

Figure 133: Selected TEM images showing fragmented DNA binding to a single AgNP@(108), supporting evidence of direct tethering of AgNP@(108) to the DNA fragment.

Lastly, no formation of silver nanowires was observed. This could be explained by the repulsion of the negative charges between the DNA and the negative zeta-potential that AgNPs have when prepared with Tollens' reagent.[100]

In conclusion, compound **(108)** successfully metallised DNA in a novel and unique pattern. The protocol used was simple and consisted in premixing the DNA, the metallisation compound **(108)** and finally the Tollens' reagent in solution in buffered water for 24 hours at room temperature, without the need of inert atmosphere.

4.3 Conclusions and Future directions

Templated DNA metallisation by using tethered sugar-DNA binders was accomplished. Results were promising: AgNPs formed with the Tollens' reagent were of small size between 6-10 nm. The DNA-binders were identified on the surface of the AgNPs and were able to bind dsDNA. A novel protocol of dsDNA metallisation in solution was developed. The inherent simplicity of the protocol

allowed fast templated metallisation of DNA. The irregular shapes and bundling of the DNA around the AgNPs hinted to the mechanism of growth. However, further understanding of AgNP process is necessary to improve the usefulness of the technique and to understand the mechanism of particle growth in the presence of polyamides and DNA. Predictable, controlled and templated metallisation would enable the creation of nanoelectronic circuits and bio-sensors with unprecedented speed and precision. The potential implications of self-assembling templated metallisation in solutions would enable the development of patterned metallised circuits controlled by DNA-programmed assembly.

4.4 Experimental

Melting temperature analysis was performed on a PerkinElmer Lambda 35 UV/Vis spectrophotometer equipped with a thermo-controlled cell holder possessing a cell path length of 1 cm. A degassed aqueous solution of 10 mM sodium cacodylate, 10 mM KCl, 10 mM $MgCl_2$, and 5 mM $CaCl_2$ at pH 7.0 was used as the analysis buffer.[162] The corresponding DNA duplex and polyamides were mixed with 1:1 stoichiometry to a final concentration of 1 μM for each experiment. Prior to analysis, samples were heated to 90 °C, and cooled to a starting temperature of 25 °C with a heating rate of 5 °C/min for each ramp. Denature profiles (Figure 105 and Figure 106) were recorded at $\lambda = 260$ nm from 40 to 85 °C. The reported melting temperatures were defined as the maximum of the first derivative of the denature profile.

Sequence of DNA **(98)**: 5'-CGATGTTCAAGC-3' ε = 127390 $M^{-1}cm^{-1}$ and complementary strand 3'-GCTACAAGTTCG-5', no mismatches, ε = 131140 $M^{-1}cm^{-1}$

Compound	T_m (°C)	ΔT_m (°C)
DNA **(98)**	49.5	-
(98) + **(93)**	64.5	15.0

Table 14: Melting temperatures of DNA (98) duplex in the absence and presence of polyamide (93)

Melting temperature analysis of the stability of DNA **(98)** in the presence of Ag^+ was conducted by equilibrating the samples at 25 °C then heated with a heating rate of 5 °C/min for each ramp (inverse ramp).

ssDNA **(106)** 48-mer of sequence 3'-ATC AGC GTT CGA TGC TTC CGA CTA ATC AGC CAT ATC AGC TTA CGA CTA-alkyne was prepared on a DNA synthesiser using commercially available phosphoramidites. MALDI-TOF *m/z*: $[M]^+$ calc. for 13A (MW 251.10), 14C (MW 227.09), 8G (MW 267.24), 13T (MW 242.23), 1alkyne (MW 98.14) 14802.52; found 14808.81

AgNP were prepared by mixing in a low-binding 1.5 mL Eppendorf tube 1 μL of 374 mM Tollens' reagent with 1 μL of 10.54 μM pUC19 plasmid, 1 μL of compound **(108)** or **(109)** 102 μM stock solutions and finally buffer to reach a final volume of 10 μL as explained in Table 13. The samples were then left

reacting at room temperature for 24h then stored at 4ºC before being imaged by TEM. Samples were diluted 1/100 before loading on TEM grids.

TEM grids were custom-made PIOLOFORM™ copper grids coated with carbon and treated with Ar-plasma for 2 seconds prior use. The crude samples were loaded onto the grid with a single 5 μL drop and left absorbing for 5 minutes then dried with filter paper, rinsed with 3x5 μL of deionised water. Samples containing DNA were also stained with 2μL uranyl acetate solution 0.2% for 20 seconds, then dried with filter paper.

For the gold nanoparticles stability tests of paragraph 4.2.2 stock solutions were prepared as following:

Solution A. 50 mM $HAuCl_4$ and 50 mM HCl

Solution B. A 50 mM $NaBH_4$ and 50 mM NaOH

Solution C. sodium citrate 50 mM

Solution D. 1 mM compound **(102)**

Solution E. 1 mM compound **(99)**

100 μL of solution A was diluted in a glass vial with 10 ml of water, solution D or E was added in variable amounts to the desired concentration to be tested, and then 50 μL of solution C was added while the solution was strongly vortexed, followed by 166 μL of solution B. AuNPs develops in less than 30 seconds during vortexing.

15nm BSPP phosphine coated AuNPs were prepared with the following recipe:[232] 10 mL of citrate coated commercially available (Sigma-Aldrich) AuNPs (~$6.0x10^{12}$ particles/mL) were mixed with 6mg of BSPP and incubated for 18 hours. Solid NaCl was added in small portions to the solutions until it turns purple. The sample was centrifuged for 10 minutes 13 krpm and the surnatant was removed. 200 μL of 2.5 mM BSPP solution in water was added and the sample was vortexed for 1 minute. 200 μL of MeOH was added and the sample was centrifuged for 10 minutes 13 krpm. After removal of the surnatant, the sample was finally re-suspended in 200 μL of 2.5 mM BSPP solution.

TBE 5X buffer was prepared accordingly to the following protocol: 54 g of Tris base, 27.5 g of boric acid, 20 ml of 0.5 M EDTA, then diluted 10 times (TBE 0.5x) for metallisation tests. Metallisation buffer was prepared by mixing solid $NaNO_3$ and sodium dodecylsulphate in 0.5x TBE buffer to reach the final concentration of 78.5 mM $NaNO_3$ and 0.02% SDS.

Semi-preparative HPLC purification of the sugars was conducted by reverse phase HPLC as explained in the experimental of Chapter 2 and purification of the PAs was conducted by reverse phase HPLC as explained in the experimental of Chapter 3

For Hoechst-PEG-galactose **(108)** see Appendix for spectroscopic data and synthetic scheme.

Gel electrophoresis was conducted using Hoefer mini 18x8 cm 10% acrylate gels prepared with the following recipe (sufficient for 2 gels): 4.0 mL of acrylate 30%, 5.6 mL H_2O, 2.4 mL TBE 5x, 200 μL Ammonium persulfate 10%, 10 μL TEMED. Samples were loaded using a 50% solution in glycerol and bromophenol blue as loading dye. Ladder shown in figures is commercially available 10 bp ladder. Gels were run in constant voltage mode using 120 V (15 V/cm), 400 mA for 60 minutes then stained using SYBR-GOLD®.

4.4.1 Synthesis of sugar-polyamide conjugates

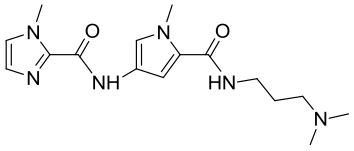

Synthesis of Boc-Im-py-ODp (102). To a solution of Boc-py-OH **(45)** (0.05 g, 0.208 mmol) in DMF (2 mL) was added HATU (0.078 g, 0.208 mmol) and DIPEA (0.107 g, 0.833 mmol). After 5 minutes under stirring, di-methylaminopropylamine **(55)** (0.0212 g, 0.208 mmol) was added and the solution stirred under nitrogen for 2 hours. HCl 1M (5 mL) was added to quench the reaction. The solid formed was centrifuged, washed with Et_2O and dried to afford Boc-py-ODp **(100)** (0.043 g, 64% yield) as a yellow glue. To a solution of Boc-py-Dp **(100)** (0.043 g, 0.208 mmol) in water (1 mL) was added TFA (2 mL). The mixture was heated at 35°C for 6 hours and the reaction monitored by TLC. The mixture was cooled, concentrated to a residue, diluted with water (5 mL) and lyophilised to afford **(101)** (0.039 g, 97% yield) as a yellow glue. To a solution of Im-OH **(52)** (0.023 g, 0.096 mmol) in DMF (2 mL) was added HATU (0.036 g,

0.096 mmol) and DIPEA (0.54 g, 0.417 mmol). After 5 minutes under stirring, NH_2-Py-Dp **(101)** (0.022 g, 0.096 mmol) was added and the solution was stirred under nitrogen for 2 hours. HCl 1M (3 mL) was added to quench the reaction. The precipitate was centrifuged, washed with Et_2O, re-dissolved water and purified by semi-preparative HPLC to afford **(102)** (0.007 g, 22% yield) as a pale yellow powder. UPLC-TOF (ESI) *m/z:* $[M+H]^+$ calc. for $C_{16}H_{25}N_6O_2$ 333.2034, found 333.2044; ^{1}H-NMR (400 MHz, DMSO-d_6) δ 10.42 (s, 1H), 8.18 (t, *J* = 5.8 Hz, 1H), 7.35 - 7.46 (m, 1H), 7.25 (d, *J* = 1.6 Hz, 1H), 7.07 - 7.09 (m, 1H), 7.02 (d, *J* = 1.6 Hz, 1H), 3.99 (s, 3H), 3.82 (br. s., 3H), 3.22 - 3.29 (m, 2H), 3.08 (br. s., 2H), 2.71 - 2.85 (m, 6H), 1.81 - 1.90 (m, 2H); ^{13}C-NMR (100 MHz, DMSO-d_6) δ 161.5, 158.2, 155.7, 138.6, 126.5, 126.3, 122.8, 121.3, 118.3, 104.6, 54.8, 42.2, 36.0, 35.5, 35.1, 24.6

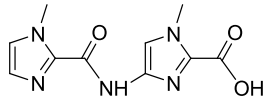

Synthesis of Im-Im-OH (67). To a solution of Im-OH **(52)** (1.000 g, 7.936 mmol) in DMF (25 mL) was added EDC (1.640 g, 7.936 mmol) and HOBt (1.071 g, 7.936 mmol). After 1 hour under stirring, NH_2-Im-OEt **(89)** (2.247 g, 7.936 mmol) was added followed by DIEA (2.047 g, 15.872 mmol) and the solution was stirred under nitrogen for 2 hours. The mixture was diluted with HCl (150mL), resulting in the precipitation of a heavy solid. The supernatant was decanted. The solid was washed with water (100 mL) then dissolved in MeOH (50 mL) and LiOH 1M (50 mL) and stirred at room temperature for 2 hours. The mixture was then acidified with HCl to pH 3, extracted with ethyl acetate (3x100 mL), and the combined organic layers were

dried over $MgSO_4$ and concentrated to residue. Lastly the residue was suspended in water (10 mL) and lyophilised to afford **(67)** (1.067 g, 54% yield) as a yellow powder. UPLC-TOF (ESI) *m/z:* $[M+H]^+$ calc. for $C_{10}H_{12}N_5O_3$ 250.0935, found 250.0944; ^{1}H-NMR (400MHz , DMSO-d_6) δ 10.37 (s, 1H), 7.65 (s, 1H), 7.45 (d, 1H), 7.07 (s, 1H), 3.99 (s, 3H), 3.94 (s, 3H); ^{13}C-NMR (100MHz , DMSO-d_6) δ 159.7, 156.0, 137.8, 135.8, 132.7, 127.5, 127.0, 114.8, 35.1, 33.6

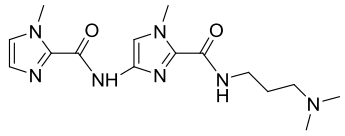

Synthesis of Im-Im-Dp (99). To a solution of Im-Im-OH **(67)** (0.050 g, 0.200 mmol) in DMF (5 mL) was added HATU (0.070 g, 0.200 mmol) and DIPEA (0.107 g, 0.833 mmol). After 15 minutes under stirring, di-methylaminopropylamine **(55)** (0.020 g, 0.200 mmol) was added and the solution was stirred under nitrogen for a further 3 hours. HCl 1M (10 mL) was added to quench the reaction. The solid formed was centrifuged, washed with Et_2O, re-dissolved in DMSO (2 mL) and purified by semi-preparative HPLC to afford **(99)** (0.0178 g, 26% yield) as a white powder. UPLC-TOF (ESI) *m/z:* $[M+H]^+$ calc. for $C_{15}H_{24}N_7O_2$ 334.1986, found 334.2000; ^{1}H NMR (400 MHz, DMSO-d_6) δ 10.82 - 11.00 (m, 1H), 9.84 (s, 1H), 8.48 (t, J = 6.1 Hz, 1H), 7.42 - 7.57 (m, 2H), 4.00 (s, 3H), 3.96 (s, 3H), 3.30 (q, J = 6.5 Hz, 2H), 2.96 - 3.12 (m, 2H), 2.71 (d, J = 4.7 Hz, 6H), 1.84 - 2.01 (m, 2H); ^{13}C-NMR (100 MHz, DMSO-d_6) δ 158.7, 155.5, 150.9, 137.6, 134.5, 134.2, 127.1, 127.0, 113.9, 54.3, 41.8, 35.7, 35.2, 35.1, 24.1

4.4.2 Synthesis of biotin conjugated sugars

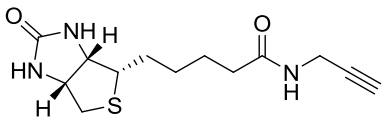

Synthesis of biotin-alkyne (103).[272,304,305] To a stirred solution of biotin-NHS (0.100 g, 0.29498 mmol) in DMF (6.6 mL) were added propargyl-amine (0.0167 g, 0.304 mmol, 21 uL) and TEA (0.141 g, 1.39 mmol, 193 uL) dropwise under an atmosphere of nitrogen. The mixture was then stirred overnight at r.t. then concentrated *in vacuo* and diethyl ether (50 mL) was added; after 5 minutes of sonication a solid crashed out, filtered, washed with diethyl ether (2 x 5 mL) and dried to afford biotin-alkyne **(103)** (0.0551 g, 47% yield) as a white powder. UPLC-TOF (ESI) *m/z*: [M^+] calc. for $C_{13}H_{19}N_3O_2S$ 281.1198, found 281.1191; ^{1}H-NMR (400 MHz, DMSO-d_6) δ 8.21 (bs, 1H), 6.42 (s, 1H), 6.35 (s, 1H), 4.28 (t, *J* = 6.4 Hz, 1H), 4.10 (q, *J* = 3.2 Hz, 1H) 3.81 (d, *J* = 2.4 Hz, 2H), 3.06 (m, 1H), 2.80 (dd, *J* = 4.8, 12.4 Hz, 1H), 2.55 (d, *J* = 12.4 Hz, 1H), 2.06 (t, *J* = 7.2 Hz, 2H), 1.59-1.24 (m, 6H); ^{13}C-NMR (100 MHz, DMSO-d_6) δ 172.5, 163.4, 82.0, 73.5, 61.7, 59.9, 56.1, 40.5, 28.8, 28.7, 28.3

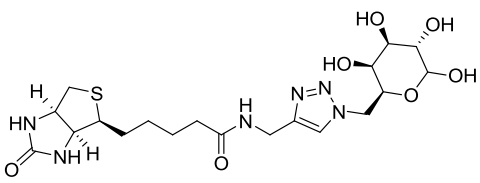

Synthesis of biotin-sugar (104). To a stirred solution of biotin-alkyne **(103)** (0.020 g, 0.0712 mmol) in DMSO (1 mL) were added 1,2,3,4-hydroxy-6-azido-galactopyranose **(7)** (0.0203 g, 0.0712 mmol) and PS-NHC-Cu(I) **(42)** 1.49 mmol/g (0.052 g, 0.07832 mmol) under a nitrogen atmosphere. The mixture was stirred at r.t. overnight, filtered and purified by semi-preparative HPLC. Biotin-sugar **(104)** was obtained (0.0091 g,

26% yield) as a white powder. UPLC-TOF (ESI) *m/z:* $[M+H]^+$ calc. for $C_{19}H_{31}N_6O_7S$ 487.1969, found 487.1981; ^{1}H-NMR (400 MHz, D_2O, mixture of 2 diastereoisomers) δ 8.35 - 8.48 (m, 1H), 7.83 - 7.92 (m, 1H), 5.14 (d, *J* = 1.0 Hz, 1H), 4.91 - 4.96 (m, 1H), 4.29 - 4.47 (m, 5H), 3.97 - 4.04 (m, 1H), 3.91 - 3.94 (m, 1H), 3.83 - 3.88 (m, 1H), 3.73 - 3.81 (m, 1H), 3.40 - 3.63 (m, 2H), 3.17 - 3.30 (m, 1H), 2.88 - 2.98 (m, 1H), 2.64 - 2.77 (m, 1H), 2.19 - 2.30 (m, 1H), 1.44 - 1.71 (m, 3H), 1.22 - 1.37 (m, 1H), 1.07 - 1.17 (m, 1H); ^{13}C-NMR (125 MHz, D_2O, mixture of 2 diastereoisomers) δ 176.9, 165.4, 124.7, 96.5, 92.4, 72.7, 71.8, 69.5, 69.1, 69.0, 68.8, 68.3, 62.1, 60.4, 55.4, 55.3, 50.9, 50.8, 39.7, 35.3, 34.4, 27.7, 27.6, 25.0

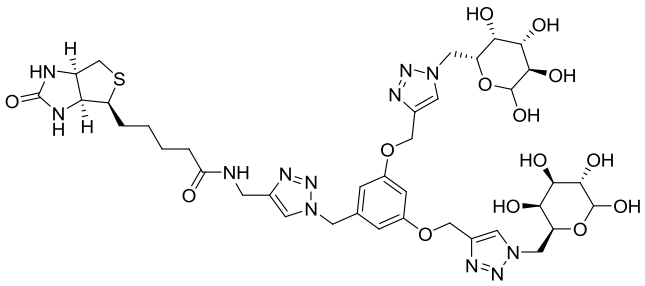

Synthesis of biotin-sugar2 (105). To a stirred solution of biotin-alkyne **(103)** (0.020 g, 0.0712 mmol) in DMSO (1 mL) were added SG1-N3 **(15)** (0.046 g, 0.0712 mmol) and PS-NHC-Cu(I) **(42)** 1.49 mmol/g (0.052 g, 0.07832 mmol) under a nitrogen atmosphere. The mixture was stirred at r.t. overnight, filtered and partitioned between water (10 mL) and ethyl acetate (10 mL). The organic phase was concentrated to obtain a crude residue (0.165 g). UPLC-TOF: m/z obs. 1093.47 $[M+H]^+$. The residue was then dissolved in water (5 mL) and TFA (5 mL) and heated at 80°C for 2 hours. The mixture was then concentrated *in vacuo* and the solid was triturated with acetone (5 mL) then diethyl ether (5 mL) to obtain a grey solid (0.158 g). Lastly the solid

was dissolved in water (1 mL) and purified by semi-preparative HPLC to afford biotin-sugar2 **(105)** (0.0052 g, 8% yield) as a white powder. UPLC-TOF (ESI) *m/z*: $[M+H]^+$ calc. for $C_{38}H_{53}N_{12}O_{14}S$ 933.3519, found 933.3538; ^{1}H-NMR (400 MHz, D_2O, mixture of 4 diastereoisomers) δ 8.26 - 8.36 (m, 1H), 8.10 - 8.16 (m, 1H), 7.81 - 8.04 (m, 1H), 7.74 - 7.80 (m, 1H), 7.67 - 7.72 (m, 1H), 6.57 - 6.62 (m, 1H), 6.47 - 6.55 (m, 1H), 6.39 - 6.45 (m, 1H), 6.28 - 6.35 (m, 1H), 5.36 - 5.41 (m, 1H), 5.04 (d, *J* = 2.9 Hz, 5H), 4.23 - 4.37 (m, 3H), 4.01 - 4.07 (m, 1H), 3.81 - 3.97 (m, 2H), 3.73 - 3.79 (m, 1H), 3.65 - 3.70 (m, 1H), 3.31 - 3.54 (m, 2H), 3.17 (dt, *J* = 3.2, 1.7 Hz, 3H), 2.98 - 3.11 (m, 1H), 2.83 - 2.94 (m, 1H), 2.62 - 2.72 (m, 1H), 2.44 - 2.56 (m, 1H), 2.04 - 2.19 (m, 1H), 1.33 - 1.49 (m, 1H), 1.21 - 1.31 (m, 1H), 0.99 - 1.19 (m, 2H), 0.69 - 0.75 (m, 1H)

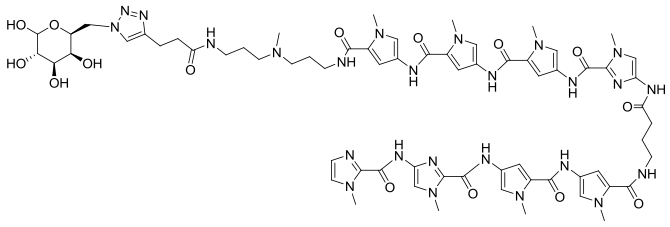

Synthesis of polyamide-galactose (109). To a stirred solution of polyamide **(93)** (0.003 g, 0.000237 mmol) in DMSO (10 uL) and DMF (20 uL) was added sugar acid **(111)** (0.000718 g, 0.000237 mmol), HTCU (0.00093 g, 0.00225 mmol) and DIPEA (0.00122 g, 0.000948 mmol). The mixture was stirred at r.t. overnight, filtered and then purified by semi-preparative HPLC to afford polyamide-galactose **(109)** (0.0006 g, 16%) as a white powder after lyophilisation. ESI-MS m/z (%): $[M\text{-Sugar}+2H]^{2+}$ calc. for $C_{61}H_{78}N_{24}O_{11}$ 661.3141, found 659 (50); UPLC-TOF (ESI) *m/z:*

$[M+4H+O]^{4+}$ calc. for $C_{70}H_{87}N_{25}O_{18}$, 391.4165, found 391.2876; UV–Vis (water): λ_{max} = 313, 274 nm.

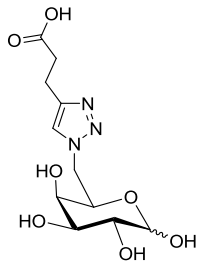

Preparation of sugar-acid (111). To a stirred solution of sugar azide **(7)** (0.432 g, 1.9 mmol.) in water (5 mL) was added pent-4-yn-oic acid **(110)** (0.405 g, 2.0 mmol.), $CuSO_4$ 0.26 M (350 uL, 0.09 mmol) and sodium L-ascorbate (0.400 g, 2.00 mmol). The mixture was stirred at r.t. overnight under nitrogen atmosphere, concentrated *in vacuo* and the product was purified by semi-preparative HPLC. Sugar acid **(111)** was recovered after lyophilisation (0.386 g, 67%) as a white powder. ESI-MS (ES+) *m/z* (%): $[M+H^+]$ calc. for $C_{11}H_{18}N_3O_7$ 304.1139, found 304 (50), 286 (40), 271 (10); ^{1}H-NMR (300 MHz, D_2O, mixture of 2 diastereoisomers) δ 7.97 - 8.04 (m, 1H), 5.08 - 5.18 (d, 1H), 4.44 - 4.53 (m), 3.64 - 4.14 (m), 3.30 - 3.60 (m), 2.88 - 3.06 (m, 1H), 2.68 - 2.85 (m, 1H), 2.58 - 2.65 (m, 1H), 2.44 - 2.55 (m, 1H); ^{13}C-NMR (100 MHz, DMSO-d_6) δ 170.6, 159.1, 142.5, 124.8, 105.2, 72.0, 68.6, 62.8, 61.1, 60.1, 49.4

References

(1) Bawa, R.; Bawa, S. R.; Maebius, S. B.; Flynn, T.; Wei, C. *Nanomed:Nanotechnol.* **2005**, *1*, 150-8.

(2) Salaita, K.; Wang, Y.; Mirkin, C. A. *Nat. Nanotechnol.* **2007**, *2*, 145-55.

(3) Ginger, D. S.; Zhang, H.; Mirkin, C. A. *Angew. Chem.* **2004**, *43*, 30-45.

(4) Huck, W. T. S. *Angew. Chem.* **2007**, *46*, 2754-7.

(5) Hatzakis, M. *IBM J. Res. Dev.* **1988**, *32*, 441-453.

(6) Sajanlal, P. R.; Sreeprasad, T. S.; Samal, A. K.; Pradeep, T. *Nano Reviews* **2011**, *2*, 1-62.

(7) Cho, E. C.; Zhang, Q.; Xia, Y. *Nat. Nanotechnol.* **2011**, *6*, 385-91.

(8) Schasfoort, R. B. M.; Tudos, A. J. *Handbook of surface plasmon resonance*; RSC, 2008; p. 403.

(9) Ozbay, E. *Science* **2006**, *311*, 189-93.

(10) Daniel, M.-C.; Astruc, D. *Chem. Rev.* **2004**, *104*, 293-346.

(11) Wunder, S.; Lu, Y.; Albrecht, M.; Ballauff, M. *ACS Catalysis* **2011**, *1*, 908-916.

(12) Stehr, J.; Hrelescu, C.; Sperling, R. a; Raschke, G.; Wunderlich, M.; Nichtl, A.; Heindl, D.; Kürzinger, K.; Parak, W. J.; Klar, T. a; Feldmann, J. *Nano Lett.* **2008**, *8*, 619-23.

(13) Narayanan, R.; El-Sayed, M. A. *Nano Lett.* **2004**, *4*, 1343-1348.

(14) Mijatovic, D.; Eijkel, J. C. T.; Berg, A. van den *Lab Chip* **2005**, *5*, 492-500.

(15) Ito, T.; Okazaki, S. *Nature* **2000**, *406*, 1027-31.

(16) Spatz, J. P.; Chan, V. Z.-H.; Mößmer, S.; Kamm, F.-M.; Plettl, A.; Ziemann, P.; Möller, M. *Adv. Mater.* **2002**, *14*, 1827-1832.

(17) Aldaye, F. A. *Nature* **2008**, 1-6.

(18) LaBean, T. H.; Li, H. *Nano Today* **2007**, *2*, 26-35.

(19) Basu, H. S.; Feuerstein, B. G.; Zarling, D. A.; Shafer, R. H.; Marton, L. J. *J Biomol Struct Dyn.* **1988**, *6*, 299-309.

(20) MANDELKERN, M. *J. Mol. Biol.* **1981**, *152*, 153-161.

(21) Basham, B. *Proc. Natl. Acad. Sci. USA* **1995**, *92*, 6464-6468.

(22) Wing, R.; Drew, H.; Takano, T.; Broka, C.; Tanaka, S.; Itakura, K.; Dickerson, R. E. *Nature* **1980**, *287*, 755-758.

(23) Looger, L. L.; Dwyer, M. A.; Smith, J. J.; Hellinga, H. W. *Nature* **2003**, *423*, 185-90.

(24) Seeman, N. C. *Nature* **2003**, *421*, 427-31.

(25) Blanksby, S. J.; Ellison, G. B. *Accounts Chem. Res.* **2003**, *36*, 255-63.

(26) Lane, A. N.; Chaires, J. B.; Gray, R. D.; Trent, J. O. *Nucleic Acids Res.* **2008**, *36*, 5482-515.

(27) Strobel, S. a; Cochrane, J. C. *Curr. Opin. Chem. Biol.* **2007**, *11*, 636-43.

(28) Abelson, J.; Trotta, C. R. *Biochemistry* 12685-12688.

(29) Jurica, M. S. *Curr. Opin. Struc. Biol.* **2008**, *18*, 315-20.

(30) Liu, Y.; West, S. C. *Nat. Rev. Mol. Cell Bio.* **2004**, *5*, 937-44.

(31) Stahl, F. W. *Genetics* **1994**, *138*, 241-6.

(32) Seeman, N. C. *J. Vac. Sci. Technol. A* **1994**, *12*, 1895.

(33) Goodman, R. P.; Schaap, I. A. T.; Tardin, C. F.; Erben, C. M.; Berry, R. M.; Schmidt, C. F.; Turberfield, A. J. *Science* **2005**, *310*, 1661-5.

(34) LaVan, D. A.; McGuire, T.; Langer, R. *Nat. Biotechnol.* **2003**, *21*, 1184-91.

(35) Erben, C. M.; Goodman, R. P.; Turberfield, A. J. *Angew. Chem.* **2006**, *45*, 7414-7.

(36) Aldaye, F. A.; Sleiman, H. F. *J. Am. Chem. Soc.* **2007**, *129*, 10070-1.

(37) Aldaye, F. A.; Sleiman, H. F. *Pure Appl. Chem.* **2009**, *81*, 2157-2181.

(38) Rothemund, P. W. K. *Nature* **2006**, *440*, 297-302.

(39) Han, D.; Pal, S.; Nangreave, J.; Deng, Z.; Liu, Y.; Yan, H. *Science* **2011**, *332*, 342-6.

(40) Berti, L.; Burley, G. A. *Nat. Nanotechnol.* **2008**, *3*, 81-7.

(41) Bloomfield, V. A.; Crothers, D. M.; Tinoco, I. J. *Nucleic Acids Structures, Properties and Functions*; University Science Books,U.S.: Berkeley, 2000; p. 794.

(42) Tse, W. C.; Boger, D. L. *Chem. Biol.* **2004**, *11*, 1607-17.

(43) Reinhardt, C. G.; Krugh, T. R. *Biochemistry* **1978**, *17*, 4845-4854.

(44) Lilley, D. *DNA-protein : structural interactions*; IRL Press at Oxford University Press: Oxford ;;New York, 1995.

(45) Eriksson, S.; Kim, S. K.; Kubista, M.; Norden, B. *Biochemistry* **1993**, *32*, 2987-2998.

(46) Bailly, C.; Henichart, J.-P.; Pommery, N.; Houssin, R. *J. Pharm. Sci.* **1989**, *78*, 910-917.

(47) Kopka, M. L.; Yoon, C.; Goodsell, D.; Pjura, P.; Dickerson, R. E. *Proc. Natl. Acad. Sci. U. S. A.* **1985**, *82*, 1376-80.

(48) Huang, W. In *ICMA*; IEEE, 2009; pp. 1427-1432.

(49) Zheng, H.; Cao, A.; Weinberger, C. R.; Huang, J. Y.; Du, K.; Wang, J.; Ma, Y.; Xia, Y.; Mao, S. X. *Nat. Comm.* **2010**, *1*, 144.

(50) Glover, R.; Miller, J. M.; Hutchison, J. E. *ACS nano* **2011**.

(51) Allis, D. G.; Drexler, E.; Drexler, K. E. *J. Comput. Theor. Nanosci.* **2005**, *2*, 45-55.

(52) Carpick, R. W. *Science* **2006**, *313*, 184-5.

(53) Narayanan, R.; El-Sayed, M. A. *J. Am. Chem. Soc.* **2003**, *125*, 8340-7.

(54) Hwang, C. *J. Catal.* **2000**, *195*, 336-341.

(55) Schmid, G. *Chemical Reviews* **1992**, *92*, 1709-1727.

(56) Brigger, I.; Dubernet, C.; Couvreur, P. *Adv. Drug Delivery Rev.* **2002**, *54*, 631-651.

(57) NEUBERGER, T.; SCHOPF, B.; HOFMANN, H.; HOFMANN, M.; VONRECHENBERG, B. *J. Magn. Magn. Mater.* **2005**, *293*, 483-496.

(58) Okitsu, K.; Yue, A.; Tanabe, S.; Matsumoto, H. *Chem. Mater.* **2000**, *12*, 3006-3011.

(59) Jones, M. R.; Osberg, K. D.; Macfarlane, R. J.; Langille, M. R.; Mirkin, C. A. *Chem. Rev.* **2011**, *111*, 3736-827.

(60) Salkar, R. a.; Jeevanandam, P.; Aruna, S. T.; Koltypin, Y.; Gedanken, a. *J. Mater. Chem.* **1999**, *9*, 1333-1335.

(61) Gottesman, R.; Shukla, S.; Perkas, N.; Solovyov, L. a; Nitzan, Y.; Gedanken, A. *Langmuir* **2011**, *27*, 720-6.

(62) Jiang, L.-P.; Wang, A.-N.; Zhao, Y.; Zhang, J.-R.; Zhu, J.-J. *Inorg. Chem. Commun.* **2004**, *7*, 506-509.

(63) Abid, J. P.; Wark, a W.; Brevet, P. F.; Girault, H. H. *Chem. Comm.* **2002**, 792-3.

(64) Sohn, J. H.; Pham, L. Q.; Kang, H. S.; Park, J. H.; Lee, B. C.; Kang, Y. S. *Radiat. Phys. Chem.* **2010**, *79*, 1149-1153.

(65) Abdullah, A.; Annapoorni, S. *Pramana* **2005**, *65*, 815-819.

(66) Lin, C. Y.; Mohanty, U. S.; Chou, J. H. *J. Alloys Compd.* **2010**, *501*, 204-210.

(67) Hartlieb, K. J.; Martin, A. D.; Saunders, M.; Raston, C. L. *New J. Chem.* **2010**, *34*, 1834.

(68) Walter, E. C.; Murray, B. J.; Favier, F.; Kaltenpoth, G.; Grunze, M.; Penner, R. M. *J. Phys. Chem. B* **2002**, *106*, 11407-11411.

(69) Rycenga, M.; Cobley, C. M.; Zeng, J.; Li, W.; Moran, C. H.; Zhang, Q.; Qin, D.; Xia, Y. *Chemical Reviews* **2011**, 3669-3712.

(70) Henglein, A.; Giersig, M. *J. Phys. Chem. B* **1999**, *103*, 9533-9539.

(71) Rosi, N. L.; Mirkin, C. a *Chem. Rev.* **2005**, *105*, 1547-62.

(72) Brust, M.; Kiely, C. J. *Colloid Surface A* **2002**, *202*, 175-186.

(73) Kim, J. H.; Min, B. R.; Won, J.; Kang, Y. S. *J. Polym. Sci. Pol. Phys.* **2006**, *44*, 1168-1178.

(74) Abdul kareem, T.; Anu kaliani, a. *Arab. J. Chem.* **2011**, *4*, 325-331.

(75) Mulfinger, L.; Solomon, S. D.; Bahadory, M.; Jeyarajasingam, A. V.; Rutkowsky, S. a.; Boritz, C. *J. Chem. Educ.* **2007**, *84*, 322.

(76) Adhikari, B.; Banerjee, A. *Chem. Mater.* **2010**, *22*, 4364-4371.

(77) Hartlieb, K. J.; Saunders, M.; Jachuck, R. J. J.; Raston, C. L. *Green Chem.* **2010**, *12*, 1012.

(78) Šileikaitė, A.; Prosyčevas, I.; Puišo, J.; Juraitis, A.; Guobienė, A. *Mater. Sci+* **2006**, *12*.

(79) Kobayashi, Y.; Katakami, H.; Mine, E.; Nagao, D.; Konno, M.; Liz-Marzán, L. M. *J. Colloid Interf. Sci.* **2005**, *283*, 392-6.

(80) Ahmad, N.; Ahmad, M.; Al-nowaiser, F. M.; Khan, Z. *Colloid Surface B* **2010**, *78*, 109-114.

(81) Khan, Z.; Al-Thabaiti, S. A.; Obaid, A. Y.; Al-Youbi, a O. *Colloid Surface B* **2011**, *82*, 513-7.

(82) Guzman, M. G.; Dille, J.; Godet, S. *Int. J. Chem. Biomol. Eng* **2009**, *2*, 104-111.

(83) Wang, W.; Chen, X.; Efrima, S. *J. Phys. Chem. B* **1999**, *103*, 7238-7246.

(84) Prathna, T. C.; Chandrasekaran, N.; Raichur, A. M.; Mukherjee, A. *Colloid Surface B* **2011**, *82*, 152-9.

(85) Ahmad, N.; Sharma, S.; Alam, M. K.; Singh, V. N.; Shamsi, S. F.; Mehta, B. R.; Fatma, A. *Colloid Surface B* **2010**, *81*, 81-6.

(86) Kamal, S. S. K.; Sahoo, P. K.; Vimala, J.; Premkumar, M.; Ram, S.; Durai, L. *Acta Chim. Slov.* **2010**, *57*, 808-812.

(87) Safaepour, M.; Shahverdi, A. R.; Shahverdi, H. R. *Avicenna J. Med. Biotechnol.* **2009**, *1*, 111-115.

(88) Nianxin, X.; Yurong, C.; Juming, Y. *Acta Chim. Sinica* **2011**, *69*, 1321-1326.

(89) Singh, C.; Sharma, V.; Naik, P. K. R.; Khandelwal, V.; Singh, H. *Dig. J. Nanomater. Bios.* **2011**, *6*, 535-542.

(90) Priya, M. M.; Selvi, B. K.; Paul, J. A. J. *Dig. J. Nanomater. Bios.* **2011**, *6*, 869-877.

(91) Rastogi, L.; Arunachalam, J. *Mater. Chem. Phys.* **2011**, *129*, 558-563.

(92) Sattler, K.; Mühlbach, J.; Recknagel, E. *Phys. Rev. Lett.* **1980**, *45*, 821-824.

(93) Marchetti, A. *Chapter 3: The Photochemistry and Photophysics of the Silver Halides*; Volman, D. H.; Hammond, G. S.; Neckers, D. C., Eds.; John Wiley & Sons, Inc.: Hoboken, NJ, USA, 1992.

(94) Tadaaki, T. *Photographic Sensitivity Theory and Mechanisms*; OXFORD UNIVERSITY PRESS, 1995; p. 263.

(95) MITCHELL, J. W. *Rep. Prog. Phys.* **1957**, *20*, 433-520.

(96) Lehtinen, K. E. J.; Backman, U.; Jokiniemi, J. K.; Kulmala, M. *J. Colloid Interf. Sci.* **2004**, *274*, 526-30.

(97) Yin, Y.; Li, Z.-Y.; Zhong, Z.; Gates, B.; Xia, Y.; Venkateswaran, S. *J. Mater. Chem.* **2002**, *12*, 522-527.

(98) Henglein, A. *J. Phys. Chem.* **1979**, *83*, 2209-2216.

(99) Le, A.-T.; Huy, P. T.; Tam, P. D.; Huy, T. Q.; Cam, P. D.; Kudrinskiy, a. a.; Krutyakov, Y. a. *Curr. Appl. Phys.* **2010**, *10*, 910-916.

(100) Soukupová, J.; Kvítek, L.; Panáček, A.; Nevěčná, T.; Zbořil, R. *Mater. Chem. Phys.* **2008**, *111*, 77-81.

(101) Pal, S.; Varghese, R.; Deng, Z.; Zhao, Z.; Kumar, A.; Yan, H.; Liu, Y. *Angew. Chem.* **2011**, *50*, 4176-9.

(102) Endo, M.; Sugiyama, H. *Chembiochem* **2009**, *10*, 2420-2443.

(103) Agard, N. J.; Prescher, J. A.; Bertozzi, C. R. *Biochemistry* **2004**, 15046-15047.

(104) Rostovtsev, V. V.; Green, L. G.; Fokin, V. V.; Sharpless, K. B. **2002**, 2596-2599.

(105) Burley, G. a; Gierlich, J.; Mofid, M. R.; Nir, H.; Tal, S.; Eichen, Y.; Carell, T. *J. Am. Chem. Soc.* **2006**, *128*, 1398-9.

(106) Gierlich, J.; Burley, G. a; Gramlich, P. M. E.; Hammond, D. M.; Carell, T. *Org. Lett.* **2006**, *8*, 3639-42.

(107) Kong, D. C. M.; Itzstein, M. von *Carbohydr. Res.* **1997**, *305*, 323-329.

(108) Morís-Varas, F.; Qian, X.-H.; Wong, C.-H. *J. Am. Chem. Soc.* **1996**, *118*, 7647-7652.

(109) VOLANTE, R. P. *Tetrahedron Lett.* **1981**, *22*, 3119-3122.

(110) Li, P.; Wang, L.; Zhang, Y. *Tetrahedron* **2008**, *64*, 10825-10830.

(111) Wu, P.; Feldman, A. K.; Nugent, A. K.; Hawker, C. J.; Scheel, A.; Voit, B.; Pyun, J.; Fréchet, J. M. J.; Sharpless, K. B.; Fokin, V. V. *Angew. Chem.* **2004**, *43*, 3928-32.

(112) *Uli Rant's group unpublished private communication, Technische Universität München (TUM) 9 November* **2009**.

(113) DION, A. S.; POMENTI, A. A. *Anal. Biochem.* **1983**, *129*, 490-496.

(114) Kimling, J.; Maier, M.; Okenve, B.; Kotaidis, V.; Ballot, H.; Plech, A. *J. Phys. Chem. B* **2006**, *110*, 15700-15707.

(115) FRENS, G. *Nat. Phys. Sci.* **1973**, *241*, 20-22.

(116) Kammerlander, N. *Metallized DNA: Synthesis, Analysis and Properties*; Diplomica Verlag, 2009; p. 118.

(117) Kvitek, L.; Vanickova, M.; Panacek, A.; Soukupova, J.; Dittrich, M.; Valentova, E.; Prucek, R.; Bancirova, M.; Milde, D.; Zboril, R. *J. Phys. Chem. C* **2009**, *113*, 4296-4300.

(118) Hao, E.; Schatz, G. C. *J. Chem. Phys.* **2004**, *120*, 357-66.

(119) Evanoff, D. D.; Chumanov, G. *Chemphyschem* **2005**, *6*, 1221-31.

(120) Mallick, K.; Witcomb, M. J.; Scurrell, M. S. *Mater. Chem. Phys.* **2005**, *90*, 221-224.

(121) Dadosh, T. *Mater. Lett.* **2009**, *63*, 2236-2238.

(122) Lee, G. P.; Bignell, L. J.; Romeo, T. C.; Razal, J. M.; Shepherd, R. L.; Chen, J.; Minett, A. I.; Innis, P. C.; Wallace, G. G. *Chem. Comm.* **2010**, *46*, 7807-9.

(123) Moerner, W. E.; Fromm, D. P. *Rev. Sci. Instrum.* **2003**, *74*, 3597.

(124) Adhikari, B.; Banerjee, A. *Chem. Mater.* **2010**, *22*, 4364-4371.

(125) Hill, H. D.; Millstone, J. E.; Banholzer, M. J.; Mirkin, C. a *ACS nano* **2009**, *3*, 418-24.

(126) Kim, T.-H.; Kang, S.-H.; Doe, C.; Yu, J.; Sim, J.-B.; Kim, J.; Kline, S. R.; Choi, S.-M. *J. Am. Chem. Soc.* **2009**, *131*, 7456-60.

(127) Cederquist, K. B.; Keating, C. D. *ACS nano* **2009**, *3*, 256-60.

(128) Rao, T. U. B.; Pradeep, T.; Udaya Bhaskara Rao, T. *Angew. Chem.* **2010**, *49*, 3925-3929.

(129) Díez, I.; Pusa, M.; Kulmala, S.; Jiang, H.; Walther, A.; Goldmann, A. S.; Müller, A. H. E.; Ikkala, O.; Ras, R. H. a *Angew. Chem.* **2009**, *48*, 2122-5.

(130) Chowdhury, M. H.; Gray, S. K.; Pond, J.; Geddes, C. D.; Aslan, K.; Lakowicz, J. R. *J. Opt. Soc. Am. B* **2007**, *24*, 2259-2267.

(131) Pease, L. F.; Tsai, D.-H.; Hertz, J. L.; Zangmeister, R. a; Zachariah, M. R.; Tarlov, M. J. *Langmuir* **2010**, *26*, 11384-90.

(132) Aroca, R.; Kovacs, G. J.; Jennings, C. A.; Loutfy, R. O.; Vincett, P. S. *Langmuir* **1988**, *4*, 518-521.

(133) Fu, Y.; Zhang, J.; Lakowicz, J. R. *J. Fluoresc.* **2007**, *17*, 811-6.

(134) Veber, D. F.; Johnson, S. R.; Cheng, H.-Y.; Smith, B. R.; Ward, K. W.; Kopple, K. D. *J. Med. Chem.* **2002**, *45*, 2615-2623.

(135) Morgan, G. T.; Drew, H. D. K. *J. Chem. Soc. Transactions* **1920**, *117*, 1456.

(136) El Aribi, H.; Rodriquez, C. F.; Shoeib, T.; Ling, Y.; Hopkinson, A. C.; Siu, K. W. M. *J. Phys. Chem. A* **2002**, *106*, 8798-8805.

(137) Souza, G. R.; Levin, C. S.; Hajitou, A.; Pasqualini, R.; Arap, W.; Miller, J. H. *Anal. Chem.* **2006**, *78*, 6232-7.

(138) Kvitek, L.; Prucek, R.; Panacek, A.; Novotn, R.; Hrb, J.; Zboil, R. *J. Mater. Chem.* **2005**, *15*, 1099.

(139) Zangger, K.; Armitage, L. M. *Metal-based drugs* **1999**, *6*, 239-45.

(140) Gallego, M. L.; Cano, M.; Campo, J. a.; Heras, J. V.; Pinilla, E.; Torres, M. R.; Cornago, P.; Claramunt, R. M. *Eur. J. Inorg. Chem.* **2005**, *2005*, 4370-4381.

(141) Gower, M. L.; Crowley, J. D. *Dalton transactions* **2010**, *39*, 2371-8.

(142) Fielding, L. *Tetrahedron* **2000**, *56*.

(143) Hynes, M. J. *J. Chem. Soc. Dalton* **1993**, 311.

(144) Kuntz, I.; Johnston, M. *J. Am. Chem. Soc.* **1967**, *89*, 6008-6017.

(145) Schields, P. J.; Dunwoody, N.; Mamak, M.; Gendron, C.; Bates, S. *JCPDS-International Centre for Diffraction Data ISSN 1097-0002* **2008**, 162-168.

(146) Jensen, T. R.; Schatz, G. C.; Duyne, R. P. Van *J. Phys. Chem. B* **1999**, *103*, 2394-2401.

(147) Meyer, M. W.; Smith, E. A. *Analyst* **2011**, *136*, 3542-3549.

(148) Stamplecoskie, K. G.; Scaiano, J. C.; Tiwari, V. S.; Anis, H. *J. Phys. Chem. C* **2011**, *115*, 1403-1409.

(149) Petroski, J.; Chou, M. H.; Creutz, C. *Inorg. Chem.* **2004**, *43*, 1597-9.

(150) Weare, W. W.; Reed, S. M.; Warner, M. G.; Hutchison, J. E. *J. Am. Chem. Soc.* **2000**, *122*, 12890-12891.

(151) Hill, H. D.; Hurst, S. J.; Mirkin, C. a. *Nano Lett.* **2009**, *9*, 1283-1283.

(152) Panacek, A.; Prucek, R.; Safarova, D.; Dittrich, M.; Richtrova, J.; Benickova, K.; Zboril, R.; Kvitek, L. *Environ. Sci. Technol.* **2011**, *45*, 4974-9.

(153) Panigrahi, S.; Praharaj, S.; Basu, S.; Ghosh, S. K.; Jana, S.; Pande, S.; Vo-Dinh, T.; Jiang, H.; Pal, T. *J. Phys. Chem. B* **2006**, *110*, 13436-44.

(154) Bosco, M.; Gall, S. L.; Rihouey, C.; Couve-Bonnaire, S.; Bardor, M.; Lerouge, P.; Pannecoucke, X. *Tetrahedron Lett.* **2008**, *49*, 2294-2297.

(155) Mourer, M.; Hapiot, F.; Monflier, E.; Menuel, S. *Tetrahedron* **2008**, *64*, 7159-7163.

(156) Dondi, R.; Su, W.; Griffith, G. a; Clark, G.; Burley, G. a *Small* **2012**, 1-7.

(157) Rucker, V. C.; Foister, S.; Melander, C.; Dervan, P. B. *J. Am. Chem. Soc.* **2003**, *125*, 1195-202.

(158) Dervan, P. B.; Edelson, B. S. *Curr. Opin. Struct. Biol.* **2003**, *13*, 284-299.

(159) Geierstanger, B. H.; Dwyer, T. J.; Bathini, Y.; Lown, J. W.; Wemmer, D. E. *J. Am. Chem. Soc.* **1993**, *115*, 4474-4482.

(160) White, S.; Szewczyk, J. W.; Turner, J. M.; Baird, E. E.; Dervan, P. B. *Nature* **1998**, *391*, 468-71.

(161) Baird, E. E.; Dervan, P. B. *J. Am. Chem. Soc.* **1996**, *118*, 6141-6146.

(162) Dose, C.; Farkas, M. E.; Chenoweth, D. M.; Dervan, P. B. *J. Am. Chem. Soc.* **2008**, *130*, 6859-6866.

(163) Marques, M. A.; Doss, R. M.; Urbach, A. R.; Dervan, P. B. *Helv. Chim. Acta* **2002**, *85*, 4485-4517.

(164) Herman, D. M.; Turner, J. M.; Baird, E. E.; Dervan, P. B. *J. Am. Chem. Soc.* **1999**, *121*, 1121-1129.

(165) Chenoweth, D. M.; Harki, D. A.; Dervan, P. B. *Org. Lett.* **2009**, *11*, 3590-3.

(166) Cohen, J. D.; Sadowski, J. P.; Dervan, P. B. *J. Am. Chem. Soc.* **2008**, *130*, 402-3.

(167) Schmidt, T. L.; Nandi, C. K.; Rasched, G.; Parui, P. P.; Brutschy, B.; Famulok, M.; Heckel, A. *Angew. Chem.* **2007**, *46*, 4382-4.

(168) Cohen, J. D.; Sadowski, J. P.; Dervan, P. B. *Angew. Chem.* **2007**, *46*, 7956-9.

(169) Fechter, E. J.; Olenyuk, B.; Dervan, P. B. *J. Am. Chem. Soc.* **2005**, *127*, 16685-91.

(170) Nandi, C. K.; Parui, P. P.; Schmidt, T. L.; Heckel, A.; Brutschy, B. *Anal. Bioanal. Chem.* **2008**, *390*, 1595-603.

(171) Best, T. P.; Edelson, B. S.; Nickols, N. G.; Dervan, P. B. *Proc. Natl. Acad. Sci. U. S. A.* **2003**, *100*, 12063-8.

(172) Edelson, B. S.; Best, T. P.; Olenyuk, B.; Nickols, N. G.; Doss, R. M.; Foister, S.; Heckel, A.; Dervan, P. B. *Nucleic Acids Res.* **2004**, *32*, 2802-18.

(173) Hsu, C. F.; Dervan, P. B. *Bioorg. Med. Chem. Lett.* **2008**, *18*, 5851-5.

(174) Denissov, S. *Transcription Regulation of Human Genes: Novel aspects and mechanisms*; LAP LAMBERT Academic Publishing, 2010; p. 184.

(175) Kageyama, Y.; Sugiyama, H.; Ayame, H.; Iwai, A.; Fujii, Y.; Huang, L. E.; Kizaka-Kondoh, S.; Hiraoka, M.; Kihara, K. *Acta Oncol.* **2006**, *45*, 317-24.

(176) Olenyuk, B. Z.; Zhang, G.-J.; Klco, J. M.; Nickols, N. G.; Kaelin, W. G.; Dervan, P. B. *Proc. Natl. Acad. Sci. U. S. A.* **2004**, *101*, 16768-73.

(177) Nickols, N. G.; Jacobs, C. S.; Farkas, M. E.; Dervan, P. B. *ACS Chem. Biol.* **2007**, *2*, 561-71.

(178) Nickols, N. G.; Dervan, P. B. *Proc. Natl. Acad. Sci. U. S. A.* **2007**, *104*, 10418-23.

(179) Muzikar, K. a; Nickols, N. G.; Dervan, P. B. *Proc. Natl. Acad. Sci. U. S. A.* **2009**, *106*, 16598-603.

(180) Hochhauser, D.; Kotecha, M.; O'hare, C.; Morris, P. J.; Hartley, J. M.; Taherbhai, Z.; Harris, D.; Forni, C.; Mantovani, R.; Lee, M.; Hartley, J. A. *Mol. Cancer Ther.* **2007**, *6*, 346-54.

(181) Takahashi, T.; Asami, Y.; Kitamura, E.; Suzuki, T.; Wang, X.; Igarashi, J.; Morohashi, A.; Shinojima, Y.; Kanou, H.; Saito, K.; Takasu, T.; Nagase, H.; Harada, Y.; Kuroda, K.; Watanabe, T.; Kumamoto, S.; Aoyama, T.; Matsumoto, Y.; Bando, T.; Sugiyama, H.; Yoshida-Noro, C.; Fukuda, N.; Hayashi, N. *Chem. Biol.* **2008**, *15*, 829-41.

(182) Mapp, a. K. *Proc. Natl. Acad. Sci.* **2000**, *97*, 3930-3935.

(183) Xiao, X.; Yu, P.; Lim, H.-S.; Sikder, D.; Kodadek, T. *Angew. Chem.* **2007**, *46*, 2865-8.

(184) Schmidt, T. L.; Nandi, C. K.; Rasched, G.; Parui, P. P.; Brutschy, B.; Famulok, M.; Heckel, A. *Angew. Chem.* **2007**, *46*, 4382-4.

(185) Schmidt, T. L.; Heckel, A. *Nano Lett.* **2011**, *11*, 1739-42.

(186) Russell, T. W.; Hoy, R. C.; Cornelius, J. E. *J. Org. Chem.* **1972**, *37*, 3552-3553.

(187) Caddick, S.; K. Haynes, A. K. de; Judd, D. B.; Williams, M. R. . *Tetrahedron Lett.* **2000**, *41*, 3513-3516.

(188) Choi, J.; Yoon, N. M. *Science* **1996**, *37*, 1057-1060.

(189) Collins, D. J.; Smith, A. D.; Davis, B. H. *Ind. Eng. Chem. Prod. RD* **1982**, *21*, 279-281.

(190) Sim, T. B.; Choi, J.; Joung, M. J.; Yoon, N. M. *J. Org. Chem.* **1997**, *62*, 2357-2361.

(191) Wang, M.; Li, H.; Wu, Y.; Zhang, J. *Mater. Lett.* **2003**, *57*, 2954 - 2964.

(192) Magoo, D. *Synlett* **2010**, *2010*, 2525-2526.

(193) Chuan, W. U. *T. Nonferr. Metal Soc.* **2007**, *17*, s1002-s1005.

(194) Sugiyama, A.; Taguchi, Y.; Nagaoka, S.; Nakajima, A. *Chem. Phys. Lett.* **2010**, *485*, 129-132.

(195) Zhou, X.; Xu, W.; Liu, G.; Panda, D.; Chen, P. *J. Am. Chem. Soc.* **2010**, *132*, 138-46.

(196) Wurtz, N. R.; Turner, J. M.; Baird, E. E.; Dervan, P. B. *Org. Lett.* **2001**, *3*, 1201-1203.

(197) Krutzik, P. O.; Chamberlin, A. R. *Bioorg. Med. Chem. Lett.* **2002**, *12*, 2129-2132.

(198) Belitsky, J. M.; Nguyen, D. H.; Wurtz, N. R.; Dervan, P. B. *Bioorg. Med. Chem. Lett.* **2002**, *10*, 2767-2774.

(199) Fattori, D.; Kinzel, O.; Ingallinella, P.; Bianchi, E.; Pessi, A. *Bioorg. Med. Chem. Lett.* **2002**, *12*, 1143-1147.

(200) Heckel, A.; Dervan, P. B.; Marques, M. A. Chapter 11 Solid-Phase Synthesis of DNA-Binding Polyamides Using Safety Catch Hydrazine Resin, California institute of technology, 2005, pp. 289-306.

(201) Hsu, C. F.; Phillips, J. W.; Trauger, J. W.; Farkas, M. E.; Belitsky, J. M.; Heckel, A.; Olenyuk, B. Z.; Puckett, J. W.; Wang, C. C. C.; Dervan, P. B. *Tetrahedron* **2007**, *63*, 6146-6151.

(202) Tsai, S. M.; Farkas, M. E.; Chou, C. J.; Gottesfeld, J. M.; Dervan, P. B. *Nucleic Acids Res.* **2007**, *35*, 307-16.

(203) Su, W.; Gray, S. J.; Dondi, R.; Burley, G. A. *Org. Lett.* **2009**, *11*, 3910-3.

(204) Wetzler, M.; Wemmer, D. E. *Org. Lett.* **2010**, *12*, 3488-90.

(205) Thern, B.; Rudolph, J.; Jung, G. *Tetrahedron Lett.* **2002**, *43*, 5013-5016.

(206) Hsu, C. F.; Phillips, J. W.; Trauger, J. W.; Farkas, M. E.; Belitsky, J. M.; Heckel, A.; Olenyuk, B. Z.; Puckett, J. W.; Wang, C. C. C.; Dervan, P. B. *Tetrahedron* **2007**, *63*, 6146-6151.

(207) Fields, C. G.; Fields, G. B. *Method. Mol. Biol.* **1994**, *35*, 29-40.

(208) Chenoweth, D. M.; Harki, D. a; Dervan, P. B. *J. Am. Chem. Soc.* **2009**, *131*, 7175-81.

(209) Nickols, N. G.; Jacobs, C. S.; Farkas, M. E.; Dervan, P. B. *Nucleic Acids Res.* **2007**, *35*, 363-70.

(210) Fechter, E. J.; Olenyuk, B.; Dervan, P. B. *Angew. Chem.* **2004**, *43*, 3591-4.

(211) Bando, T.; Narita, A.; Asada, K.; Ayame, H.; Sugiyama, H. *J. Am. Chem. Soc.* **2004**, *126*, 8948-55.

(212) Bando, T.; Sugiyama, H. *Acc. Chem. Res.* **2006**, *39*, 935-944.

(213) Qian, S.; Wang, C.; Wang, Q.; Finn, G. M. G.; Fokin, V.; Thomson, J.; Burley, C.; Batchelor, M.; Convine, N.; Davies, K.; Farrington, K.; Howes, L.; Kirk, A.; Cockrill, J.; Orchard, J.; Warncke, L.; Wilson, E. *Chemical Society Reviews*. 2010, pp. 1223-1230.

(214) Hein, J. E.; Tripp, J. C.; Krasnova, L. B.; Sharpless, K. B.; Fokin, V. V. *Angew. Chem.* **2009**, *48*, 8018-21.

(215) Fiore, M.; Marra, A.; Dondoni, A. *J. Org. Chem.* **2009**, *74*, 4422-5.

(216) Bremer, R. E.; Szewczyk, J. W.; Baird, E. E.; Dervan, P. B. *Bioorg. Med. Chem.* **2000**, *8*, 1947-55.

(217) Nguyen, D. H.; Szewczyk, J. W.; Baird, E. E.; Dervan, P. B. *Bioorg. Med. Chem.* **2001**, *9*, 7-17.

(218) Boren, B. C.; Narayan, S.; Rasmussen, L. K.; Zhang, L.; Zhao, H.; Lin, Z.; Jia, G.; Fokin, V. V. *Science* **2008**.

(219) Grehn, L.; Ding, L.; Ragnarsson, U.; Kim, B. H.; Pihlaja, K.; Maartmann-Moe, K.; Wold, S. *Acta Chem. Scand.* **1990**, *44*, 67-74.

(220) Wolter, F. E.; Molinari, L.; Socher, E. R.; Schneider, K.; Nicholson, G.; Beil, W.; Seitz, O.; Süssmuth, R. D. *Bioorg. Med. Chem. Lett.* **2009**, *19*, 3811-5.

(221) Schneider, K.; Keller, S.; Wolter, F. E.; Röglin, L.; Beil, W.; Seitz, O.; Nicholson, G.; Bruntner, C.; Riedlinger, J.; Fiedler, H.-peter; Süssmuth, R. D. *Angew. Chem.* **2008**, *47*, 3258-61.

(222) Bailly, C.; Henichart, J.-P.; Pommery, N.; Houssin, R. *J. Pharm. Sci.* **1989**, *78*, 910-917.

(223) Grehn, L.; Ragnarsson, U. *J. Org. Chem.* **1981**, *46*, 3492-3497.

(224) Hewlett, N. M.; Tepe, J. J. *Org. Lett.* **2011**, *13*, 4550-3.

(225) Keifer, P. A.; Schwartz, R. E.; Koker, M. E. S.; Hughes, R. G.; Rittschof, D.; Rinehart, K. L. *J. Org. Chem.* **1991**, *56*, 2965-2975.

(226) Wallace, D. M.; Leung, S. H.; Senge, M. O.; Smith, K. M. *J. Org. Chem.* **1993**, *58*, 7245-7257.

(227) Heckel, A.; Dervan, P. B. *Chem. Eur. J.* **2003**, *9*, 3353-66.

(228) Nishiwaki, N.; Ogihara, T.; Takami, T.; Tamura, M.; Ariga, M. *J. Org. Chem.* **2004**, *69*, 8382-6.

(229) Hale, W. J.; Hoyt, W. V. *J. Am. Chem. Soc.* **1915**, *37*, 2538-2552.

(230) Mancini, I.; Cavazza, M.; Guella, G.; Pietra, F. *J. Chem. Soc. Perk. T. 1* **1994**, 2181.

(231) Bremer, R. E.; Wurtz, N. R.; Szewczyk, J. W.; Dervan, P. B. *Bioorg. Med. Chem.* **2001**, *9*, 2093-103.

(232) Mirkin, C. A.; Letsinger, R. L.; Mucic, R. C.; Storhoff, J. J. *Nature* **1996**, *382*, 607-9.

(233) Kallenbach, N. R.; Ma, R.-I.; Seeman, N. C. *Nature* **1983**, *305*, 829-831.

(234) Erben, C. M.; Goodman, R. P.; Turberfield, A. J. *J. Am. Chem. Soc.* **2007**, *129*, 6992-3.

(235) Mastroianni, A. J.; Claridge, S. a; Alivisatos, a P. *J. Am. Chem. Soc.* **2009**, *131*, 8455-9.

(236) Rinker, S.; Ke, Y.; Liu, Y.; Chhabra, R.; Yan, H. *Nat. Nanotechnol.* **2008**, *3*, 418-22.

(237) Gothelf, K. V.; Labean, T. H. *DNA Sequence* **2005**, 4023-4037.

(238) Aldaye, F. A.; Palmer, A. L.; Sleiman, H. F. *Science* **2008**, *321*, 1795-9.

(239) Aldaye, F. A.; Sleiman, H. F. *J. Am. Chem. Soc.* **2007**, *129*, 4130-1.

(240) Aldaye, F. A.; Sleiman, H. F. *Angew. Chem.* **2006**, *45*, 2204-9.

(241) Pal, S.; Deng, Z.; Ding, B.; Yan, H.; Liu, Y. *Angew. Chem.* **2010**, *49*, 2700-4.

(242) Ding, B.; Deng, Z.; Yan, H.; Cabrini, S.; Zuckermann, R. N.; Bokor, J. *J. Am. Chem. Soc.* **2010**, *132*, 3248-9.

(243) Bandy, T. J.; Brewer, A.; Burns, J. R.; Marth, G.; Nguyen, T.; Stulz, E. *Chemical Society reviews* **2011**, *40*, 138-48.

(244) Stulz, E. *Chem. Eur. J.* **2012**.

(245) Pinheiro, A. V.; Han, D.; Shih, W. M.; Yan, H. *Nat. Nanotech.* **2011**, *6*, 763-72.

(246) Labean, T. H.; Li, H. *Nature* **2007**, *2*, 26-35.

(247) Berti, L.; Alessandrini, A.; Facci, P. *J. Am. Chem. Soc.* **2005**, *127*, 11216-7.

(248) Samson, J.; Varotto, A.; Nahirney, P. C.; Toschi, A.; Piscopo, I.; Drain, C. M. *ACS nano* **2009**, *3*, 339-44.

(249) Braun, E.; Eichen, Y.; Sivan, U.; Ben-Yoseph, G. *Nature* **1998**, *391*, 775-8.

(250) Park, S. H.; Prior, M. W.; LaBean, T. H.; Finkelstein, G. *Appl. Phys. Lett.* **2006**, *89*, 033901.

(251) Gu, Q.; Cheng, C.; Gonela, R.; Suryanarayanan, S.; Anabathula, S.; Dai, K.; Haynie, D. T. *Nanotechnology* **2006**, *17*, R14-R25.

(252) Gu, Q.; Cheng, C.; Haynie, D. T. *Nanotechnology* **2005**, *16*, 1358-1363.

(253) Richter, J.; Seidel, R.; Kirsch, R.; Mertig, M.; Pompe, W.; Plaschke, J.; Schackert, H. K. *Adv. Mater.* **2000**, *12*, 507-510.

(254) Stoltenberg, R. M.; Woolley, A. T. *Biomed. Microdevices* **2004**, *6*, 105-111.

(255) Monson, C. F.; Woolley, A. T. *Nano Lett.* **2003**, *3*, 359-363.

(256) Bagkar, N.; Choudhury, S.; Bhattacharya, S.; Yakhmi, J. V. *J. Phys. Chem. B* **2008**, *112*, 6467-72.

(257) Fischler, M.; Simon, U.; Nir, H.; Eichen, Y.; Burley, G. A.; Gierlich, J.; Gramlich, P. M. E.; Carell, T. *Small* **2007**, *3*, 1049-55.

(258) Lindahl, T.; Nyberg, B. *Biochemistry* **1972**, *11*, 3610-8.

(259) Frederico, L. A.; Kunkel, T. A.; Shaw, B. R. *Biochemistry* **1993**, *32*, 6523-30.

(260) Lindahl, T.; Andersson, A. *Biochemistry* **1972**, *11*, 3618-23.

(261) Sagripanti, J.-L.; Goering, P. L.; Lamanna, A. *Toxicol. Appl. Pharmacol.* **1991**, *110*, 477-485.

(262) Barber, R. *Biochim. Biophys. Acta* **1971**, *238*, 60-6.

(263) Eichhorn, G. L.; Butzow, J. J.; Shin, Y. a. *J. Bioscience* **1985**, *8*, 527-535.

(264) Ames, B. N.; Gold, L. S. *Mutat. Res.* **1991**, *250*, 3-16.

(265) Karadeniz, H.; Erdem, A.; Caliskan, A.; Pereira, C. M.; Pereira, E. M.; Ribeiro, J. A. *Electrochem. Commun.* **2007**, *9*, 2167-2173.

(266) Hsu, C. F.; Phillips, J. W.; Trauger, J. W.; Farkas, M. E.; Belitsky, J. M.; Heckel, A.; Olenyuk, B. Z.; Puckett, J. W.; Wang, C. C. C.; Dervan, P. B. *Tetrahedron* **2007**, *63*, 6146-6151.

(267) Zhu, H.-F.; Fan, J.; Okamura, T.-aki; Sun, W.-Y.; Ueyama, N. *Cryst. Growth Des.* **2005**, *5*, 289-294.

(268) Roldan, M.; Scaffardi, L.; Desanctis, O.; Pellegri, N. *Mater. Chem. Phys.* **2008**, *112*, 984-990.

(269) Dash, P.; Scott, R. W. J. *Chem. Comm.* **2009**, 812-4.

(270) Martin, M. N.; Basham, J. I.; Chando, P.; Eah, S.-K. *Langmuir* **2010**, *26*, 7410-7.

(271) Green, N. M. *Adv. Protein Chem.* **1975**, *29*, 85-133.

(272) Susumu, K.; Mei, B. C.; Mattoussi, H. *Nature protocols* **2009**, *4*, 424-36.

(273) SLOCIK, J. M.; GOVOROV, A. O.; NAIK, R. R. *Supramol. Chem.* **2006**, *18*, 415-421.

(274) Velev, O. *Adv. Biophys.* **1997**, *34*, 139-157.

(275) Huang, X.; Du, D.; Gong, X.; Cai, J.; Tu, H.; Xu, X.; Zhang, A. *Electroanalysis* **2008**, *20*, 402-409.

(276) Hegde, S.; Kapoor, S.; Joshi, S.; Mukherjee, T. *J. Colloid Interf. Sci.* **2006**, *297*, 637-43.

(277) Garlick, R. K.; Giese, R. W. *Biochem. J.* **1990**, *268*, 611-613.

(278) Baer, D. R.; Gaspar, D. J.; Nachimuthu, P.; Techane, S. D.; Castner, D. G. *Anal. Bioanal. Chem.* **2010**, *396*, 983-1002.

(279) Drummond, T. G.; Hill, M. G.; Barton, J. K. *Nat. Biotechnol.* **2003**, *21*, 1192-9.

(280) Genereux, J. C.; Boal, A. K.; Barton, J. K. *J. Am. Chem. Soc.* **2010**, *132*, 891-905.

(281) Rant, U.; Arinaga, K.; Fujita, S.; Yokoyama, N.; Abstreiter, G.; Tornow, M. *Nano Lett.* **2004**, *4*, 2441-2445.

(282) Rant, U.; Arinaga, K.; Fujita, S.; Yokoyama, N.; Abstreiter, G.; Tornow, M. *Langmuir* **2004**, *20*, 10086-92.

(283) Takeishi, S.; Rant, U.; Fujiwara, T.; Buchholz, K.; Usuki, T.; Arinaga, K.; Takemoto, K.; Yamaguchi, Y.; Tornow, M.; Fujita, S.; Abstreiter, G.; Yokoyama, N. *J. Chem. Phys.* **2004**, *120*, 5501-4.

(284) Rant, U.; Pringsheim, E.; Kaiser, W.; Arinaga, K.; Knezevic, J.; Tornow, M.; Fujita, S.; Yokoyama, N.; Abstreiter, G. *Nano Lett.* **2009**, *9*, 1290-5.

(285) Rosi, N. L.; Giljohann, D. A.; Thaxton, C. S.; Lytton-Jean, A. K. R.; Han, M. S.; Mirkin, C. A. *Science* **2006**, *312*, 1027-30.

(286) Zuker, M. *Nucleic Acids Res.* **2003**, *31*, 3406-15.

(287) Mathews, D. H.; Sabina, J.; Zuker, M.; Turner, D. H. *J. Mol. Biol.* **1999**, *288*, 911-40.

(288) Hänni, K. D.; Leigh, D. A. *Chemical Society reviews* **2010**, *39*, 1240-51.

(289) El-Sagheer, A. H.; Brown, T. *Chemical Society reviews* **2010**, *39*, 1388-405.

(290) Chan, T. R.; Hilgraf, R.; Sharpless, K. B.; Fokin, V. V. *Org. Lett.* **2004**, *6*, 2853-5.

(291) Presolski, S. I.; Hong, V.; Cho, S.-hye; Finn, M. G. *J. Am. Chem. Soc.* **2010**, *132*, 14570-6.

(292) Hong, V.; Presolski, S. I.; Ma, C.; Finn, M. G. *Angew. Chem.* **2009**, *48*, 9879-83.

(293) Branham, W. S.; Melvin, C. D.; Han, T.; Desai, V. G.; Moland, C. L.; Scully, A. T.; Fuscoe, J. C. *BMC biotechnology* **2007**, *7*, 8.

(294) Curry, A.; Nusz, G.; Chilkoti, A.; Wax, A. *Opt. Express* **2005**, *13*, 2668.

(295) Mertig, M.; Colombi Ciacchi, L.; Seidel, R.; Pompe, W.; Vita, A. De *Nano Lett.* **2002**, *2*, 841-844.

(296) Liu, J.; Geng, Y.; Pound, E.; Gyawali, S.; Ashton, J. R.; Hickey, J.; Woolley, A. T.; Harb, J. N. *ACS NANO* **2011**, *5*, 2240-2247.

(297) Vieira, J.; Messing, J. *Gene* **1982**, *19*, 259-68.

(298) Brazas, M. D.; Yamada, J. T.; Ouellette, B. F. F. *Nucleic Acids Res.* **2010**, *38*, W3-6.

(299) McGowan, P. F.; Hurst, R. E.; Bass, R. A.; Wilcox, L. J.; Hemstreet, G. P.; Postier, R. G. *J. Histochem. Cytochem.* **1988**, *36*, 757-762.

(300) Palomba, S.; Novotny, L.; Palmer, R. *Opt. Commun.* **2007**, *281*, 480-483.

(301) Hurst, S. J.; Hill, H. D.; Mirkin, C. a *J. Am. Chem. Soc.* **2008**, *130*, 12192-200.

(302) Liu, Y. *Front. Biosci.* **2008**, *13*, 923.

(303) Inman, R. B.; Jackson, J. F. *Gene* **1989**, *84*, 221-226.

(304) Liu, S.; Zhou, B.; Yang, H.; He, Y.; Jiang, Z.-X.; Kumar, S.; Wu, L.; Zhang, Z.-Y. *J. Am. Chem. Soc.* **2008**, *130*, 8251-60.

(305) Meier, J. L.; Mercer, A. C.; Rivera, H.; Burkart, M. D. *J. Am. Chem. Soc.* **2006**, *128*, 12174-84.

(306) Schnier, P. D.; Klassen, J. S.; Strittmatter, E. F.; Williams, E. R. *J. Am. Chem. Soc.* **1998**, *120*, 9605-13.

(307) Chenoweth, D. M.; Harki, D. a; Phillips, J. W.; Dose, C.; Dervan, P. B. *J. Am. Chem. Soc.* **2009**, *131*, 7182-8.

POSTGRADUATE ACTIVITIES

Demonstrator to MSc Cancer Chemistry

Presentation of the PhD project at the "Postgraduate Annual Seminar"

Attendance to *42nd IUPAC Congress on Chemistry Solutions* in Glasgow in August 2009

Attendance to Workshop *Investigating Chemical Processes through Designed Experiments* University of Southampton in September 2008

Attendance to *Leicester Organic and Physical Chemistry Seminars*.

Attendance to *RSC symposia* in different universities like Nottingham, Loughborough, and Leicester.

Validation of 10 credits in course BS2056 Molecular Machines

Validation of 10 credits in course BS2052 Gene expression and regulation

Supervision of 3rd year BSc projects and summer students.

Firefighting and fire prevention training at the University of Leicester.

LIST OF PUBLICATIONS

Su, W.; Gray, S. J.; Dondi, R.; Burley, G. A. *Org. Lett.* **2009**, 11, 3910-3

Dondi, R.; Su, W.; Griffith, G. A.; Clark, G.; Burley, G. A. *Small* **2012**, 1-7.